The Role of Nickel in the Survival of the Basidiomycete Fungus *Cryptococcus neoformans*

Robert Panting

Thesis submitted in accordance with the regulations of Newcastle University for the degree of Doctorate of Philosophy

September 2011

Abstract

Cryptococcus neoformans is a basidiomycete fungus that is found throughout the world living as a saprophyte. It is an opportunistic pathogen in humans and prevalence has increased significantly with the spread of HIV-AIDS, particularly in sub-Saharan Africa. *C. neoformans* infects the body via inhalation into the lung and dissemination around the body, including the central nervous system. Infection of the brain is fatal if untreated. The virulence of this organism is dependent on the enzyme urease, which catalyses the degradation of urea to ammonia and carbamate. The molecular role of urease during infection is not clear, although there is evidence that it is involved in the ability of *C. neoformans* to cross the blood brain barrier. Urease enzymes require an iron or nickel cofactor to function, which suggests that acquisition and distribution of this cofactor is important for the virulence of this yeast. The homeostasis of transition metals in living organisms is tightly regulated by a number of mechanisms including; metallochaperones, selective metal permeases, metal-sensors and compartmentalisation. Cases of *in vivo* mis-population of metal proteins are extremely rare.

In this project *C. neoformans* urease is identified as a nickel binding enzyme and regulation of urease activity in response to the available nitrogen source is characterised. The accumulation of nickel in *C. neoformans* is responsive to the available nitrogen source and a putative nickel-importer, *Cn*Nic1, is identified as the primary means of nickel accumulation. The urease accessory protein *Cn*UreG is essential for urease maturation and binds two equivalents of nickel with high affinity. *Cn*UreG is proposed to be a novel nickel chaperone for urease. Cobalt inhibits cryptococcal urease *in vivo* by binding to the protein and preventing nickel insertion into the active site. Urease inhibition by cobalt occurs at relatively low cobalt concentrations and therefore *C. neoformans* does not appear to have evolved effective mechanisms to protect against cobalt mis-population.

Declaration

I certify that this thesis contains my own work, except where acknowledged, and that no part of this material has previously been submitted for a qualification at this or any other university.

Acknowledgements

My greatest thanks are extended to my supervisor, Dr. Julian Rutherford, for his support and advice throughout this project. I would also like to thank Dr. Kevin Waldron, Prof. Christopher Dennison and Dr. Janet Quinn for their help, advice and extreme patience without which this project would not have been possible. For their moral and technical support I must thank Stephen Allen, Helen Crook, Abdelnasser El Ghazouani, Jonathon Brown and Miranda Patterson, who helped me stay motivated and focused.

To my parents, Dr. Caroline Carr and Dr. Gerard Panting, I would like to offer thanks for their support and guidance throughout my life and particularly during the writing of this thesis. To my girlfriend Christie Waddington I offer my heart-felt thanks for enduring the late nights and stress and always helping to relax and reassure me after a long day in the lab.

This project was support by funding from the Biotechnology and Biological Sciences Research Council.

Table of Contents

List of Figures

Chapter 1.

Chapter 3.

Chapter 4.

Chapter 5.

Chapter 6.

Chapter 8.

List of Abbreviations

HEPES	4-(2-hydroxyethyl)-1-piperazineethanesulfonic acid
AIDS	Acquired immune deficiency syndrome
N-terminus(al)	Amino-terminus(al)
AAS	Atomic absorption spectroscopy
ATP	Adenosine triphosphate
ABC	ATP-binding cassette
B. pasteurii	*Bacillus pasteurii*
*Bp*UreE	*Bacillus pasteurii* UreE
*Bp*UreG	*Bacillus pasteurii* UreG
BCG	Bacillus Calmette-Guérin
bp	Base pair
CIAP	Calf intestinal alkaline phosphatase
C-terminus(al)	Carboxyl-terminus(al)
k_{cat}	Catalytic constant
CDF	Cation diffusion facilitator
CNS	Central nervous system
CoCBS	Cobalt cystathionine β-synthase
CoPPIX	Cobalt protoporphyrin IX
C. immitis	*Coccidioides immitis*
*Ci*Nic1	*Coccidioides immitis* Nic1
C. posadasii	*Coccidioides posadasii*

cDNA	Complementary deoxyribonucleic acid
CuRE	Copper-responsive *cis*-acting element
CD	Circular dichroism
C. gattii	*Cryptococcus gattii*
C. neoformans	*Cryptococcus neoformans*
*Cn*Nic1	*Cryptococcus neoformans* Nic1
*Cn*UreG	*Cryptococcus neoformans* UreG
C. necator	*Cupriavidus necator*
*Cn*HoxN	*Cupriavidus necator* HoxN
CBS	Cystathionine β-synthase
CSD	Cysteine sulphinate desulphinase pathway
dATP	Deoxyadenosine triphosphate
dCTP	Deoxycytidine triphosphate
dGTP	Deoxyguanosine triphosphate
DNA	Deoxyribonucleic acid
dTTP	Deoxythymidine triphosphate
Kd	Dissociation constant
DTT	Dithiothreitol
EPR	Electron paramagnetic resonance
E. coli	*Escherichia coli*
EDTA	Ethylenediaminetetraacetic acid
EXFAS	Extended X-ray absorption fine structure
Far-UV	Far-ultraviolet

g	Gram
GTP	Guanosine triphosphate
H. felis	*Helicobacter felis*
H. mustelae	*Helicobacter mustelae*
H. pylori	*Helicobacter pylori*
*Hp*UreA	*Helicobacter pylori* UreA
*Hp*UreB	*Helicobacter pylori* UreB
*Hp*UreE	*Helicobacter pylori* UreE
*Hp*UreG	*Helicobacter pylori* UreG
CTAB	Hexadecyltrimethylammonium bromide
High-MW	High-molecular weight
HPLC	High pressure liquid chromatography
HT	High tension
hr(s)	Hour(s)
HIV	Human immunodeficiency virus
hph	Hygromycin resistance cassette
IMAC	Immobilized metal ion affinity chromatography
ICP-MS	Inductively coupled plasma mass spectrometry
FePPIX	Iron protoporphyrin IX
[Fe-S] cluster	Iron-sulphur cluster
ISC	Iron-sulphur cluster pathway
FeSOD	Iron-superoxide dismutase
IPTG	Isopropyl β-D-1-thiogalactopyranoside

kB	Kilo base pair
kDa	Kilo Dalton
K. aerogenes	*Klebsiella aerogenes*
*Ka*HypB	*Klebsiella aerogenes* HypB
*Ka*UreE	*Klebsiella aerogenes* UreE
*Ka*UreG	*Klebsiella aerogenes* UreG
LMCT	Ligand to metal charge transfer
LC/MS/MS	Liquid chromatography-mass spectrometry-mass spectrometry
l	Litre
LB	Luria broth
MHCII	Major histocompatibility Class II complex
MBP	Maltose Binding Protein
MnSOD	Manganese- superoxide dismutase
B_{max}	Maximal binding capacity
MALDI-PMF	Matrix-assisted laser desorption/ionization-protein mass fingerprinting
MALDI-TOF	Matrix-assisted laser desorption/ionization-time of flight
µg	Microgram
µl	Microlitre
µm	Micrometer
µM	Micromolar
mg	Milligram
ml	Millilitre

mm	Millimeter
mM	Millimolar
min	Minute(s)
M	Molar
MWCO	Molecular weight cut off
M. tuberculosis	*Mycobacterium tuberculosis*
*Mt*UreG	*Mycobacterium tuberculosis* UreG
nm	Nanometer
nM	Nanomolar
Nramp	Natural resistance-associated macrophage protein
NEO	Neomycin resistance cassette
NiCoT	Nickel/cobalt transporter
NCR	Nitrogen catabolite repression
ORF	Open reading frame
$OD_{(x)}$	Optical Density (at x nm)
ppb	Parts per billion
PMSF	Phenylmethanesulfonyl fluoride
PEG	Polyethylene Glycol
PCR	Polymerase chain reaction
kpsi	Pounds per square inch (thousands)
PCA	Principle component analysis
PC	Principle component
RND	Resistance and nodulation

RNA	Ribonucleic acid
krpm	Rotations per minute (thousands)
S. cerevisiae	*Saccharomyces cerevisiae*
S. pombe	*Schizosaccharomyces pombe*
*Sp*Nic1p	*Schizosaccharomyces pombe* Nic1
s	Seconds
SDS	Sodium dodecyl sulphate
SDS-PAGE	Sodium dodecyl sulphate polyacrylamide gel electrophoresis
*St*UreG	*Solanum tuberosum* ssp. *tuberosum* UreG
SUF	Sulphur assimilation pathway
SOD	Superoxide dismutase
tRNA	Transfer ribonucleic acid
Tris	Tris(hydroxymethyl)aminomethane
UV	Ultraviolet
w/v	Weight for volume
YPD	Yeast, peptone, dextrose medium
ZnPP	Zinc protoporphyrin

1. Introduction

1.1. *Cryptococcus neoformans*

Cryptococcus neoformans is a basidiomycete fungus that is capable of causing disease in humans (Lazera *et al.*, 1996; Bicanic and Harrison 2004). It is normally isolated as a spherical budding yeast of between 5 and 10 μM in diameter, although it has sometimes been found as slight hyphal and filamentous forms (Okagaki *et al.*, 2010; Gupta *et al.*, 2010). *C. neoformans* is sub-dived into two variants which are defined by their serotype, the antigens recognised by the immune system. The variants are serotype A, *C. neoformans var. grubii*, and serotype D, *C. neoformans var. neoformans*. Serotypes B and C have recently been classified as a separate species, *Cryptococcus gattii*, which diverged from *C. neoformans* some 40 million years ago (Levitz, 1991; Casadevall and Perfect, 1998; Franzot *et al.*, 1999).

C. neoformans is found world-wide, normally living as a saprophyte and is associated with rotting bark, soil and bird, particularly pigeon, excreta (Ellis and Pfeiffer, 1990a; Lazera *et al.*, 1996; Casadevall and Perfect, 1998). It has been proposed that *C. neoformans* has been spread world-wide by migratory pigeons (Nielsen *et al.*, 2007). *C. gattii* is associated with the bark of tropical trees and is not isolated from pigeon excreta (Ellis and Pfeiffer, 1990b; Sorrel *et al.*, 1996). As *C. gattii* tends only to be found in tropical regions, along with some other isolated areas, this supports the theory of pigeon-related *C. neoformans* distribution.

1.2. Infection by C*ryptococcus neoformans*

C. neoformans is an opportunistic pathogen in humans and infection does not form part of the normal life cycle (Perfect *et al.*, 1998). As an opportunistic pathogen *C. neoformans* is associated with immunocompromised or immunosuppressed individuals. This includes patients under immunosuppressive therapy, but is in particularly associated with HIV-AIDS sufferers (Bicanic and Harrison, 2005). Indeed, the spread of HIV-AIDS across the world had led to a global increase in the prevalence of *C. neoformans* infection. Cryptococcal infection now accounts for a significant proportion of HIV related deaths. The most notable increase is in the developing world, particularly sub-Saharan Africa, from which 70% of reported

cases of *C. neoformans* infection originate (Okongo *et al.*, 1998; French *et al.*, 2002). This is because the region is where the spread of HIV-AIDS has been most prolific and access to effective anti-fungal treatments is extremely limited (Robinson *et al.*, 1999). *C. gattii*, on the other hand, infects predominantly immunocompetent individuals, but accounts for far fewer cases than the *C. neoformans* species (Mitchell and Perfect, 1995; Kidd *et al.*, 2007).

The model of infection starts with inhalation of the fungal spores or dried and aerosolised cells into the lungs (Figure 1). The fungus then lodges in the alveoli and, in an immunocompetent individual, encounters the alveolar macrophages that trigger an immune response which normally clears the infection (Sukroongreung *et al.*, 1998; Bicanic and Harrison, 2004). In an immunocompromised individual, rather than being confined to the primary sites of infection, the *C. neoformans* cells can grow and escape the lung into the blood stream. Once in the blood stream the fungus can disseminate through the entire body, including the central nervous system (CNS). If *C. neoformans* crosses the blood-brain barrier it can cause meningoencephalitis, which is fatal if untreated (White *et al.*, 1992; Koguchi and Kawakami, 2002).

To be able to infect a human host *C. neoformans* has several virulence factors. These virulence factors include the ability to grow a polysaccharide capsule, melanin production, urease activity, ability to grow at 37^{o}C and spore formation (Casadevall *et al*., 2003). Capsule formation and urease activity are described in greater detail below. Melanin production protects the cell from reactive oxygen species and so defends the fungal cell from attack by phagocytic immune cells (Wang *et al.*, 1995; Wang *et al.*, 1996; Liu *et al.*, 1999). The ability to grow at 37^{o}C allows *C. neoformans* to survive and grow in a human host. Spore formation, as described above, facilitates entry to the lungs and establishment of primary sites of infection (Bicanic and Harrison, 2004). As infection does not form part of the *C. neoformans* lifecycle these virulence factors will not have evolved to facilitate human infection. One theory is that these virulence factors which protect against phagocytic attack, evolved to protect *C. neoformans* from predation by amoeba or nematode worms that are also present in environments with which *C. neoformans* is associated (Casadevall *et al.*, 2003).

A

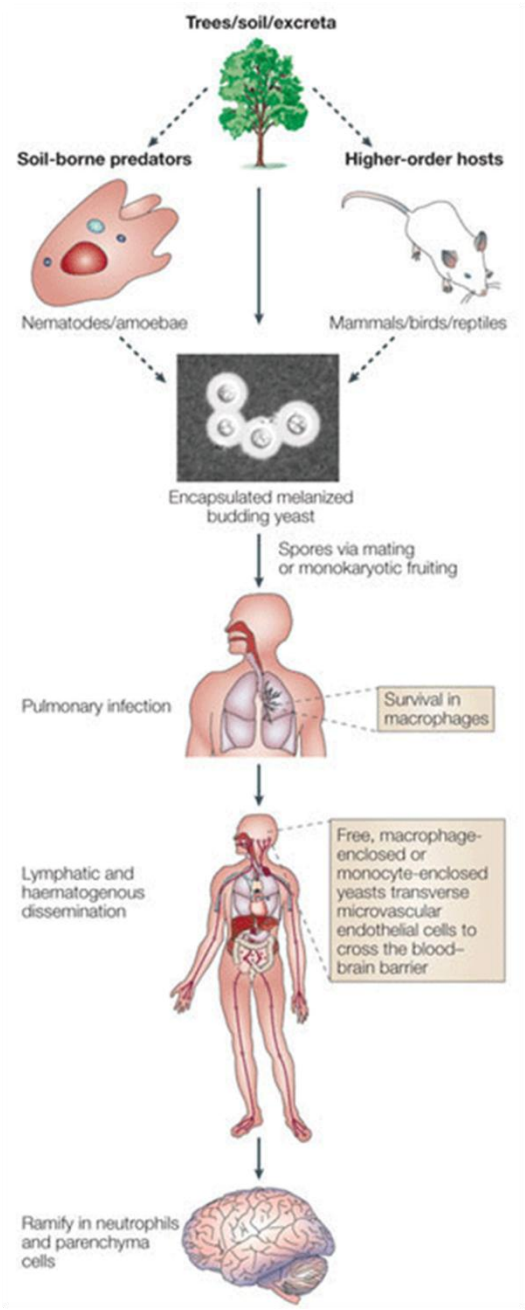

B

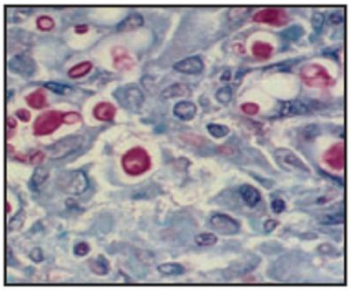

C

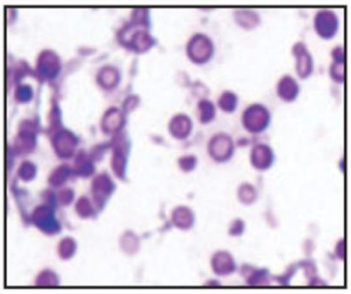

Figure 1 - Infection by *C. neoformans.*

A - *C. neoformans* enters the body by inhalation into the lungs and, if able to survive, disseminates through the body. Infection of the brain occurs if the yeast is able to cross the blood brain barrier. Panel adapted from Idnurm *et al*., 2005.

B - Lung tissue of an AIDS patient infected with *C. neoformans*. The cells are stained with Mucicarmine which binds to the inner polysaccharide capsule giving red colouration. Panel adapted from Doering, 2009.

C - Brain tissue infected with *C. neoformans*. The fungal cells are stained with Methenamine silver stain which binds to the cell wall giving a dark colouration. Panel adapted from Doering, 2009.

1.2.1. Urease Activity

Urease is an enzyme that catalyses the degradation of urea to ammonia, which is utilised as a source of nitrogen. To do this urease requires a nickel or iron cofactor, absence of which abolishes catalytic activity (Carter *et al.*, 2009; Carter *et al.*, 2011). How urease facilitates *C. neoformans* infection is not fully understood. Urease-negative *C. neoformans* is avirulent in a mouse model of infection, as mice infected with urease-negative *C. neoformans* have a significantly longer survival time than those infected with wild-type *C. neoformans* (Cox *et al.*, 2000; Olszewski *et al.*, 2004). Mice infected with urease-negative *C. neoformans* also have a lower fungal burden in the CNS than wild-type infected mice, while the fungal burden of other organs were broadly similar. Urease is required, either directly or indirectly, to cross the blood-brain barrier and infect the brain. Ammonia produced by urease may destroy the epithelial cells to facilitate transmigration (Shi *et al.*, 2010a).

Although the role of urease is unclear in *C. neoformans* infection, it has been well studied in bacterial pathogens (Mobley *et al.*, 1995; Canteros *et al.*, 1996). In bacteria urease usually facilitates infection by localised alkalisation due to the production of ammonia. In *Helicobacter pylori*, which colonises the human stomach, the increase in pH creates a pH-neutral microenvironment in which the bacteria can survive and grow (Scott *et al.*, 2002). The bacteria *Mycobacterium tuberculosis* infects human lungs and is capable of surviving when internalised by alveolar macrophages, even for long periods of time (Clemens *et al.*, 1995). In this instance the ammonia produced by urease neutralises the acidic phagosome of the macrophage and so helps prevent intra-cellular killing. Urease activity in experimental tuberculosis (BCG) has also been shown to inhibit presentation of the major histocompatibility class II (MHCII) complex at the macrophage cell surface and so prevent escalation of the immune response. Interestingly, when purified urease was attached to latex beads and phagocytised by macrophages the same inhibition of MHCII complex presentation was observed (Sendide *et al.*, 2004). This suggests that this could be a common role for urease in the survival of pathogens internalised by phagocytic immune cells. Urease is present in other pathogenic fungi that invade the lungs, such as *Coccidioides immitis*, *Coccidioides posadasii* and *Aspergillus niger* (Ghasemi *et al.*, 2004; Mirbond-Donovan *et al.*, 2006). *C.*

neoformans can therefore be used as a model to study urease activity, function and maturation in pathogenic fungi.

1.2.2. The Polysaccharide Capsule

The polysaccharide capsule is considered to be the most important of the virulence factors of *C. neoformans* infection (Bose *et al.*, 2003). The capsule surrounds the fungal cell wall and can be many times the volume of the cell itself. This acts as a barrier against the immune system, protecting against phagocytosis by inhibiting recognition and internalisation, as well as acting as a physical barrier to the cytotoxic agents of intracellular killing (Kozel *et* al., 1988). The capsule also reduces inflammation and can bind to, and thus inhibit, components of the complement pathway (Buchanan and Murphy, 1998).

The capsule is primarily made of a mannose back-bone with xylosyl and glucuronyl side chains (Cherniak *et al.*, 1998). This carbohydrate structure gives *C. neoformans* colonies expressing the polysaccharide capsule a distinctive mucoid appearance. The standard test for capsule formation is an India ink stain. The pigment of the ink is excluded from the cell by capsule, so that under microscopic examination a distinctive 'halo' is seen around an encapsulated cell (Figure 2) (Pierini and Doering, 2001).

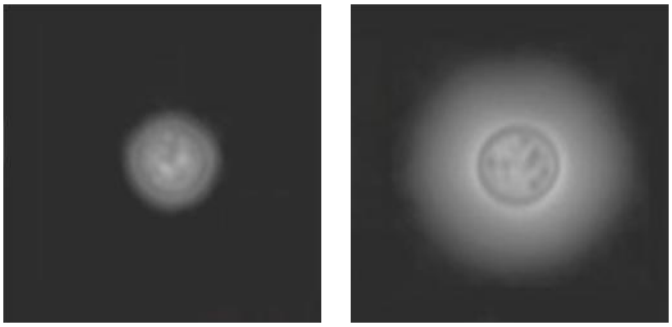

Figure 2 - Capsule detection by India ink stain.

C. neoformans with small (left panel) and large (right panel) capsule growth stained with India ink.

The figure was adapted from Guimarães *et al.*, 2010.

Capsule formation is regulated in response to a number of different factors including; low iron bio-availability, pH of the media and high CO_2 concentrations (Granger *et al.*, 1985; Vartivarian *et al.*, 1993). During infection capsule formation is induced to varying degrees depending on tissue location (Rivera *et al.*, 1998). More recently Lee *et al.* demonstrated that capsule formation is regulated in response to the available nitrogen source. Specifically, uric acid, urea and creatine induce capsule production, while ammonia inhibits production, even when added with those nitrogen sources which promote capsule production (Lee *et al*., 2011).

1.2.3. The Effect of Cell Size on Pathogenicity

How *C. neoformans* crosses the blood-brain barrier is not fully understood. A theory is that fungal cells lodge in capillaries of the CNS and cross directly to the brain, bypassing the meninges (Olszewski *et al.*, 2004; Shi *et al.*, 2010a). This requires the cells to be smaller than the capillary diameter. Cell gigantism, in which the cell diameter can increase up to 100 μM (excluding capsule), has been implicated in protecting against phagocytosis. When cell gigantism is induced the ability of *C. neoformans* to cross the blood-brain barrier is reduced in a mouse model of infection (Zaragoza *et al.*, 2010). This supports the theory that cell size is an important determinant for the ability of *C. neoformans* to infect the brain.

1.3. Nitrogen Catabolite Repression

Fungi use nitrogen for a number of different roles, including incorporation into macromolecules such as proteins, DNA and RNA. This means that the acquisition of nitrogen is of paramount importance to the fungal cell. While fungi can utilise a variety of nitrogen sources, they do not all result in the same rate of growth (Cooper, 1982). It is then in the interest of the fungi to use the nitrogen sources that provide the best growth conditions. This is achieved by a process known as Nitrogen Catabolite Repression (NCR) or Nitrogen Metabolite Repression, the terms can be used interchangeably (Wiame et al., 1985; Magasanik and Kaiser, 2002). By NCR the pathways that utilise nitrogen sources that result in poorer growth conditions are down-regulated in the presence of better nitrogen sources, which are considered 'preferred' nitrogen sources (Schure *et al.*, 2000).

In the model yeast *Saccharomyces cerevisiae* all nitrogen sources are degraded to ammonium or glutamine, which are the preferred nitrogen sources. Other nitrogen sources are therefore utilised less preferentially (Cooper, 1982; Wiame *et al*., 1985). For example, the proline utilisation pathway is down-regulated in the presence of ammonia. The existing proline acquisition permeases, Gap1p and Put4p, are inactivated and degraded while their transcription is repressed (Grenson, 1983; Jauniaux *et al*., 1987; Jauniaux and Grenson, 1990; Stanbrough and Magasanik, 1995). Transcriptional control is regulated through GATA transcription factors Gln3p and Gat1p, which bind to the promoters of NCR sensitive genes and promote expression in the absence of ammonia (Minehart and Magasanik, 1991; Coffman *et al.*, 1996). The negative acting transcription factors Dal80p and Deh1p, which are also in the GATA class of transcription factor, down-regulate the expression of NCR sensitive genes (Daugherty *et al.*, 1993; Coffman *et al.*, 1996; Schure *et al.*, 2000).

In *C. neoformans* only one NCR transcription factor has been identified, Gat1, which shares limited sequence homology to the GATA factors of *S. cerevisiae* (Kmetzsch *et al*., 2011). This is similar to *Aspergillus nidulans* and *Neurospora crassa*, which also have only one NCR transcription factor AreA and Nar1, respectively (Stewart and Vollmer, 1986; Fu and Marzluf, 1987a; Fu and Marzluf, 1987b; Hensel *et al.*, 1998). Deletion of *GAT1* in *C. neoformans* results in loss of ability to grow on minimal synthetic media in which urea, ammonia, or any amino acid are the sole nitrogen source, with the exception of arginine and proline. Microarray analysis demonstrated that *GAT1* was involved in the transcriptional regulation of NCR genes (Kmetzsch *et al.*, 2011). During the course of this study, NCR has been shown to be involved in the expression of *C. neoformans* virulence factors. Capsule growth is induced in response to urea, uric acid or creatine and repressed by ammonia. However, melanin production is repressed by urea, uric acid or creatine and recovered by ammonia (Lee *et al.*, 2011). Despite opposite effects on capsule and melanin production it is evident that nitrogen source availability and, by extension, NCR are involved in the regulation of virulence factors in *C. neoformans*.

1.3.1. Uric Acid Metabolism

Uric acid is a potential nitrogen source that is highly abundant in bird excreta, one of the environments with which *C. neoformans* is most associated. *C. neoformans* is able to grow on media based on pigeon guano (Nielsen *et al.*, 2007). The predicted degradation of uric acid is outlined in Figure 3. The final stage in this pathway is the degradation of urea to ammonia by the enzyme urease (Figure 3) (Rouf and Lomprey, 1968). Interestingly, primates are the only mammals which do not degrade uric acid. The first enzyme in the pathway, urate oxidase or uricase, is a non-functional gene in primates (Proctor, 1970). As a result uric acid is present in the human blood stream, as is urea at around 2.5 mM, both are potential sources of nitrogen to *C. neoformans* during infection (Proctor, 1970; Zielinski *et al.*, 1999; Ronne-Engström *et al.*, 2001; Tyvold 2007; Waring *et al.*, 2008). It is then possible that urease is required for virulence simply to allow *C. neoformans* to metabolise available nitrogen sources. It is also possible that urease has an effect on the expression of other virulence factors by indirect regulation of NCR.

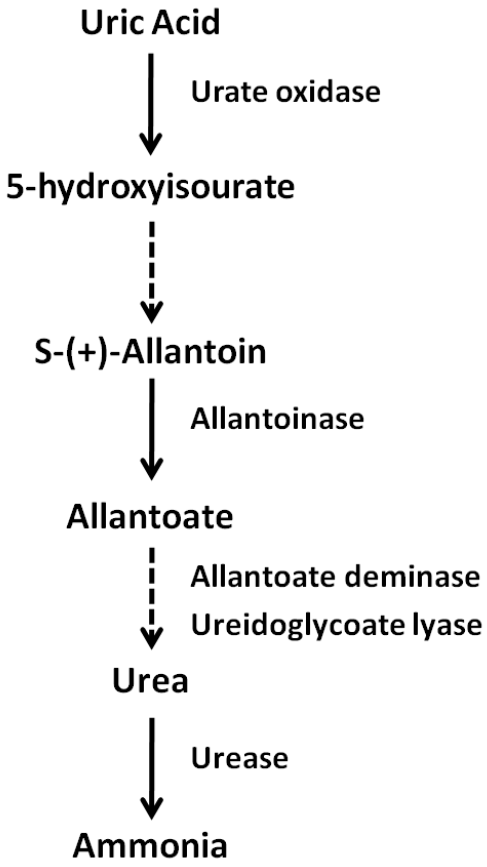

Figure 3 - The degradation of uric acid.

The predicted pathway of uric acid metabolism in *C. neoformans*. The enzyme involved at each stage is indicated. A dashed arrow indicates that more than one reaction takes place.

The figure was adapted from Lee *et al.*, 2011.

1.4. Metals in Biology

Protein-bound transition metals are utilised across all kingdoms of life in a variety of roles and are essential for cell survival. Structural metals, such as zinc in zinc-finger proteins, provide mechanical support to the protein backbone and can help facilitate folding. Other metals, such as copper in copper/zinc superoxide dismutase, are required in the catalytic core of enzymes (Matthews *et al.*, 2009; Liochev and Fridovich, 2010). Between a quarter and a third of all proteins are thought to be metal binding, therefore the insertion of the correct metal into the protein metal-binding site is essential for cell survival (Waldron and Robinson, 2009). However, high concentrations of unbound transition metals can be toxic to the cell. In the cases of copper, nickel or zinc, any free atoms of these metals in the cell can be considered a high concentration. Free metals are able to bind the incorrect protein or other macromolecules and inhibit function. In the case of iron and copper, oxidative stress can be caused by hydroxyl radicals generated by Fenton chemistry. Therefore elaborate homeostatic mechanisms have evolved to control the concentration and distribution of metals in the cell.

The homeostasis of metals is complicated by the different affinities of ligands for metals, as described by the Irving-Williams series. This series orders the general affinity of ligands for divalent transition metals as Mn^{2+} and $Ca^{2+} < Fe^{2+} < Co^{2+} < Ni^{2+} < Cu^{2+} > Zn^{2+}$, with copper having the highest affinity and magnesium and calcium the lowest (Irving and Williams, 1948; Irving and Williams, 1953; Fraústo da Silva and Williams, 2001). Therefore, if the metal binding proteins of a cell were to be produced in a solution with equal concentrations of each of these metals all the proteins would bind to copper (Waldron *et al.*, 2009). To prevent this a selection of metal homeostatic mechanisms have evolved, including; metallochaperones, selective metal-transporters, metal-sensors and compartmentalisation of metals and metal binding proteins.

1.4.1. Metal Transporters and Their Regulation

The import of metals into the cytoplasm is carefully controlled via metal specific transporters. In bacteria there are a variety of transporter types responsible for metal uptake, such as the ATP-binding cassette (ABC) family that includes importers for

nickel, zinc, iron and manganese, and P-type ATPases that may be involved in the import of a range of metals including copper (Ferguson and Deisenhofer, 2004; Lu and Solioz, 2002). Both of these systems use ATP hydrolysis to drive metal uptake. Other transporters, such as the natural resistance associated macrophage protein (Nramp) family use a proton gradient to drive metal uptake (Kehres *et al.*, 2000). In the yeast *S. cerevisiae* copper uptake is mediated via the high-affinity transporters Ctr1p and Ctr3p (Labbé *et al.*, 1997). The *S. cerevisiae* iron uptake system is divided between siderophore uptake by the Arn family of transporters, Fre1-4 reductase linked import via the high-affinity Fet3/Ftr1 transporter complex and the low-affinity transporter Fet4p (Yun *et al.*, 2000; Waters and Eide, 2002). *S. cerevisiae* zinc uptake is via the high-affinity Zrt1p and Zrt2p transporters and low affinity Fet4p transporter (Waters and Eide, 2002; Zhao and Eide, 1996a; Zhao and Eide, 1996b). To prevent over-accumulation of metals, bacteria express export proteins that transport metals out of the cytoplasm in high metal concentrations. The cation diffusion facilitator (CDF) family drive excess metal transport from the cytoplasm to the periplasm of gram-negative bacteria and the resistance and nodulation (RND) family drive transport across the outer membrane (Saier *et al.*, 1994; Anton *et al.*, 1999). In *S. cerevisiae* an excess of potentially useful metal is not exported from the cell but is stored in the vacuole for potential use in the future (MacDiarmid *et al.*, 2000; Li *et al.*, 2001; MacDiarmid *et al.*, 2002).

The concentration of metals in the cytoplasm is controlled by the expression levels of metal transporters. In *Escherichia coli* the metal importers are expressed in metal limiting conditions and exporters in high metal conditions to maintain appropriate cytosolic concentrations (Waldron *et al.*, 2009). This is commonly mediated by metal sensing transcription factors. The copper sensor CueR binds copper at 10^{-21} molar concentrations. When copper-bound, CueR transcriptionally activates the expression of CopA and CueO which export copper from the cytoplasm, thus keeping the copper concentration in the sub-femtomolar range (Wayne Outten *et al.*, 2000; Changela *et al.*, 2003). A similar system is present for zinc regulation, the zinc sensors ZntR and Zur have 10^{-15} molar affinities for zinc and when zinc bound transcriptionally activate expression of zinc export proteins such as ZntA (Rensing *et al.*, 1999; Outten and O'Halloran, 2001). The nickel sensor NikR binds nickel via 2 sites, with 10^{-7} and 10^{-12} molar affinities. Binding of both sites increases DNA

binding which represses expression of the NikABCDE importer complex (Eitinger and Mandrand-Berthelot, 2000; Waldron and Robinson, 2009). These systems all have very tight binding affinity for their respective metal and thus keep the cytosolic concentration extremely low, in the cases of copper and zinc below 1 atom per cell.

The metal homeostatic systems in *S. cerevisiae* activate transcription of metal importers during metal starvation and mediate the internalisation and degradation of the importers in metal replete conditions. In parallel to this process, in metal replete conditions useful metals are stored in the vacuole and in metal limiting conditions the metals are released (Rutherford and Bird, 2004). The expression of the copper importers Ctr1p and Ctr3p is induced in low copper conditions by the transcription factor Mac1p, which binds to copper-responsive *cis*-acting elements (CuREs) in the promoter region of these genes. Under copper replete conditions these transporters are internalised and degraded via a Mac1p mediated pathway (Yamaguchi-Iwai *et al.*, 1996: Ooi *et al.*, 1996; Labbé *et al.*, 1997; Yonkovich *et al.*, 2002). Iron homeostasis in *S. cerevisiae* is mediated by the Aft1 and Aft2 transcription factors that respond to iron concentration and oxidative stress by nuclear localisation regulated by Grx3 and Grx4 (Pujol-Carrion *et al*., 2006). In low iron conditions iron uptake transporters are expressed and the vacuolar iron stores released via expression of the Fet5/Fth1 system (Casas *et al.*, 1997; Blaiseau *et al*., 2001; Rutherford and Bird, 2004). However, Aft1 is also responsive to glucose levels independently of iron. Iron uptake genes have increased expression on the switch to respiratory metabolism in a Snf1/Snf4 and Aft1 dependent manner (Haurie *et al.*, 2003). The zinc responsive transcription factor, Zap1, induces expression of Zrt1, Zrt2 and Fet3 under zinc limiting conditions as well as increasing expression of the vacuole efflux pump Zrt3. Zrt1 is endocytosed and degraded in response to high zinc (Waters and Eide, 2002; Zhao and Eide, 1996a; Zhao and Eide, 1996b; MacDiarmid *et al.*, 2000; Eide, 2003). A common theme to each of these metal regulation systems is the direct regulation by the metal binding to the transcription factor; Mac1p binds DNA in a copper dependent interaction, Aft1 binding [Fe-S] clusters induces nuclear export, Zap1 binds zinc and DNA via zinc-finger motifs that regulates DNA binding (Jensen and Winge, 1998; Bird *et al.*, 2000; Rutherford and Bird, 2004; Ueta *et al*., 2007).

1.4.2. Metallochaperones

The concentration of transition metals is kept extremely low by the cell, but metal binding proteins still require access to the appropriate metal during or soon after folding. This presents a problem as there are many potential metal binding sites in the cell, so the probability of the few atoms of the correct metal finding the correct binding site is small. Also, the incorrect metal may fill the binding site and lead to inactive protein (Waldron and Robinson, 2009; Robinson and Winge, 2010). To overcome these problems a class of proteins known as metallochaperones has evolved. Metallochaperones bind metal and dock with the target protein via protein-specific interactions and transfer the metal to the target by ligand exchange reactions (Furukawa *et al.*, 2004). The protein-protein interaction provides specificity to the transfer and prevents transfer to the wrong protein or insertion of the wrong metal to the target. An example of this is the copper chaperone to cyanobacterium P-type ATPases, Atx1, which forms a homodimer with the copper transporters CtaA and PacS to facilitate copper transfer. However, Atx1 cannot interact with the zinc P-type ATPases, ZntA and ZiaA, and so does not transfer copper to the wrong protein, despite close homology of transporter cytoplasmic regions (Banci *et al.*, 2002; Tottey *et al.*, 2002; Robinson and Winge, 2010). How metallochaperones acquire the metal is not fully understood, but systematic deletion of copper importers in *S. cerevisiae* does not result in loss of metal-binding by specific chaperones, indicating that chaperones do not accept metal exclusively from one transporter (Portnoy *et al.*, 2001). However, interactions between the copper importer Ctr1p and the copper chaperone Atx1 result in copper transfer *in vitro* (Xiao and Wedd, 2002).

Metallochaperones have been described for copper, nickel and iron (Waldron *et al.*, 2009). The three most studied copper chaperones in yeast are Atx1, which transfers copper to the P-type ATPases on the Golgi membrane, Cox17, which transfer copper to cytochrome *c* oxidase via Sco1 and Cox11, and Ccs1, the copper chaperone for superoxide dismutase 1 (Huffman and O'Halloran, 2001; Singleton and Le Brun, 2007; Robinson and Winge, 2010). Bacterial nickel chaperones include UreE, the chaperone to urease, which is discussed in more detail below, and the HypA-HypB complex, which supplies nickel to the NiFe-hydrogenase. The HypA-HypB complex accepts nickel from the NikABCDE system and transfers it in a GTP hydrolysis dependent step to the hydrogenase apo-enzyme (Eitinger and Mandrand-Berthelot,

2000; Rowe *et al.,* 2005). Iron being assembled into iron-sulphur ([Fe-S]) clusters in bacteria is delivered to the assembly factor scaffold by the protein CyaY, which therefore acts as an iron chaperone (Fontecave and Ollagnier-de-Choudens, 2008).

1.4.3. Compartmentalisation

The folding of a nascent polypeptide exposes potential metal binding sites to the metals of its local environment. Those metals with the highest affinity in the local environment will bind the protein. Similarly proteins with exposed metal binding sites that bind weak affinity metals, such as manganese or iron, are liable to have the metal exchanged with any available higher affinity metals, such as copper (Waldron *et al.,* 2009). A strategy to overcome this problem is to exploit the compartments of a cell, by folding low-affinity metal-binding proteins in compartments devoid of tightly binding metals. This is exemplified by MncA and CucA from the cyanobacterium *Synechocystis*. MncA is a manganese binding protein and CucA is a copper binding protein, both are localised to the periplasm which is rich in copper. However, the proteins have identical metal binding sites and *in vitro* MncA binds copper with 10^4 times higher affinity than manganese. The insertion of manganese into MncA is achieved by folding of the protein in the cytoplasm, which is depleted of copper but manganese replete, prior to export to the periplasm. Once loaded with manganese the metal binding site of MncA is buried, thus preventing substitution with copper. In comparison, CucA is folded in the periplasm and so binds copper directly (Tottey *et al.,* 2008). In eukaryotes the number of organelles and compartments provides opportunity for similar metal regulation and some evidence for this exists. In mammals the delivery of copper to tyrosinase can only occur at specific compartments of the secretory pathway (Setty *et al*., 2008). The plant *Arabidopsis thaliana* localises manganese transporters to sub-populations of the post-Golgi compartments (Li *et al.,* 2008). In *S. cerevisiae* the vacuole is used for metal storage and thus protects the cytoplasm from high concentrations of useful but toxic metals (Li *et al.,* 2001; MacDiarmid *et al*., 2000; MacDiarmid *et al*., 2002; Eide, 2003).

1.4.4. Metal Mis-population

A large number of metal binding proteins have been discovered and studied. Despite the general lack of discrimination between metals by proteins *in vitro*, only a handful of cases of incorporation of the incorrect metal have been documented *in vivo* (Waldron *et al*., 2009). This demonstrates how well regulated metal homeostasis is across different species. However, the few cases of metal mis-population that are documented can give valuable insight into the mechanism and evolution of metal homeostasis by identification of how and why the wrong metal was incorporated.

[Fe-S] clusters are utilised by proteins with various biological functions, including; electron transfer, regulation of transcription and in the catalytic core of enzymes (Beinert *et al.,* 1997). The correct incorporation of these clusters is therefore vital for many aspects of cell survival but in *E. coli* formation and incorporation of an [Fe-S] cluster can be inhibited by cobalt *in vivo* (Ranquet *et al.,* 2007). The [Fe-S] clusters form as either [4Fe-4S], [3Fe-4S] or [2Fe-2S] and are generated by the iron-sulpher cluster (ISC), sulphur assimilation (SUF) or cysteine sulphinate desulphinase (CSD) machinery. The ISC machinery generates [Fe-S] clusters under normal conditions and the SUF is used during oxidative stress or iron limiting conditions. Both systems utilise a cysteine desulfurase, IscS and SufSE, which donates sulphur to the [Fe-S] cluster during biogenesis (Barras *et al*., 2005). Addition of cobalt to the *E. coli* growth medium inhibits growth rates, decreases iron accumulation to around half wild-type levels and results in significantly increased cobalt accumulation (Ranquet *et al.*, 2007). Deletion of the CorA transporter abolishes cobalt accumulation but does not rescue iron accumulation, indicating that cobalt enters the cell via this transporter and blocks iron accumulation by a different mechanism. The activity of the [Fe-S] proteins aconitase, MiaB and FhuF was studied *in vivo* in normal and high-cobalt (200 μM) conditions. Aconitase and MiaB, both [4Fe-4S] enzymes, had reduced activity in high cobalt conditions, which was rescued by deletion of CorA. FhuF, a [2Fe-2S] protein, was found by UV-visible absorbance, electron paramagnetic resonance (EPR) and atomic absorbance spectroscopy (AAS) to have reduced iron and increased cobalt content. When the same proteins were examined *in vitro*, iron loaded MiaB and FhuF were not inactived by incubation of cobalt and aconitase was only inactivated by switching from anaerobic to aerobic conditions and back in the presence of cobalt, which causes iron to dissociate and allows cobalt to

bind. This indicated that cobalt entered the iron homeostatic pathway *in vivo*. The scaffold proteins IscU and SufA are able to assemble and transfer [Fe-S] clusters to target proteins. When these proteins were incubated with cobalt the UV-visible spectrum revealed peaks indicative of cobalt binding. IscU was also able to transfer cobalt to apoMiaB *in vitro*. The model put forward was that cobalt inhibited some iron uptake but also replaced iron in the [Fe-S] cluster biogenesis pathway, effectively inhibiting the formation of a range of important [Fe-S] cluster binding proteins (Ranquet *et al.*, 2007).

The effect of copper on [Fe-S] clusters has also been investigated. To *E. coli*, growth in minimal media with excess copper is highly toxic (Macomber and Imlay, 2009). In addition to oxidative stress caused by copper redox chemistry the [Fe-S] containing dehydratase enzymes fumarase A, 6-phosphogluconate dehydratase and isopropylmalate isomerase were inhibited *in vivo* in high copper conditions. However, unlike the [Fe-S] biogenesis proteins, fumarase A could be inactivated by copper *in vitro* independently of oxidative stress. The addition of copper released iron from the [Fe-S] cluster but the presence of Cu-Fe-S intermediates was not detected, indicating that the copper does not replace iron in the cluster. The recovery of the fumarase A activity, after copper inactivation, by the addition of iron also indicated that copper caused the degradation of the [Fe-S] cluster rather than binding in the place of iron. In agreement with this, copper stress induces the expression of [Fe-S] biogenesis factor in *Bacillus subtilis* (Chillappagari *et al*., 2010). Although this example is not direct mis-population of a metal binding site it does demonstrate that *in vivo* enzyme inhibition can arise from other effects of aberrant metal homeostasis.

Another iron containing compound, haem, can also be mis-populated by other transition metals. The final stage in haem biosynthesis is the incorporation of iron into protoporphyrin by the enzyme ferrochelatase (Lange *et al.*, 1999). However when iron is limiting zinc can compete for the same site, resulting in the production of zinc-protoporphyrin (ZnPP) (Camadro and Labbé, 1982; Camadro *et al.*, 1982). The structure of ferrochelatase is conserved from bacteria to humans and ZnPP levels are used as an indicator of iron deficiency in humans, indicating that poor metal specificity of ferrochelatase may be common to many species (Al-Karadaghi *et al.*, 1997; Labbé and Dewanji, 2004). Therefore under normal conditions iron

outcompetes zinc to bind protoporphyrin, but when iron is limiting zinc is able to partially outcompete iron and form ZnPP. The incorporation of cobalt into haem has also been documented in *E. coli* (Majtan *et al*., 2011). When *E. coli* cells are grown in high (150 μM) cobalt media the formation of cobalt protoporphyrin IX (CoPPIX) can be detected in place of normal haem (FePPIX). The CoPPIX was incorporated into the normally haem containing enzyme, cystathionine β-synthase (CBS). The CoCBS had an activity nearly as high (~95 %) as the wild-type FeCBS, which is likely to be a reflection of the non-catalytic role of haem in CBS. The incorporation of CoPPIX into enzymes which utilise a catalytic haem core, such as cytochromes, may result in reduced activity (Majtan *et al*., 2011).

The superoxide dismutase (SOD) family of proteins has Cu/Zn, Ni, Fe and Mn members. The FeSOD and MnSOD share significant sequence and structural homology (Culotta *et al.*, 2006). Very unusually for a metal enzyme, MnSOD of *E. coli* is purified in 3 forms, a Mn_2, a Mn,Fe and an Fe_2 form (Beyer *et al.*, 1991). Analysis of MnSOD *in vitro* revealed equal binding affinities for manganese and iron (Mizuno *et al.*, 2004). However, iron bound MnSOD is inactive and therefore metal selection affects enzyme function (Whittaker, 2003). This may result from the binding environment of MnSOD being inappropriate for iron based redox reactions (Culotta *et al.*, 2006). This is an unusual example in which metal mis-population *in vivo* occurs without the aberrant metal being added to non-physiological levels. Although MnSOD mis-population is observed in bacteria, iron binding to the normally manganese binding SOD2 of eukaryotes is only observed in conditions where iron homeostasis is disrupted. In this case iron would not normally reach SOD2, which is in the mitochondrial matrix, however mutations which increase mitochondrial iron content result in the inhibition of SOD2 by iron binding (Dancis, 1998; Yang *et al.*, 2006; Culotta *et al.*, 2006).

1.5. Urease Maturation

1.5.1. The Urease Enzyme

The urease of *Canavalia ensiformis*, or jack bean, was the first enzyme to be crystalised, in 1926, although the structure was not solved (Sumner, 1926). Jack bean urease was also the first enzyme demonstrated to utilise nickel (Dixon *et al.*, 1975). Urease catalyses the degradation of urea to ammonia and carbamate, which spontaneously degrades to ammonia and carbon dioxide. The structure of urease enzymes from different sources (bacteria, plants and fungi) are very similar and involve the formation of a trimeric complex with 3 catalytic cores (Carter *et al.*, 2009). The urease enzymes of most bacteria, including *Klebsiella aerogenes* and *Bacillus pasteurii*, are comprised of 3 subunits, UreA, UreB and UreC, which form a heterotrimer that forms a complex comprised of 3 of these trimers, a $(UreABC)_3$ complex (Figure 4A) (Jabri *et al.*, 1995; Benini *et al.*, 1999). The urease of *H. pylori* is comprised of 2 subunits, *Hp*UreA and *Hp*UreB. *Hp*UreA represents a fusion of UreA and UreB from other bacterial urease enzymes and *Hp*UreB is homologous to the UreC of other bacteria. The *H. pylori* urease forms a $(UreAB)_3$ complex similar to that of *K. aerogenes* and *B. pasteurii* (Ha *et al.*, 2001). Despite the early work on jack bean urease crystallisation the structure has only recently been solved to high resolution (Balasubramanian and Ponnuraj, 2010). The plant urease enzymes are composed of a single poly-peptide chain equivalent to a fusion of the 3 subunits found in bacteria. Jack bean urease forms a trimer analogous to the $(UreABC)_3$ complex of bacterial urease enzymes, which then forms a hexamer (Figure 4B) (Sheridan *et al.*, 2002). Urease enzymes from different species form different higher order complexes; the *H. pylori* urease forms a $((UreAB)_3)_4$ complex and the jack bean urease forms a hexamer in solution (Ha *et al.*, 2001; Balasubramanian and Ponnuraj, 2010).

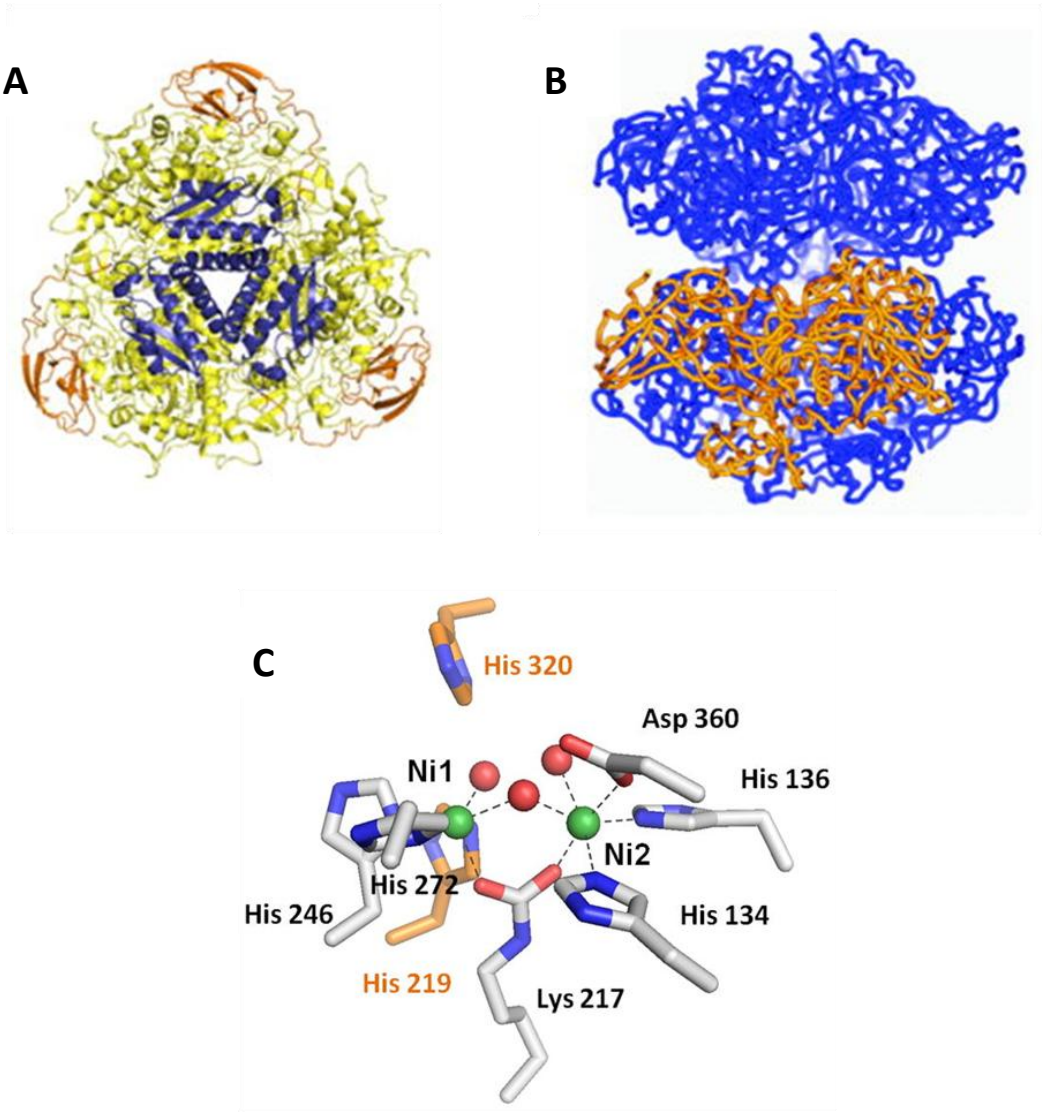

Figure 4 - The structures of urease enzymes.

A - The crystal structure of *K. aerogenes* urease in a $(UreABC)_3$ complex with UreA coloured blue, UreB coloured orange and UreC coloured yellow.

B - The crystal structure of *C. ensiformis* urease in a hexameric complex. A single subunit is highlighted in orange.

C - The active site of *K. aerogenes* urease. Nickel atoms are coloured green and water molecules are coloured red. Metal binding amino acid residues are coloured white and residues proposed to be involved in urea hydrolysis are coloured orange.

Figure adapted from Carter *et al.*, 2009.

The active site of urease is highly conserved in those enzymes for which there are structures (Carter *et al.*, 2009; Balasubramanian and Ponnuraj, 2010). Urease utilises two nickel atoms in catalytic core, Ni1 and Ni2. In *K. aerogenes* urease Ni1 is coordinated by two histidine residues, H246 and H272, a water molecule and a modified lysine residue, K217. Ni2 is coordinated by two histidine residues, H134 and H136, an aspartate residue, D360, a water molecule, the same molecule which coordinates Ni1, and the modified lysine, K217 (Figure 4C) (Pearson *et al.*, 1997). The lysine residue which links the two nickel atoms is carbamylated, a modification that is conserved between species and which is essential for urease maturation (Pearson *et al.*, 1997; Balasubramanian and Ponnuraj, 2010). Extended X-ray absorption fine structure (EXFAS) studies of jack bean urease are consistent with the crystal structure (Alagna *et al.*, 1984). The mechanism of urea breakdown by urease is not fully understood, but various models have been put forward since the identification of urease as a nickel enzyme. A recently proposed mechanism is as follows; the urea substrate interacts with Ni1 via the carbonyl oxygen atom and the water bridging the two nickel atoms (nucleophilically charged by interaction with Ni2) performs a nucleophilic attack on the urea carbon forming an intermediate complex. The adjacent H320 then accepts the electron and the intermediate complex collapses thus releasing one nitrogen atom as ammonia and leaving carbamate which spontaneously degrades to ammonia and carbon dioxide (Carter *et al.*, 2009). Other models differ on which water molecule performs the nucleophilic attack and what acts as the acid to accept the electron on breakdown of the intermediate complex (Dixon *et al.*, 1980; Andrews *et al.*, 1986; Carter *et al.*, 2009).

The maturation of urease normally requires several protein cofactors, but can be achieved *in vitro* with relatively low efficiency. *K. aerogenes* apo-urease is activated to ~15% of wild-type levels when incubated with nickel and bicarbonate (Park and Hausinger, 1996). When in solution bicarbonate is in equilibrium with carbon dioxide, the covalent binding of CO_2 to the terminal amine group of K217 produces the carbamoyl group (R-NH-COOH). As the reaction is the addition of a carboxyl group to the K217 residue, this modification is sometimes referred to as carboxylation rather than carbamylation. Also investigated was the effect of metal ions other than nickel binding in the active site. Incubation of apo-urease with bicarbonate and zinc or copper resulted in inactive enzyme. However incubation with

manganese or cobalt generated ~2% of activity compared to nickel, indicating that other metals can substitute for nickel but result in lower enzyme activity. In the case of cobalt this only occurs in a C319A mutant, as cobalt incubated with the wild-type urease bound to C319 and did not produce any urease activity (Park and Hausinger, 1996; Yamaguchi and Hausinger, 1997). The exposure of nickel-bound jack bean urease to zinc and cobalt, for 51 and 87 days respectively, resulted in partial replacement of the catalytic core and a drop in enzyme activity. The nickel was partially replaced by zinc and cobalt and thought to result in mixed-metal active sites that were inactive (King and Zerner, 1997). The long incubation periods indicate that replacement of nickel in the mature urease is very inefficient.

The urease activity of gastric pathogens allows the creation of a pH neutral microenvironment that is essential for colonisation. The *Helicobacter* species which populate the stomachs of plant eating hosts are able to acquire nickel for urease from the plant matter that is ingested. However those species which colonise carnivore stomachs may be more limited for nickel as animals are not known to require nickel or accumulate it and so nickel-rich food will seldom be ingested (Solomons *et al.*, 1982). A second form of the urease was identified in the species *Helicobacter felis*, UreA2 and UreB2 which have 46% and 73% sequence identity to the *H. felis* UreA and UreB respectively (Pot *et al.*, 2007). The homologous urease system of *Helicobacter mustelae* is expressed in nickel limiting conditions (Stoof 2008). *H. mustelae* UreA2B2 was iron bound when purified from *H. mustelae* cells. This iron-urease coordinated iron at the active site in an arrangement and with ligands indistinguishable from those of nickel-urease enzymes. The quaternary structure formed a $((UreA2B2)_3)_4$ complex in a manner identical to the *H. pylori* $((UreAB)_3)_4$ complex (Ha *et al.*, 2001; Carter *et al.*, 2011). The high degree of similarity between the iron- and nickel-urease sequence, structure and active-site architecture suggest that to confirm which metal a urease enzyme binds direct, *in vivo* evidence is required.

1.5.2. Assembly of the Urease Maturation Complex

The maturation of urease has been most thoroughly studied in the bacterium *K. aerogenes*, which requires 4 accessory proteins to activate urease, UreD, UreE, UreF and UreG. Deletion of these accessory proteins results in abolished urease activity *in*

vivo (Lee *et al.*, 1992; Mulrooney *et al.*, 2005). Low levels, ~15%, of *K. aerogenes* apo-urease can be activated *in vitro* by modification of the conserved lysine with CO_2 and the binding of nickel to the active site (Park and Hausinger, 1996). The activation of urease *in vivo* is achieved via assembly of the urease-UreDEFG complex, which is thought to occur in a step-wise process (Figure 5) (Lee *et al.*, 1990). The urease activation complex assembly begins with the binding of UreD to urease. When UreD is highly expressed with urease *in vivo* a urease-UreD complex is formed and cross-linking studies have confirmed UreD binding to urease (Park *et al.*, 1994; Chang *et al*., 2004). This binding event appears to induce a conformational change that partially opens the active site, as the *in vitro* activation of urease in the urease-UreD complex is approximately 30%, twice the activity of urease alone (Park *et al.*, 1994; Park and Hausinger, 1996).

The subsequent step is binding of UreF to the urease-UreD complex. Over-expression *in vivo* of UreF alongside UreD and urease resulted in the formation of a urease-UreDF complex. Significantly, the over-expression of UreF alone with urease does not result in the formation of a complex, indicating that UreD is required to mediate the UreF-urease interaction. An anti-UreD antibody is unable to bind to the urease-UreDF complex but can bind to urease-UreD, indicating that UreF covers the UreD epitope (Moncrief and Hausinger, 1996; Moncrief and Hausinger, 1997). The binding of UreF to the urease-UreD complex prevents crosslinking of urease and UreD. This indicates that UreF binding causes a conformational change in the complex and UreD moves away from urease (Chang *et al.*, 2004). The *in vitro* levels of activity of urease-UreDF are equal to that of urease-UreD, suggesting that the active site structure has not been significantly altered by UreF binding (Moncrief and Hausinger, 1996).

The third stage in complex assembly is the binding of UreG to the urease-UreDF complex. The co-expression of *K. aerogenes* urease, UreD, UreF and UreG resulted in the formation of a urease-UreDFG complex which was also assembled by mixing of the components *in vitro* (Park and Hausinger, 1995; Soriano and Hausinger, 1999). The *in vitro* activity of urease in this complex was above 60% of wild-type levels and was enhanced by hydrolysis of GTP. UreG contains a GTPase domain known as a P-loop and mutation of this region abolished the enhanced activation of urease-UreDFG in the presence GTP. Similarly GTP did not enhance activation of

the urease-UreD or urease-UreDF complex (Soriano and Hausinger, 1999). This suggests that UreG is a GTPase and UreF may be a GTPase activating enzyme. The expression of UreD, UreF and UreG without urease results in the formation of an insoluble UreDFG complex, it has been suggested that this complex is pre-formed and then binds urease (Moncrief and Hausinger, 1997; Carter *et al*., 2009).

The final stage of urease activation is the delivery of nickel to the urease-UreDFG complex by the nickel chaperone, UreE (Colpas *et al.*, 1999; Colpas and Hausinger, 2000). Activity *in vitro* of urease-UreDFG incubated with UreE is equal to wild-type levels of urease activation (Soriano *et al.*, 2000). This result indicates that urease-UreDFG is the physiologically relevant activation complex and UreE is required to transport nickel to the active site (Carter *et al.*, 2009).

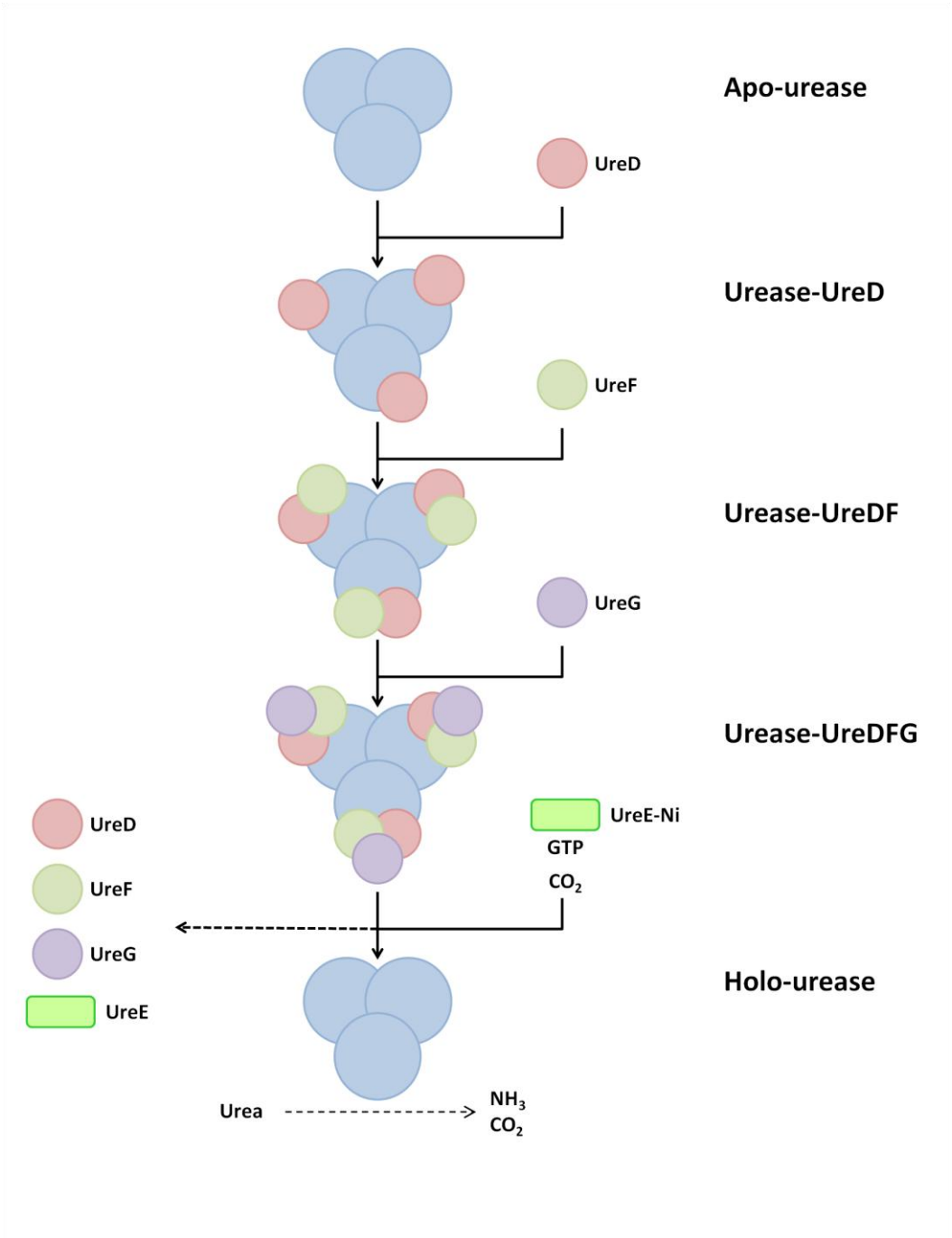

Figure 5 - The step-wise assembly of the urease maturation complex.

The formation of the urease-UreDEFG complex occurs in a step-wise manner of UreD, UreF, UreG and UreE binding sequentially to the urease apo-enzyme. After nickel loaded UreE binds the active site lysine residue is modified and nickel inserted in a GTP hydrolysis dependent manner. After maturation the accessory proteins dissociate.

1.5.3. UreE

UreE is considered to be the nickel chaperone to urease. To date UreE has been predominantly studied in three bacterial species, *B. pasteurii* (*Bp*UreE), *K. aerogenes* (*Ka*UreE) and *H. pylori* (*Hp*UreE). UreE is not essential for urease maturation, but deletion of UreE results in reduced urease activity that can be recovered by addition of nickel (Brayman and Hausinger, 1996). Each UreE protein contains a putative peptide binding domain and a conserved metal binding domain, which resemble the copper chaperone Atx1 (Song *et al*., 2001; Won *et al.*, 2004; Bellucci *et al.*, 2009). A non-conserved 15 residue C-terminal region is present in *Ka*UreE which contains 10 histidine residues. A smaller C-terminal region containing 2 histidine residues is present in *Bp*UreE and only 1 C-terminal histidine residue is present in *Hp*UreE (Brayman and Hausinger, 1996; Remaut *et al.*, 2001; Benoit and Maier, 2003). At low micromolar concentrations UreE forms a dimer in solution via a non-metal mediated hydrophobic interaction (Musiani *et al*., 2004).

The nickel binding properties of *Ka*UreE, *Bp*UreE and *Hp*UreE have been investigated. *Ka*UreE binds 6 nickel atoms per dimer with an average Kd of 9.6 μM but a truncated from, H144**Ka*UreE, which lacks the C-terminal histidine residues binds 2 nickel atoms per dimer with Kd = 0.78 μM and Kd = 85 μM (Lee *et al.*, 1993; Brayman and Hausinger, 1996). *Bp*UreE binds 2 nickel atoms per dimer with Kd = 1.4 μM and Kd = 25 μM (Stola *et al.*, 2006). *Hp*UreE binds only 1 nickel atom per dimer with a Kd = 1 μM (Benoit and Maier, 2003). Nickel binds in 3 separate sites of UreE and the difference in binding capacity between each species is due to the presence or absence of some of these sites (Figure 6). A central binding site utilises a highly conserved histidine ligand from each subunit in the dimer that is present in each UreE protein (H96 in *Ka*UreE, H100 in *Bp*UreE and H102 in *Hp*UreE) and binds nickel in an octahedral coordination geometry (Stola *et al*., 2006). A peripheral nickel binding site utilises H110 and H112 in *Ka*UreE and H145 and H147 in *Bp*UreE and is also thought to bind nickel in an octahedral coordination geometry. Whether one nickel atom is bound by ligands from both subunits or each subunit is capable of binding one nickel atom is unclear (Song *et al.*, 2001; Won and Lee 2004; Mulrooney *et al.*, 2005). *Hp*UreE does not possess this peripheral binding site and mutation of the only histidine residue in this region does not affect overall nickel binding (Bellucci *et al*., 2009). The final binding site is the histidine-rich C-

terminal extension present on some UreE proteins, such as *Ka*UreE. As deletion of this region reduces the nickel binding capacity of *Ka*UreG from 6 atoms per dimer to 2 the remaining 4 atoms appear to bind in this region (Brayman and Hausinger, 1996). As the H145 and H147 of *Bp*UreE are in the extreme C-terminus of the peptide, nickel binding by these residues may be more analogous to that of the *Ka*UreE C-terminal extension rather than the peripheral binding site. In *Bp*UreE the H145/H147 peripheral binding site has a lower affinity than the central binding site (Won *et al.*, 2004).

The central binding site is the key site in transfer of nickel to urease. Mutation of the conserved central histidine residue of UreE *in vivo* results in lower urease activity than in a UreE deletion mutant (Stola *et al.*, 2006). This has lead to a model whereby nickel is bound by the peripheral or C-terminal binding sites and transferred to urease via the central binding site upon binding to the urease-UreD-UreF-UreG complex or GTP hydrolysis by UreG. UreE is not required for nickel insertion to the urease active site provided sufficient nickel can reach the assembly complex. UreE lacking the central binding site, due to residue mutation, binds nickel at the peripheral sites but is not able to transfer it to urease, thus resulting in lower availability of nickel to urease than the absence of UreE. The peripheral sites are also important in urease activation. Expression of H144**Ka*UreE with mutations in H110 or H112, which abolish nickel binding in the peripheral site, results in lower urease activation *in vivo* (Colpas *et al.*, 1999). Activation of urease in *H. pylori* requires the nickel chaperones to hydrogenase, HypA and HypB, but deletion of these proteins can be compensated for by the expression of *Hp*UreE with a 6 Histidine tag (Benoit and Maier, 2003; Benoit *et* al., 2007). This is consistent with the above model, as nickel transfer from either a native or artificial UreE peripheral nickel site or from another nickel chaperone is required for high levels of urease maturation.

The binding of nickel to *Bp*UreE gives rise to slight changes in the secondary structure consistent with a decrease of random coil and an increase of α-helix observed by Far-UV CD spectroscopy (Lee *et al.*, 2002a). However, measurements by NMR do not detect any significant changes upon nickel binding *Bp*UreE (Lee *et al.*, 2002b; Won *et al.*, 2004). As the C-terminus of both *Bp*UreE and *Ka*UreE is absent in the crystal structure this indicates that this is a flexible region (Shi *et al.*, 2010b). Despite the relatively small structural change, nickel binding to *Bp*UreE did

confer significantly increased thermal stability indicating that nickel binding provides some structural support to UreE (Lee *et al*., 2002a). Metal binding to UreE at higher concentrations can result in the formation of a dimer of dimers. In this tetramer formation a single metal atom is coordinated by the conserved central histidine residue from each subunit, H100 in *Bp*UreE (Remaut *et al.*, 2001). As the tetramer only forms at high, >25 μM, concentrations of UreE or during crystallisation this form does not appear to be physiologically relevant (Musiani *et al*., 2004).

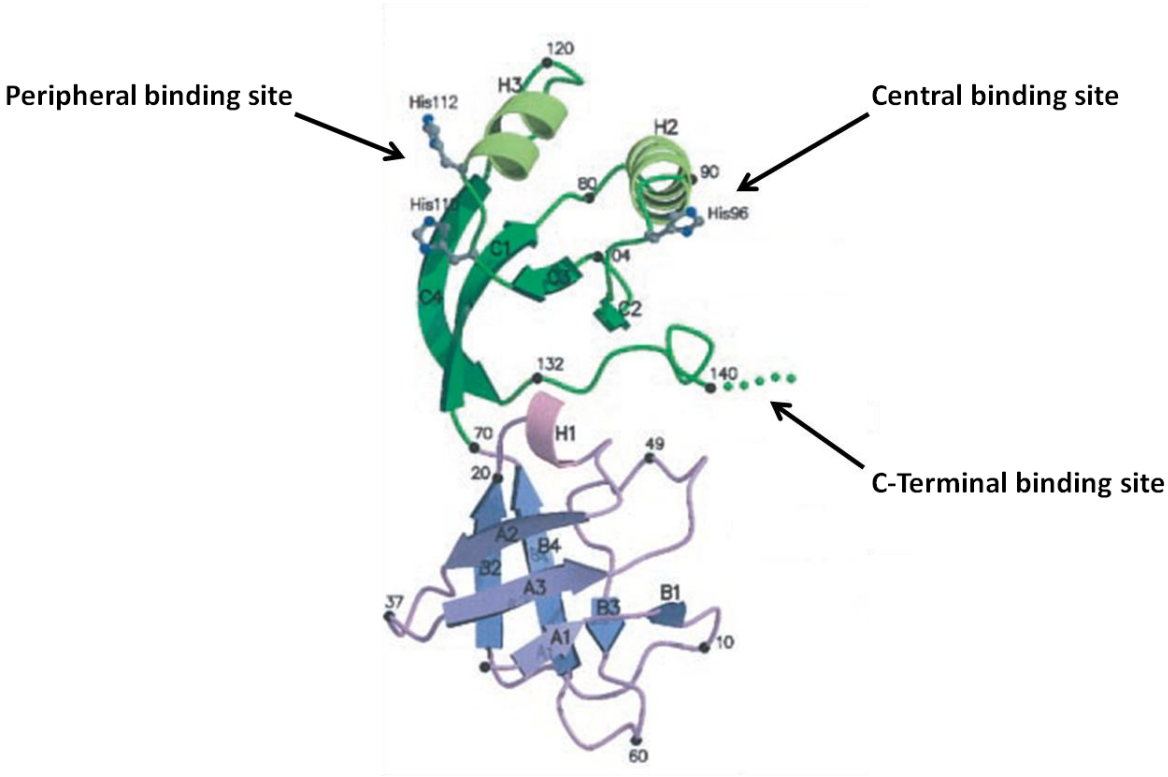

Figure 6 - The crystal structure of *Ka*UreE.

The crystal structure of the *Ka*UreE monomer, the metal binding domain is coloured green and the protein interaction domain is coloured purple. The proposed metal binding sites are indicated. The C-Terminal structure was not solved, but the location of the proposed binding site is indicated.

Figure adapted from Song *et al.*, 2001.

1.5.4. UreG

UreG is a urease accessory protein that is essential to urease activation *in vivo*. Like UreE, UreG has been predominately studied in *K. aerogenes* (*Ka*UreG), *B. pasteurii* (*Bp*UreG) and *H. pylori* (*Hp*UreG) as well as *M. tuberculosis* (*Mt*UreG). Due to the conservation of the GTP binding P-loop and the switch 1 and switch 2 sequences between UreG proteins and the hydrogenase accessory protein *Ka*HypB, which is a GTPase required for nickel transfer, UreG is considered to be a GTPase (Moncrief and Hausinger, 1997). When studied *in vitro* GTPase activity in UreG proteins is low, k_{cat} = 0.01 min^{-1} in *Hp*UreG, k_{cat} = 0.04 min^{-1} in *Bp*UreG and GTP hydrolysis is undetectable in *Ka*UreG, compared with a k_{cat} = 0.17 min^{-1} in *Ka*HypB (Moncrief and Hausinger, 1997; Zambelli *et al.*, 2005; Zambelli *et al.*, 2007). Mutations in the P-loop region of *Ka*UreG results in a loss of urease activation *in vivo* and *in vitro* urease activation in a UreD-UreF-UreG-urease complex is increased in the presence of GTP (Moncrief and Hausinger, 1997; Soriano and Hausinger, 1999). A similar result is reported for mutation of the *Hp*UreG P-loop domain *in vivo* (Mehta *et al.*, 2003a). This has lead to the conclusion that UreG acts as a GTPase in urease active site assembly but that interaction with the other accessory proteins or the urease apo-enzyme is required to activate GTP hydrolysis (Benoit *et al*., 2007; Maier *et al*., 2007). The energy derived from GTP hydrolysis is likely to be required for modification of the lysine in the urease active site or to facilitate transfer of nickel from the accessory proteins to urease.

To date a crystal structure of UreG from any species has not been solved and this has been identified as an important step in understanding the function of UreG (Carter *et al*., 2009). NMR spectroscopy has revealed that *Bp*UreG and *Mt*UreG have little or no tertiary structure. Far-UV CD indicated that *Bp*UreG secondary structure was composed of 15% α-helix, 29% β-sheet, 26% turns and 30% random coil, similarly *Mt*UreG was determined to be composed of 8% α-helix, 29% β-sheet, 19% turns and 45% random coil (Zambelli *et al.*, 2005; Zambelli *et al*., 2007). This indicated that these proteins are intrinsically disordered and offers an explanation as to why a crystal structure has been so difficult to produce. In contrast *Hp*UreG showed a more rigid tertiary structure by NMR and Far-UV CD revealed 31% α-helix, 11% β-sheet and 58% turns (Zambelli *et al*., 2009). This demonstrated that there is inconsistency in the biochemical properties of UreG between bacterial species but why *Hp*UreG

should be different is unclear. The activation of urease in *H. pylori* requires the HypA and HypB proteins, which has not been observed in other species (Olson *et al*., 2001). The involvement of additional factors in the urease assembly complex may explain the different properties of *Hp*UreG. Computational models based on sequence homology between UreG proteins from different species have been generated for *Hp*UreG, *Bp*UreG and *Mt*UreG and in the case of *Hp*UreG is partially based on the crystal structure of HypB from *Methanocaldococcus jannaschii* with which it shares 29% identity. The secondary structure composition of these models is at some variance with that determined by Far-UV CD (stated above), for the *Bp*UreG model the structure was composed of 36% α-helix, 22% β-sheet and 42% turns and random coil and the *Mt*UreG model was composed of 36% α-helix, 19% β-sheet and 44% turns and random coil (Figure 7) (Zambelli *et al*., 2005; Zambelli *et al*., 2007; Zambelli *et al*., 2009). In both cases the model included a far greater proportion of α-helix and β-sheet than experimentally determined for the protein *in vitro*. Whether these models represent a folded form of UreG in complex with other accessory proteins is not clear and still requires confirmation by solving of a crystal structure.

The metal binding properties of UreG proteins has been investigated. *Ka*UreG binds 1 nickel atom, Kd = 16 μM, per monomer (Boer *et al.*, 2010). *Bp*UreG binds 4 nickel atoms, Kd = 360 μM, or 2 zinc atoms, Kd = 42 μM, per dimer (Zambelli *et al.*, 2005). *Hp*UreG binds 4 nickel atoms, Kd = 10 μM, or 1 zinc atom, Kd = 0.33 μM, per dimer (Zambelli *et al*., 2009). This is another demonstration that the properties of bacterial UreG proteins are not always consistent between species. However, it is important to note that nickel binding affinity of the UreG of any species is significantly lower than that of the conjugate UreE. The zinc binding of *Hp*UreG stabilises the homodimer interaction by the conserved C66 and H68 residue from each monomer interacting with the single zinc atom (Zambelli *et al.*, 2009). The analogous cysteine residues in *Bp*UreG and *Mt*UreG, C68 and C90 respectively, are oxidised during homodimer formation (Zambelli *et al*., 2007; Neyroz *et al*., 2006). *Ka*UreG is a monomer in solution and the analogous residue, C72, is involved in nickel binding and required for *in vivo* activation of urease (Boer *et al.*, 2010). Whether the data reported represent physiological differences between urease maturation systems in these bacteria or are the result of *in vitro* artefacts is not clear. The requirement of *Ka*UreG C72 for *in vivo* urease activity indicates that nickel

binding in this site is important for urease maturation and that this may be a transient binding site during a stepwise transfer of nickel from UreE to urease.

The interaction between UreG and UreE is potentially important for the maturation of urease. In both *H. pylori* and *K. aerogenes* metal binding stabilises the interaction between UreG and UreE. In *H. pylori* when zinc is incubated with *Hp*UreG monomer and the *Hp*UreE dimer an *Hp*UreG$_2$(*Hp*UreE$_2$) complex is formed. This complex has a high affinity zinc binding site, Kd = 1.5 nM, and a lower affinity binding site, Kd = 0.67 μM. The C66 and H68 residues of *Hp*UreG are thought to form the low affinity binding site, and the H102 and H152 the high affinity binding site. Nickel does not stabilise this complex (Bellucci *et al*., 2009). In *K. aerogenes Ka*UreG and *Ka*UreE interact in a zinc or nickel dependent manner to form a (*Ka*UreG(*Ka*UreE)$_2$)$_3$ complex (Boer *et al.*, 2010). That nickel stabilises the complex is suggested as evidence that nickel is passed from *Ka*UreE to *Ka*UreG during urease maturation. However, the C72 of *Ka*UreG is suggested as part of the nickel binding site involved in transfer of nickel to urease, but the equivalent residue in *Hp*UreG is involved in zinc binding and *Hp*UreG does not show nickel-mediated stabilisation (Bellucci *et al.*, 2009). Once again the cause of these differences between species is not clear.

Eukaryotic UreG proteins have also been studied, although in much less detail than those of bacteria. The UreG of the potato plant *Solanum tuberosum* ssp. *tuberosum* (*St*UreG) and that of soybean *Eu3* both contain a histidine-rich N-terminal domain. *St*UreG N-terminal domain contains 17 histidine residues and *Eu3* contains 22 (Freyermuth *et al*., 2000, Witte *et al.*, 2001). Despite these domains being identified as potential metal binding sites and the lack of a UreE homologue for either species in the NCBI database, the metal binding properties of *St*UreG were not studied and metal binding by *Eu3* was only crudely demonstrated. *Eu3* was passed through a Ni-sepharose resin and could only be eluted by washing with imidazole, but the same result was observed when *Eu3* was passed through a Co-sepharose resin (Freyermuth *et al*., 2000). This established that *Eu3* was able to bind nickel and cobalt, but did not indicate affinity or capacity and so does not distinguish *Eu3* from bacterial UreG proteins.

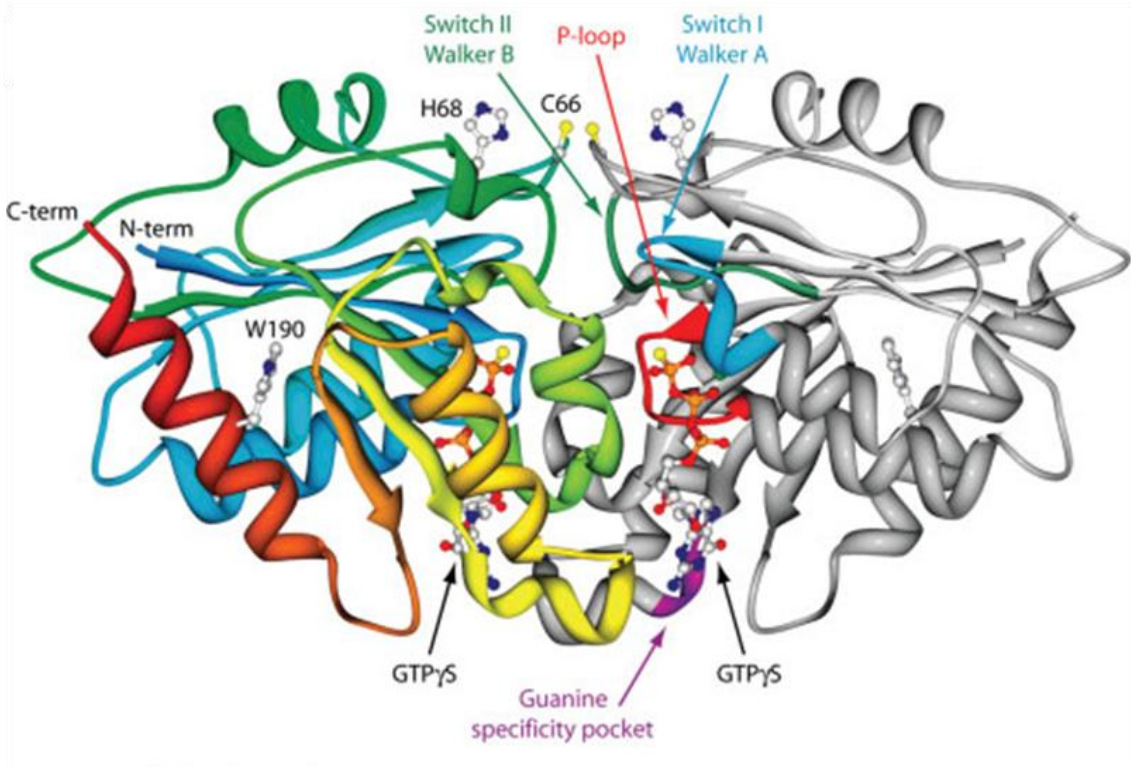

Figure 7 - The model structure of *Hp*UreG.

A structural model of dimeric *Hp*UreG based on sequence homology of UreG proteins. The left subunit is coloured blue at the N-terminus to red at the C-terminus. GTPase features including the P-loop, Switch I, Switch II and GTP binding site are indicated and coloured on the right subunit. The proposed metal binding residues C66 and H68 are labelled.

The figure was adapted from Zambelli *et al.*, 2009.

1.5.5. UreD and UreF

The attempted expression of both *K. aerogenes* UreD and UreF in *E. coli* resulted in insoluble bodies (Park *et al.*, 1994; Moncrief and Hausinger, 1996). Recently *Ka*UreD has been purified as part of a fusion with the maltose binding protein (MBP) (Carter and Hausinger, 2010). When expressed with the *K. aerogenes* urease cluster lacking UreD the fusion was shown to be functional by activating urease to approximately 33% of wild-type levels. The metal binding characteristics were investigated and UreD was found to bind 2.5 nickel atoms per monomer with a Kd of 50 μM and 4 Zn atoms per monomer with a Kd of 5 μM, which compete for the same binding sites as nickel as well as one additional site. This indicates that UreD may bind nickel during its transfer from UreE to the urease active site. The metal binding properties of the MBP were accounted for to calculate these values. The UreD-MBP fusion formed a urease-UreD-MBP-UreFG complex and a UreD-MBP-UreFG complex *in vivo*, supporting the theory that the UreDFG complex is physiologically relevant.

UreF from *K. aerogenes* has also been expressed as part of a fusion with MBP and has been expressed as a UreF-UreE fusion (Kim *et al*., 1999; Kim *et al.*, 2006). The UreF-UreE fusion was functional and formed a urease-UreFE-UreDG complex *in vivo* and a urease-UreD-UreEF complex *in vitro*. Mutation of residues revealed that the UreF C-terminal domain is required to form the urease maturation complex and the N-terminal domain is required for urease activation. The UreF of *B. pasteurii* has been structurally modelled based on sequence homology with known proteins and conservation of sequences among UreF proteins (Salomone-Stagni *et al.*, 2007). The model was based on a class of GTPase activating proteins, which indicated that UreF may act as a UreG regulating protein to control the biosynthesis of the urease active site.

1.5.6. Other Proteins Involved in Urease Maturation

The maturation of urease in *H. pylori* requires factors in addition to the four accessory proteins described for *K. aerogenes* (the UreD homologue of *H. pylori* is known as UreH). The hydrogenase accessory proteins HypA and HypB are essential for urease activation (Voland *et al.*, 2003; Olson *et al.*, 2001). HypA is considered to

be a nickel chaperone for hydrogenase activation, and binds 2 nickel atoms per dimer (Mehta *et al.*, 2003a; Mehta *et al.*, 2003b). HypA interacts with *Hp*UreE *in vivo* and expression of the *H. pylori* urease in *E. coli* revealed a dependence on HypA for activation only in nickel limiting conditions (Benoit *et al.*, 2007). As *Hp*UreE is only able to bind 1 nickel atom per dimer, compared to 6 per dimer of *Ka*UreE, this suggests that the HypA is required to chaperone nickel to the urease maturation complex. The HypB protein is a GTPase required for hydrogenase activation and mutations in the P-loop domain effectively abolish hydrogenase and urease activity, indicating GTP hydrolysis by HypB is required to activate urease (Mehta *et al.*, 2003b). Why *H. pylori* urease requires an extra GTPase for activation is not clear. HypA or HypB interact in a 1:1 ratio to activate hydrogenase, which suggests a HypA-HypB complex may be required for urease activation (Olson *et al.*, 2001). How the balance of HypA-HypB and HypA-*Hp*UreE interactions is regulated and facilitates urease activation is still unclear.

The histidine rich proteins Hpn and Hpn-like in *H. pylori* are short peptides with large proportions of histidine residues, 28 of 60 residues and 18 of 75 residues respectively, Hpn-like also contains 31 glutamine residues (Gilbert *et al.*, 1995; Seshadri *et al.*, 2007). Deletion of either of these proteins increases the urease activity and the nickel associated with urease increases. However the sensitivity to nickel, cadmium and cobalt in the deletion mutants is also increased (Seshadri *et al.*, 2007). Hpn binds 5 atoms of Ni per monomer at a neutral pH, but the nickel is released when the pH is lowered (Ge *et al.*, 2006). This indicates that Hpn and Hpn-like are nickel storage or detoxification proteins, that can release nickel to urease when increased ammonia production is required to increase the pH.

1.5.7. Nickel Transporters

The environmental nickel concentration is very low with salt and freshwater nickel concentrations being around 30 nm and 5 nm respectively (Eitinger and Mandrand-Berthelot, 2000). This means that those organisms that require nickel to function must be able to selectively uptake it even at these low concentrations. To do this a range of nickel transporters are utilised. The nickel/cobalt transporter (NiCoT) family has homologues in bacteria and fungi (Eitinger *et al.*, 2005). The HoxN protein of *Cupriavidus necator* is a high-affinity, low-capacity nickel transporter, deletion of

which significantly reduces nickel uptake (Eitinger and Friedrich, 1991). HoxN is comprised of 8 transmembrane domains with both the N-terminus and C-terminus on the cytosolic face. On the second transmembrane domain is a HAVDADH sequence which is partially conserved across NiCoTs and sometimes referred to as the HX_4DH motif. Mutation of the first histidine residue reduces the affinity of HoxN for nickel and mutation of the second abolishes nickel transport. Mutation of the valine residue to phenylalanine reduces specificity of HoxN for nickel, allowing cobalt transport, but increases capacity. The NiCoT Nh1F of *Rhodococcus rhodochrous* transports both nickel and cobalt and has a HAFDADH sequence on the second transmembrane domain and mutation of the phenylalanine to valine significantly reduces activity (Eitinger *et al.*, 1997; Degen *et al.*, 1999; Degen and Eitinger, 2002). These results indicate that the two histidine residues are required for metal transport while other residues in the region determine specificity and capacity. Nic1p is a fungal NiCoT identified in the fission yeast *Schizosaccharomyces pombe* (*Sp*Nic1p)(Eitinger *et al*., 2000). *Sp*Nic1p, like HoxN, is a specific nickel transporter but activity is inhibited by cobalt. The HX_4DH sequence of *Sp*Nic1p is HALDADH. The presence of leucine rather than valine or phenylalanine may explain the specific nickel transport but inhibition by cobalt, a combination of features not observed for HoxN or Nh1F (Degen *et al.*, 1999; Degen and Eitinger, 2002).

NikABCDE is a nickel transport system which belongs to the ATP-binding cassette (ABC) family (Navarro *et al*., 1993; Higgins, 2001). The Nik system was discovered in *E. coli* where each of the components of the transporter NikA, NikB, NikC, NikD, NikE and NikR are encoded in a single operon regulated by the nickel binding transcription factor NikR. Homologous systems have since been discovered in a range of bacteria (Leitch *et al*., 2007; Li and Zamble, 2009). The Nik systems transport nickel from the periplasm to the cytoplasm in an ATP hydrolysis dependent manner. The transmembrane regions NikB and NikC form a nickel channel and NikD and NikE are nucleotide binding proteins which bind NikB and NikC on their cytosolic face (Navarro *et al.*, 1993). NikA is a periplasmic nickel binding protein that specifically binds nickel and chaperones it to the NikBCDE complex to be transported into the cytoplasm (de Pina *et al.*, 1995).

At higher nickel concentrations transport through non-specific low-affinity transporters is possible (Eitinger and Mandrand-Berthelot, 2000). The magnesium transporter CorA has been demonstrated to transport nickel and cobalt with relatively low affinities (Hmiel *et al.*, 1986; Snavely *et al*., 1989; Wang *et al.*, 2006; Niegowski and Eshaghi, 2007). The Nramp homologue of *C. neoformans*, Cramp, is also able to transport both nickel and cobalt, although at a much lower rate than iron and manganese (Agranoff *et al.*, 2005). The Nramp homologue of *S. pombe* is also a potential low-affinity nickel transporter (Eitinger *et al*., 2000). The transport of nickel by these proteins is not likely to be physiologically relevant, but in studies investigating nickel-specific permeases excess magnesium is often added to growth media to inhibit nickel transport via low-affinity transporters (Eitinger *et al.*, 2000; Eitinger and Mandrand-Berthelot, 2000).

1.6. Aims and Context

The *C. neoformans* gene database contains urease and homologues to the bacterial urease accessory proteins UreD, UreF and UreG. No homologue of the nickel chaperone UreE is present in *C. neoformans*, however, cryptococcal UreG contains a histidine-rich N-terminal domain that my facilitate a metal chaperone function. It is also unclear whether cryptococcal urease utilises iron or nickel within its catalytic core. The *C. neoformans* gene database also contains a homologue of the *S. pombe* nickel transporter Nic1p, as well as a homologue of the metal transporter CorA and the Cramp protein.

The overall aims of this project are to investigate urease maturation in *C. neoformans* and to establish *C. neoformans* as a model of fungal urease maturation and homeostasis. A primary aim is to establish which metal urease utilises and also how that metal reaches the apo-enzyme, in particular what role cryptococcal UreG plays in urease maturation. This project will also investigate the regulation of urease activity including how metal accumulation in the yeast cell affects enzyme activity, in particular the role of the cryptococcal Nic1p homologue which is a putative nickel importer.

2. Methods

2.1. Media, Strains and Competent Cell Preparation

2.1.1. Strain List

C. neoformans strains generated in this study are derived from wild-type strain *H99* (Serotype A, *MATα*) (Perfect *et al.*, 1993).

Strain	**Genotype**	**Source**
H99	*MATα*	Perfect *et al.*, 1993
ure1Δ	*MATα ure1::hph*	This study
nic1Δ	*MATα nic1::NEO*	This study
nic1Δ+NIC1	*MATα nic1::NEO NIC1::hph*	This study
ureGΔ	*MATα ureG::NEO*	This study
ureGΔ+UREG	*MATα ureG::NEO UREG::hph*	This study
B-4131	*MATα cap59*	Chang and Kwon-Chung, 1994 García-Rivera *et al.*, 2004

Table 1 - *C. neoformans* strains used in this study.

2.1.2. Generation of *ure1Δ, nic1Δ, nic1Δ+NIC1, ureGΔ* and *ureGΔ+UREG*

The mutant strains generated in this study (*ure1Δ*, *nic1Δ* and *ureGΔ*) were made in an *H99* background by biolistic transformation of targeted *ure1Δ*, *nic1Δ* and *ureGΔ* knock-out cassettes which conferred resistance to hygromycin (*ure1Δ*) and neomycin (*nic1Δ* and *ureGΔ*) (Toffaletti *et al.* 1993). The *ure1Δ* knock-out cassette integrated in the *URE1* ORF, excising ~500bp of the coding region. The *nic1Δ* and *ureGΔ* cassette integrated at the *NIC1* locus and *UREG* locus, respectively, replacing the entire ORF. The knock-out cassettes were amplified by PCR from the plasmids pRS426-*ure1Δ,* pRS426-*nic1Δ* and pRS426-*ureGΔ* using the T7 and T3 primers.

pRS426-*ure1Δ* was created by separately amplifying 3 PCR products. Part 1, using primers *ure1Δ*1F, *ure1Δ*1R and *H99* genomic DNA, amplified ~1 kb of the *URE1* promoter and coding region. Part 2, using primers *ure1Δ*2F, *ure1Δ*2R and pAG32 as template, amplified the *hph* cassette, which confers resistance to hygromycin (Goldstein and McCusker, 1999). Part 3, using primers *ure1Δ*3F, *ure1Δ*3R and genomic DNA, amplified a portion of the *URE1* ORF ~500bps upstream of part 1. The 3 parts were cloned into pRS426 that had been previously digested with HindIII, by homologous recombination in the *S. cerevisiae* strain MLY40 (Lorenz and Heitman, 1997). pRS426-*nic1Δ* and pRS426-*ureGΔ* were created by the same method. pRS426-*nic1Δ*: part 1 - using *nic1Δ*1F, *nic1Δ*1R and genomic DNA amplified ~1 kb of the *NIC1* promoter region, part 2 - using primers *nic1Δ*2F, *nic1Δ*2R and pJAF1, amplified the *NEO* cassette, part 3 - using primers *nic1Δ*3F, *nic1Δ*3R and genomic DNA, amplified ~1 kb of *NIC1* terminator sequence (Fraser *et al*., 2003). pRS426-*ureGΔ*: part 1 - using *ureGΔ*1F, *ureGΔ*1R and genomic DNA amplified ~1 kb of the *UREG* promoter region, part 2 - using primers *ureGΔ*2F, *ureGΔ*2R and pJAF1, amplified the *NEO* cassette, part 3 - using primers *ureGΔ*3F, *ureGΔ*3R and genomic DNA, amplified ~1 kb of *UREG* terminator sequence.

Post-transformation cultures were plated on YPD agar medium containing either G418 (200 μg/ml), for *nic1Δ* and *ureGΔ*, or Hygromycin B (200 μg/ml), for *ure1Δ*, and incubated at 30^{o}C until colonies grew. Colonies were screened for lack of urease activity on Christensen's medium. In each case correct integration was confirmed by Southern blot.

The *NIC1* ORF was reconstituted into the *nic1Δ* strain to generate the *nic1Δ::NIC1* strain. The entire *NIC1* ORF along with the *hph* cassette was inserted back to the original locus by biolistic transformation of the pAG32-*NIC1* plasmid digested with SphI. pAG32-*NIC1* was created by amplification of the *NIC1* ORF, including ~1 kb of the promoter and ~500 bp of the terminator regions, using primers *NIC1*RcnF, *NIC1*RcnR and genomic DNA. The PCR fragment was digested with BamHI followed by ligation into pAG32, previously digested with BamHI and treated with alkaline phosphatase. pAG32-*NIC1* was digested with BsgI, which cut in the promoter region, to target integration at the *NIC1* locus. Colonies were screened for urease activity on Christensen's medium. Correct integration was confirmed by Southern blot and PCR, using primers *NIC1*RcnCheckF and *NIC1*RcnCheckR.

The *UREG* ORF was reconstituted into the *ureGΔ* strain to generate the *ureGΔ::UREG* strain. The entire *UREG* ORF along with the *hph* cassette was inserted back to the original locus by biolistic transformation of the pAG32-*UREG* plasmid digested with SphI. pAG32-*UREG* was created by amplification of the *UREG* ORF, including ~1 kb of the promoter and ~500 bp of the terminator regions, using primers *UREG*RcnF, *UREG*RcnR and genomic DNA. The PCR fragment was digested with BamHI followed by ligation into pAG32, previously digested with BamHI. pAG32-*UREG* was digested with SphI, which cut in the promoter region, to target integration at the *UREG* locus. Colonies were screened for urease activity on Christensen's media. Correct integration was confirmed by Southern blot and PCR, using primers *UREG*RcnCheckF and *UREG*RcnCheckR.

2.1.5. *C. neoformans* Growth Media and Conditions

C. neoformans cultures were grown in enriched YPD media (10 g/l yeast extract, 10 g/l peptone, 2 % glucose) or minimal synthetic media (1.7g/l yeast nitrogen base, 2% glucose) with either ammonium sulphate (5 g/l), urea (2.27 g/l), uric acid sodium salt (0.8 g/l), glutamine (5.53 g/l) or glutamic acid (14.16 g/l) added as a source of nitrogen. Christensen's urea agar medium (sigma, 27048) was used to qualitatively assay for urease activity. Where indicated agar was added to 2 % before autoclaving to produce solid medium.

2.1.6. Preparation of Competent *E. coli*

To prepare competent *E. coli* the strain, either DH5α or BL21, was pre-grown in LB medium (5 g/l yeast extract, 10 g/l tryptone, 10 g/l NaCl) for ~16 hrs at 37^{o}C. This culture was used to inoculate 500 ml of 2XL medium (10 g/l yeast extract, 20 g/l tryptone, 1g/l NaCl) to OD_{595} 0.05. The culture was incubated at 30^{o}C, at OD_{595} 0.2 10 ml $MgCl_2$ (1 M) was added and at OD_{595} 0.5 the culture was moved to an ice-water bath for 2 hrs. The cells were then pelleted by centrifugation (5 minutes, 900 g, 4^{o}C), resuspended in 250 ml ice-cold calcium/manganese medium (100 mM $CaCl_2$, 70 mM $MnCl_2$, 40 mM $C_2H_3O_2Na$, pH 5.5) and incubated on ice for 2 hrs. The cells were then pelleted by centrifugation (5 minutes, 900 g, 4^{o}C) and resuspended in 25 ml calcium/manganese medium with glycerol (15 % w/v). Aliquots (0.2 ml) were transferred to 1.5 ml eppendorfs, snap frozen in liquid nitrogen and stored at -80^{o}C.

2.1.7. Preparation of Competent *S. cerevisiae*

To prepare competent cells of the *S. cerevisiae* strain MLY40 (*MATα ura3-52*) the cells were pre-grown in YPD (5 ml) for ~16 hrs at 30°C (Lorenz and Heitman, 1997). The culture was used to inoculate YPD medium (50 ml) to OD_{600} 0.1 and incubated at 30°C. When the culture reached OD_{600} 0.7 the cells were pelleted by centrifugation (3 krpm, 5 min), washed twice in sterile water and resuspended in 300 µl lithium acetate (100 mM). The cells were either used for transformation immediately or stored at 4°C for up to 3 days.

2.2. *In Vivo* Biochemical Analysis Techniques

2.2.1. Protein Extraction and Urease Activity Assays

C. neoformans protein extraction was performed essentially as described previously (Chai and Tay, 2008). 10 ml *C. neoformans* culture was grown to OD_{600} 4 in minimal media, (nitrogen source indicated in text) and the cells were harvested by centrifugation at 3 krpm for 5 minutes in a 15 ml corning tube. The pellet was washed twice in 2 ml of cold nano-pure water, remaining liquid was removed and the pellet snap frozen in liquid nitrogen. The pellet was thawed on ice and resuspended in 500 µl of extraction buffer (40 mM Tris-HCl, 20 mM DTT, 4 % Triton X-100, 1 mM EDTA, 2 mM PMSF, pH 9) and transferred to a screw top microcentrifuge tube. An equal volume of 0.5 µm glass beads were added and samples bead beaten for 6 cycles of 20 s, with 2 min on ice between cycles. Samples were then subject to centrifugation at 13 krpm for 10 minutes at 4°C. The supernatant was carefully removed and assayed for protein concentration with Bradford reagent.

To assay urease activity 200 µg of *C. neoformans* protein extract was added to 1.6 ml of 66 mM urea solution in Reaction buffer (10 mM Potassium Phosphate, 10 mM Lithium Chloride, 1 mM EDTA, pH 8.2), mixed by inversion and incubated in a water bath at 30°C. At 0, 10, 20, 30 and 40 minutes 150 µl was removed from the reaction and added to 750 µl Nessler's colour reagent (20% Nessler's Reagent (Sigma, 345148), 0.08% Ficoll). Absorbance at 480 nm was measured and used to calculate ammonia production over time. Units of urease given equate to the liberation of 1 µM of ammonia per minute at pH 8.2 at 30°C.

2.2.2. Metal Accumulation Assays

To measure metal accumulation of cells 10 ml of culture was grown in conditions indicated in the text. The cells were harvested by centrifugation at 3 krpm for 10 min in a clean 15 ml corning tube. The cell pellet was washed twice in cold nano-pure water and excess water carefully removed and the pellet frozen at -20^{o}C. During the centrifugation steps the cell number was measured. The pellet was then thawed at room temperature and 1 ml of 65 % Suprapur nitric acid (VWR, 1.00441) added. The samples were incubated at room temperature for 3 days with occasional vortexing to fully digest the cells. The digested samples were subject to centrifugation at 3 krpm for 30 min to remove insoluble particles. 0.8 ml of the supernatant was removed and diluted to 5 ml in 2% Suprapur nitric acid followed by analysis by ICP-MS (Thermo Electron Corp., X-Series).

2.2.3. Metal Profiles

Metal Profiles were performed as previously described (Tottey *et al*., 2008). *C. neoformans* culture (1 l) was grown to OD 4 in media as described in the text. The cells were harvested by centrifugation (3 krpm, 10 minutes), washed in nano-pure water and snap frozen in liquid nitrogen. The pellet was thawed in HEPES buffer (50 mM, pH 8.8) and cells lyses performed by grinding with pestle and morta under liquid nitrogen. The broken cells were thawed under anaerobic conditions, unbroken cells and membrane was removed by centrifugation at 8 krpm for 15 min followed by ultra-centrifugation at 30 krpm for 30 min. The protein concentration of the supernatant was determined by Bradford Assay. Cell extract (30 mg) was loaded onto a 1 ml Hi-Trap QFF anion exchange column (GE Healthcare). Cell extract was eluted in steps of 1 ml in buffer (50 mM Tris-HCl, pH 8.8) containing 100, 200, 300 and 400 mM NaCl. Aliquots of each fraction (200 µl) were subjected to size-exclusion HPLC on a TSK-SW3000 column (Tosoh Biosciences) in HPLC buffer (10mM Tris-HCl, 50 mM NaCl, pH 7.5). Elution fractions (500 µl) were collected, an aliquot (200 µl) was analysed for metal content by ICP-MS. Urease activity of the fractions was determined by addition of an aliquot (5 µl) of each fraction to urea solution (45 µl, 66 mM) in urease reaction buffer and incubating at 30^{o}C for 40 minutes followed by addition of Nessler's colour reagent (200 µl).

2.3. *In Vitro* Biochemical Analysis Techniques

2.3.1. Purification of *Cn*UreG

Recombinant *Cn*UreG was expressed in the *E. coli* strain BL21 from the plasmid pET29a-UreG. pET29a-UreG was generated by amplification of *Cn*UreG cDNA from *C. neoformans* mRNA using primers UreGNdeIF and UreGNdeIR. The cDNA was digested with NdeI and ligated into pET29a, previously digested with NdeI. Correct amplification and cloning was confirmed by sequencing.

pET29a-UreG was transformed into BL21 competent cells, which were plated onto LB agar medium with kanamycin (50 μg/ml) and incubated at 37^{o}C for ~16 hrs. A single colony was used to inoculate 50 ml of liquid LB medium containing kanamycin (50 μg/ml) which was incubated for ~16 hrs at 37^{o}C. The 50 ml culture was used to inoculate 4 l of LB medium with kanamycin (50 μg/ml). The cultures were incubated at 37^{o}C to OD_{595} 0.6 then were moved to 30^{o}C, $NiSO_4$ added to 1 mM and *Cn*UreG expression induced by addition of IPTG to 1 mM. 6 hrs after induction the cells were harvested by centrifugation at 8 krpm for 10 minutes and frozen at -20^{o}C.

The cells were resuspended in Binding buffer (50 mM Tris-HCl, 300 mM NaCl, pH 8) with imidazole (10 mM) and subject to lysis by French press (3 passages at 25 kpsi). The crude extract was subject to centrifugation (30 krpm for 20 min) to remove insoluble cell fragments. The extract was then loaded onto a 5 ml His-trap column (GE) followed by washing with 4 column volumes of Binding buffer. 2 elution steps were used to purify *Cn*UreG. The first elution step was a linear gradient over 20 column volumes from 10 mM to 300 mM Imidazole in Binding buffer. 2.5 ml fractions were collected and analysed by SDS-PAGE. Fractions containing *Cn*UreG were pooled and diluted 10 times in binding buffer before re-loading onto the His-Trap column. The 2nd elution step was a linear gradient over 80 column volumes from 60 mM to 200 mM Imidazole in Binding buffer. 5 ml fractions were collected and analysed by SDS-PAGE, those containing pure *Cn*UreG were pooled and diluted 5 times in Binding buffer. The purified *Cn*UreG was concentrated by re-loading onto a 5 ml His-Trap column followed by a single elution step at 300 mM imidazole in Binding buffer. Metal bound to *Cn*UreG was removed by addition

of EDTA to 1 mM and incubation at 4^{o}C for ~72hrs. Imidazole, EDTA and NaCl were removed by serial buffer exchanges into 20 mM Tris-HCl pH 8. An Amicon filter (Ultra-15, MWCO 30 kDa (Sigma Z717185)) was used to perform 10 serial 1 in 15 exchanges. The metal content of *Cn*UreG was then analysed by ICP-MS.

2.3.2. Desalting Column Metal Binding Assay

The metal binding capacity of *Cn*UreG was assayed by retention of pre-loaded metal when passed through a desalting column. 1 ml of UreG (3 μM) was incubated separately with 20 molar equivalents of $NiSO_4$, $ZnCl_2$ or $CoCl_2$ at 4^{o}C. The *Cn*UreG-metal mixture was then loaded onto a PD10 desalting column (GE) and 1 ml fractions eluted. The metal concentration of the eluted fractions was determined by ICP-MS and protein concentration determined by Bradford assay.

2.3.3. UV-visual Spectroscopic Analysis

The absorbance of *Cn*UreG across the UV-visible spectrum (200-800 nm) was measured using a Perkin-Elmer λ35 UV/vis spectrophotometer. 1 ml of UreG (8 μM) was incubated with or without $NiSO_4$ (1, 2, 3, 5, and 10 molar equivalents) for 16 hrs at 4^{o}C. The samples were subject centrifugation at 13 krpm for 10 minutes prior to analysis to remove any precipitation. After analysis the 5 and 10 molar equivalent samples were loaded onto a PD10 desalting column and eluted in 1 ml fractions. The absorbance of fractions containing *Cn*UreG was analysed, followed by ICP-MS and Bradford assay to determine metal to protein ratio.

2.3.4. Circular Dichroism

Secondary structure of *Cn*UreG was studied using Far-UV Circular Dichroism. *Cn*UreG (14.86 μM) in Tris-HCl (20 mM, pH 8) was incubated with or without metal, as indicated in text, for 16 hrs at 4^{o}C. Analysis was performed using a 0.02cm path length in a Jasco J-810 spectropolarimeter. Circular dichroism of each sample was recorded (190 to 250 nm) ten times and averaged. All samples were blanked against buffer containing the same concentration of metal. Secondary structure composition was quantified using the K2d server (Andrade *et al*., 1993).

2.2.5. Equilibrium Dialysis

Equilibrium dialysis was used to confirm the stoichiometery of metal binding to *Cn*UreG and indicate binding affinity. 500 µl of *Cn*UreG (3 µM) was dialysed against 500 ml of Tris-HCl buffer (10 mM, pH 8), with $NiSO_4$, $ZnCl_2$ or $CoCl_2$ added to concentrations indicated in the text, for 72hrs without agitation. The metal concentration of the sample and assay volumes were determined by ICP-MS and used to calculate the concentration of *Cn*UreG associated metal. The dissociation constant, Kd, and binding capacity, B_{max}, were determined using a Hill plot (Origin software).

2.2.6. Size Exclusion Chromatography

Gel filtration of *Cn*UreG semi-purified after the first step of IMAC was performed using a Superdex 200 column (GE Healthcare). Sample (approximately 5 mg) was analysed in size exclusion buffer (20 mM $NaPO_4$, 300 mM NaCl, pH 8) at a flow rate of 1 ml/min over one column volume (120 ml) and the absorbance at 280 nm was recorded. The column was calibrated by filtration of ferritin (440 kDa), catalase (232 kDa), aldolase (158 kDa), BSA (66.4 kDa), chicken albumin (43 kDa) and cytochrome C (13.7 kDa) at 0.4 ml/min in filtration buffer (50 mM $NaPO_4$, 150 mM NaCl, pH 7).

Size exclusion HPLC of pure *Cn*UreG was performed using a TSK-SW3000 column (Tosoh Biosciences). *Cn*UreG (2 µg) was incubated in the presence or absence of 2 molar equivalents of $NiSO_4$ in HPLC buffer (10mM Tris-HCl, 50 mM NaCl, pH 7.5) prior to analysis. The samples were analysed at a flow rate of 3 ml/min and 500 µl fractions were collected and protein content determined by Bradford assay. The column was calibrated with jack bean urease (90.8 kDa) and BSA (66.4 kDa) under the same conditions.

2.4. Molecular Biology Techniques

2.4.1. Oligonucleotide list

The oligonucleotides used in this study were synthesized by Sigma-Aldrich and the sequences are listed in Table 2.

Oligonucleotide	**Sequence 5' - 3'**
T7	AAT TAA CCC TCA CTA AAG GG
T3	TAA TAC GAC TCA CTA TAG GG
*ure1Δ*1F	T TTG GTA CCG GGC CCC CCC TCG AGG TCG ACG GTA TCG ATA CGT CAG GAA AGG TGT TCC AGA
*ure1Δ*1R	ATG TCC ATA TGG TGC ACT CTC CCA GCT TTA CCA ATA CCA ACA
*ure1Δ*2F	TGT TGG TAT TGG TAA AGC TGG GAG AGT GCA CCA TAT GGA CAT
*ure1Δ*2R	ACC TCA GTC ATG AGT TGA GGA CAG GTT AAC CTG GCT TAT CGA
*ure1Δ*3F	TCG ATA AGC CAG GTT AAC CTG TCC TCA ACT CAT GAC TGA GGT
*ure1Δ*3R	A GAA CTA GTG GAT CCC CCG GGC TGC AGG AAT TCG ATA TCA CAC CCT GTT GTT GTC TCT CGT
*nic1Δ*1F	TTGG GTA CCG GGC CCC CCC TCG AGG TCG ACG GTA TCG ATA CGC AAA TGA CAC ACC ATA ATG
*nic1Δ*1R	CAT GGT CAT AGC TGT TTC CTG CAG GCA GAC GAT GGT TCG TTG
*nic1Δ*2F	CAA CGA ACC ATC GTC TGC CTG CAG GAA ACA GCT ATG ACC ATG
*nic1Δ*2R	GCA TGC CAA TTA TTA GTT CGC GTA ATA CGA CTC ACT ATA GGG
*nic1Δ*3F	CCC TAT AGT GAG TCG TAT TAC GCG AAC TAA TAA TGG GCA TGC

*nic1Δ*3R	A GAA CTA GTG GAT CCC CCG GGC TGC AGG AAT TCG ATA TCA GAC ACC CTC CTT GAA ATT CG
*NIC1*RcnF	GCG GGA TCC AGC ATT CCA TCC GTC ATG TAC
*NIC1*RcnR	GTA GGA TCC GGA ACT CAT AGA GAA CGA GTG
*NIC1*RcnCheckF	GTC TTT TGA CCG ATC TGT ACC
*NIC1*RcnCheckR	AGC GTT AAA GAG TAA CTC TCC
*ureGΔ*1F	TTGG GTA CCG GGC CCC CCC TCG AGG TCG ACG GTA TCG ATA GCG AAA GCG TCA TAG TCA AGG
*ureGΔ*1R	CAT GGT CAT AGC TGT TTC CTG GTC GTC TGC GAA TGT TGA AAG
*ureGΔ*2F	CTT TCA ACA TTC GCA GAC GAC CAG GAA ACA GCT ATG ACC ATG
*ureGΔ*2R	G ACA TAT TGC TAC ATT TTG GTG GTA ATA CGA CTC ACT ATA GGG
*ureGΔ*3F	CCC TAT AGT GAG TCG TAT TAC CAC CAA ATT GTA GCA ATA TGT C
*ureGΔ*3R	A GAA CTA GTG GAT CCC CCG GGC TGC AGG AAT TCG ATA TCA CAA ATG TGA ATT GGA CAT GTG
*UREG*RcnF	GCG GGA TCC GCG AAA GCG TCA TAG TCA AGG
*UREG*RcnR	GTA GGA TCC GCG TGA ATA ACG AAG TTG CAG
*UREG*RcnCheckF	CTT TAA ACG CTG CCT TGA AGG
*UREG*RcnCheckR	CAG CAT TGA GAG CTG TTG CCA
UreGNdeIF	ATA GAA TTC CAT ATG GCA GTG CCT GCT CAG
UreGNde1R	AAG GCT AAG GCA TAA CAT ATG TAT CTT AAG
Pb1F	CTC ATG TCA TGG ACT CAA TCT
Pb1R	GCT TAT TAT GTA CCC AGT GAC
Pb2F	TTG CTA GGA TAC AGT TCT CAC
Pb2R	ATC ACA GTT TGC CAG TGA TAC
Pb3F	TGA TCC TGG ATG AAT TTG GTC

Pb3R	TCA GCG GAG CTC CGA GCT GTC
Pb4F	TCC ATT GCA TTG CTT GCT ATC
Pb4R	TGA ATG AAA GGG ATG ACA TGG
Pb5F	CCA ACG CTA TGT CCT GAT AGC
Pb5R	TGA ATG AAC TGC AGG ACG AGG
Pb6F	CGT GAC TTT GGG ACA AAT GTC
Pb6R	TTG CTT CCA TCA TCT TCC ATC

Table 2 - DNA oligonucleotides used in this study.

2.4.2. Polymerase Chain Reaction (PCR) and Cloning

PCR reactions for plasmid or strain generation were performed using VentR high fidelity PCR system (NEB) in a Labnet MultiGene II Personal Thermal Cycler. PCR reactions to generate Southern probes or to analyse genomic sequence were performed using GoTaq (Promega). PCR reaction mixtures had a final volume of 50 µl and included 1 µg template DNA, 200 µM each of dATP, dCTP, dGTP and dTTP, 100 pmol of each oligonucleotide primer, 1 x reaction buffer (supplied by manufacturer) and 1 unit of polymerase (as described by manufacturer). Each reaction included an initial denaturation step at 95^{o}C for 5-20 minutes and 30 cycles of denaturation at 95^{o}C for 30 s, primer annealing at 50-66^{o}C for 1-3 minutes (dependant upon primers used) and elongation at 72^{o}C for 30 s to 5 minutes (1 kb per min for GoTaq and 500 bp per min for VentR) followed by a final elongation step at 72^{o}C for 5-10 minutes.

Cloning was performed using DNA endonucleases, DNA ligase and calf intestinal alkaline phosphatase (CIAP) supplied by Promega. DNA digestion with endonucleases was performed at 37^{o}C for 30 minutes to 16 hrs according to the manufacturer's instructions. DNA ligation and alkaline phosphatase reactions were performed according to the manufacturer's instructions. After incubation ligation reactions were transformed into competent DH5α cells.

2.4.3. Electrophoresis

DNA samples were resolved over a 1 % agarose gel containing Ethidium Bromide (0.5 μg/ml) in 1x TBE buffer (10.8 g/l Tris-base, 5.5 g/l boric acid, 25 mM EDTA pH 8) at 100v, unless stated otherwise. DNA migration was examined by exposure of the gel to UV light and fragment size determined by comparison with the 1 kb DNA ladder (Promega). The GenElute Gel Extraction Kit (Sigma-Aldrich) was used to recover DNA samples from agarose gels.

Protein samples were resolved in denaturing conditions by SDS-PAGE. A 12 % separating gel (325 mM Tris-HCl pH 8.8, 0.1 % SDS (w/v), 12 % Acrylamide/Bis-acrylamide, 0.05 % ammonium persulfate (w/v), 0.07 % TEMED) and a 4 % stacking gel (125 mM Tris-HCl pH 6.8, 0.1 % SDS (w/v), 4 % Acrylamide/Bis-acrylamide, 0.05 % ammonium persulfate (w/v), 0.1 % TEMED) were used unless stated otherwise. The gels were run at 200 v for ~1 hr in 1x Running buffer (25mM Tris-base, 200 mM glycine, 0.1 % SDS (w/v)). After running gels were stained in Coomassie stain (10 % glacial acetic acid, 40% methanol, 0.01 % Brilliant Blue (w/v)) followed by destaining in water or were incubated with Oriole Fluorescent Gel Stain (Bio-rad) for ~1 hr and protein migration visualised by exposure to UV light.

2.4.4. Southern Blotting

Southern blot analysis was used to confirm the correct genotype of the strains generated this study. Genomic DNA (30 μg) was digested by restriction endonucleases, as indicated in the text, for ~16 hrs at 37^{o}C. The digested DNA was resolved on a 1% agarose gel for ~3 hrs at 80 v. The migration distance of the 1 kb DNA ladder (Promega) was noted and then the gel blotted onto a nylon membrane (GeneScreen Plus, Perkin Elmar) using the alkaline transfer protocol as described by the manufacturer. Sequence specific radio-labelled probes were generated using PCR products (Table 3), dCTP containing ^{32}P (Perkin Elmar) and the Prime-a-Gene Labelling System (Promega) by following the manufacturer's instructions. The blots were pre-hybridised with 10 ml Modified Church's Buffer (0.36 M Na_2HPO_4, 0.14 M NaH_2PO_4, 1 mM EDTA, SDS 7 %) for 30 minutes at 65°C. The radio-labelled probe was then added to the buffer and incubated at 65^{o}C for 10-16 hrs. The blots

were then washed for 15 minutes at 65°C twice in each Wash Buffer 1 (0.1% SDS, 30mM Sodium Citrate, 0.3M NaCl), followed by Wash Buffer 2 (0.1% SDS, 7.5mM Sodium Citrate, 75mM NaCl) then Wash buffer 3 (0.1% SDS, 1.5mM Sodium Citrate, 15mM NaCl). The blots were exposed to x-ray film (Fujifilm) for 2-72 hours.

Probe	Region to which probe anneals	Primers
1	*URE1* ORF	Pb1F and Pb1R
2	*hph* antibiotic marker	Pb2F and Pb2R
3	*NIC1* promoter region	Pb3F and Pb3R
4	*NIC1* ORF	Pb4F and Pb4R
5	*NEO* antibiotic marker	Pb5F and Pb5R
6	*UREG* promoter region	Pb6F and Pb6R

Table 3 - Southern blot probes used in this study.

2.4.5. *E. coli* Transformation and Plasmid Recovery

To transform *E. coli* strains with a plasmid or ligation mixture the competent cells were thawed on ice and incubated with the DNA for 30 min to 1 hr on ice. The samples were then heat shocked at 42°C for 45 s followed by cooling on ice. LB medium (1 ml) was added to each sample followed by incubation at 37°C for 40 min. The cells were harvested by centrifugation (5 krpm, 5 minutes), washed in sterile water and plated on LB media containing selective antibiotics.

Plasmids were recovered from *E. coli* cells using a GenElute HP Plasmid Miniprep Kit (Sigma-Aldrich) using the manufacturer's instructions.

2.4.6. *S. cerevisiae* Transformation and Plasmid Recovery

To transform *S. cerevisiae* strains with a plasmid or ligation fragments the DNA was added to 240 µl PEG 4000 (50 % (w/v)), 10 µl sonicated salmon sperm DNA (5 mg/ml) and 50 µl of competent cells in lithium acetate. The mixture was vortexed, 32 µl lithium acetate (1 M, pH 7.5) was added followed by further mixing by vortex.

The mixture was then incubated at 30°C for at least 20 minutes followed by heat shock at 42°C for 15 min. Cells were harvested by centrifugation (3 krpm, 5 minutes), resuspended in 150 µl sterile water, plated on selective medium and incubated at 30°C until colonies appeared.

To recover plasmid DNA from *S. cerevisiae* cells were grown in selective medium for ~16 hrs at 30°C. The cells were harvested by centrifugation (3 krpm, 5 minutes) and resuspended in 100 µl STET buffer (8 % sucrose (w/v), 50 mM Tris-HCl pH 8, 50 mM EDTA, 5 % Triton X-100 (w/v)). Glass beads were added and each sample beaten for 5 cycles of 20 s interspaced by 2 minutes on ice and another 100 µl STET buffer added. The samples were incubated at 100°C for 3 minutes followed by incubation of ice for 5 minutes. The samples were subject to centrifugation (13 krpm, 10 minutes, 4°C), 100 µl of the supernatant collected and transferred to 50 µl ammonium acetate (7.5 M). The samples were stored at -80°C for 10 minutes, subject to centrifugation (13 krpm, 10 minutes, 4°C), 100 µl of the supernatant was transferred to 200 µl ice-cold ethanol (100%) and subject to centrifugation (13krpm, 10 minutes, 4°C) and the supernatant removed. The pellet was washed in ethanol (70 %), dried in air and resuspended in sterile water (30 µl). 15 µl of the DNA was used to transform into the *E. coli* strain dH5α.

2.4.7. *C. neoformans* Genomic DNA extraction

To isolate genomic DNA from *C. neoformans* the strain was grown in 50 ml YPD medium for ~16 hrs at 30°C. The cells were pelleted by centrifugation (3 krpm, 10mins) in a 50ml corning tube, washed in water and snap frozen in liquid nitrogen. The frozen pellets were dried by lyophilization for 10-16 hrs. 15ml Glass beads (2 mm) were added and the sample vortexed until a fine powder was created. 10 ml CTAB buffer (100 mM Tris-HCl pH 7.5, 0.7 M NaCl, 10 mM EDTA, 1 % CTAB (hexadecyltrimethylammonium bromide), 1 % β-mercaptoethanol) added, the sample was mixed by gentle inversion, incubated at 65°C for 30 minutes then cooled to room temperature. Phenol-chloroform (10 ml) was added and the sample mixed for 1 min. The sample was subject to centrifugation (3 krpm, 10 minutes), the supernatant transferred to a fresh 50 ml corning tube, 10 ml isopropanol added and mixed by inversion. The samples were subject to centrifugation (3 krpm, 10 minutes), the supernatant discarded, the pellet washed in ethanol (70 %) and resuspended in sterile

nano-pure water. RNase A was added to 20 µg/ml and samples incubated at 37^{o}C for 1 hr.

2.5. Microbiological Techniques

2.5.1. Cell Counting and Microscopy

Cell or particle size and number were determined by measurement on a CASY Cell Counter and Analyser System (Schärfe Systems). Cell aggregation was visualised using a Zeiss Axiovert with a 100x oil immersion objective and the Axiovision imaging system. Cell capsule was visualised by staining in India ink and microscopic examination. Cells were picked from colonies grown on an agar plate, suspended in India ink and transferred to a microscope slide with cover slip.

2.5.3. Colony Imaging

Cells were pre-grown in liquid ammonia based SD medium (5 ml) for ~16 hrs at 30^{o}C, spotted onto urea or ammonia SD agar plates and incubated at 30^{o}C for 10 days. Colonies were photographed using a Canon PowerShot A640 digital camera linked to a Zeiss Stemi 2000-C stereo microscope.

3. The Activation of Urease and the Roles of Nic1 and *Cn*UreG

3.1. Introduction

Urease is a nickel or iron utilising enzyme that catalyses the degradation of urea to ammonia and carbamate and is a virulence factor in some microorganisms. The role of urease during infection by bacteria is associated with a localised increase in pH, due to the production of ammonia (Scott *et al*., 2002; Sendide *et al.,* 2004). Urease has also been identified as a virulence factor in pathogenic fungi, including *C. neoformans* (Cox *et al.,* 2000). The role of urease in *C. neoformans* infection is not fully understood, but invasion of the brain by the yeast cell crossing cerebral capillaries is dependent on urease (Olszewski *et al.*, 2004; Shi *et al.*, 2010a). The degradation of uric acid for use as a nitrogen source is via a pathway which includes urease (Lazera *et al.*, 1996; Nielsen *et al.*, 2007). Urea and uric acid are available throughout the human body and are therefore potential nitrogen sources for invading pathogens (Proctor, 1970; Zielinski *et al.*, 1999; Ronne-Engström *et al.*, 2001; Tyvold 2007; Waring *et al.*, 2008)

The maturation of bacterial urease requires several cofactors including a GTPase, UreG, and a nickel chaperone, UreE (Carter *et al.*, 2009). *C. neoformans* lacks the chaperone UreE and *Cn*UreG possesses an N-terminal histidine-rich region. The function of this domain is unknown but potentially involves nickel binding. *C. neoformans* also contains a homologue of the high-affinity nickel transporter of *S. pombe*, *Sp*Nic1p, which is a putative nickel importer that may be required for urease activation.

The aims of this chapter are to outline the growth characteristics of *C. neoformans* utilising different nitrogen sources and to investigate how different nitrogen sources affect the levels of urease activity and nickel accumulation. In addition the roles of urease, *Cn*Nic1 and *Cn*UreG in the utilisation of urea as a nitrogen source and the accumulation of nickel are analysed. The data establish that urease activity and nickel accumulation increase in response to urea. *Cn*Nic1 is established as the primary means of nickel accumulation in response to urea and *Cn*UreG is required for urease activity. Virulence factors other than urease are shown to be responsive to urea.

3.2. Phenotypic Characterisation of Wild-type *C. neoformans*

3.2.1. Growth of *C. neoformans* Utilising Different Nitrogen Sources

To date the growth characteristics of *C. neoformans* utilising different nitrogen sources has not been studied in detail. To establish the parameters that would be used to study urease maturation, the growth of *C. neoformans* in batch culture was analysed. The wild-type strain was grown in minimal media containing either ammonium or urea as the sole source of nitrogen. Cultures were inoculated at OD_{600} 0.1 and monitored until stationary phase (Figure 8A). The urea grown cells reached a higher optical density as compared to the ammonium grown cells, growing to OD_{600} ~12 and ~9 respectively. In each case logarithmic growth occurred between OD_{600} 1-6. This established that *C. neoformans* cultures at OD_{600} ~4 are in the mid-log growth phase.

To determine which other nitrogen sources *C. neoformans* can utilise, wild-type cells were grown in media containing either ammonium, urea, glutamine or glutamic acid as the sole source of nitrogen. The level of growth was determined by measuring the optical density of each culture. The glutamine, glutamic acid and urea grown cultures grew to equal levels (Figure 8B). This established that *C. neoformans* is able to utilise ammonium, urea, glutamine and glutamic acid as sources of nitrogen.

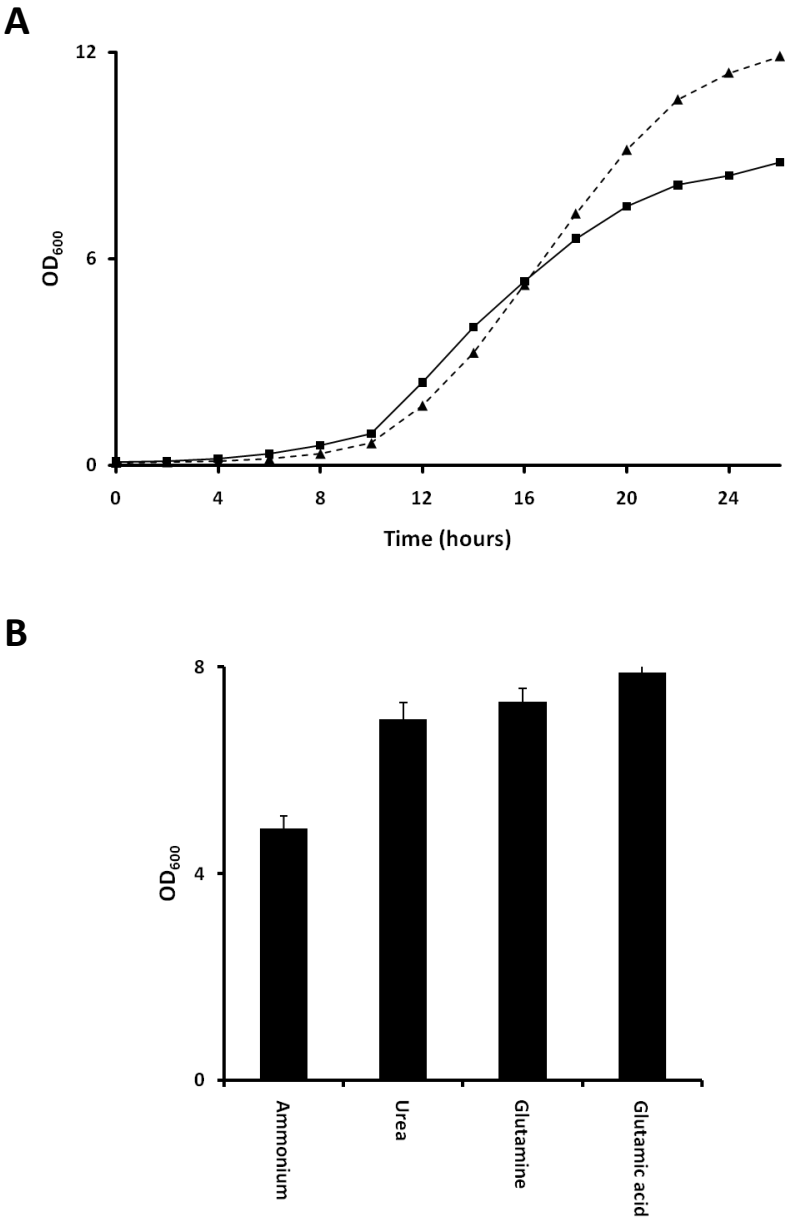

Figure 8 - The wild-type strain of *C. neoformans* is able to grow in a variety of nitrogen sources.

A - Cultures of the wild-type strain were inoculated to OD_{600} 0.1 in media containing either ammonium (squares) or urea (triangles) as the sole source of nitrogen and incubated at 30^{o}C with agitation in baffled flasks. The optical density was recorded every 2 hours. Data is representative of 3 repeat experiments.

B - Wild-type cultures inoculated to OD_{600} 0.1 in media containing either ammonium, urea, glutamine or glutamic acid as the sole source of nitrogen and incubated at 30^{o}C with agitation in baffled flasks. After 18 hours the optical density was recorded. Data points shown represent the mean of 3 repeat experiments and error bars represent the standard deviation.

While investigating the growth of *C. neoformans* it was observed that ammonium grown cells aggregated, while urea grown cells did not. To examine this phenotype further, wild-type cells were grown in ammonium and urea media and particle volume was measured using a cell counter at 2 hour intervals. The urea grown cultures maintained a mean particle volume of between 55.6 and 78.8 fl without any increasing or decreasing trend. In the ammonium grown cultures the mean particle size increased from 96 to 260 fl (Figure 9A). Microscopic examination established that ammonium grown cells formed large aggregates while urea grown cells did not (Figure 9B). Therefore the type of nitrogen source utilised by *C. neoformans* affects the characteristics of cell aggregation.

It was also observed that wild-type colonies grown on urea agar developed a mucoid appearance which is characteristic of polysaccharide capsule growth. To analyse this phenotype further, wild-type cells were pre-grown over-night in ammonium medium, washed in nano-pure water and then plated onto minimal agar media containing either urea or ammonium as the sole nitrogen source. The plates were then incubated at 30^{o}C for 10 days. The colonies grown on urea plates developed a marked mucoid morphology, while the ammonium grown colonies did not. India ink staining was then used to study the cells microscopically. The urea grown cells exhibited clear capsule growth, while the ammonium grown cells showed no capsule production (Figure 10). This established that capsule growth is regulated in response to nitrogen source and that urea promotes capsule production.

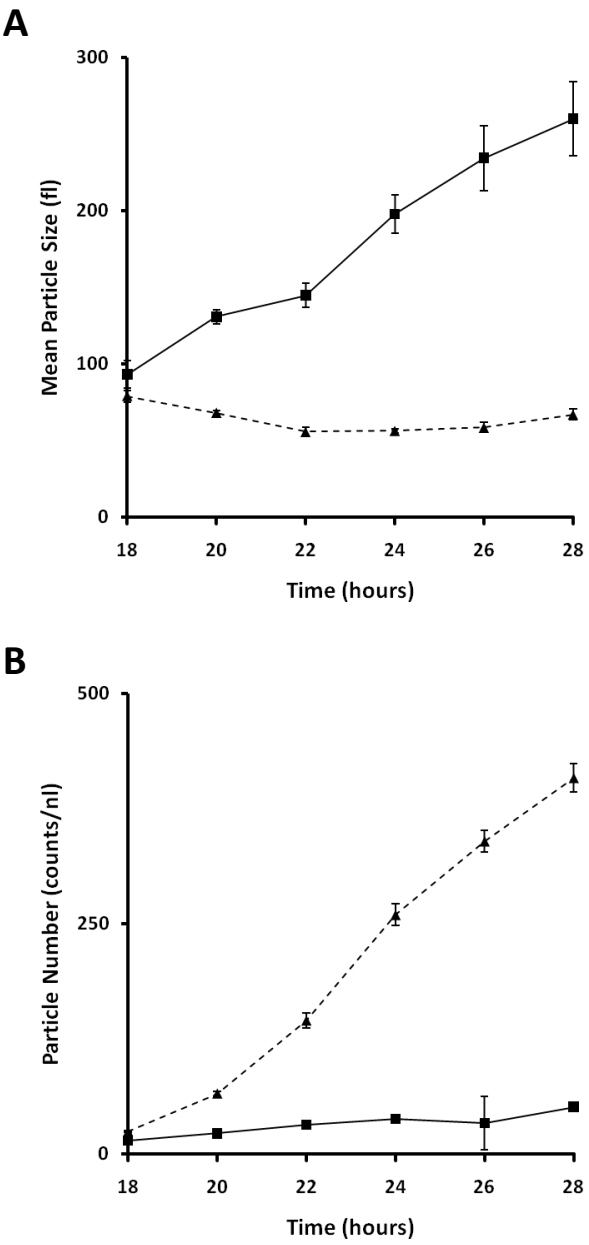

C

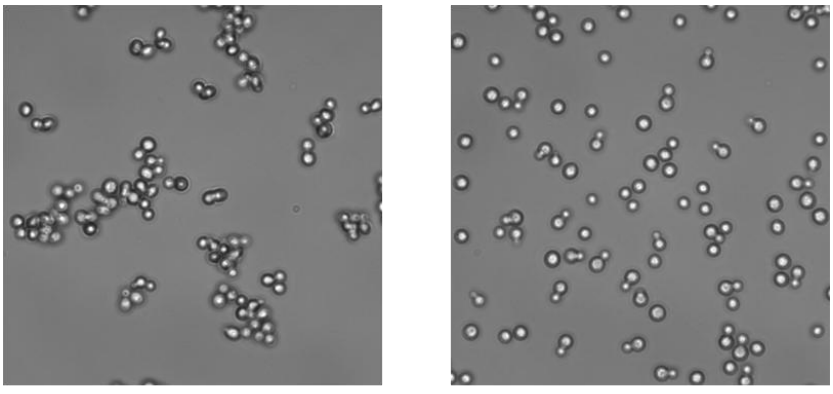

Ammonium

Urea

Figure 9 - Growth in ammonium media induces cell aggregation.

A and B - The mean particle size (A) and particle number (B) recorded over the late log and early stationary growth phases of wild-type cultures in ammonium (squares) and urea (triangles) media, using a CASY cell counter (Schärfe System). Data points shown represent the mean of 3 repeat experiments and error bars represent the standard deviation.

C - The cultures were subject to microscopic analysis after 28 hours of growth. Cell images were captured using a Zeiss Axiovert 200 M inverted microscope (100x). Data are representative of 3 repeat experiments.

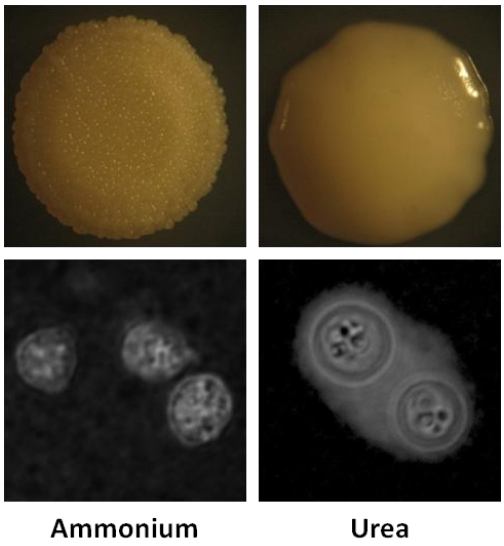

Figure 10 - Growth on urea medium induces mucoid colony morphology and capsule formation.

Colonies were plated on minimal agar media containing ammonium or urea as the sole nitrogen source and incubated at 30^{o}C for 10 days. The colonies were photographed (top panels) and a sample of each stained with India ink (lower panels). Data are representative of 3 repeat experiments.

3.2.2. Urease Activity is Responsive to the Available Nitrogen Source

It is not known if cryptococcal urease activity varies in response to the available nitrogen source. To investigate this, urease activity was quantified in wild-type cultures grown to mid-log in enriched YPD medium or minimal synthetic media containing either ammonium, urea, glutamine or glutamic acid as the sole source of nitrogen. The urea grown cells exhibited the highest levels of urease activity, while the YPD grown cells had very low levels. Urease activity in the ammonium grown cells was approximately half the level of activity detected in the urea grown cells (Figure 11A). The glutamine and glutamic acid samples' activity was between those of the ammonium and urea extracts. This demonstrates that urease activity is regulated in response to the available nitrogen source and the lack of urea does not repress urease activity.

The production of ammonium by urease can be utilised to neutralise acidic environments. To determine if urease activity is responsive to the pH of the environment, the wild-type strain was grown in ammonium and urea media buffered with 100 mM HEPES and the pH adjusted to 4, 5.5 or 6. The pH of standard minimal media is pH 5.5. The urease activity in each pH was equal in both ammonium and urea grown cells (Figure 11B). This established that *C. neoformans* urease activity is not responsive to the pH of the media.

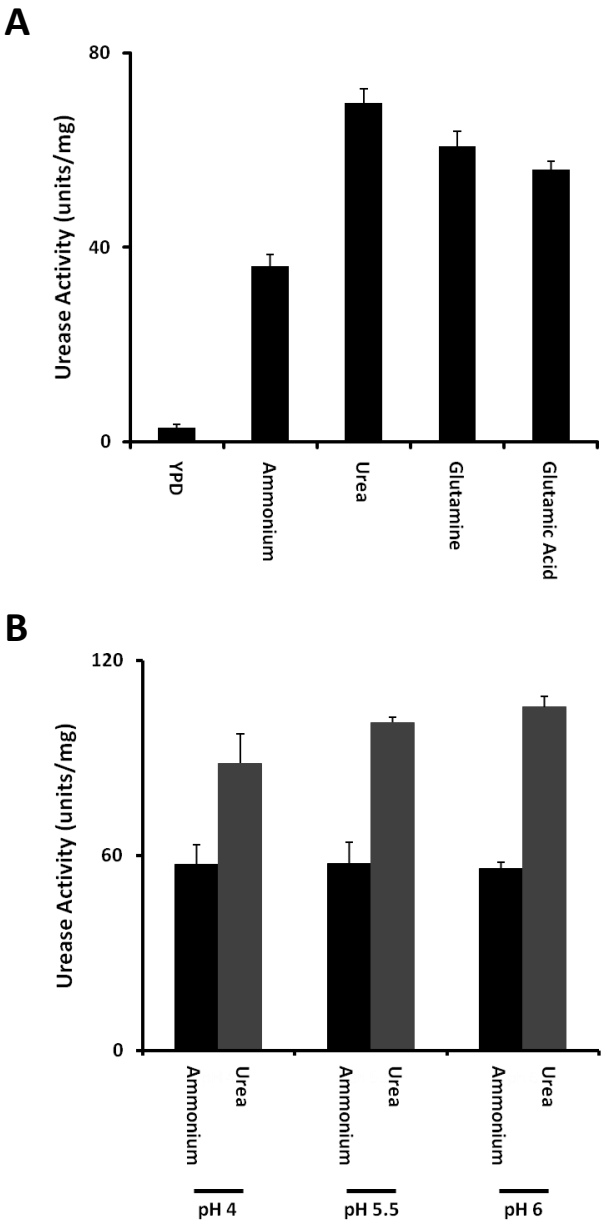

Figure 11 - Urease activity is regulated in response to utilised nitrogen source.

A - The wild-type strain was grown to mid-log in minimal media containing ammonium, urea, glutamine or glutamic acid as the sole source of nitrogen, or YPD medium. Protein extracts (200 μg) were incubated in 66 mM urea solution at 30^{o}C and rate of ammonia production determined by Nessler's colour reagent. Units are in μM of ammonium produced per minute at pH 8.2 and 30^{o}C, per mg of protein extract.

B- The wild-type strain was grown to mid-log in ammonium or urea media adjusted to pH 4, 5.5 or 6 and buffered with 100 mM HEPES. Protein was extracted and the urease activity determined.

Data points shown represent the mean of 3 repeat experiments and error bars represent the standard deviation.

3.2.3. Nickel is Accumulated in Response to Nitrogen Source

It is not known how cryptococcal urease is regulated, but may include regulation of the uptake or incorporation of the metal cofactor. To determine if metal accumulation in *C. neoformans* varies in response to the growth conditions the metal content of cells was measured by ICP-MS. Samples were analysed from cultures grown in YPD medium or minimal synthetic media containing ammonium, urea, glutamine or glutamic acid as the sole source of nitrogen. The levels of nickel were significantly higher in urea, glutamine and glutamic acid samples than the ammonium sample. Levels of zinc were relatively constant between the samples and iron levels were higher in glutamine cells (Figure 12A-C). This established that nickel accumulation is regulated in response to the utilised nitrogen source. The levels of cobalt also increased in urea, glutamine and glutamic acid compared to ammonium (Figure 12D).

Capsule production in response to growth in urea was a concern to the metal accumulation studies due to the potential metal chelating capacity of the capsule. Although capsule growth in mid-log liquid culture was not observed confirmation that it was not a factor in nitrogen source specific metal accumulation was necessary. Nickel accumulation of the wild-type strain and an acapsular strain B-4131 was compared. The strains were grown in minimal media containing ammonium or urea as the sole source of nitrogen. The nickel accumulation in the wild-type and B-4131 strains was comparable with low levels of nickel accumulation in ammonium increasing significantly in urea (Figure 13). The ability of the wild-type and B-4131 strains to grow capsule was tested by growth on solid ammonium and urea based media, which showed that the wild-type produced capsule in response to urea and B-4131 did not (Figure 14). This established that the increased nickel accumulation in urea grown cells compared to ammonia grown cells is not due to capsule formation.

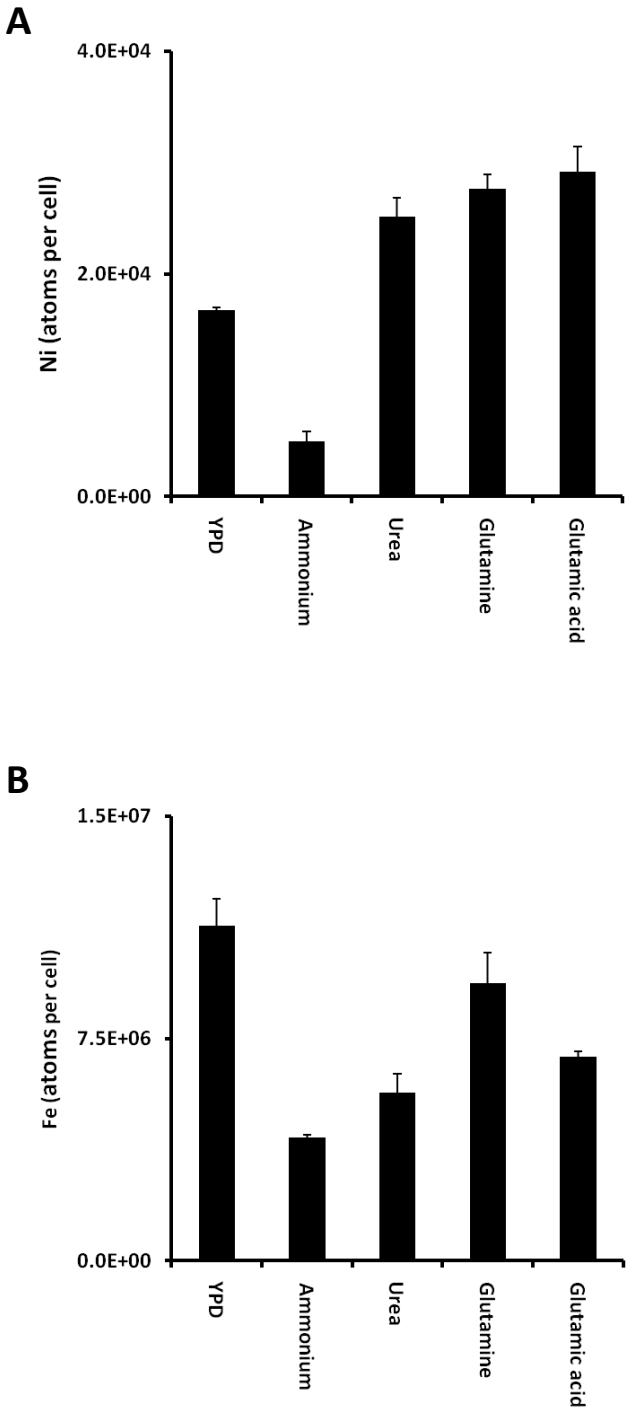
A
4.0E+04
2.0E+04
0.0E+00
Ni (atoms per cell)
YPD
Ammonium
Urea
Glutamine
Glutamic acid
B
1.5E+07
7.5E+06
0.0E+00
Fe (atoms per cell)
YPD
Ammonium
Urea
Glutamine
Glutamic acid

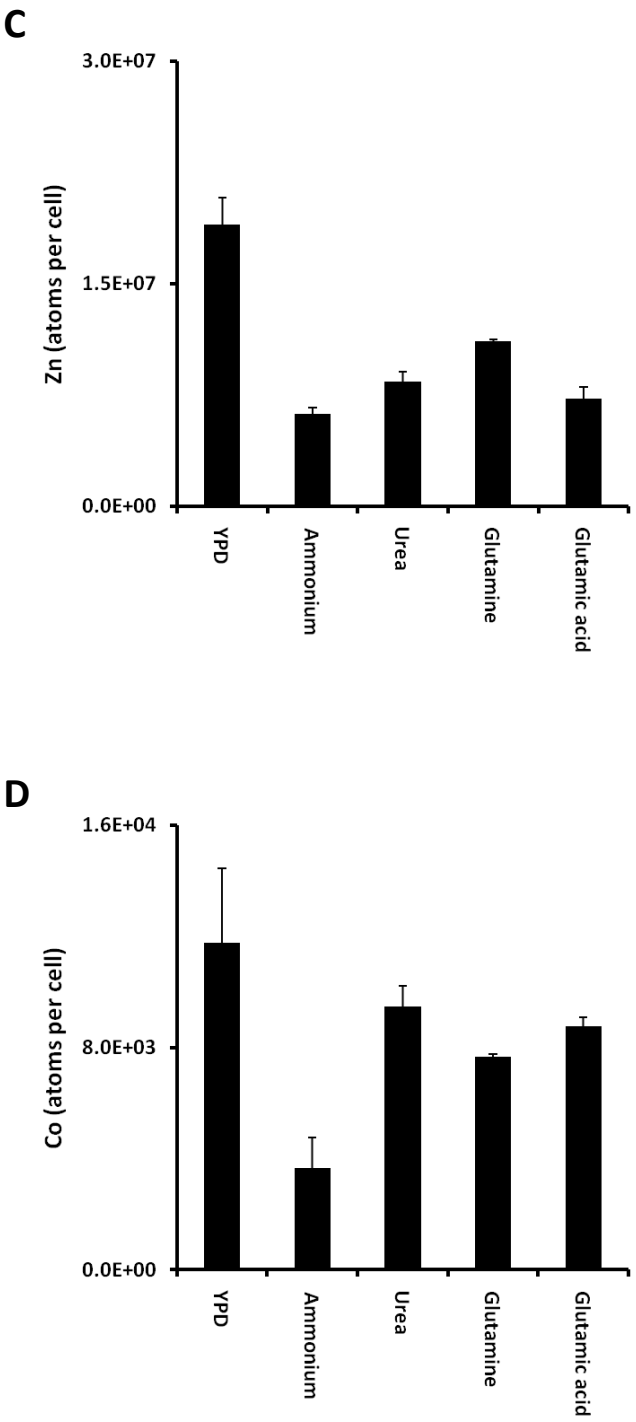

Figure 12 - Metal accumulation in response to nitrogen source.

The wild-type strain was grown to mid-log in YPD or minimal media containing ammonium, urea, glutamine or glutamic acid as the sole source of nitrogen. Cells were harvested and washed in nano-pure water to remove growth media, digested in 65 % nitric acid and analysed by ICP-MS. Cellular accumulation for nickel (A), iron (B), zinc (C) and cobalt (D) was calculated. Data points shown represent the mean of 3 repeat experiments and error bars represent the standard deviation.

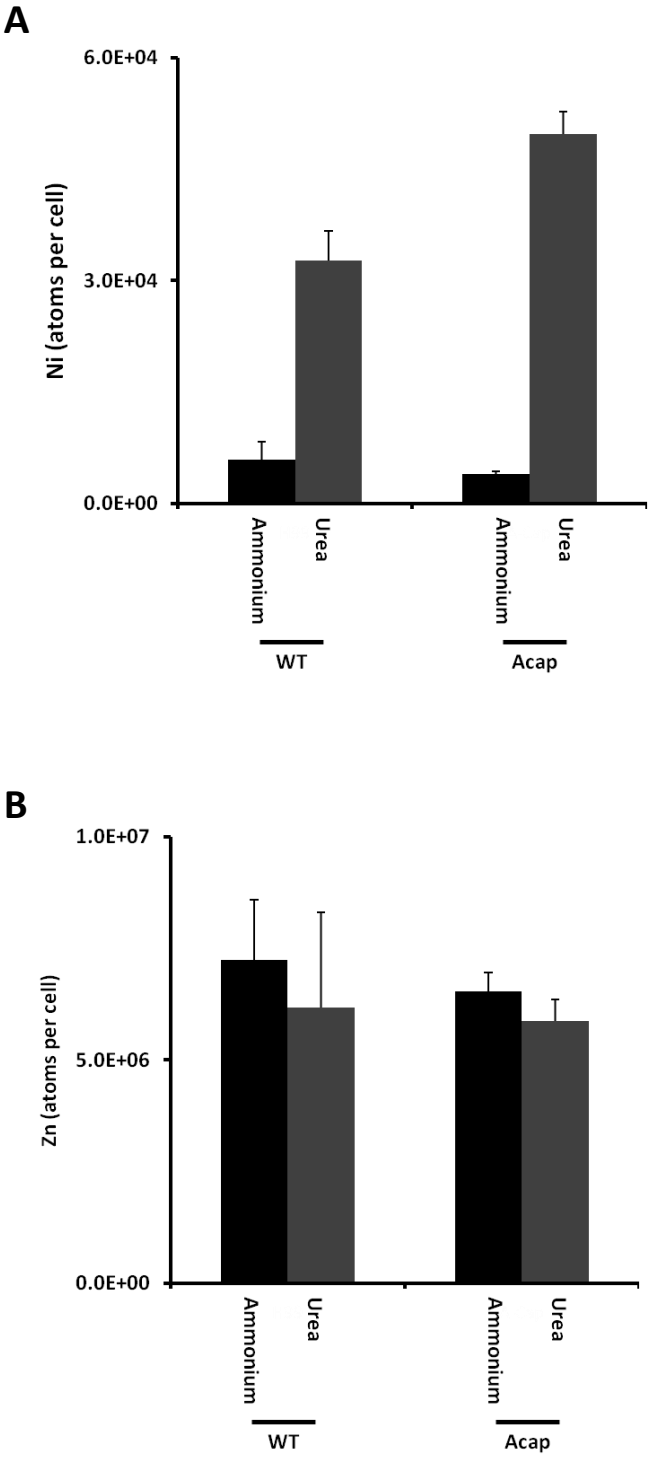

Figure 13 - The metal accumulation of the wild-type and acapsular strains.

Cultures of the wild-type and B-4131 (Acap) strains were grown to mid-log in ammonium and urea based minimal media. Nickel (A) and zinc (B) cellular concentrations were calculated. Data points shown represent the mean of 3 repeat experiments and error bars represent the standard deviation.

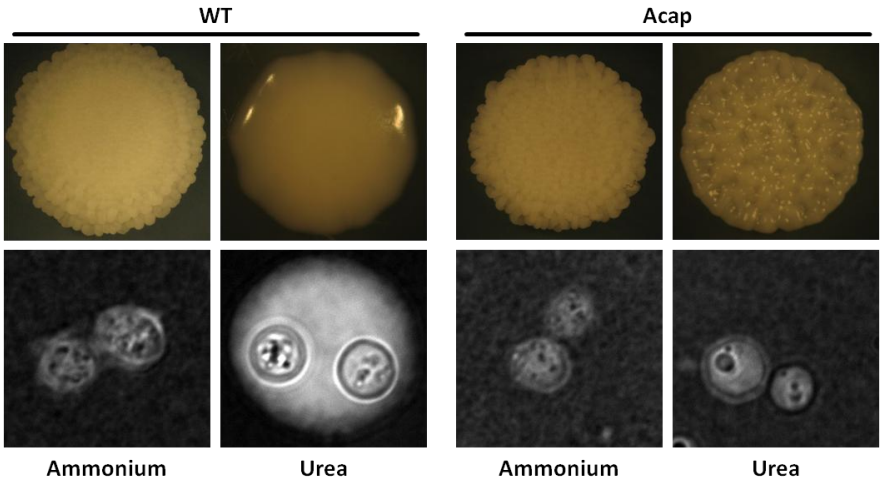

Figure 14 - The B-4131 strain does not form capsule.

Colonies of the wild-type and B-4131 (Acap) strains were grown on ammonium and urea minimal media for 10 days at 30^{o}C. Colony morphology was photographed and capsule formation assayed by India ink. Data are representative of 3 repeat experiments.

3.3. Creation and Confirmation of Mutant Strains

3.3.1. Generation of Mutant Strains

To study the roles of urease, *Cn*Nic1 and *Cn*UreG, deletion mutants lacking each gene were generated. A *ure1Δ* strain was generated by interruption of the *URE1* coding sequence by integration of an antibiotic resistance marker, *hph*, conferring resistance to Hygromycin B. A *nic1Δ* strain and a *ureGΔ* strain were generated by replacement of the *NIC1* and *UREG* coding regions with the *NEO* resistance marker, which confers resistance to neomycin (G418 was used in this study). In each case integration of the relevant deletion cassette into the wild-type genome was achieved by biolistic transformation. The deletion cassette for the *ure1Δ* strain consisted of the *hph* marker flanked by ~1 kb of sequence homologous to the *URE1* promoter region and ~1 kb of sequence homologous to the *URE1* coding region. This facilitated integration of the *hph* marker into the coding region of *URE1*, excising ~500 bp of coding sequence (Figure 16A-C). The deletion cassettes for the *nic1Δ* and *ureGΔ* strains contained the *NEO* marker flanked by ~1 kb of promoter and terminator regions of the respective genes. This facilitated integration of the *NEO* marker and deletion of the complete open reading frame (Figure 17A-C, Figure 18A-C). Transformation colonies were selected by the ability to grow on YPD medium containing the relevant antibiotics and screened for loss of ability to turn Christensen's medium from yellow to pink, a qualitative test of urease activity (Figure 15, Figure 20A, Figure 24A, Figure 28A).

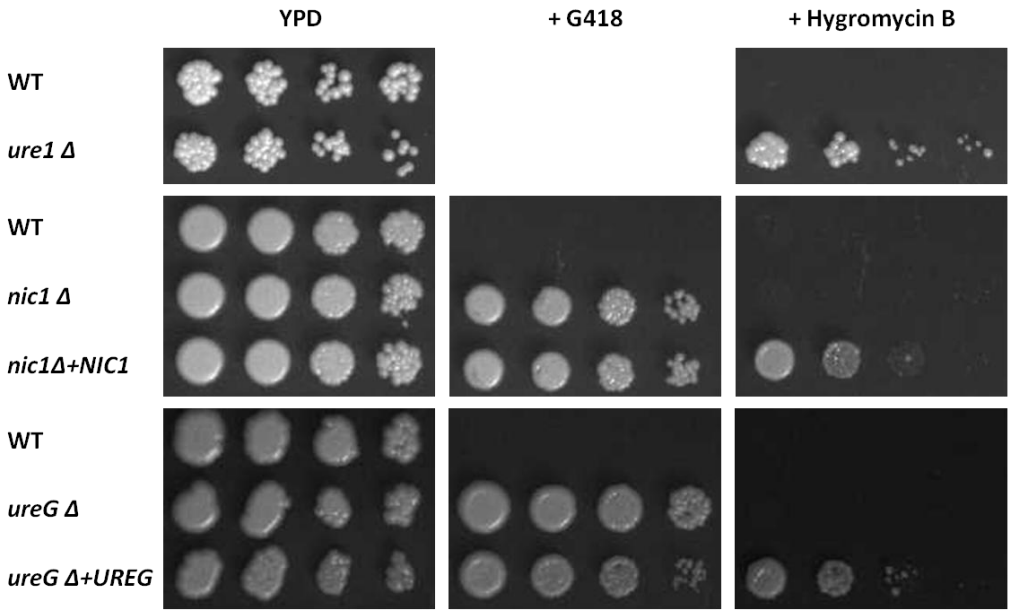

Figure 15 - Antibiotic resistance of strains generated in this study.

The ability of the wild-type, *ure1Δ*, *nic1Δ*, *nic1Δ+NIC1*, *ureGΔ* and *ureGΔ+UREG* to grow in the presence of G418 and Hygromycin B was assayed by plating serial dilutions of each strain onto YPD, YPD with 200 μg/ml G418 and YPD with 200 μg/ml Hygromycin B. The plates were incubated at 30°C for 3 days. Data are representative of 3 repeat experiments.

The *nic1Δ* and *ureGΔ* deletion strains were reconstituted with the wild-type *NIC1* and *UREG* genes, respectively. In each case the entire coding region with ~1 kb of promoter and ~500 bp of terminator sequence, was re-introduced into the original locus with the *hph* antibiotic resistance marker. This was achieved by integration of a reconstitution plasmid into the deletion strain by biolistic transformation (pAG32-*NIC1* into *nic1Δ* and pAG32-*UREG* into *ureGΔ*). The plasmids were linearised in the promoter region of the gene which targeted integration of the plasmid into the promoter region of the wild-type locus (Figure 16D-F, Figure 17D-F). Transformation colonies were selected by the ability to grow on YPD medium containing Hygromycin B and screened for ability to turn Christensen's medium from yellow to pink (Figure 15, Figure 20, Figure 24 and Figure 28).

3.3.2. Confirmation of Generated Strains by Southern Blot

Southern blot analysis was used to confirm that the deletion cassettes and reconstitution plasmids integrated into the correct locus and that only one copy integrated into the genome. To confirm the correct integration of the *ure1Δ* deletion cassette DNA was extracted from the wild-type and *ure1Δ* strains and digested with ApaI and BglI. A probe specific for the *URE1* promoter and coding regions annealed to DNA fragments of 5.6 kb and 4.0 kb in the wild-type and *ure1Δ* strains respectively (Figure 16D). This established the integration of the *ure1Δ* deletion cassette at the *URE1* locus. Three non-specific bands were also observed. A second probe specific to the *hph* marker annealed to a 4.0 kb fragment from the *ure1Δ* strain and no fragment in the wild-type strain (Figure 16D). This established single integration of the *ure1Δ* cassette.

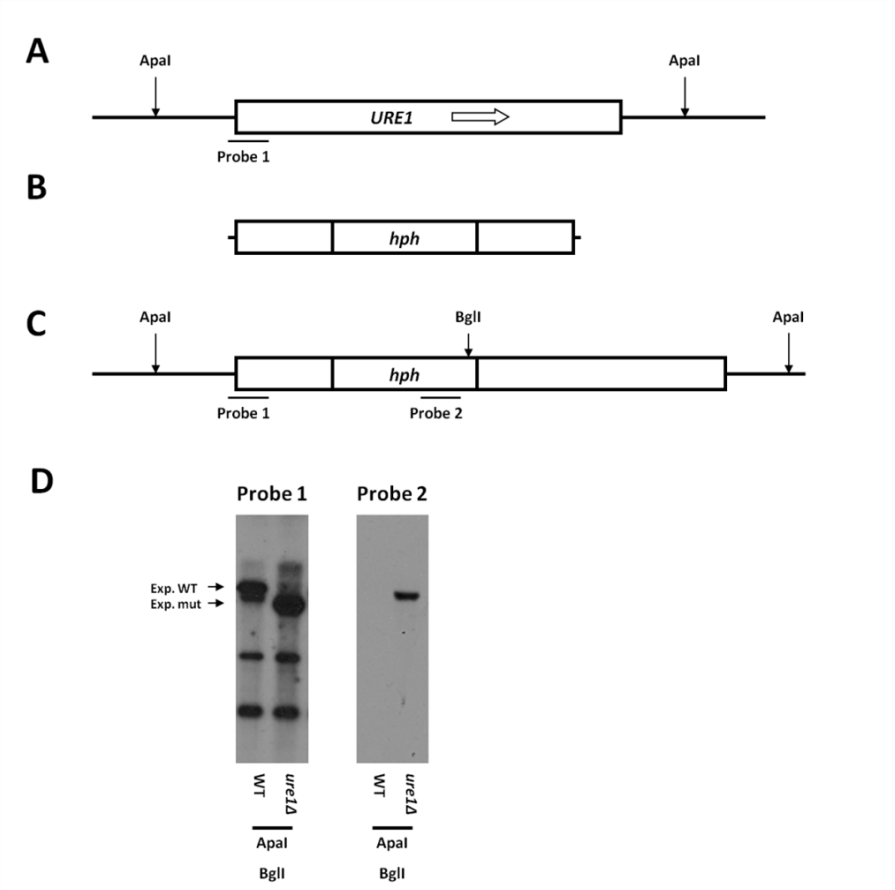

Figure 16 - Southern blot analysis of the *ure1Δ* strain.

A-C - Schematic representation of the wild-type *URE1* locus (A), the *ure1Δ* deletion cassette (B) and the *ure1Δ* locus (C). Relevant sites of restriction digest and probe binding locations are indicated.

D - Southern blots to confirm integration of the *ure1Δ* deletion cassette at the correct site (probe 1, left hand panel) and a single integration event (probe 2, right hand panel) after digestion with ApaI and BglI. Expected fragment sizes are indicated by arrows where relevant.

To confirm the correct integration of the *nic1Δ* deletion cassette DNA was extracted from the wild-type and *nic1Δ* strains and digested with BsrGI and XbaI. A probe specific for the *NIC1* promoter region annealed to DNA fragments of 4.1 kb and 3.1 kb from the wild-type and *nic1Δ* strains respectively (Figure 17F). This established integration of the *nic1Δ* deletion cassette at the *NIC1* locus. A second probe specific for the *NEO* marker annealed to a 3.1 kb fragment from the *nic1Δ* strain but no fragment from the wild-type strain. This established the single integration of the *nic1Δ* deletion cassette.

To confirm the correct integration of the *NIC1* reconstitution plasmid DNA was extracted from the *nic1Δ* and *nic1Δ+NIC1* strains and was digested with BglII and separately with ClaI. A probe specific for the *hph* marker annealed to a single DNA fragment in *nic1Δ+NIC1* strain of 8.4 kb, for the BglII digestion, and 7.6 kb, for the ClaI digestion, and no fragment in the *nic1Δ* strain (Figure 17G). To confirm that the *NIC1* reconstitution plasmid integrated into the promoter region of the wild-type locus, the *nic1Δ* and *nic1Δ+NIC1* strain DNA was digested with BsrGI. A probe specific for the *NIC1* coding region annealed to a DNA fragment of 7.7 kb in the *nic1Δ+NIC1* strain and no fragment in the *nic1Δ* strain (Figure 17G). This established the single integration of the *NIC1* reconstitution plasmid. To further confirm the correct integration of the *NIC1* reconstitution plasmid, PCR was performed using primers N1rnF (which anneals in the *NIC1* promoter region) and N1rnR (which anneals in the *NIC1* coding region). A PCR product of 1.4 kb was generated when DNA from the wild-type and *nic1Δ+NIC1* strains was used as template (Figure 19), which was subsequently sequenced. These data established the integration of the *NIC1* reconstitution plasmid at the *NIC1* locus in the *nic1Δ* strain.

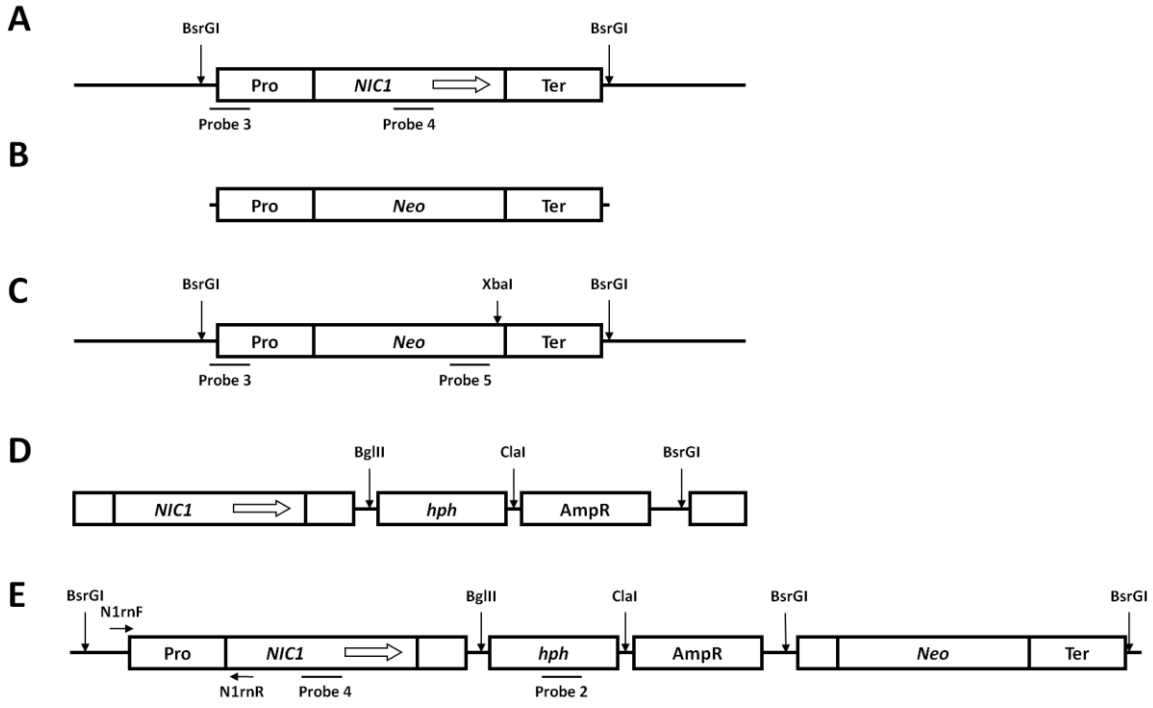
A
BsrGI
BsrGI
Pro
NIC1
Ter
Probe 3
Probe 4
B
Pro
Neo
Ter
C
BsrGI
XbaI
BsrGI
Pro
Neo
Ter
Probe 3
Probe 5
D
BglII
ClaI
BsrGI
NIC1
hph
AmpR
E
BsrGI
N1rnF
BglII
ClaI
BsrGI
BsrGI
Pro
NIC1
hph
AmpR
Neo
Ter
N1rnR
Probe 4
Probe 2

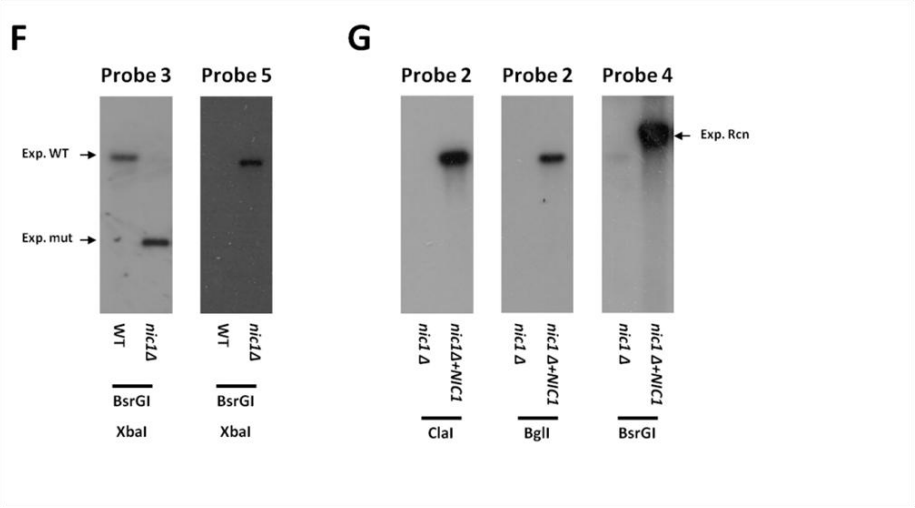
F
Probe 3
Probe 5
Exp. WT
Exp. mut
WT
nic1Δ
WT
nic1Δ
BsrGI
XbaI
BsrGI
XbaI
G
Probe 2
Probe 2
Probe 4
Exp. Rcn
nic1 Δ
nic1Δ+NIC1
nic1 Δ
nic1 Δ+NIC1
nic1 Δ
nic1 Δ+NIC1
ClaI
BglI
BsrGI

Figure 17 - Southern blot analysis of the *nic1Δ* and *nic1Δ+NIC1* strains.

A-E - Schematic representation of the wild-type *NIC1* locus (A), the *nic1Δ* deletion cassette (B), the *nic1Δ* locus (C), the *NIC1* reconstitution vector pAG32-*NIC1* digested by BsgI (D) and the *nic1Δ+NIC1* locus (E). Relevant sites of restriction digest, probe and primer binding locations are indicated.

F - Southern blots to confirm integration of the *nic1Δ* deletion cassette at the correct locus (probe 3, left hand panel) and a single integration event (probe 5, right hand panel) after digestion with BsrGI and XbaI. Expected fragment sizes are indicated by arrows where relevant.

G - Southern blots to confirm a single integration of pAG32-*NIC1* into *nic1Δ* (probe 2, left and centre panels) after digestion, separately, with ClaI and BglI and to confirm correct site of integration (probe 4, right hand panel) after digestion with BsrGI. Expected fragment sizes are indicated by arrows where relevant.

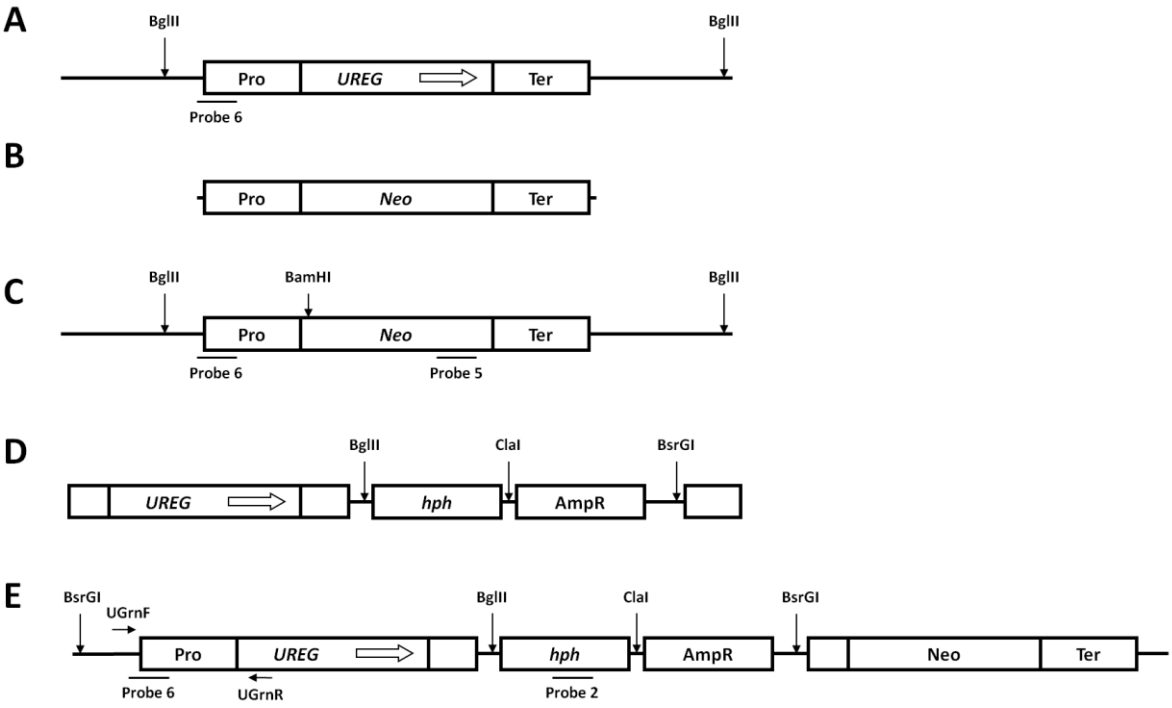
A
BglII
BglII
Pro
UREG
Ter
Probe 6
B
Pro
Neo
Ter
C
BglII
BamHI
BglII
Pro
Neo
Ter
Probe 6
Probe 5
D
BglII
ClaI
BsrGI
UREG
hph
AmpR
E
BsrGI
UGrnF
BglII
ClaI
BsrGI
Pro
UREG
hph
AmpR
Neo
Ter
Probe 6
UGrnR
Probe 2

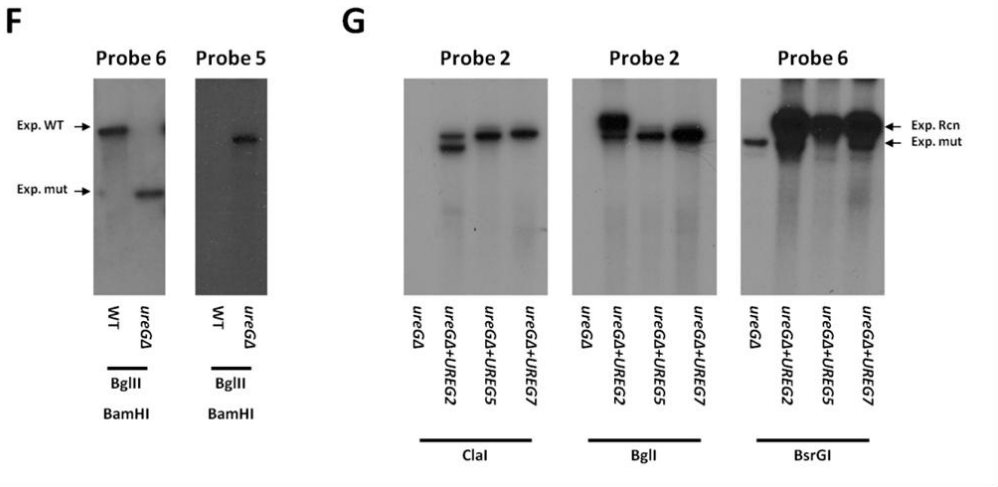
F
Probe 6
Probe 5
Exp. WT
Exp. mut
WT
ureGΔ
WT
ureGΔ
BglII
BamHI
BglII
BamHI
G
Probe 2
Probe 2
Probe 6
Exp. Rcn
Exp. mut
ureGΔ
ureGΔ+UREG2
ureGΔ+UREG5
ureGΔ+UREG7
ureGΔ
ureGΔ+UREG2
ureGΔ+UREG5
ureGΔ+UREG7
ureGΔ
ureGΔ+UREG2
ureGΔ+UREG5
ureGΔ+UREG7
ClaI
BglI
BsrGI

Figure 18 - Southern blot analysis of the *ureGΔ* and *ureGΔ+UREG* strains.

A-E - Schematic representation of the wild-type *UREG* locus (A), the *ureGΔ* deletion cassette (B), the *ureGΔ* locus (C), the *UREG* reconstitution vector pAG32-*UREG* digested by SphI (D) and the *ureGΔ+UREG* locus (E). Relevant sites of restriction digest, probe and primer binding locations are indicated.

F - Southern blots to confirm integration of the *ureGΔ* deletion cassette at the correct locus (probe 6, left hand panel) and a single integration event (probe 5, right hand panel) after digestion with BglII and BamHI. Expected fragment sizes are indicated by arrows where relevant.

G - Southern blots to confirm a single integration of pAG32-*UREG* into *ureGΔ* (probe 2, left and centre panels) after digestion, separately, with ClaI and BglI and to confirm correct site of integration (probe 6, right hand panel) after digestion with BsrGI. Expected fragment sizes are indicated by arrows where relevant. *ureGΔ+UREG2*, *ureGΔ+UREG5* and *ureGΔ+UREG7* are separate isolates of the *UREG* reconstitution transformations into the *ureGΔ* background.

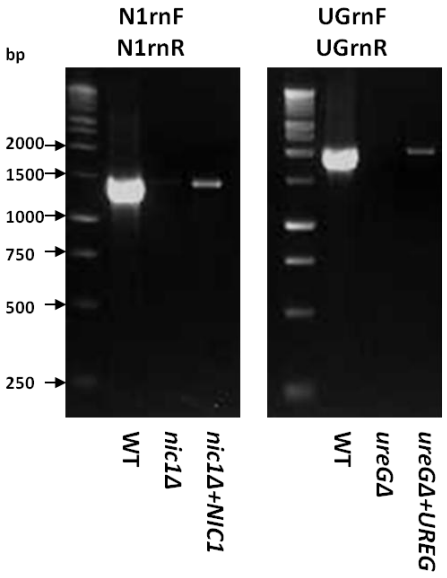

Figure 19 - Confirmation of *nic1Δ+NIC1* and *ureGΔ+UREG* by PCR.

The integration of pAG32-*NIC1* and pAG32-*UREG* into the promoter region of the *nic1Δ* locus and the *ureGΔ* locus, respectively, was confirmed by PCR. N1rnF and N1rnR primers were used to analyse the *nic1Δ+NIC1* strain which produced a product of 1.4 kb (left hand panel). UGrnF and UGrnR primers were used to analyse the *ureGΔ+UREG* strain which produced a product of 2 kb (right hand panel).

To confirm the correct integration of the *ureGΔ* deletion cassette DNA was extracted from the wild-type and *ureGΔ* strains and digested with BamHI and BglII. A probe specific for the *UREG* promoter region annealed to DNA fragments of 6.7 kb and 1.6 kb from the wild-type and *ureGΔ* strains respectively (Figure 18F). This established integration of the *ureGΔ* deletion cassette at the *UREG* locus. A probe specific for the *NEO* marker annealed to a 5.8 kb DNA fragment from the *ureGΔ* strain and no fragment from the wild-type strain (Figure 18F). This established the single integration of the *ureGΔ* deletion cassette.

To confirm the correct integration of the *UREG* reconstitution plasmid DNA extract from the *ureGΔ* and *ureGΔ+UREG* strains was digested separately with BglII and ClaI. A probe specific to the *hph* marker annealed to a single DNA fragment from the *ureGΔ+UREG* strain of 11.1 kb, for the BglII digestion, or 10.1 kb, for the ClaI digestion, and no fragments in the *ureGΔ* strain (Figure 18G). This established the single integration of the *UREG* reconstitution plasmid. To confirm integration of the *UREG* reconstitution plasmid into the *UREG* promoter region DNA was extracted from the *ureGΔ* and *ureGΔ+UREG* strains and digested with BsrGI. A probe specific for the *UREG* promoter region annealed to DNA fragments of 5.8 kb and 7.7 kb in the *ureGΔ* and *ureGΔ+UREG* strain respectively (Figure 18G). To further confirm the correct integration of the *UREG* reconstitution plasmid PCR was performed using primers UGrnF (which anneals in the *UREG* promoter) and UGrnR (which anneals in the *UREG* coding region). A product of 2 kb was generated when DNA from the wild-type and *ureGΔ+UREG* strains was used as template, which was subsequently sequenced (Figure 19). These data established the integration of the *UREG* reconstitution plasmid at the *UREG* locus in the *ureGΔ* strain.

3.4. Identification and Analysis of the Role of Urease, Nic1 and UreG

3.4.1. *URE1*

The urease gene, *URE1*, has been previously identified in *C. neoformans*. Like other plant and fungal urease enzymes, the urease in *C. neoformans* is a single poly-peptide representing a fusion of the three sub-units found in most bacterial urease enzymes. *C. neoformans* contains the conserved lysine residue in the active site, which is carbamylated, and the histidine residues involved in nickel binding (Cox *et al.*, 2000).

The *ure1Δ* strain has previously been described as avirulent but during that study the effect of urease deletion on growth under different conditions was not studied (Olszewski *et al.*, 2004). In *S. cerevisiae*, which lacks a urease gene, urea is metabolised via the Dur1,2 system, comprised of two fused sub-units, which is part of the allantoin degradation system and is NCR sensitive (Cunningham and Cooper, 1991). Homologues to each of the Dur1,2 subunits exist in *C. neoformans* and so represent a potential secondary pathway for utilisation of urea as a nitrogen source (ORFs CANG_07944 and CNAG_01680, NCBI database). To investigate the role of *URE1*, the wild-type and *ure1Δ* strains were plated in serial dilutions onto minimal agar media containing either ammonium, urea or uric acid as the sole nitrogen source. As urea specific accumulation of nickel was observed in the wild-type strain, the medium was or was not supplemented with 10 μM $NiSO_4$. The *ure1Δ* strain showed little or no growth on urea or uric acid media compared to the wild-type strain and growth could not be recovered by addition of nickel (Figure 20). This established that urease is essential for *C. neoformans* growth utilising urea as the sole nitrogen source.

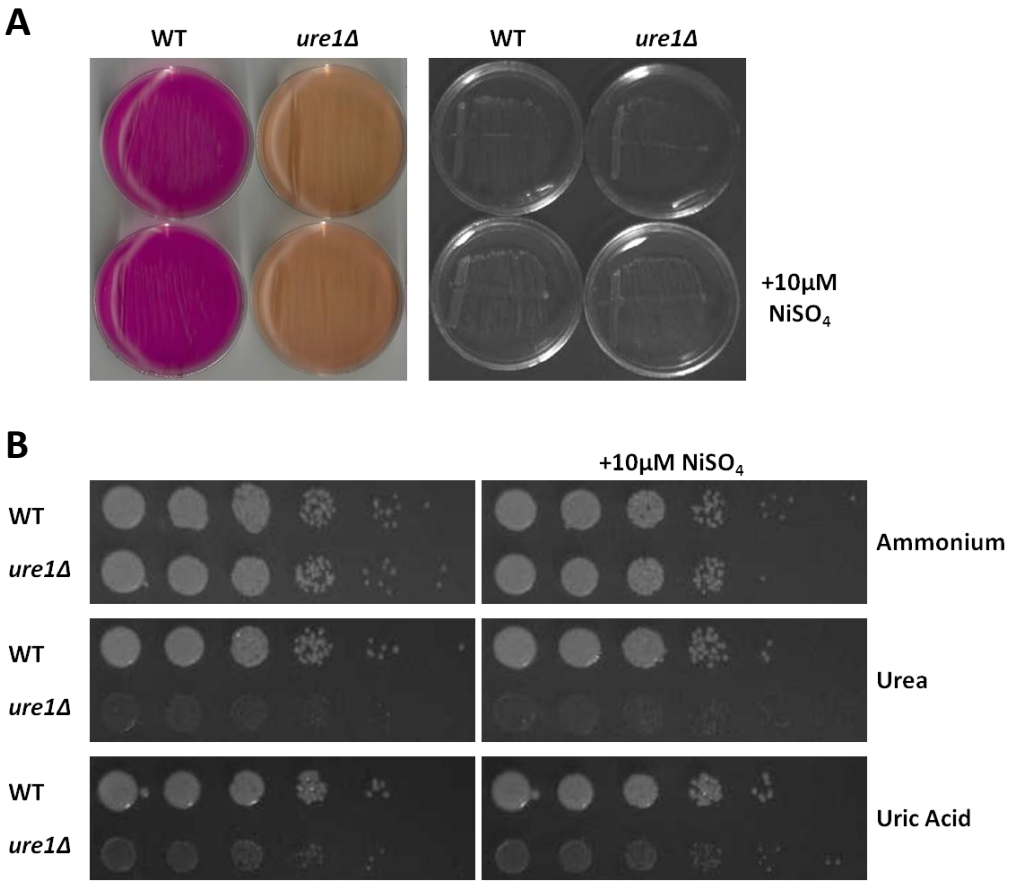

Figure 20 - *ure1Δ* cannot grow on urea and uric acid based media.

A - The wild-type and *ure1Δ* strains were streaked onto Christensen's urea agar with and without $NiSO_4$ added to 10 μM. Ability to change the media from yellow to pink was recorded by colour scan (left hand panel) and equal loading confirmed by grey-scale photograph (right hand panel).

B - The wild-type and *ure1Δ* strains were plated in serial dilutions onto minimal media containing either ammonium, urea or uric acid as the sole source of nitrogen both with and without $NiSO_4$ added to 10 μM. The plates were incubated at 30°C for 3 days and then photographed.

Data are representative of 3 repeat experiments.

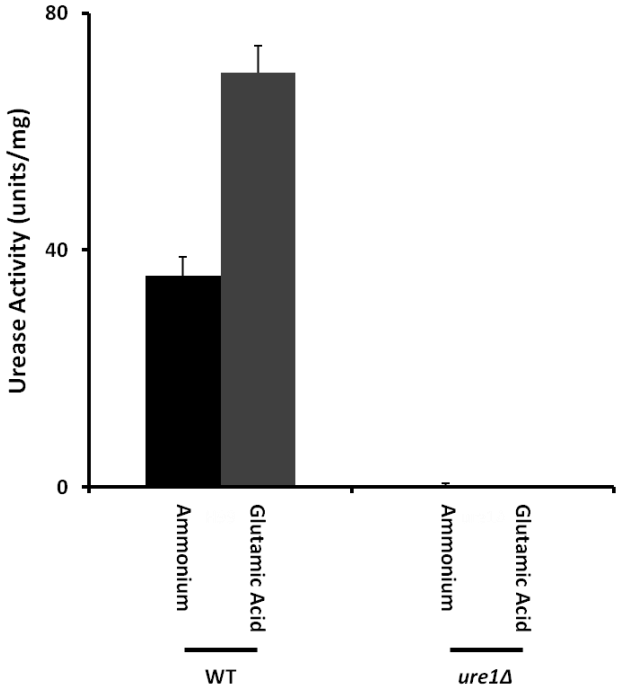

Figure 21 - *ure1Δ* does not have urease activity.

The wild-type and *ure1Δ* strains were grown to mid-log in minimal media containing ammonium or glutamic acid as the sole source of nitrogen. The urease activity of protein extracts was determined. Data points shown represent the mean of 3 repeats and error bars represent the standard deviation.

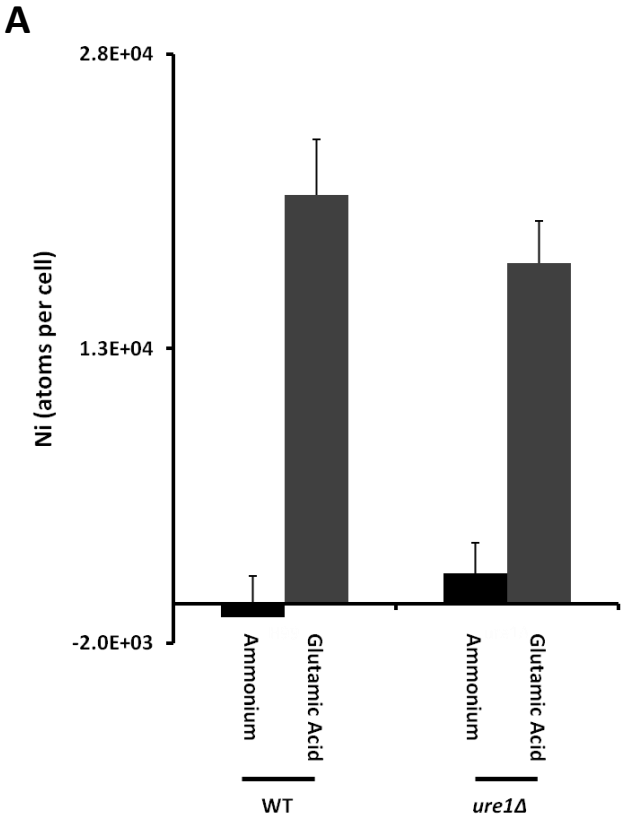
A
2.8E+04
1.3E+04
-2.0E+03
Ni (atoms per cell)
Ammonium
Glutamic Acid
Ammonium
Glutamic Acid
WT
ure1Δ

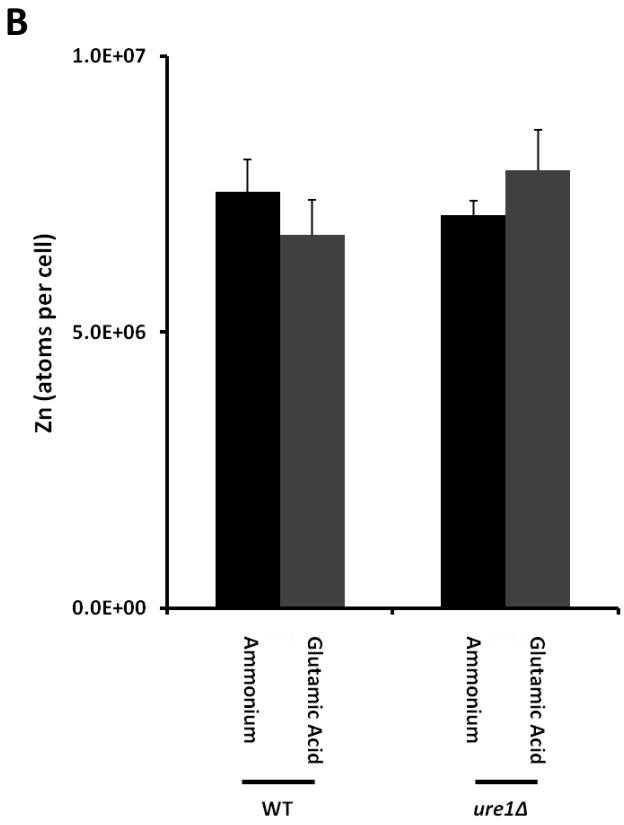
B
1.0E+07
5.0E+06
0.0E+00
Zn (atoms per cell)
Ammonium
Glutamic Acid
Ammonium
Glutamic Acid
WT
ure1Δ

Figure 22 - Nickel accumulation in the *ure1Δ* strain.

The wild-type and *ure1Δ* strains were grown to mid-log in minimal media containing ammonium or glutamic acid as the sole source of nitrogen. The cellular concentration of nickel (A) and zinc (B) was determined by ICP-MS. Data points shown represent the mean of 3 repeat experiments and error bars represent the standard deviation.

To quantify urease activity in cells utilising different nitrogen sources the enzyme activity of the wild-type and *ure1Δ* strains was compared. Each strain was grown to mid-log at 30^{o}C in minimal media containing ammonium or glutamic acid and urease activity quantified. No urease activity was detected in the *ure1Δ* strain (Figure 21). This established that urease is the only means by which *C. neoformans* degrades urea.

To investigate whether urease is a store for nickel, metal accumulation in wild-type and *ure1Δ* cells grown in ammonium and glutamic acid media was determined. The loss of urease did not abolish nickel accumulation in response to glutamic acid, although there was a small but consistent reduction compared to the wild-type strain (Figure 22). This established that nickel is accumulated in a urease independent manner. The small decrease seen between wild-type and *ure1Δ* glutamic acid grown cells may reflect the nickel atoms associated with urease.

3.4.2. *NIC1*

The predicted product of ORF CNAG_03664.2 in the *C. neoformans* genome has a high degree of homology (40% identity) to the nickel transporter *Sp*Nic1p of *S. pombe* (Eitinger *et al*., 2000) and is designated *Cn*Nic1. *Cn*Nic1 is well conserved with the HoxN members of the NiCoTs family, including HoxN from the bacteria *Cupriavidus necator* with which it shares 35% identity, determined by ClustalW2 alignment (Eitinger *et al.*, 1991). *Cn*Nic1 contains the HX_4DH motif that is essential for nickel transport and 8 transmembrane sequences, predicted by SOUSI, consistent with high-affinity transporters of the HoxN family (Figure 23). In addition *Cn*Nic1 has a large cytosolic loop between the predicted sixth and seventh transmembrane domains that is not present in HoxN or *Sp*Nic1p but is present in the Nic1 homologue of *C. gattii*, a species closely related to *C. neoformans*.

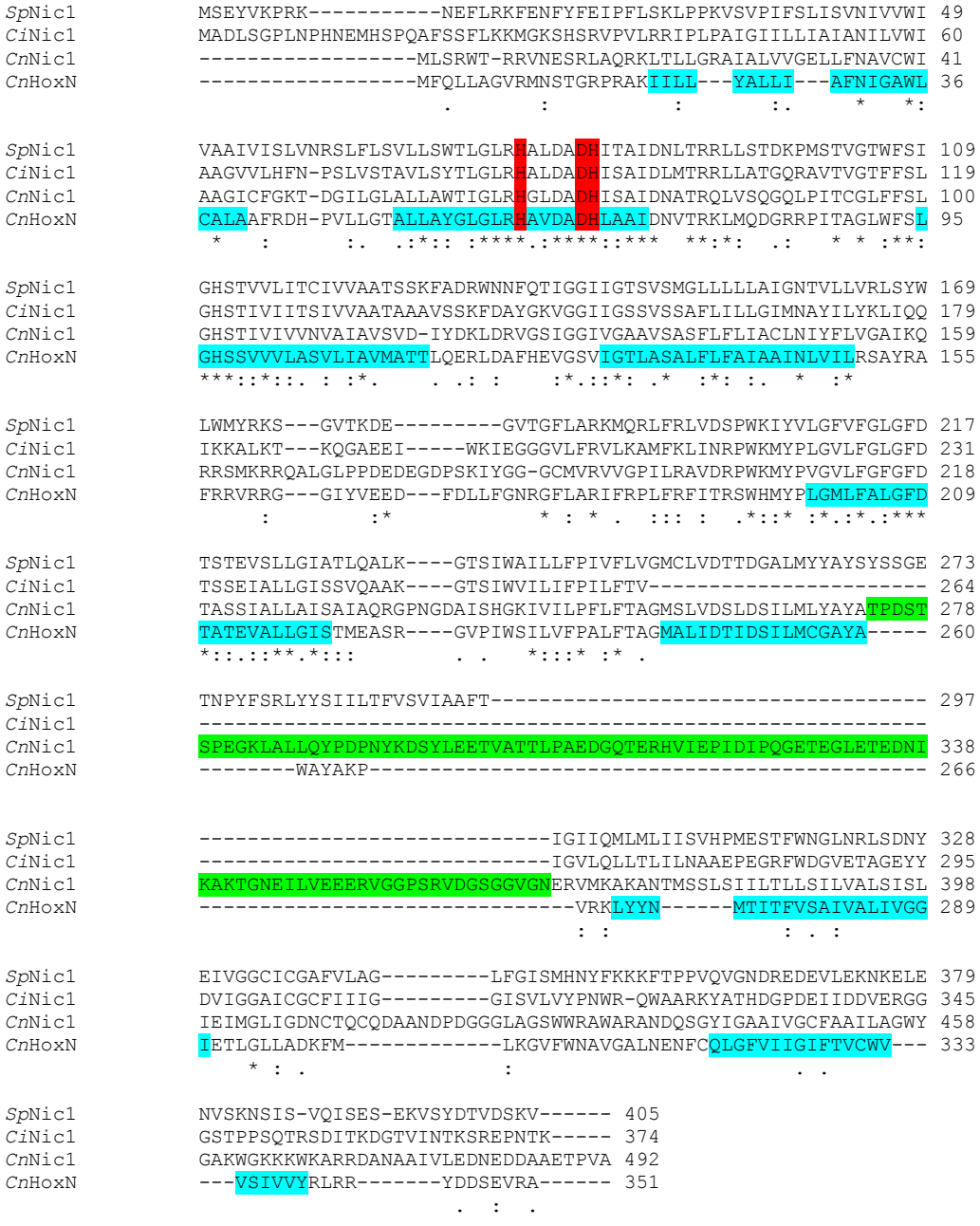

Figure 23 - Sequence alignment of nickel transporters.

A ClustalW2 alignment of Nic1 from *C. neoformans* (*Cn*Nic1), *C. immitis* (*Ci*Nic1), *S. pombe* (*Sp*Nic1) and HoxN from *C. necator* (*Cn*HoxN). The transmembrane domains of *Re*HoxN previously described are highlighted in cyan and the essential nickel-binding motif in red (Eitinger *et al.*, 97). The cytosolic loop between transmembrane domains 6 and 7, found only in *Cn*Nic1, is highlighted in green.

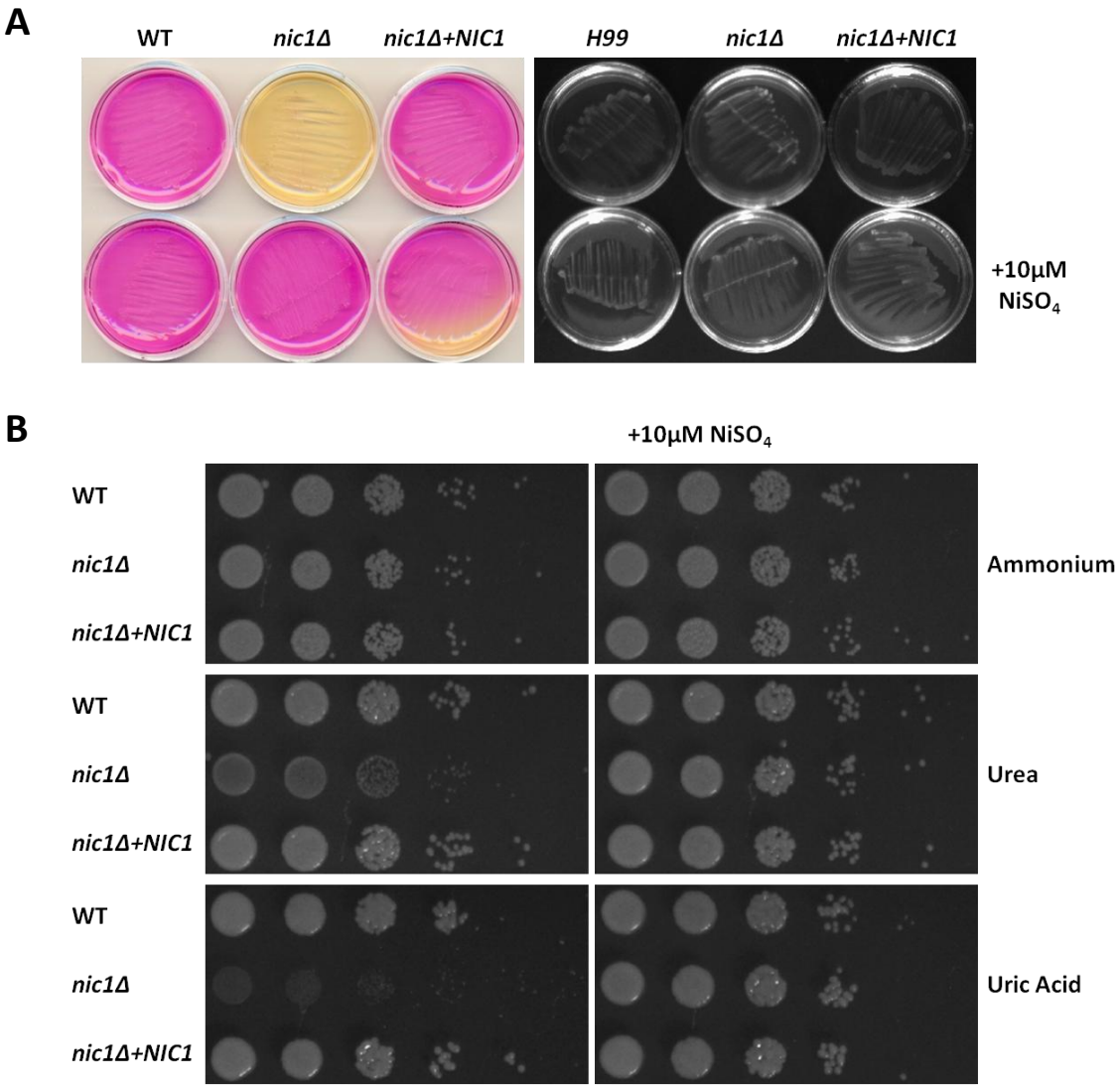

Figure 24 - The growth of *nic1Δ* on urea media is recovered by addition of nickel.

A - The wild-type, *nic1Δ* and *nic1Δ+NIC1* strains were streaked onto Christensen's urea agar with and without $NiSO_4$ added to 10 µM. Ability to change the media from yellow to pink was recorded by colour scan (left hand panel) and equal loading confirmed by grey-scale photograph (right hand panel).

B - The wild-type, *nic1Δ* and *nic1Δ+NIC1* strains were plated in serial dilutions onto minimal media containing either ammonium, urea or uric acid as the sole source of nitrogen both with and without $NiSO_4$ added to 10 µM. The plates were incubated at 30^{o}C for 3 days and then photographed.

Data are representative of 3 repeat experiments.

*Cn*Nic1 is a putative nickel transporter in *C. neoformans* that may supply urease with nickel. To determine if *Cn*Nic1 is required for cryptococcal urease activity the wild-type, *nic1Δ* and *nic1Δ+NIC1* strains were plated in serial dilutions on minimal agar media containing either ammonium, urea or uric acid as a source of nitrogen, with or without 10 μM $NiSO_4$. The *nic1Δ* strain showed a significantly reduced ability to grow on media utilising urea or uric acid as a source of nitrogen, but wild-type levels of growth were recovered by the addition of nickel to the media (Figure 24). This is consistent with *Cn*Nic1 being a nickel importer that is required to deliver nickel to urease.

To determine the effect of the loss of *Cn*Nic1 on urease activity, urease assays were performed using cell extract from the wild-type, *nic1Δ* and *nic1Δ+NIC1* strains grown in minimal media containing ammonium or urea as the sole source of nitrogen. The *nic1Δ* strain is able to grow in urea based media at a slower rate than the wild-type strain. The urease activity of the *nic1Δ* cell extract was significantly reduced compared to extract from wild-type cells (Figure 25A). No urease activity was detected in extracts from the *ure1Δ* strain (Figure 21). Wild-type levels of activity were recovered in the *nic1Δ* strain on addition of 10 μM nickel to the growth media (Figure 25B, C). The addition of either cobalt, copper, iron or zinc to urea medium did not recover activity (Figure 25D). This established that *Cn*Nic1 is required for urease activity when cells are grown in standard minimal media. The addition of nickel to the wild-type cells did not significantly increase urease activity, indicating that *C. neoformans* is not limited for nickel under standard growth conditions.

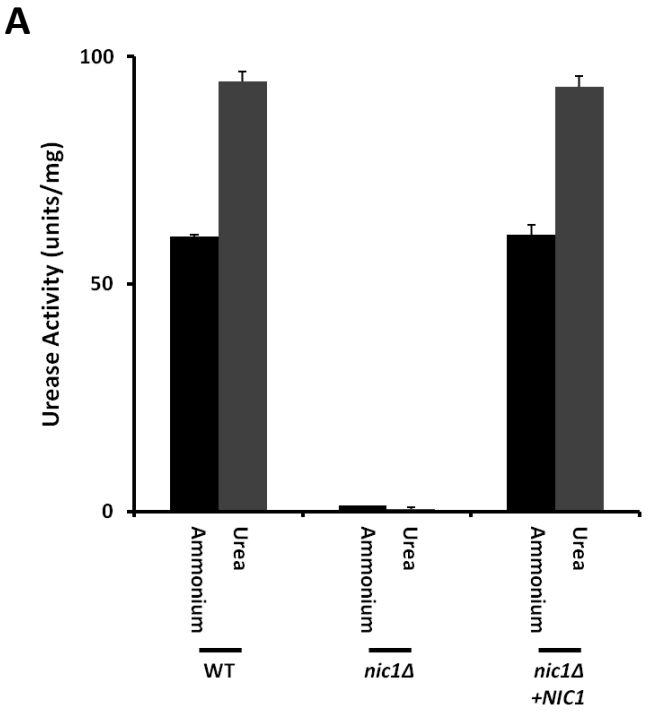
A
100
50
0
Urease Activity (units/mg)
Ammonium
Urea
Ammonium
Urea
Ammonium
Urea
WT
nic1Δ
nic1Δ
+NIC1

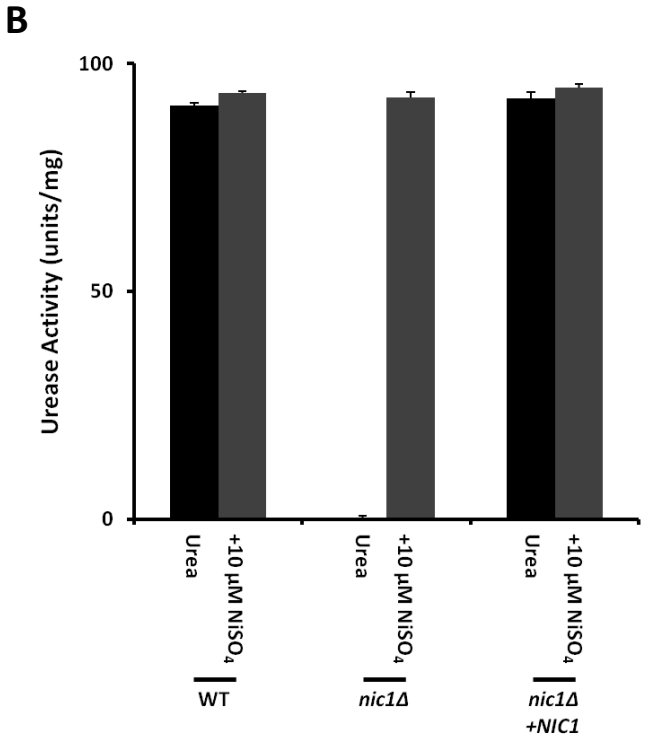
B
100
50
0
Urease Activity (units/mg)
Urea
+10 μM NiSO4
Urea
+10 μM NiSO4
Urea
+10 μM NiSO4
WT
nic1Δ
nic1Δ
+NIC1

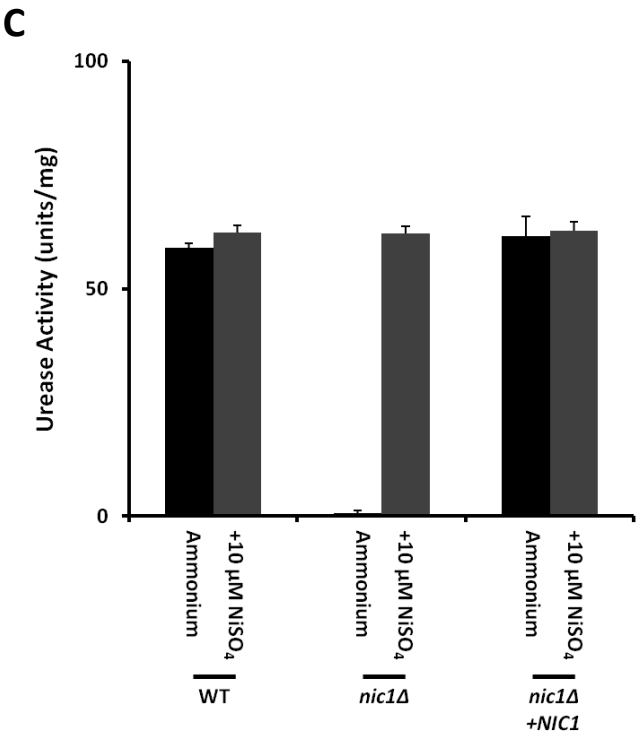
C
100
50
0
Urease Activity (units/mg)
Ammonium
+10 µM NiSO4
Ammonium
+10 µM NiSO4
Ammonium
+10 µM NiSO4
WT
nic1Δ
nic1Δ
+NIC1

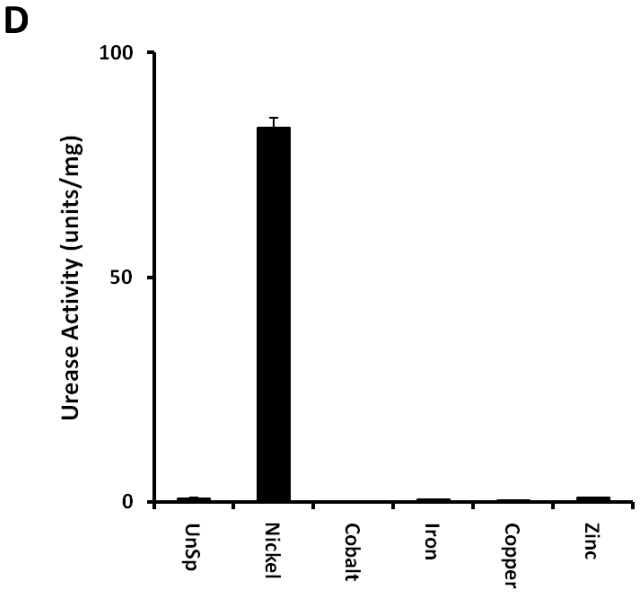
D
100
50
0
Urease Activity (units/mg)
UnSp
Nickel
Cobalt
Iron
Copper
Zinc

Figure 25 - The urease activity of *nic1Δ* is restored by addition of nickel.

A - The wild-type, *nic1Δ* and *nic1Δ+NIC1* strains were grown to mid-log in minimal media containing ammonium or urea as the sole source of nitrogen. The urease activity of protein extracts was determined.

B and C - The wild-type, *nic1Δ* and *nic1Δ+NIC1* strains were grown to mid-log in minimal media containing urea as the sole source of nitrogen with or without nickel added to 10 μM (B), and in ammonium based minimal media with or without 10 μM nickel (C). The urease activity of each sample was then determined.

D- The *nic1Δ* strain was grown to mid-log in urea media either unsupplemented (UnSp) or with 10 μM $NiSO_4$, $CoCl_2$, $Fe_2(SO_4)_3$ or $ZnCl_2$ added. Protein was extracted and the urease activity of each sample was determined.

Data points shown represent the mean of 3 repeat experiments and error bars represent the standard deviation.

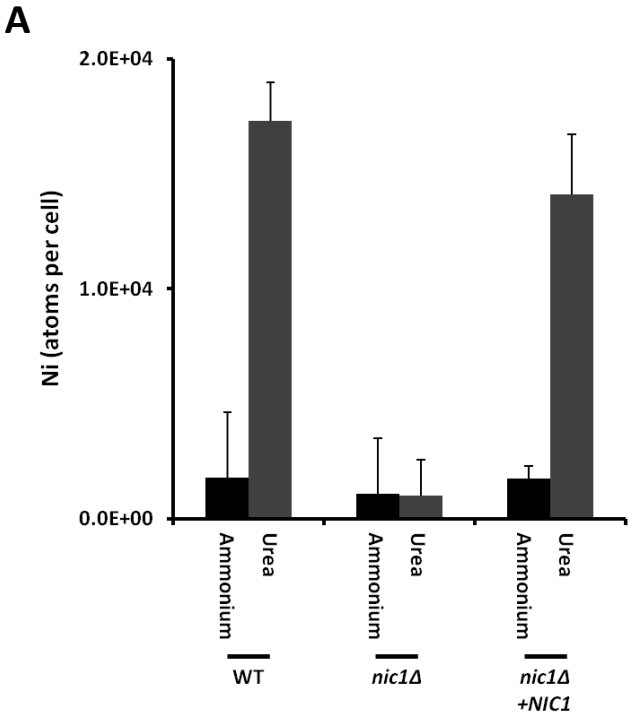
A
2.0E+04
1.0E+04
0.0E+00
Ni (atoms per cell)
Ammonium
Urea
Ammonium
Urea
Ammonium
Urea
WT
nic1Δ
nic1Δ
+NIC1

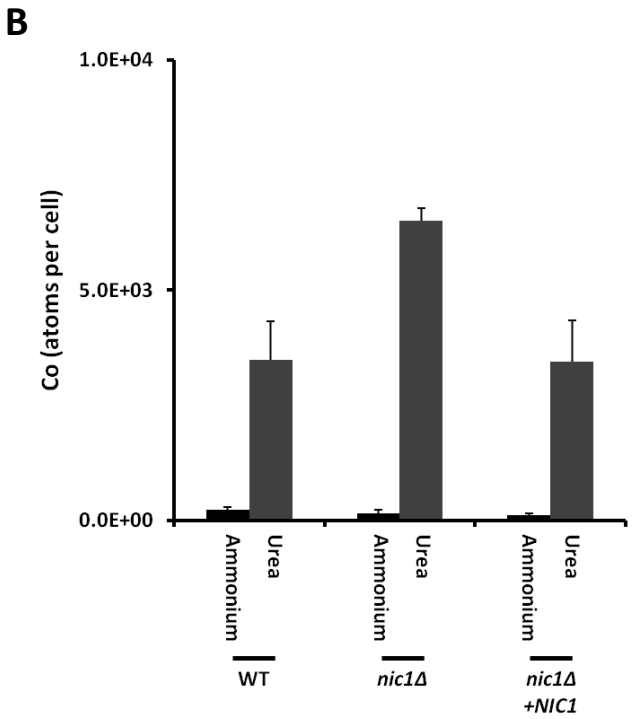
B
1.0E+04
5.0E+03
0.0E+00
Co (atoms per cell)
Ammonium
Urea
Ammonium
Urea
Ammonium
Urea
WT
nic1Δ
nic1Δ
+NIC1

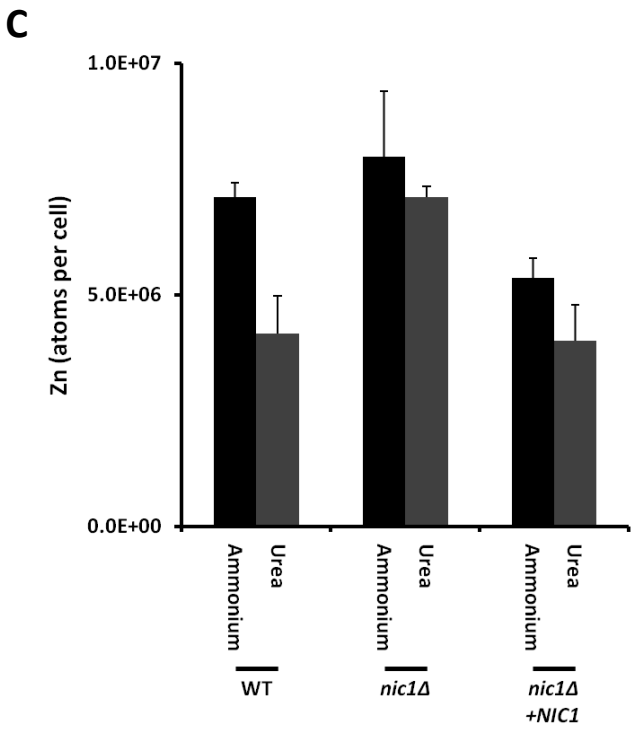

Figure 26 - *NIC1* is required for nickel accumulation.

The wild-type, *nic1Δ* and *nic1Δ+NIC1* strains were grown to mid-log in minimal media containing ammonium or urea as the sole source of nitrogen. Cell number was recorded. The cellular concentration of nickel (A), cobalt (B) and zinc (C) was determined by ICP-MS. Data points shown represent the mean of 3 repeat experiments and error bars represent the standard deviation.

The reduced urease activity in the *nic1Δ* strain is consistent with *Cn*Nic1 being a nickel transporter. To investigate the role of *Cn*Nic1 in nickel accumulation, metal levels were quantified in wild-type, *nic1Δ* and *nic1Δ+NIC1* cells grown in minimal media containing ammonium or urea as the sole source of nitrogen. The *nic1Δ* strain did not accumulate nickel in response to urea as observed for the wild-type strain (Figure 26A). This established that *Cn*Nic1 is required for nickel accumulation in *C. neoformans*. Levels of cobalt accumulation in the *nic1Δ* strain are greater when grown in urea compared to ammonium media (Figure 26C). Therefore, *Cn*Nic1 is not required for the accumulation of cobalt in response to urea.

3.4.3. *UREG*

The product of CNAG_00678 in the *C. neoformans* genome database is highly homologous to the UreG of *H. pylori* (55% identity) and is designated *Cn*UreG. *Cn*UreG contains sequences conserved with the UreG proteins from other species, including the GTP-binding P-loop and a conserved cysteine residue, which is predicted to oxidise to form a homodimer in *Bp*UreG and *Mt*UreG and be part of a metal binding site in *Hp*UreG and *Ka*UreG (Figure 27). These similarities are consistent with *Cn*UreG being a GTPase involved in nickel insertion into the urease active site.

The *Cn*UreG has an N-terminal extension containing 17 histidine residues the function of which is unknown. This region is common to urease expressed in fungi including *S. pombe* and *C. immitis* (Figure 27). *Mt*UreG has a similar extension that is shorter and contains 4 histidine residues. All of these species lack the nickel chaperone UreE. As histidine is a good metal ligand, this domain of the protein has a potential role in nickel binding for storage or as a chaperone.

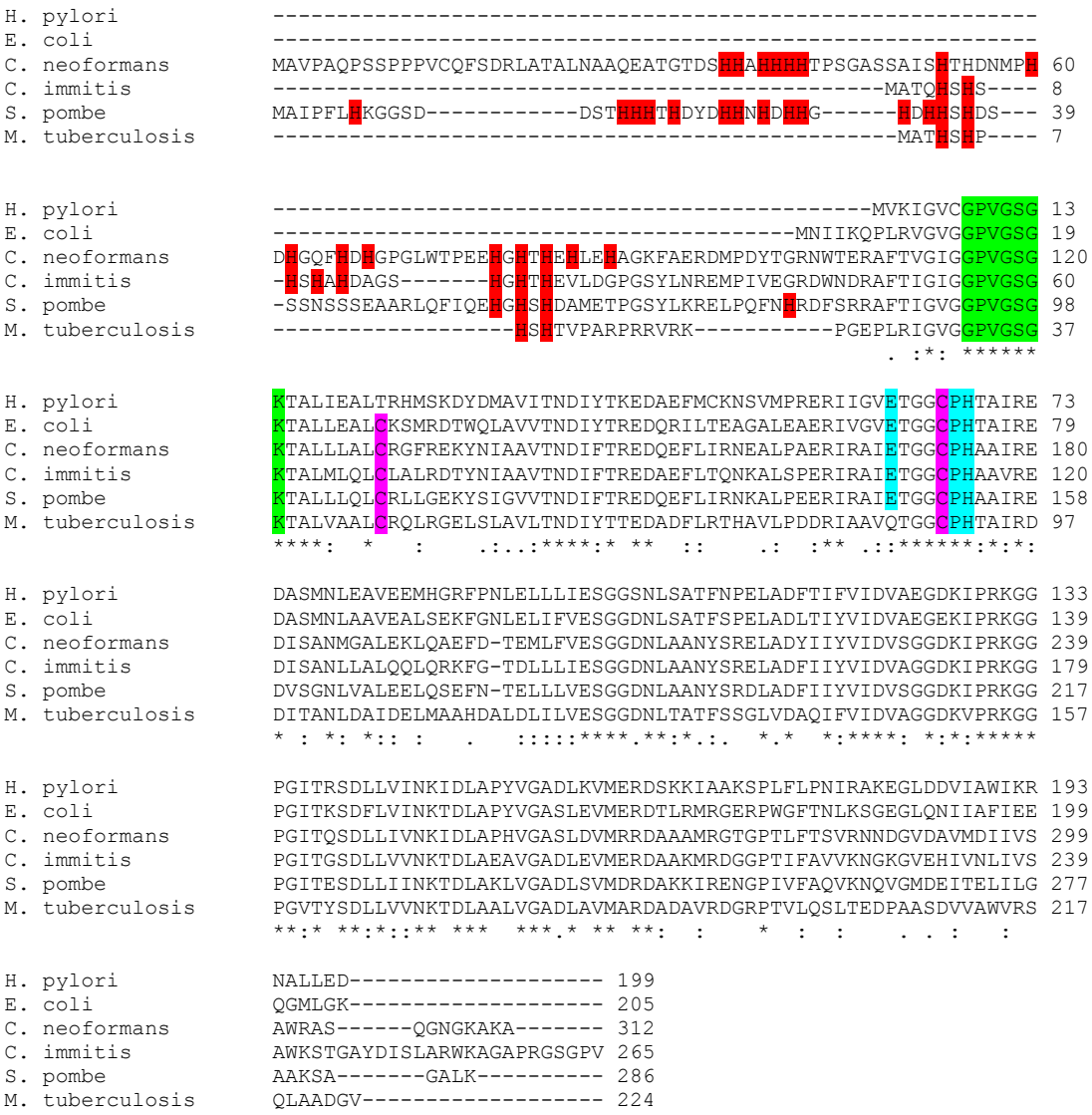

Figure 27 - UreG sequence alignment from multiple species.

A ClustalW2 alignment of the UreG protein sequence from *H. pylori*, *E. coli*, *C .neoformans*, *C. immitis*, *S. pombe* and *M. tuberculosis*. The GTP binding P-loop is highlighted in green, the putative zinc-binding site of *Hp*UreG in cyan, the conserved cysteine residues in pink and the N-terminal histidine residues in red.

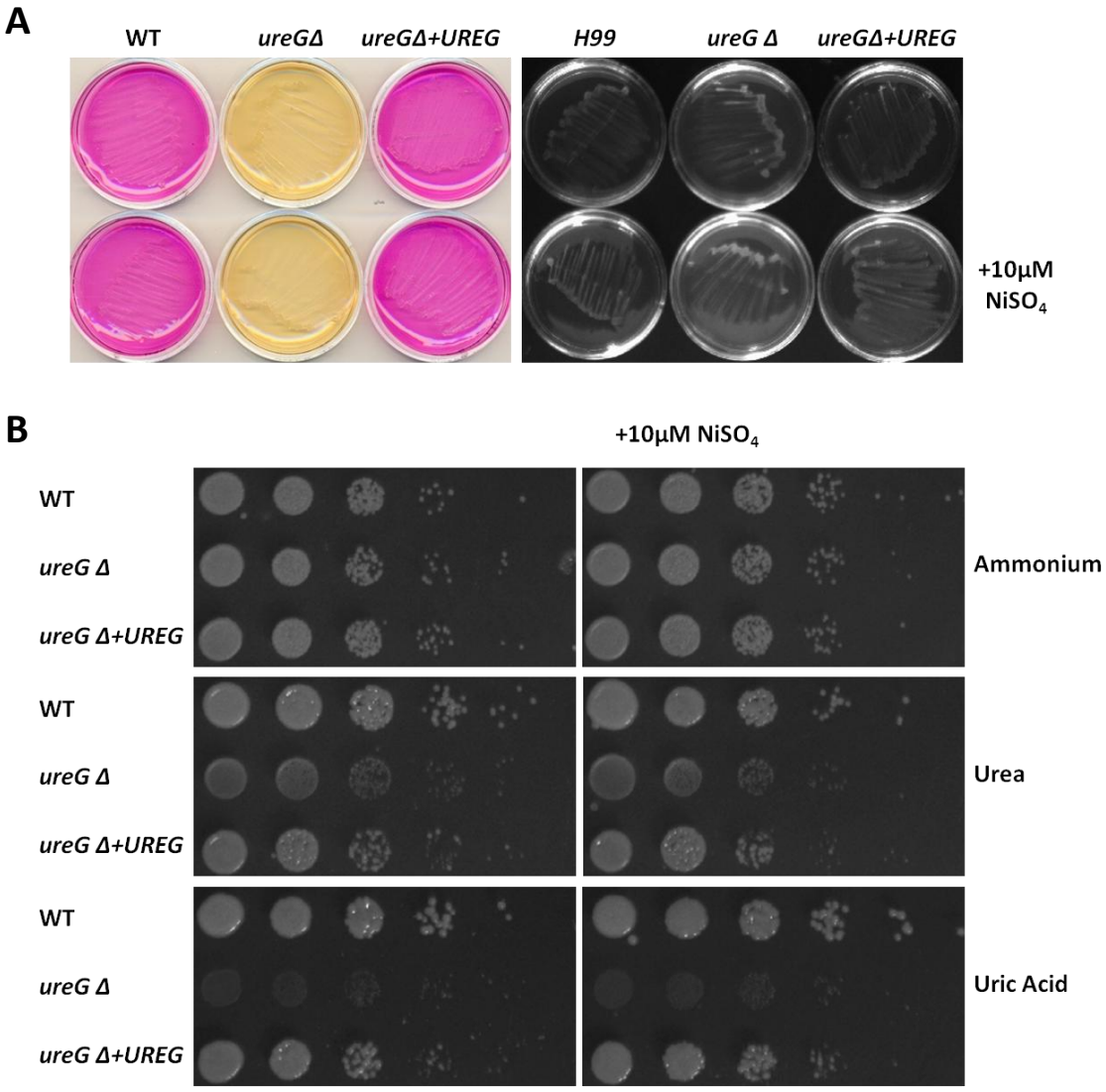

Figure 28 - *UREG* is required for growth on urea and uric acid based media.

A - The wild-type, *ureGΔ* and *ureGΔ+UREG* strains were streaked onto Christensen's urea agar with and without $NiSO_4$ added to 10 µM. Ability to change the media from yellow to pink was recorded by colour scan (left hand panel) and equal loading confirmed by grey-scale photograph (right hand panel).

B - The wild-type, *ureGΔ* and ureG*Δ+UREG* strains were plated in serial dilutions onto minimal media containing either ammonium, urea or uric acid as the sole source of nitrogen both with and without $NiSO_4$ added to 10 µM. The plates were incubated at 30^{o}C for 3 days and then photographed.

Data are representative of 3 repeat experiments.

To determine if *Cn*UreG is required for the utilisation of urea as a nitrogen source the wild-type, *ureGΔ* and *ureGΔ+UREG* strain were plated in serial dilutions on minimal agar media containing ammonium, urea or uric acid as the sole source of nitrogen. The *ureGΔ* strain showed a significantly reduced ability to grow utilising urea or uric acid as a source of nitrogen (Figure 28). Growth could not be recovered by addition of nickel as in the case of the *nic1Δ* strain which might be expected for a mutant lacking a nickel chaperone.

To quantify urease activity in the *ureGΔ* strain, urease activity assay were performed using cell extracts from the wild-type, *ureGΔ* and *ureGΔ+UREG* strains grown in media containing ammonium or glutamic acid as the sole source of nitrogen. No urease activity was detected in the *ureGΔ* cell extract, comparable to that of the *ure1Δ* cell extract (Figure 21, Figure 29). This is consistent with UreG acting as a GTPase that is required for maturation of the urease active site.

To investigate the role of *Cn*UreG in nickel accumulation, nickel levels were quantified in wild-type, *ureGΔ*, and *ureGΔ+UREG* cells grown in minimal ammonium or glutamic acid media. The *ureGΔ* strain accumulated nickel in response to glutamic acid, but similar to the *ure1Δ* strain showed a small but consistent reduction compared to the wild-type strain (Figure 30). As UreG is required for maturation, and thus nickel loading, this supports the theory that this decrease represents urease associated nickel.

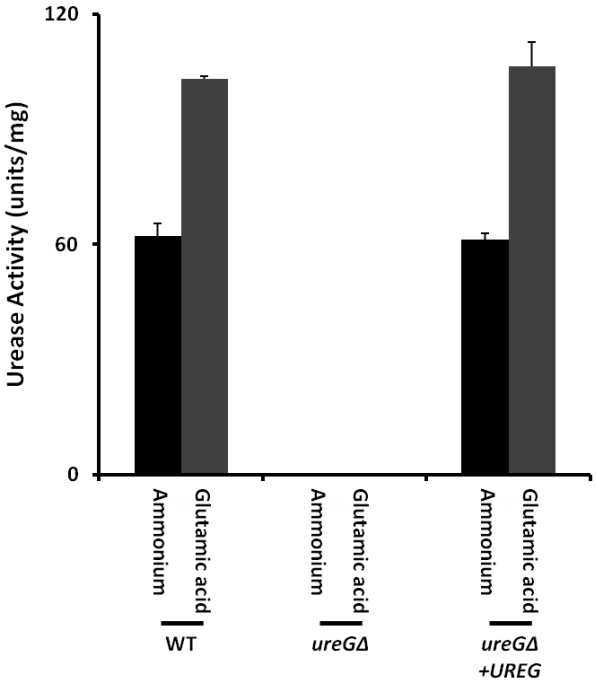

Figure 29 - *UREG* is required for urease activity.

The wild-type, *ureGΔ* and ureG*Δ+UREG* strains were grown to mid-log in minimal media containing ammonium or glutamic acid as the sole source of nitrogen. Urease activity of protein extracts was determined. Data points shown represent the mean of 3 repeat experiments and error bars represent the standard deviation.

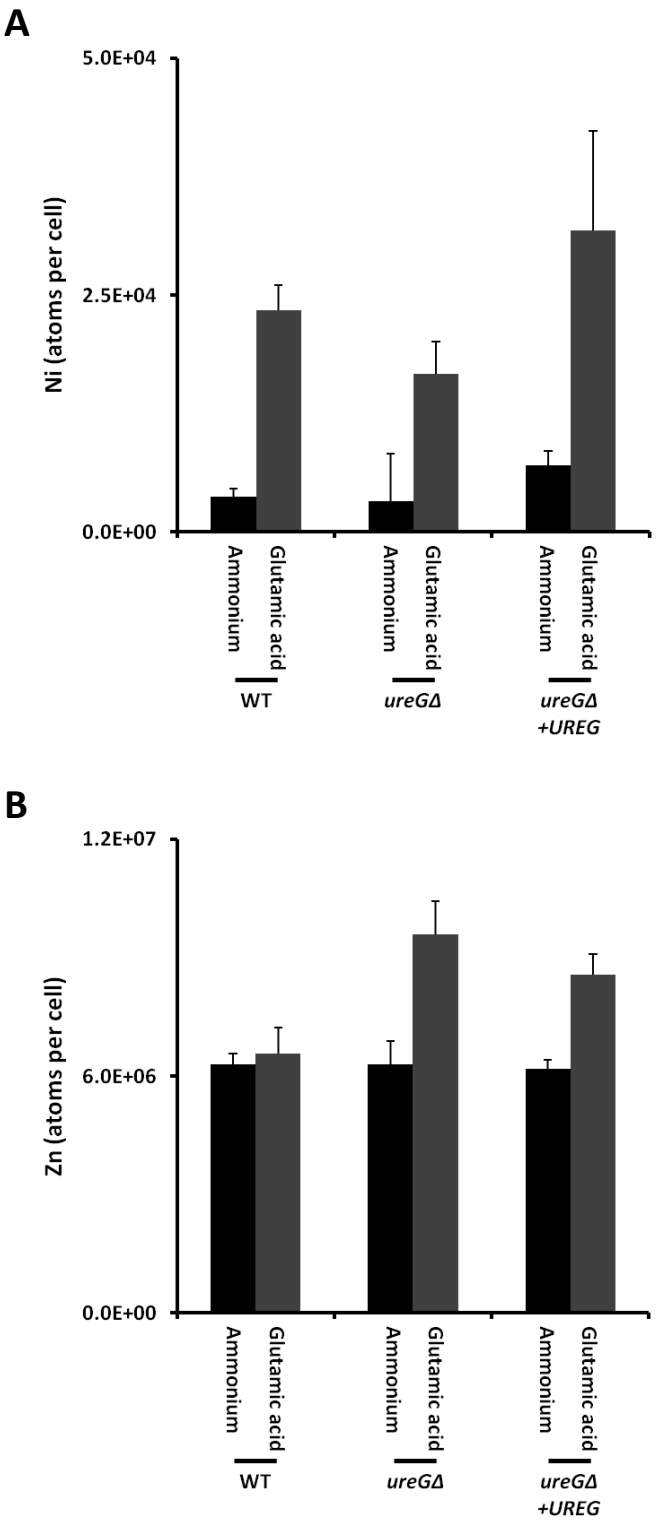

Figure 30 - *UREG* is not required for nickel accumulation.

The wild-type, *ureGΔ* and ureG*Δ+UREG* strains were grown to mid-log in minimal media containing ammonium or glutamic acid as the sole source of nitrogen. The cellular concentration of nickel (A) and zinc (B) was determined by ICP-MS. Data points shown represent the mean of 3 repeat experiments and error bars represent the standard deviation.

3.7. Discussion

The metabolism of urea to ammonium by *C. neoformans* has been identified as a virulence factor. As the enzyme urease requires a nickel or iron cofactor the homeostasis of these metals is potentially linked to virulence. The ability of *C. neoformans* to grow utilising different nitrogen sources was investigated to outline experimental parameters of growth. Growth of *C. neoformans* in uric acid was also of interest as it is degraded for use as a nitrogen source by a pathway that includes urease, is present in human blood and a major component of bird excreta, with which *C. neoformans* is commonly associated.

It was observed that capsule formed in response to urea. A similar result was published during the course of this study (Lee *et al*., 2011). The capsule is considered an important *C. neoformans* virulence factor and provides protection to the cell by inhibiting recognition by the host immune system, protecting the cell against phagocytosis and providing a barrier to cytotoxic agents (Bose *et al.*, 2003). Therefore regulation of capsule formation is important during infection. Ammonium grown cells exhibited a cell aggregation phenotype that the urea grown cells did not. In both cases the presence of urea induces a phenotype that may be linked to *C. neoformans* virulence (Olszewski *et al*., 2004; Okagaki *et al*., 2010). *C. neoformans* is likely to have access to between 2.5-6.6 mM urea in the human body which is sufficient for growth (Waring *et al.*, 2008). Whether urease activity is required to produce capsule or prevent cell aggregation in urea medium is not clear, but these phenotypes may be induced by urea in a urease independent manner. As the *ure1Δ* strain cannot grow utilising urea as the sole source a direct comparison with the wild-type strain under these conditions is not possible. Although the formation of cell aggregates may hinder entry to the small cerebral capillaries this model is not consistent with the data presented by *Shi et al.*, which established that urease is required for *C. neoformans* to transmigrate the capillary wall and deletion of urease does not affect entry and trapping of cells in the capillaries (Shi *et al.*, 2010a).

The levels of urease activity were responsive to the available nitrogen source. Higher levels of enzyme activity were observed for urea than ammonium grown cells. The glutamine and glutamic acid grown cells had intermediate levels of urease activity. This suggests that ammonium suppresses urease activity, as activity is lower in

ammonium grown cells than cells grown in any other individual nitrogen source. This also indicates that there is a level of positive regulation in response to urea. Regulation of urease may be achieved by a number of mechanisms; the accumulation of nickel, transcription of the urease gene, degradation of urease or maturation of the urease active site. The control of gene expression via nitrogen catabolite repression (NCR) has been well studied in *S. cerevisiae* (Magasanik and Kaiser, 2002). NCR utilises GATA transcription factors that regulate the expression of genes involved in nitrogen metabolism depending on the available nitrogen source. If a preferred nitrogen source is present expression of genes required for metabolism of less preferential nitrogen sources are repressed while those required to metabolise the preferred nitrogen source are up-regulated. In *C. neoformans* the Gat1 protein is the only NCR transcription factor and deletion of Gat1 abolishes growth when urea or uric acid are utilised as the nitrogen source. As the expression of *URE1* is increased in response to uric acid, NCR and gene transcription are likely to be involved in regulation of urease activity (Lee *et al*., 2011). A media switch experiment could be used to investigate this further, in which the wild-type and *gat1Δ* strains are grown in ammonium medium before switching to urea medium and *URE1* transcript levels of each strain determined before and after switching. This would establish if *URE1* transcription is up-regulated in urea and if Gat1 is required. A similar experiment could be used to determine if urease degradation is affected by available nitrogen source. Wild-type cells grown in urea media would be split into fresh ammonium and urea media samples and protein synthesis stopped by addition of cycloheximide. The levels of urease could then be monitored over time by western blot and relative rates of degradation of urease determined in each sample. To investigate if urease maturation regulates activity comparison of urease protein levels by western blot and urease activity would reveal if differences in activity are matched by differences in protein level between urea and ammonium grown cells. However, post-translational modifications to deactivate urease would not be detected by this assay. To investigate this a protein degradation assay in which urease activity was also measured could be used.

The regulation of nickel accumulation is responsive to the available nitrogen source, but does not correlate with urease activity. The loss of urea induced nickel accumulation in the *nic1Δ* strain demonstrated that *Cn*Nic1 is the primary means of

nickel accumulation and is therefore a putative nickel importer. The regulation of iron and copper uptake in *S. cerevisiae* utilises metal responsive transcription factors with degradation of the metal transporters. In copper regulation the high-affinity copper uptake systems, Ctr1p and Ctr3p, are expressed in response to low copper condition via the Mac1p transcription factor and degraded in copper replete conditions in a Mac1p dependent manner (Yamaguchi-Iwai 1996, Ooi 1996, Labbé 1997, Yonkovich 2002). The regulation of iron uptake systems in *S. cerevisiae* is responsive to iron bio-availability by the Aft1 and Aft2 transcription factors that activate expression of iron uptake genes when iron is limiting (Casas *et al*., 1997; Blaiseau *et al*., 2001). Aft1 is also responsive to levels of available glucose via Snf1, which activates increased iron uptake to facilitate aerobic respiration (Haurie *et al*., 2003). It is not clear if *Cn*Nic1 expression in *C. neoformans* is regulated in response to nickel availability. This could be investigated by determination of *Cn*Nic1 protein or mRNA levels in cells grown in nickel limiting and nickel replete media. The nitrogen source responsive accumulation of nickel indicates that regulation of nickel accumulation may be NCR responsive and controlled by the Gat1 transcription factor. This could be investigated further by determination of *Cn*Nic1 protein and mRNA levels in cells grown in ammonium and urea media.

The low levels of urease activity in YPD grown cells indicate that either one or more of the many potential nitrogen sources in the medium significantly suppresses urease activity. The levels of nickel accumulated in YPD grown cells is higher than those of ammonium grown cells. This is likely to be due to higher concentration of metals in YPD compared to minimal media. Therefore metal accumulation in YPD grown cells cannot be fairly compared with metal accumulation in cells grown in minimal media.

The level of urease activity is approximately half in ammonium grown cells compared to urea grown cells, however nickel accumulation in ammonium grown cells is a fraction of that in urea grown cells. This indicates that nickel is imported in excess of requirement to activate urease when urea is utilised as a nitrogen source. The *ure1Δ* and *ureGΔ* strains show a small decrease in nickel accumulation compared to wild-type in glutamic acid medium. As neither strain is able to insert nickel into urease this decease may be representative of nickel which is associated with urease. The excess nickel accumulated in response to urea cannot be stored in either urease or *Cn*UreG as the *ure1Δ* and *ureGΔ* strains accumulate significantly

more nickel when grown in glutamic acid compared to ammonium media. Although it is possible there are nickel storage proteins in *C. neoformans* which provide a similar function to hpn and hpn-like proteins of *H. pylori* there are no proteins with significant sequence homology to either in the *C. neoformans* genome. It is more likely that *C. neoformans* stores excess nickel in the vacuole, as *S. cerevisiae* does for surplus metals (MacDiarmid *et al*., 2000; Li *et al*., 2001). This could be investigated by separation of membrane bound organelles from the cytoplasm by centrifugation and analysis of metal content by ICP-MS.

Cobalt was accumulated in response to urea, glutamine and glutamic acid in a trend which closely resembles that of nickel accumulation. As cobalt was still accumulated in the absence of *Cn*Nic1 the uptake of cobalt cannot be via this transporter. *Cn*Nic1 belongs to a family of nickel-specific transporters. The low levels of urease activity in the *nic1Δ* strain and recovery of activity by addition of nickel to the media indicate that nickel is imported in the absence of *Cn*Nic1. Therefore there is a secondary nickel import system which has a lower affinity for nickel than *Cn*Nic1. Nickel import systems which utilise a high-affinity nickel-specific transporter and low-affinity non-specific transporter have been documented but the affinity of a non-specific transporter for nickel may be too low to facilitate significant levels of nickel accumulation in media without nickel supplementation (Eitinger and Mandrand-Berthelot, 2000). Two potential candidates for a secondary nickel import protein are Cramp, a natural resistance-associated macrophage protein (Nramp) homologue, and the *C. neoformans* homologue of CorA. CorA is a magnesium transporter which is also capable of transporting both nickel and cobalt (Niegowski and Eshaghi, 2007). The Cramp protein of *C. neoformans* has previously been demonstrated to transport both nickel and cobalt when expressed in *Xenopus laevis* oocytes (Agranoff *et al*., 2005). The localisation of Cramp and CorA in *C. neoformans* cells is unknown. A similar accumulation of cobalt in response to urea was recorded in wild-type and *nic1Δ* strains of *S. pombe*, which was attributed to the Nramp homologues of that species (Eitinger *et al.*, 2000). The generation of deletion mutants for these proteins in the wild-type and *nic1Δ* strain background would allow investigation into the roles of these transporters in nickel accumulation and urea metabolism.

4. Characterisation of the Nickel binding protein *Cn*UreG

4.1. Introduction

The maturation of urease is not fully understood but several accessory proteins that are required for maturation have been identified. In most bacterial urease maturation systems these include a nickel chaperone, UreE (Hausinger, 1994). In some bacteria the HypB nickel chaperone of the hydrogenase enzyme is also required to deliver nickel to urease (Olson *et al.*, 2001; Maier *et al*., 2007). No eukaryotic UreE or other known nickel chaperone is present in the NCBI database. Bacteria utilise nickel chaperones and it is reasonable to expect eukaryotes to do the same but it is unclear what acts as the nickel chaperone in eukaryotic urease systems. One candidate for this role in *C. neoformans* is *Cn*UreG.

UreG is a GTPase required for urease maturation along with other urease accessory proteins. *Cn*UreG has an approximately 100 amino acid N-terminal extension which includes 17 histidine residues and 1 cysteine residue. Histidine and cysteine are good metal ligands. Histidine rich N-terminal regions are only found on UreG in organisms that lack UreE. The nickel binding properties of UreG from *K. aerogenes*, *B. pasteurii* and *H .pylori* have been investigated; *Ka*UreG binds 1 nickel atom per monomer with a Kd of 16 μM, *Bp*UreG binds 4 nickel atoms per homodimer with a Kd of 360 μM and *Hp*UreG binds 4 nickel atoms per homodimer with a Kd of 10 μM (Zambelli *et al*., 2005; Zambelli *et al.*, 2009; Boer *et al*., 2010). The UreE proteins of these organisms bind nickel significantly more tightly. The highest affinity sites in *Ka*UreE, *Bp*UreE and *Hp*UreE are 0.78, 1.4 and 1 μM respectively (Brayman and Hausinger, 1996; Benoit and Maier, 2003; Stola *et al*., 2006). The characteristics of eukaryotic UreG proteins have been studied in little detail and metal binding affinities and capacities have not been determined (Freyermuth *et al*., 2001; Witte *et* al., 2001).

The aim of this chapter was to investigate the metal binding properties of *Cn*UreG. Recombinant *Cn*UreG was expressed and purified using immobilised metal ion affinity chromatography (IMAC). The binding capacity and affinity were determined for nickel, zinc and cobalt. Effects of metal binding on secondary structure were

analysed and the effect of nickel binding on the UV-visible profile of *Cn*UreG investigated.

4.2. Over-Expression and Purification of *Cn*UreG

4.2.1. Over-Expression of Soluble *Cn*UreG

Recombinant UreG was expressed from the plasmid pET29a-UreG under the inducible T7 promoter and without amino acid tags in the *E. coli* BL21 strain. *Cn*UreG was inducibly expressed at low levels and tended to be insoluble (Figure 31A). As CnUreG was expressed from *C. neoformans* cDNA many of the codons are rare in the BL21 *E. coli* strain. Rare codon tRNAs are present at low concentrations and so can be a rate limiting step in translation. To address this *Cn*UreG was expressed from the same plasmid in the Rosetta strain of *E. coli*, which expresses higher levels of eukaryotic tRNAs (Novagen). This did not increase either levels of *Cn*UreG expression or solubility (Figure 31B). *Cn*UreG is a potential metal binding protein and binding of a cofactor can help stabilise and solubilise a protein. To test if nickel increased expression or solubility *Cn*UreG was induced and expressed in the presence of 1 mM $NiSO_4$ for 6 hrs. This increased the solubility but did not increase the expression levels of *Cn*UreG (Figure 31C).

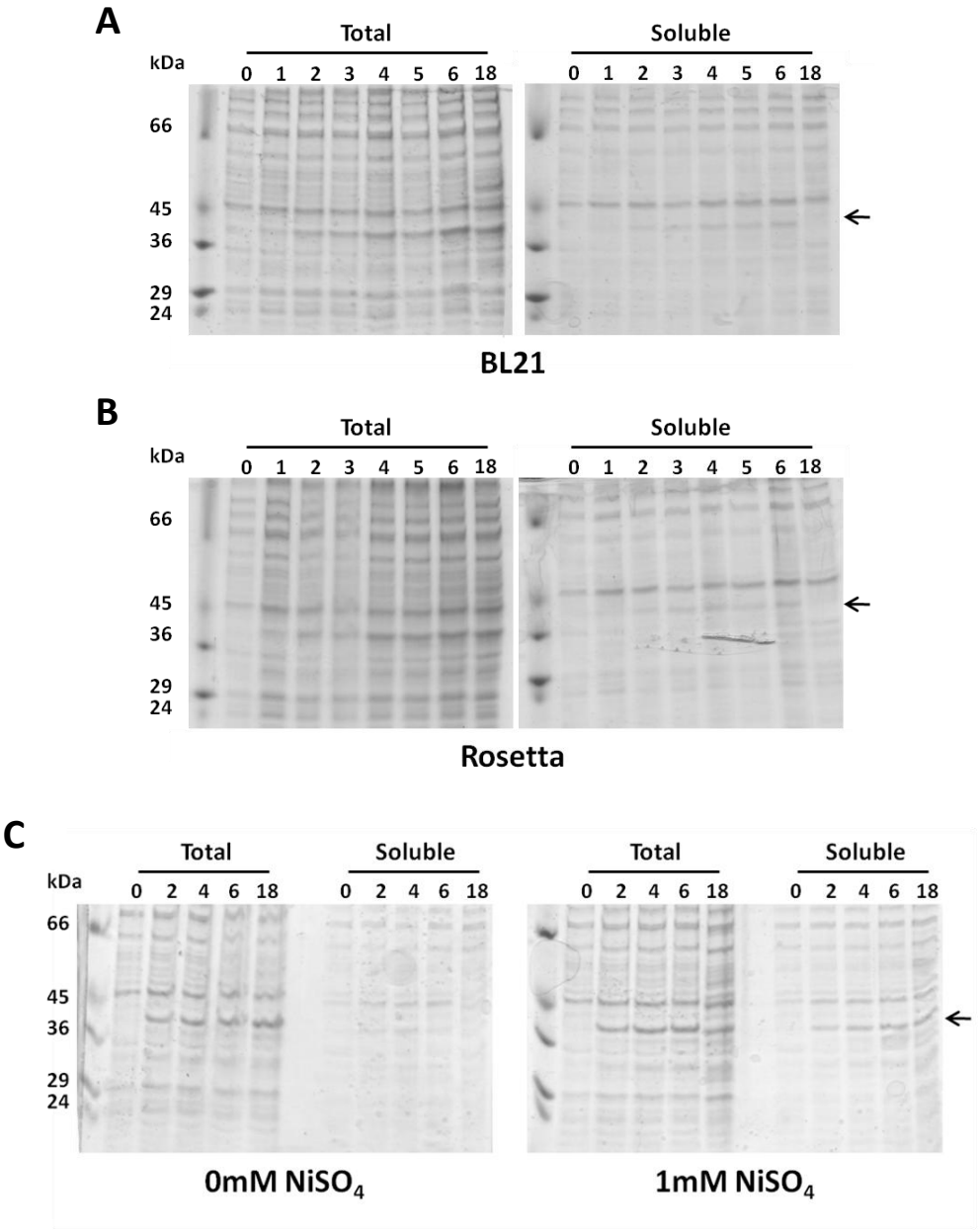

Figure 31 - Over-expression of soluble *Cn*UreG.

Native full length *Cn*UreG was expressed from the pET29a vector in BL21 (A) and Rosetta (B) strains of *E. coli*. $NiSO_4$ (1 mM) was added at the point of induction to increase *Cn*UreG solubility (C). Hours after induction are indicated above each lane. Soluble fractions were subject to centrifugation at 13 krpm to remove insoluble components. *Cn*UreG is indicated by black arrows to the right of each gel.

4.2.2. Purification by Tandem Nickel-Affinity Chromatography

Following the induction of *Cn*UreG, cells were pelleted then lysed by passage through a French pressure cell and the lysate subject to centrifugation to remove insoluble components. IMAC was used as an initial means of purification. The crude lysate was loaded onto a 5 ml His-Trap column and eluted over 20 column volumes on a 10-300 mM imidazole gradient in 2.5 ml fractions. *Cn*UreG eluted between fractions 16 and 42, which were collected and concentrated (Figure 32A). Analysis of this pooled fraction by SDS-PAGE revealed 3 major protein species in the mixture. Each of these was identified as *Cn*UreG by MALDI-PMF. MALDI-TOF was used to confirm that the size of the largest of these species was 33.6 kDa consistent with full length *Cn*UreG. This indicated that the smaller species were truncated forms of *Cn*UreG or degradation products. Attempts to separate the truncated forms of *Cn*UreG from the full length protein by anion exchange, cation exchange and size exclusion were unsuccessful. During the initial IMAC purification it was noted that truncated forms of *Cn*UreG resolved differently from the full length *Cn*UreG. Full length *Cn*UreG elution peaked around fraction 24 and the lower band around fraction 20 (Figure 32A). To separate the different *Cn*UreG forms the sample was loaded onto a 5 ml His-Trap column and eluted over 80 column volumes on a 60-200 mM imidazole gradient with 5ml fraction volumes. *Cn*UreG eluted across fractions 15 to 72 (Figure 32B). To prevent collection of the truncated forms of *Cn*UreG only fractions 28 to 72 were collected. These fractions were concentrated by re-loading onto a 5 ml His-Trap column and single-step elution at 300 mM imidazole (Figure 32C).

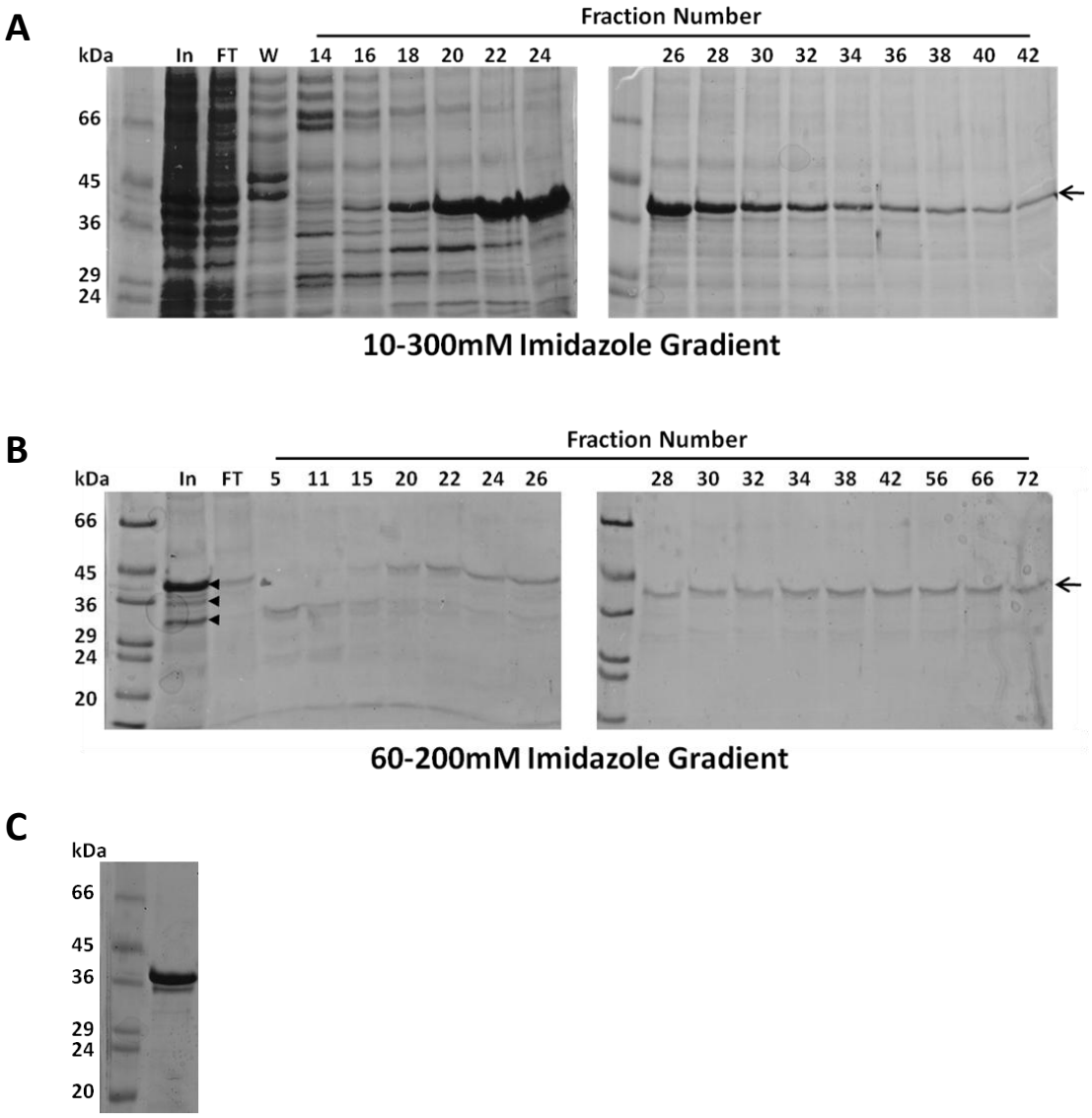

Figure 32 - Purification of *Cn*UreG by tandem IMAC.

A - The initial *Cn*UreG purification was performed using a 5 ml His-Trap column. Cell lysate was subject to centrifugation and supernatant loaded onto the column. Elution was performed over 20 column volumes on a 10-300 mM imidazole gradient using a 2.5 ml fraction volume. Input to the column (In) and the flow through (FT) are indicated. The position of *Cn*UreG is indicated by the black arrow to the right of the gel.

B - To further purify *Cn*UreG the sample was re-loaded onto a 5 ml His-Trap column. Elution was performed over 80 column volumes on a 60-200 mM gradient using 5 ml fraction volumes. The position of full length *Cn*UreG is indicated by the black arrow to the right of the gel. The 3 major components of the input (In) are indicated by black arrows to the right of that lane.

C - The fractions containing full length *Cn*UreG were collected and pooled. The sample was concentrated by re-loading onto a 5 ml His-Trap column and a single elution step at 300 mM imidazole.

The purified *Cn*UreG was analysed by ICP-MS and found to contain ~1 equivalent of nickel. This was removed by incubation of the sample with 1 mM EDTA for 72 hours at 5^{o}C. The EDTA was removed by buffer exchange and the sample re-analysed by ICP-MS and found to contain <0.005 equivalents of nickel. *Cn*UreG is predicted to have a mass of 33.6 kDa and resolved with an apparent mass of ~40 kDa by SDS-PAGE. An increased apparent mass has been previously observed in histidine-rich protein but not bacterial UreG proteins (Ge *et al*., 2006).

4.3 *Cn*UreG is Able to bind Ni, Zn and Co *in vitro*

4.3.1. Determination of Stoichiometery and Affinity for Ni, Zn and Co

The ability of *Cn*UreG to bind metal had been indicated by the increased solubility during expression in the presence of nickel, it's ability to bind to a nickel column and the nickel associated with the protein after purification. To investigate the metal binding stoichiometery of *Cn*UreG a desalting column based assay was used. Apo-*Cn*UreG was separately incubated with 20 molar equivalents of nickel, zinc and cobalt at 4^{o}C for 1 hour prior to passage through a desalting column. The eluted fractions were collected. Protein concentration was determined by Bradford assay and metal concentration quantified by ICP-MS. The results established that *Cn*UreG binds 1.94 +/- 0.12 (mean +/- SD) equivalents of nickel, 3.78 +/- 0.18 equivalents of zinc and 1.70 +/- 0.12 equivalents of cobalt.

A

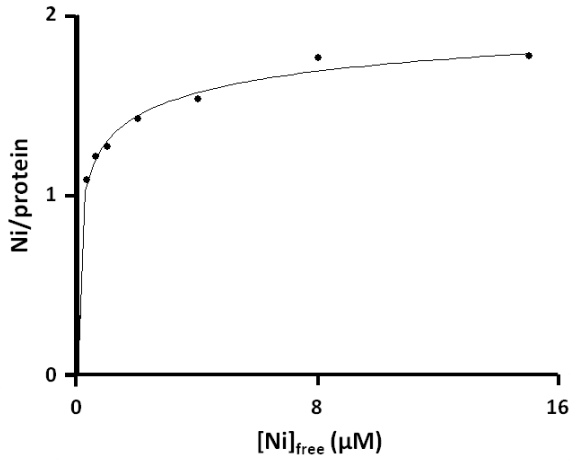
2
1
0
Ni/protein
0
8
16
[Ni]free (μM)

B

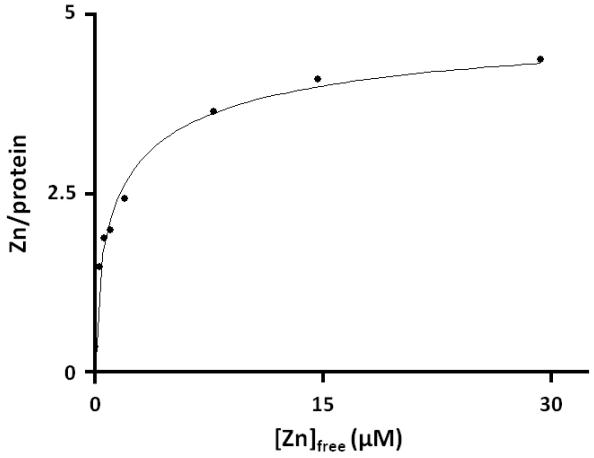
5
2.5
0
Zn/protein
0
15
30
[Zn]free (μM)

C

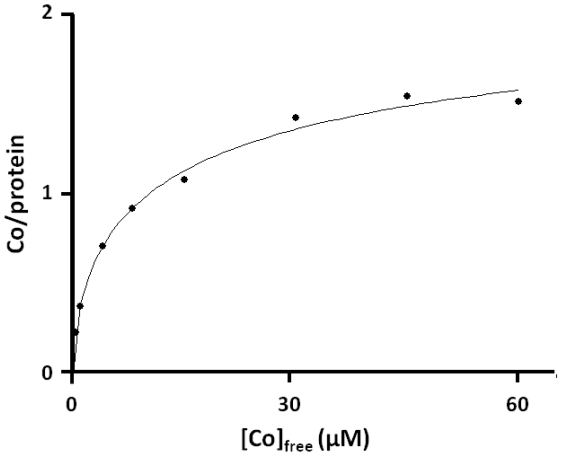
2
1
0
Co/protein
0
30
60
[Co]free (μM)

Figure 33 - Determination of binding capacity and Kd for nickel, zinc and cobalt.

Kinetics of metal binding to *Cn*UreG was determined by equilibrium dialysis. Apo-*Cn*UreG (3 μM) was dialysed overnight against increasing concentrations of nickel (A), zinc (B) and cobalt (C). Metal concentration on each side of the dialysis membrane was determined by ICP-MS. Metal binding capacity and Kd were determined using a Hill plot. Data are representative of 3 repeat experiments.

Equilibrium dialysis was used to further investigate the binding of metals to *Cn*UreG. Apo-*Cn*UreG was dialysed against increasing concentrations of nickel, zinc and cobalt. The metal concentration on each side of the dialysis membrane was determined by ICP-MS and used to calculate the level of *Cn*UreG bound metal. These data were then analysed using a Hill plot to determine B_{max} and Kd. The binding capacity determined in each case was; nickel 2.18 +/- 0.21, cobalt 2.26 +/- 0.39 and zinc 5.26 +/- 0.39 (Figure 33). Therefore, *Cn*UreG is capable of binding 2 equivalents of nickel or cobalt and up to 5.5 equivalents of zinc. The Kd determined in each case was; nickel <1 μM, cobalt 17.31 μM +/- 1.31 and zinc 2.14 μM +/- 0.93 (Figure 33). This established that nickel is bound significantly more tightly to *Cn*UreG than cobalt. The Kd is calculated as an average for all of the metal binding sites so relative nickel and zinc affinity is not clear. To determine whether nickel or zinc had the higher affinity a modification of the desalting column assay was used. Apo-*Cn*UreG was incubated with 2 equivalents nickel and increasing equivalents of zinc added prior to passage through a desalting column. The eluted fractions were analysed for protein and metal content. This showed that more nickel is bound to *Cn*UreG even when equal amounts of nickel and zinc were added (Figure 34).

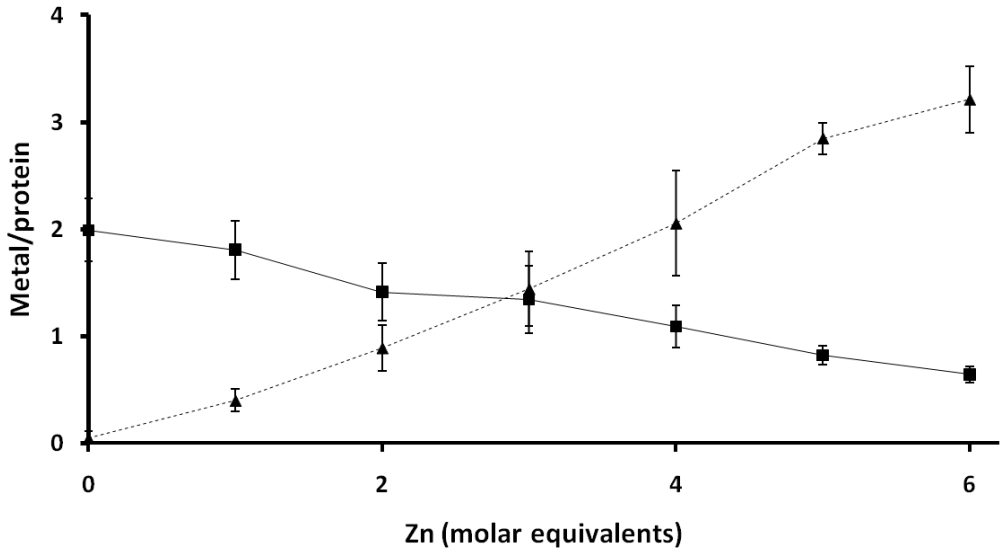

Figure 34 - Nickel-zinc binding competition assay.

Relative ability of nickel and zinc to bind *Cn*UreG was determined by a desalting column based assay. Apo-*Cn*UreG (2 μM) was incubated with 2 molar equivalents of nickel and increasing equivalents of zinc prior to passage through a PD10 desalting column. The fractions containing *Cn*UreG were analysed for protein concentration by Bradford assay and metal concentration by ICP-MS. Nickel (squares) and zinc (triangles) molar equivalents to *Cn*UreG were calculated and plotted. Data points represent the mean and error bars the standard deviation of 3 repeat experiments.

4.3.2. UV-Vis Spectroscopic Analysis of Metal Binding

The binding of metals to ligands, including amino acid residues of proteins, can result in changes in absorbance across the UV-visible spectrum caused by ligand to metal charge transfer (LMCT). To study the effects of nickel binding to *Cn*UreG the absorbance across this spectrum was recorded following the addition of 0, 1, 2, 3 5 and 10 molar equivalents of nickel to the apo-protein (Figure 35A). When the apo-*Cn*UreG spectrum was subtracted from the nickel-*Cn*UreG spectra it was apparent that 3 peaks in absorbance at 287, 293 and 326 nm were generated (Figure 35B). There was also a general increase in absorbance between 250-500 nm, which can result from nickel binding to histidine residues (Ge *et al*., 2006). The peak at 326nm is apparent even without subtraction of the apo-*Cn*UreG sample (Figure 35A). The bands at 287 and 293 nm appear when 1 and 2 equivalents of nickel were added. The 326 nm peak was only apparent after 3 or more equivalents of nickel had been added and continued to increase with each subsequent addition of nickel. The spectrum could not be recorded for higher than 10 equivalents of nickel due to protein precipitation.

The stoichiometery of nickel binding to *Cn*UreG has been established at 2 equivalents suggesting that the 326 nm peak represents super-stoichiometric nickel binding. To confirm this, the 5 and 10 molar equivalent samples were passed through a desalting column to remove loosely bound nickel. The UV-visible spectra of the samples were monitored and the protein concentration was determined by Bradford assay and the nickel concentration by ICP-MS analysis. The eluted samples no longer generated an absorbance peak at 326 nm and the ratio of nickel to *Cn*UreG was 2.09 and 1.90 for the 5 and 10 nickel equivalent samples, respectively (Figure 36). This established that *Cn*UreG is able to bind 2 equivalents of nickel with high affinity and additional nickel atoms at a lower affinity. The lower affinity sites give rise to the 326 nm peak and the general increase in absorbance across 250-500 nm.

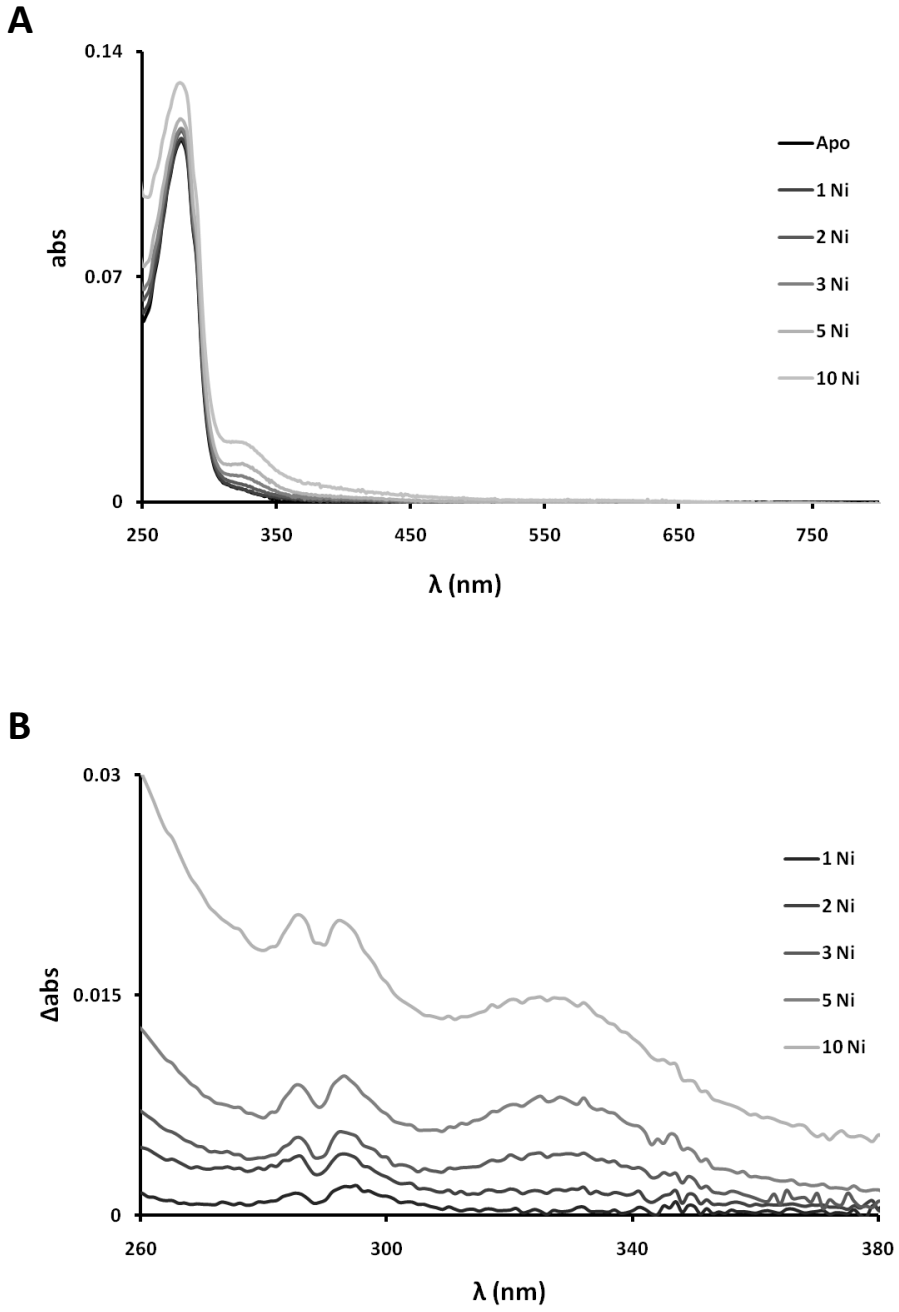

Figure 35 - The UV-visible absorbance spectrum of *Cn*UreG changes on nickel binding.

A - UV-visible absorbance spectra of *Cn*UreG (8 μM) incubated in the absence and presence of nickel. Apo-*Cn*UreG was incubated with 0, 1, 2, 3, 5 and 10 molar equivalents of nickel prior absorbance measurements.

B - Differential UV-visible absorbance spectra of nickel binding to *Cn*UreG. Spectra for 1, 2, 3, 5 and 10 molar equivalent incubated with *Cn*UreG following subtraction of the apo-*Cn*UreG spectrum.

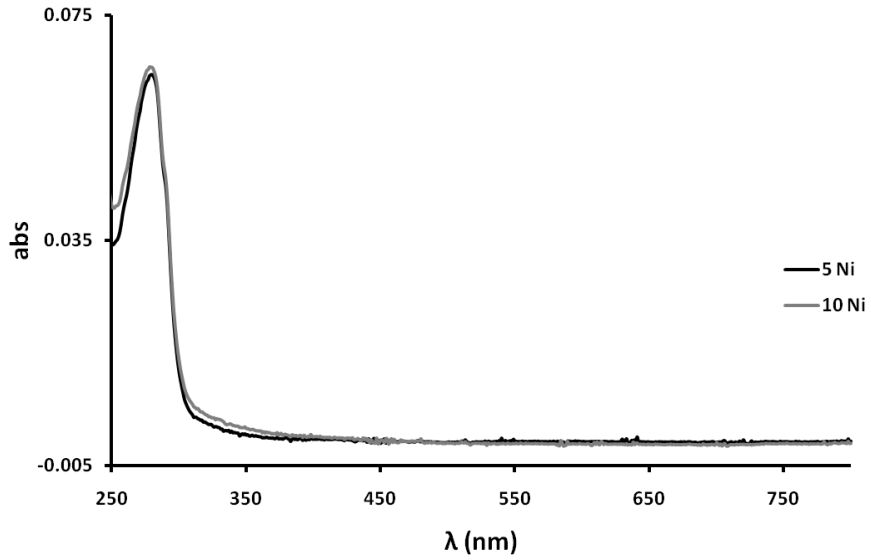

Figure 36 - The UV-visible absorbance spectrum of nickel-loaded *Cn*UreG.

UV-visible absorbance spectra for nickel loaded samples after desalting. The 5 and 10 molar equivalent samples were passed through a desalting column. The eluted fractions containing *Cn*UreG were collected and the absorbance spectra recorded. Relative protein and metal concentrations were determined by Bradford assay and ICP-MS.

4.3.3. Metal Binding Alters the Secondary Structure of *Cn*UreG

The secondary structure of a protein can be analysed by using CD spectroscopy across the Far-UV spectrum. The Far-UV CD profile for *Cn*UreG was analysed and revealed a profile very similar to those of *Bp*UreG and *Mt*UreG (Zambelli *et al*., 2005; Neyroz *et al*., 2006). The deep negative peak at 206 nm is indicative of a largely unstructured protein and the positive peak at 190 nm suggests some β-sheet and the shoulder between 212-222 nm indicates a small proportion of α-helix (Figure 37). When the *Cn*UreG spectra was analysed using the K2D server a composition of 9 % α-helix, 36 % β-sheet and 55 % random coil was calculated, indicating that *Cn*UreG is less structured than either *Bp*UreG or *Mt*UreG (K2d site). Addition of nickel caused a reduction in the negative 206nm peak, an increase in the 190nm peak and increased definition of the 212-222 nm shoulder. This suggests that *Cn*UreG is folding in the presence of nickel. This folding only represents a small change in the overall structure, which may be due to a single region folding or a small change across the whole protein. The most significant changes in the CD spectra occur between 0 and 1 molar equivalents of nickel. This shows the folding of *Cn*UreG occurs in the presence of only 1 nickel atom.

The Far-UV CD spectra of *Cn*UreG samples with up to 6 molar equivalents of zinc added was recorded. Addition of zinc reduced the random coil signal and increased the β-sheet signal, however the α-helix content appeared unchanged. Structural changes occurred responsive to the full range of zinc additions, indicating that *Cn*UreG folds differently in the presence of zinc and nickel (Figure 38). The effect of cobalt binding to *Cn*UreG on the Far-UV CD spectrum was also investigated. Addition of cobalt produced relatively little change in the secondary structure of *Cn*UreG compared to addition of nickel or zinc, but small changes in the α-helix and β-sheet signal were observed (Figure 39).

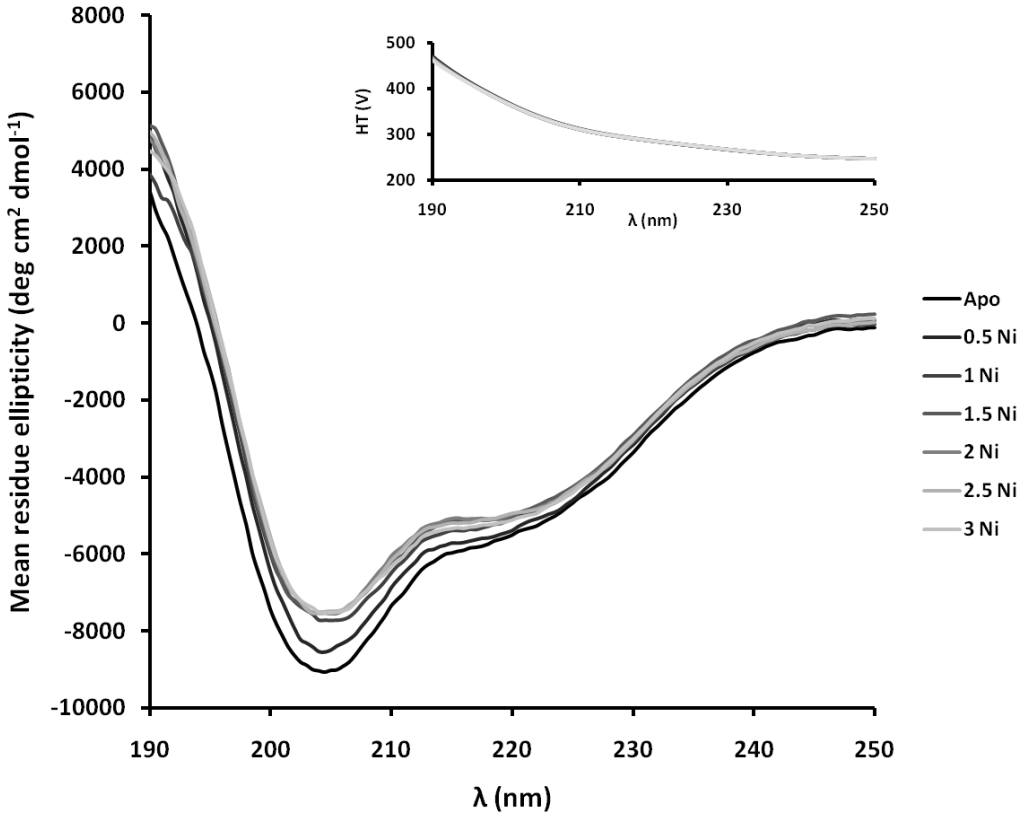

Figure 37 - The effect of nickel binding on *Cn*UreG secondary structure.

Secondary structure of *Cn*UreG was examined in the presence and absence of nickel by far-UV circular dichroism. Data were collected for 0.5mg/ml *Cn*UreG incubated in 20mM Tris-HCl, pH 8 with 0-3 molar equivalents of nickel added in 0.5 equivalent increments. Values are presented in mean residue ellipticity. The insert shows the High Tension (HT) measured over the same spectrum. Data are representative of 3 repeat experiments.

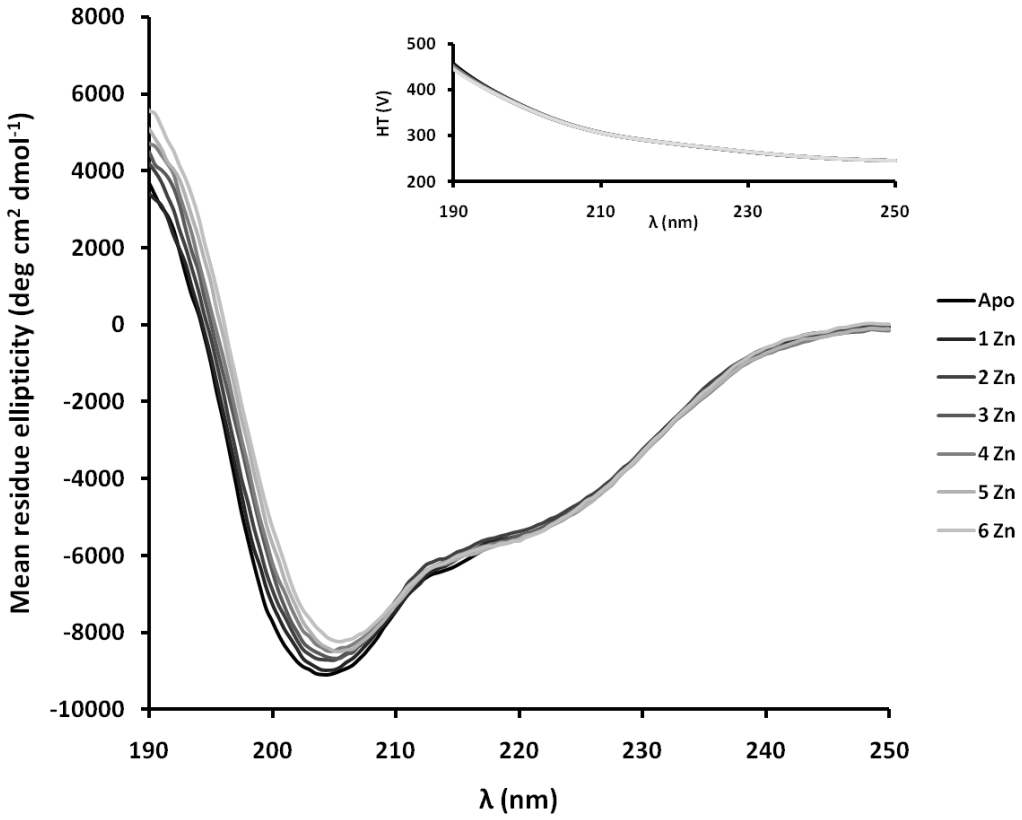

Figure 38 - The effect of zinc binding on *Cn*UreG secondary structure.

Secondary structure of *Cn*UreG was examined in the presence and absence of zinc by Far-UV circular dichroism. Data were collected for 0.5 mg/ml *Cn*UreG incubated in 20 mM Tris-HCl, pH 8 with 0-6 molar equivalents of zinc added in 1 equivalent increments. Values are presented in mean residue ellipticity. The insert shows the High Tension (HT) measured over the same spectrum. Data are representative of 3 repeat experiments.

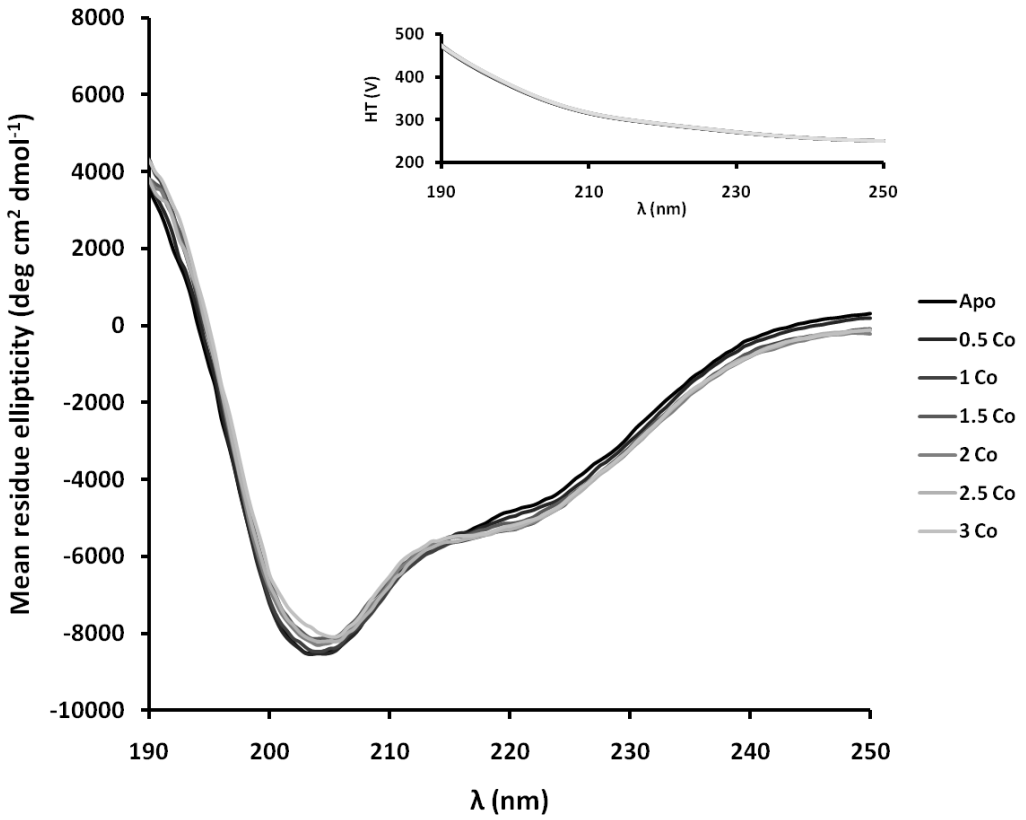

Figure 39 - The effect of cobalt binding on *Cn*UreG secondary structure.

Secondary structure of *Cn*UreG was examined in the presence and absence of cobalt by far-UV circular dichroism. Data were collected for 0.5 mg/ml *Cn*UreG incubated in 20 mM Tris-HCl, pH 8 with 0-3 molar equivalents of cobalt added in 0.5 equivalent increments. Values are presented in mean residue ellipticity. The insert shows the High Tension (HT) measured over the same spectrum. Data are representative of 3 repeat experiments.

4.3.4. UreG Forms a High-MW Species When Nickel-Loaded

During the purification of recombinant *Cn*UreG size exclusion chromatography did not separate full length *Cn*UreG from its truncated forms. *Cn*UreG was eluted in fractions that included a 47.3 kDa peak and a high molecular weight peak that eluted in the column void and was therefore larger than 440 kDa (Figure 40A). The UreG proteins of some bacterial species form a dimer in solution, but not higher weight complexes (Zambelli *et al*., 2009). The broad low-molecular weight peak appears to represent a mixture of monomer and dimer forms or may be caused by *Cn*UreG interacting with the column matrix and retarding elution (Figure 40A). Histidine rich proteins can form large multimeric complexes when bound to nickel, so the *Cn*UreG size exclusion profile might reflect a combination of dimerisation and nickel-dependent multimerisation (Ge *et al.*, 2006). To test this, the fractions collected from the size exclusion column were analysed by ICP-MS. The fraction containing the high-MW species contained nickel at a concentration of 3.091 ppb, where those of the monomer/dimer contained nickel up to 0.1607 ppb. Nickel is therefore associated with the multimeric form.

To confirm the formation of high-MW species an HPLC size exclusion column was used. Pure *Cn*UreG was incubated with and without 2 molar equivalents of nickel prior to passage through the column. The nickel-loaded *Cn*UreG produced a single peak that was significantly larger than 90 kDa (Figure 40B). In addition the eluted protein did not represent all the protein loaded onto the column. When apo-*Cn*UreG was loaded onto the HPLC column, protein was not eluted and could not be removed from the column by washing with EDTA. This suggests that the nickel bound form of *Cn*UreG caused the formation of high-MW forms that alter the affinity of the protein for the column matrix.

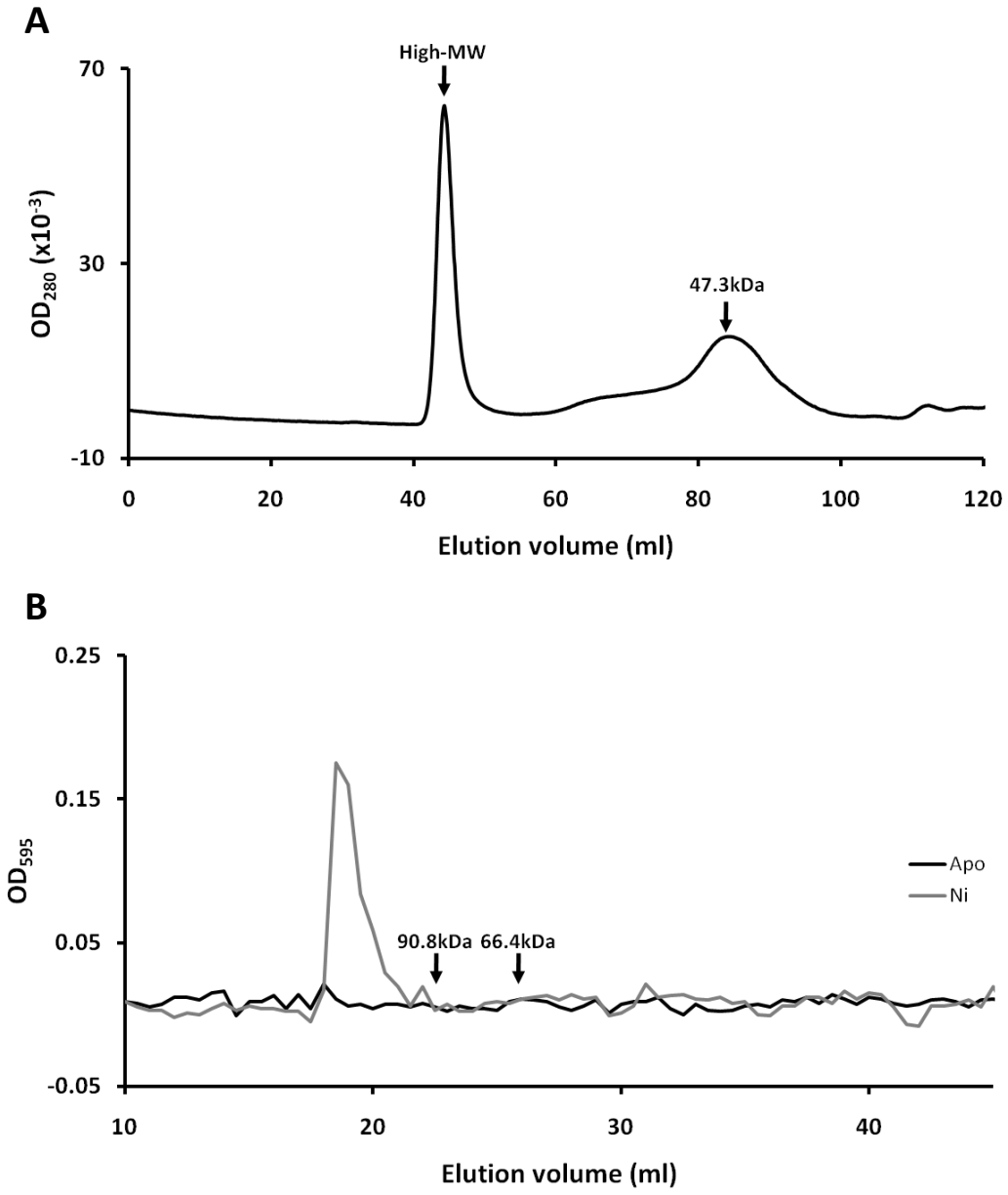

Figure 40 - *Cn*UreG is capable of forming high-MW complexes.

A- Partially pure *Cn*UreG was subject to size exclusion chromatography. Semi-pure *Cn*UreG was loaded onto a size exclusion column and eluted over 1 column volume (120 ml). Protein was detected in the eluate by absorbance at 280 nm. Molecular weights indicated by black arrows were calculated as described in methods.

B- Pure *Cn*UreG was subject to HPLC size exclusion chromatography. *Cn*UreG (2 μM) was incubated in the absence and presence of 2 molar equivalents of nickel prior to HPLC. Fractions were collected and analysed for protein content by addition of Bradford reagent and measurement of absorbance at 595 nm. Elution peaks of Jack Bean Urease (90.8kDa) and BSA (66.4kDa) are indicated by black arrows. Data is representative of 2 repeat experiments.

4.4. Discussion

The histidine-rich N-terminal region of *Cn*UreG is a potential metal binding domain. This region is only present in the UreG protein of species in which the nickel chaperone to urease, UreE, is not present in the NCBI database. Therefore these forms of UreG may act as nickel chaperones in addition to their predicted role as GTPases. To investigate the metal binding capacity of *Cn*UreG two approaches were taken, a desalting column based assay and equilibrium dialysis. In each case *Cn*UreG was shown to bind 2 molar equivalents of nickel per monomer and the equilibrium dialysis revealed an apparent average Kd of <1 μM. The investigation of metal binding to bacterial UreG proteins has revealed a range of nickel binding capacity and affinity, *Ka*UreG binds 1 atom of nickel per monomer with a Kd of 16 μM, *Bp*UreG binds 4 atoms of nickel per dimer with a Kd of 360 μM and *Hp*UreG binds 4 nickel atoms per dimer with a Kd of 10 μM (Zambelli *et al*., 2005; Zambelli *et al*., 2009; Boer *et al*., 2010). *Cn*UreG therefore binds nickel with significantly higher affinity than bacterial UreG proteins. The UreE proteins of various bacteria have been studied with reference to nickel binding and are able to bind nickel at sites with comparable high affinity, *Ka*UreE has a Kd of 0.78 μM in the 1st site, *Bp*UreE has a Kd of 1.4 μM in the 1st site and *Hp*UreE has a Kd of 0.15 μM (Brayman and Hausinger, 1996; Stola *et al*., 2006; Bellucci *et* al., 2009). These data demonstrate that in bacteria UreG binds nickel with low affinity and UreE with high affinity, however in *C. neoformans* UreG binds nickel with high affinity. Therefore, this is consistent with *Cn*UreG acting as a nickel chaperone. The UV-visible spectral analysis of *Cn*UreG revealed a band at 326 nm that was due to a low-affinity nickel binding event. A similar band was observed for nickel binding to *Ka*UreG, which is a monomer in solution, and was attributed to nickel binding the C72 residue (Boer *et al*., 2010). Therefore the low affinity site in *Cn*UreG may include the analogous residue, C173. In *Bp*UreG and *Mt*UreG the equivalent residue, C68 and C90 respectively, forms a disulphide bridge during dimerisation and therefore cannot be involved in metal binding and the equivalent residue in *Hp*UreG, C66, binds zinc at the dimer interface (Neyroz *et al*., 2006; Zambelli *et al*., 2007; Zambelli *et al*., 2009). Whether these results reflect the physiological conditions or are *in vitro* artefacts is not clear. The size exclusion profile of *Cn*UreG indicates that dimerisation is occurring, however the mechanism is unknown. To investigate if *Cn*UreG forms a

dimer in a nickel dependent manner, pure *Cn*UreG in the apo- and nickel-bound forms could be analysed by size-exclusion chromatography or native-PAGE. The C173 residue could be mutated to determine if it is involved in dimerisation. However, *Cn*UreG cannot pass reliably through a size exclusion column and does not resolve on a native-PAGE gel and so these experiments were not attempted.

*Cn*UreG binds 2 equivalents of cobalt with a Kd of over 17 μM. Cobalt may occupy the same binding sites as nickel, as both tend to have octahedral coordination geometries and have the same binding stoichiometery to *Cn*UreG. The low affinity suggests that cobalt binding to *Cn*UreG is not physiologically relevant. *C. neoformans* has no known use for cobalt. *Cn*UreG was able to bind up to 5.5 equivalents of zinc with a Kd of 2.14 μM. Where these zinc atoms are binding is not clear. The binding of zinc to bacterial UreG proteins has been investigated, *Bp*UreG binds 2 zinc atoms per dimer with a Kd of 42 μM and *Hp*UreG binds 1 zinc atom per dimer with a Kd of .33 μM (Zambelli *et al.*, 2005; Zambelli *et al*., 2009). Therefore the binding of so many zinc atoms to *Cn*UreG may represent zinc binding to the equivalent sites of *Bp*UreG or *Hp*UreG as well as to the histidine-rich N-terminal domain. That different numbers of nickel and zinc atoms may bind in this region is likely to be due to the different coordination geometries each atom preferentially adopts. Nickel tends to bind in an octahedral geometry, binding 6 ligands, and zinc in a pyramidal, binding 4 ligands (Waldron *et al*., 2009). Due to the different number and orientation of ligands the binding environment is likely to differ significantly.

Investigation of the secondary structure of apo-*Cn*UreG by far-UV CD revealed a profile similar to that of bacterial UreG proteins. Although largely unstructured, *Cn*UreG possesses regions of α-helix and β-sheet. Addition of nickel to *Cn*UreG reduced the random coil signal and the α-helix and β-sheet signals increased slightly. This indicated that *Cn*UreG was folding in the presence of nickel. As the changes were relatively small this suggests that either a small domain folds on addition of nickel or that a small change occurs across a large portion of the protein. Structural changes have been reported in *Hp*UreG on zinc binding that are linked to dimerisation and are not consistent with the changes reported here (Zambelli 2009). The structural changes of *Cn*UreG on binding nickel may therefore represent folding of the N-terminal domain on binding nickel. The changes in secondary structure of *Cn*UreG on binding cobalt are much smaller compared to binding nickel. The much

lower affinity of *Cn*UreG for cobalt than nickel may be partially due to the protein remaining relatively unstructured in the N-terminal region. The binding of zinc to *Cn*UreG produced different structural changes compared to nickel binding. The changes associated with nickel binding occurred between 0-1 equivalents, whereas changes associated with zinc binding occurred over 0-6 equivalents. The binding of nickel increased both α-helix and β-sheet signal, whereas zinc binding only increased β-sheet signal. This indicates that different folding events are taking place in each case. This may be due to the different preferential coordination geometry for each metal.

Spectroscopic analysis was used to investigate the nature of *Cn*UreG-nickel interactions. Peaks were apparent at 283 and 297 nm in the presence of nickel and these were attributed to LMTC bands from nickel binding to the protein ligands. A third peak at 326 nm and a general increase in absorbance from 250-500 nm was observed above 2 equivalents of added nickel. The stoichiometery of *Cn*UreG binding nickel had been established at 2 equivalents of nickel, so these features represented super-stoichiometric binding of nickel. As both features were removed by passage through a desalting column they may result from much weaker interactions than the 2 nickel atoms retained after desalting. As discussed above the peak at 326 nm may results from nickel binding the C173 residue. A general increase in absorbance across 250-500 nm is indicative of multiple nickel-histidine interactions (Ge *et al.*, 2006). This suggests that nickel can bind to the histidine-rich N-terminal domain with low affinity. The N-terminal domain may then bind 2 atoms of nickel with high affinity, which alters the secondary structure, and histidine residues not involved in the high affinity sites may interact other nickel atoms with a lower affinity. The effect of zinc binding on the *Cn*UreG spectrum could not be studied due to protein precipitation.

The formation of high-MW complexes by *Cn*UreG was observed during purification. A partially pure *Cn*UreG was eluted from size exclusion chromatography as a high molecular weight species. Nickel was only found in the high-MW fractions. Apo-*Cn*UreG was not eluted from a HPLC size exclusion column and nickel-loaded *Cn*UreG eluted only a high-MW species. Bacterial UreG proteins have previously been shown to form dimers in solution (Zambelli *et al.*, 2005; Zambelli *et al.*, 2007; Zambelli *et al.*, 2009). Formation of high-MW complexes has been reported in the

histidine rich protein, hpn, in the presence of nickel (Ge *et* al., 2006). Therefore *Cn*UreG may form multimeric complexes via nickel binding to the N-terminal histidine residues. Whether the formation of high-MW species has a physiological role is unclear as this may be an artefact of *in vitro* analysis. Further investigation is required to determine any physiological role of the high-MW *Cn*UreG complex formation.

*Cn*UreG is able to bind nickel and zinc with similar affinity, however the physiological relevance is not known. UreG has not been shown to bind nickel or zinc *in vivo* in any organism. Comparison between the two showed that nickel binds slightly more tightly than zinc. Affinity alone does not demonstrate which, if any, metal binds under physiological conditions. In the context of urease activation, *Cn*UreG binding nickel serves a potential function whereas binding of zinc does not. Although binding of a single, structural zinc at the conserved putative zinc-binding site is not excluded by the binding of stoichiometric levels of nickel in the N-terminal region. Therefore *Cn*UreG may bind 2 nickel atoms in the N-terminal domain as well as 1 zinc atom at another site, which may include C173.

Understanding the metal binding role of *Cn*UreG is important to understand urease maturation in *C. neoformans*. The lack of the usual nickel chaperone to urease, UreE, suggests that another mechanism of trafficking nickel to urease is required. The data presented here suggests that *Cn*UreG is a good candidate for the nickel chaperone to urease. To confirm the role of *Cn*UreG as a nickel chaperone *in vivo* studies should be used. Expression *in vivo* and *in vitro* of *Cn*UreG with and without the N-terminal region would demonstrate if this region is required for nickel delivery to urease and mutation of potential metal ligands would indicate which residues are used in metal binding. A crystal structure of *Cn*UreG would allow investigation of which ligands bind metals. To date no UreG crystal structure has been solved. Future studies on *Cn*UreG should focus on demonstration of a chaperone role *in vivo* and confirmation that nickel binds in the N-terminal region. Nickel binding in the N-terminal region may indicate that this is a common feature of all eukaryotic UreG proteins. The data presented here distinguishes *Cn*UreG from bacterial UreG proteins and suggests that there are different urease maturation systems in fungi and bacteria.

5. Metal Binding and Inhibition of Urease *in vivo*

5.1. Introduction

The urease enzyme of *C. ensiformis*, jack bean, was the first enzyme to be crystalised and the first to be identified as utilising nickel for catalytic function (Summer, 1926; Dixon *et al*., 1975). Since then the structure of the urease enzymes from *H. pylori, K. aerogenes* and *B. pasteurii* have been solved and been shown to utilise nickel (Jabri *et al*., 1995; Benini *et al*., 1999; Ha *et al*., 2001). The conservation of the structure of the active site of the enzyme and sequence homology between these urease proteins led to the general assumption that all urease enzymes are nickel proteins (Carter *et al*., 2009). More recently, iron containing urease enzymes have been identified in species of bacteria that colonise the stomachs of carnivores, where nickel is scarce but urease is required for survival in the acidic conditions (Pot *et al*., 2006; Stoof *et al*., 2008; Carter *et al*., 2011). The sequence similarity between the iron and nickel urease enzymes and the conserved structure of the active site suggests that homology to known urease enzymes is not sufficient to determine if a urease utilises iron or nickel. To date the metal which the urease enzyme of *C. neoformans* utilises has not been demonstrated.

A large number of metal binding proteins have been identified and studied, but *in vivo* mis-population of the metal binding site with the incorrect metal has been reported in very few cases (Waldron *et al*., 2009). Cobalt can populate the iron binding sites of proteins involved in Fe-S cluster biogenesis, can be incorporated into haem binding proteins required for respiration and can mimic hypoxia by replacing iron bound to the HIF1 transcription factor (Schofield and Ratcliffe, 2004; Ranquet *et al*., 2007; Majtan *et al*., 2010). Cobalt incorporation into the apo-urease active site has been shown *in vitro* and generated low levels of enzyme activity, however the replacement of incorporated nickel with another metal in the active site is very inefficient (King and Zerner, 1997; Yamaguchi and Hausinger, 1997, Carter *et al*., 2009).

The aims of this chapter were to determine which metal *C. neoformans* urease binds *in vivo*, to investigate a nickel-binding role for *Cn*UreG *in vivo* and to investigate the effect of cobalt on urease activity. The data establish that *C. neoformans* urease is a

nickel containing enzyme and that a *Cn*UreG dependent nickel pool exists. The *in vivo* inhibition of urease by cobalt is observed and shown to be due to binding of cobalt to urease, which excludes nickel from binding urease.

5.2. The Urease of *C. neoformans* is a Nickel Enzyme

Urease is a putative nickel protein in *C. neoformans* but the number and size of nickel pools in this yeast are unknown. To determine the number of cryptococcal nickel pools, cell extracts from the wild-type strain grown in urea and glutamic acid media were resolved by anion exchange chromatography followed by size exclusion HPLC. The metal concentration of the eluted fractions was quantified by ICP-MS. The profiles included three significant nickel peaks that eluted at a volume which indicated they were associated with proteins. In addition nickel peaks eluted at a volume indicative of low molecular weight that may result from nickel associated with small ligands such as histidine. The nickel profiles were consistent between urea and glutamic acid grown cell extracts (Figure 41, Figure 42). This established that multiple protein-associated nickel pools exist in *C. neoformans*, which are consistent between urea and glutamic acid grown cells. To determine what proteins were associated with the nickel pools the fractions associated with each pool were resolved by SDS-PAGE and analysed using Principal Component Analysis (PCA). PCA compares the distribution of data sets, in this case protein and nickel concentrations, by reducing the variance in data sets to principle components (PC) that are further reduced to form more principle components (PC1, PC2, PC3 etc.). Comparison of the principle components from each data set indicates how the data sets correlate to each other. This did not identify alignment of any protein and nickel concentrations establishing that PCA could not be used to identify the proteins associated with the nickel pools (Figure 43) (See appendix; Figure 56, Figure 57, Figure 58).

Urease of *C. neoformans* has been reported as an extracellular protein which would exclude it from the cell extract and metal profiles (Rodrigues *et al*., 2007; Rodrigues *et al*., 2008). To determine if urease is excreted into the growth medium the wild-type strain was grown in urea medium, the cells were harvested, cell extract isolated and the medium collected. The protein extract and medium were normalised for volume and urease activity determined. The activity of the cell extracts was

significantly higher than that of the medium (Figure 44A). This established that urease is not excreted into the growth medium. Urease may also have been associated with the membrane as has been suggested for *H. pylori*, which would also exclude it from the metal profile (Voland *et al*., 2003). To determine if urease is in the soluble or membrane fractions the wild-type strain was grown in urea medium and cell extract isolated. The extract was divided into 2 aliquots and 1 was subject to centrifugation to separate the soluble and insoluble components and the urease activity of each fraction determined. The urease activity of the soluble fraction was equal to that of the total fraction but the membrane fraction activity was significantly lower (Figure 44B). This established that urease is a soluble protein.

To determine which metal *C. neoformans* urease utilises the urease activity and metal concentration of each fraction in the wild-type and *ure1Δ* strain profiles was determined. A single peak of urease activity was identified which co-eluted with nickel peak 3. This nickel peak was not present in the *ure1Δ* strain extracts (Figure 45, Figure 46). The lack of urease activity in the *ure1Δ* strain extracts did not correlate with any change in the iron profiles of the wild-type and *ure1Δ* strains (Figure 47). This established that the urease of *C. neoformans* is a nickel binding enzyme.

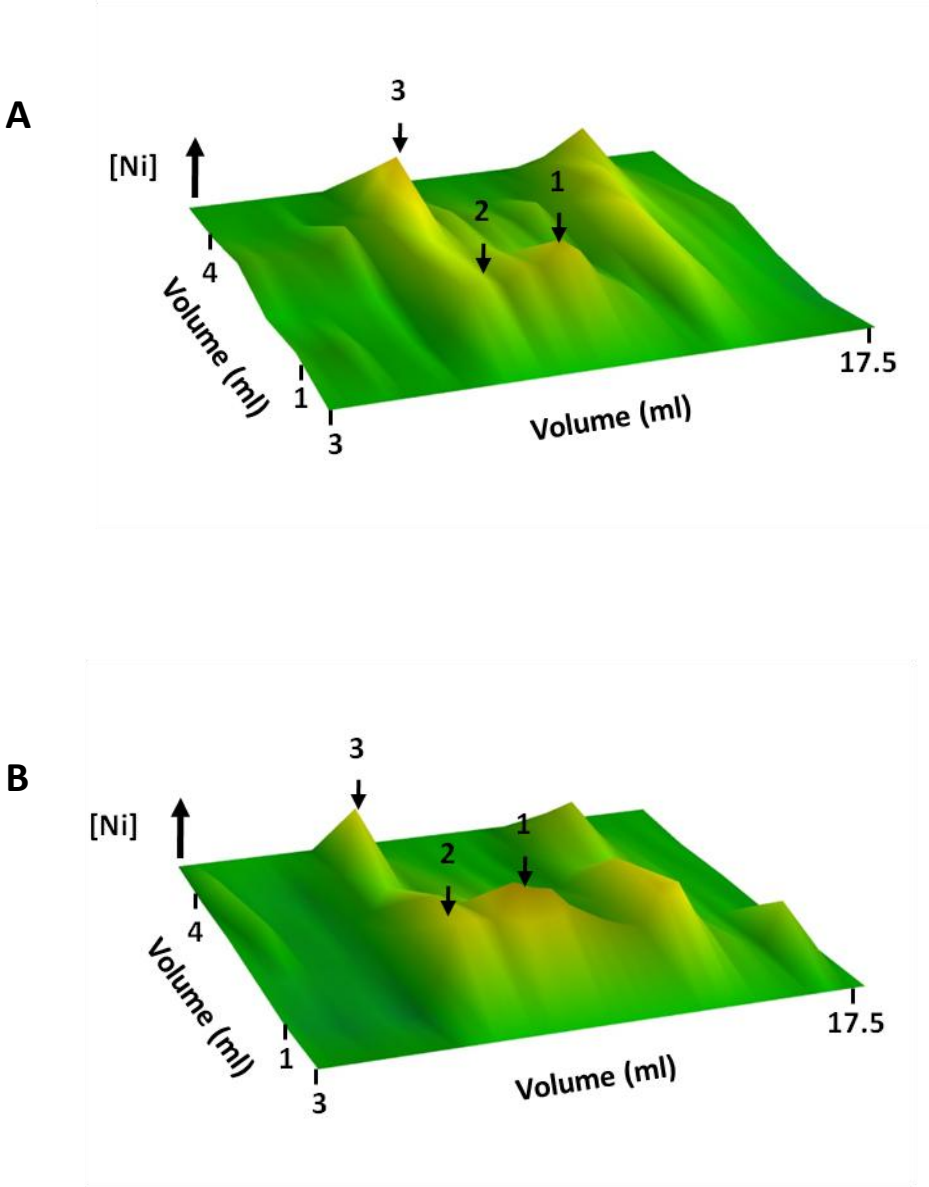

Figure 41 - A 3D representation of the wild-type nickel profile.

The nickel concentration (z axis) displayed for profiles showing two-dimensional chromatography based on size exclusion HPLC (y axis) and anion exchange chromatography (x axis) of wild-type cell extract from urea (A) and glutamic acid (B) grown cultures.

Metal concentration was determined by ICP-MS. nickel peaks 1, 2 and 3 are indicated by black arrows. Data are representative of 2 repeat experiments.

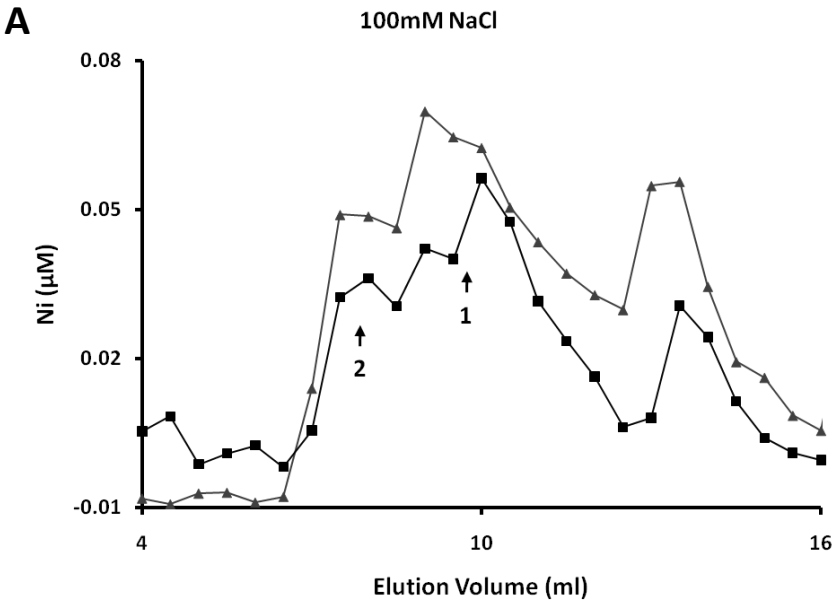
A
100mM NaCl
0.08
0.05
0.02
-0.01
Ni (µM)
1
2
4
10
16
Elution Volume (ml)

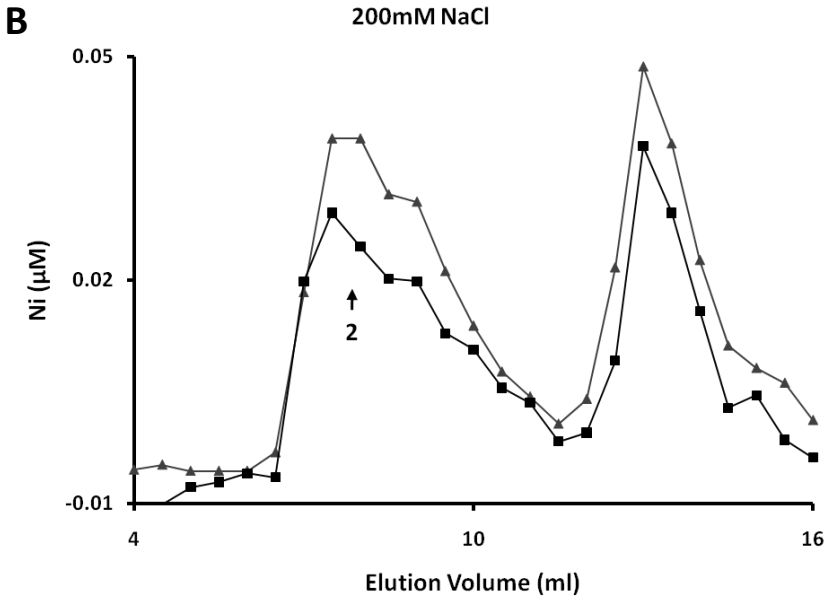
B
200mM NaCl
0.05
0.02
-0.01
Ni (µM)
2
4
10
16
Elution Volume (ml)

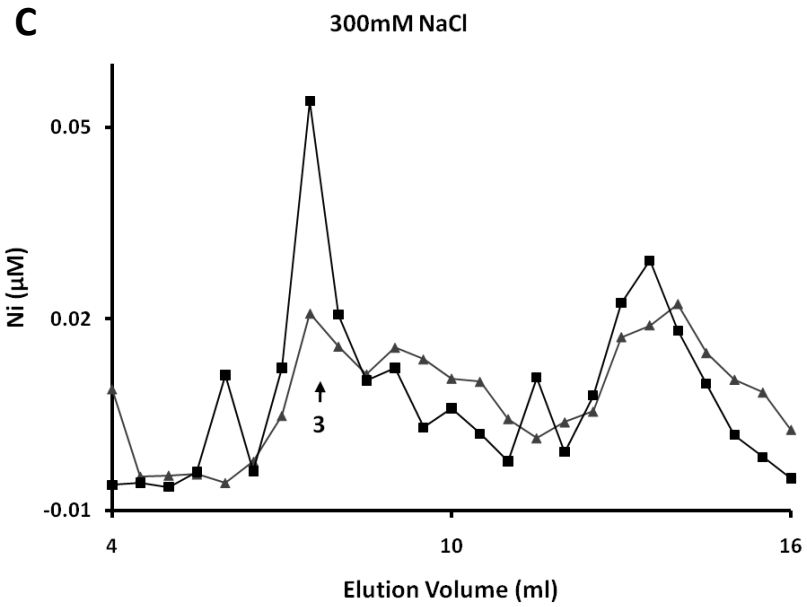
C
300mM NaCl
0.05
0.02
-0.01
Ni (µM)
3
4
10
16
Elution Volume (ml)

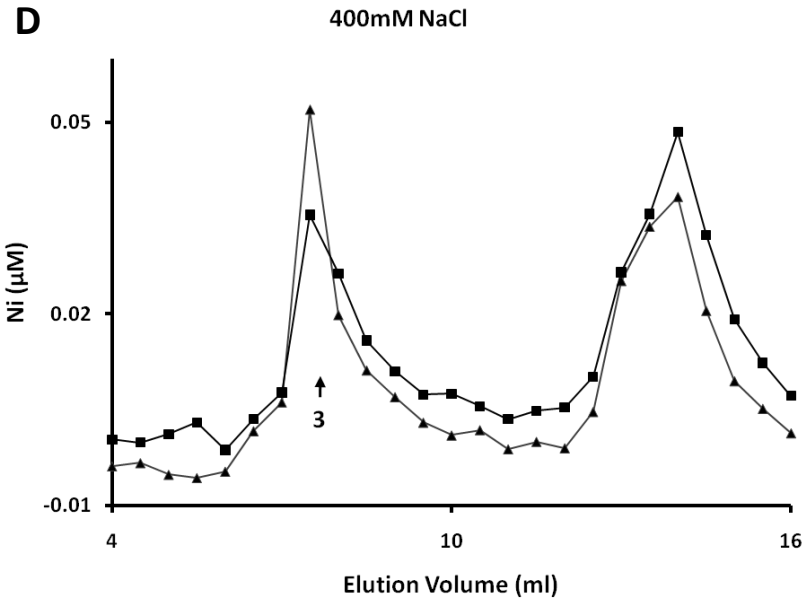
D
400mM NaCl
0.05
0.02
-0.01
Ni (µM)
3
4
10
16
Elution Volume (ml)

Figure 42 - A 2D representation of the wild-type nickel profile.

Size-exclusion HPLC for 100 (C), 200 (D), 300 (E) and 400 (F) mM NaCl anion exchange elution steps displaying the nickel concentration for wild-type cell extract of urea (black squares) and glutamic acid (grey triangles) cultures.

Metal concentration was determined by ICP-MS. nickel peaks 1, 2 and 3 are indicated by black arrows. Data are representative of 2 repeat experiments.

A

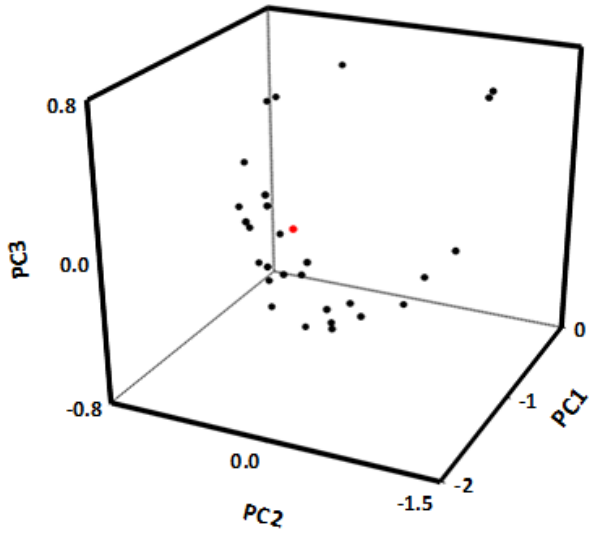

B

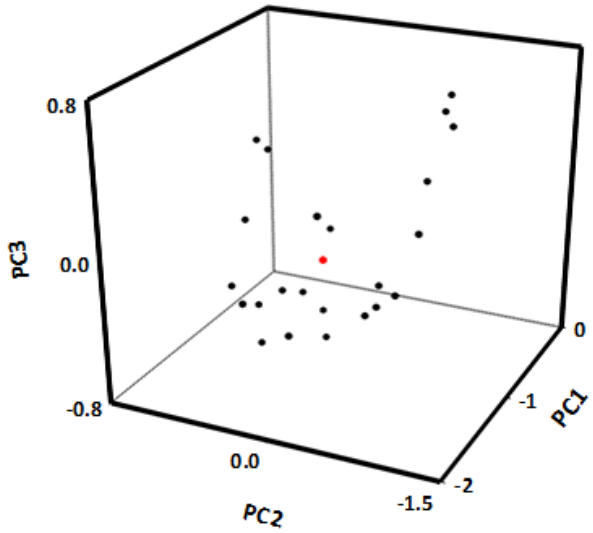

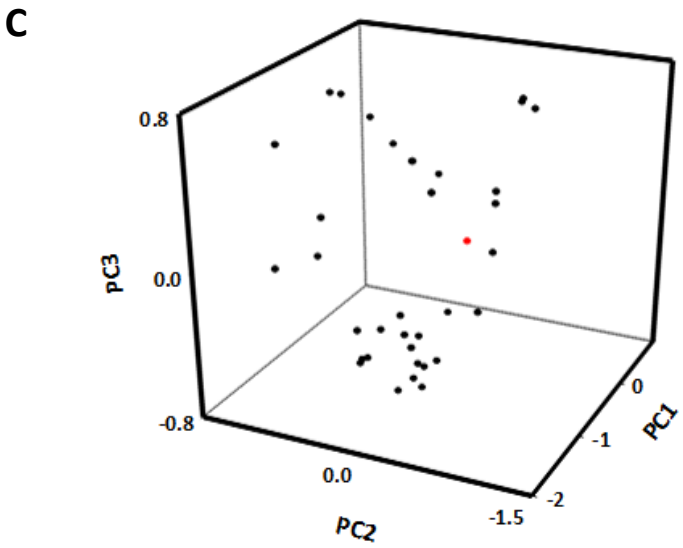

Figure 43 - PCA of the wild-type nickel peaks.

The principle component distribution for nickel peaks 1 (A), 2 (B) and 3 (C).Comparing nickel (red) distribution to protein (black) distribution in a three-dimensional plot. Data are representative of 2 repeat experiments.

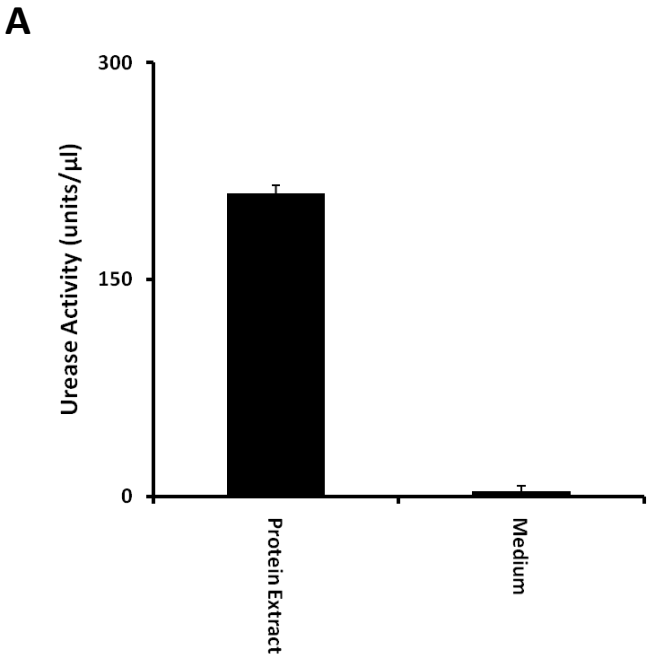
A
300
150
0
Urease Activity (units/µl)
Protein Extract
Medium

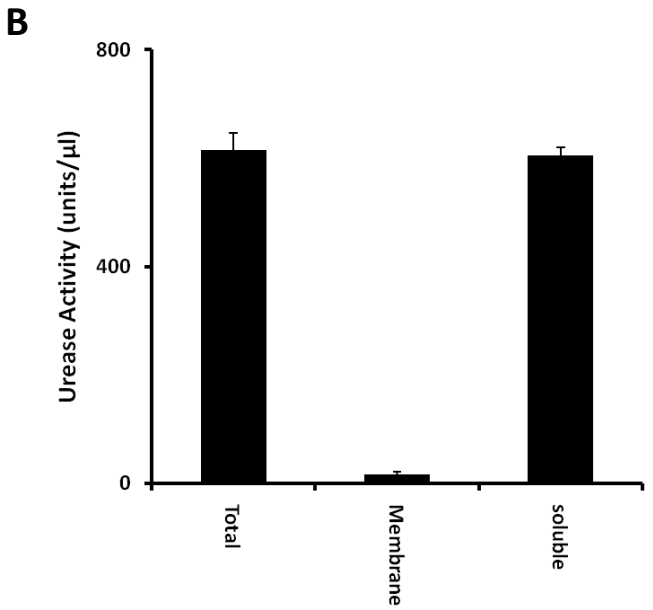
B
800
400
0
Urease Activity (units/µl)
Total
Membrane
soluble

Figure 44 - Urease is a non-excreted soluble protein.

A - The wild-type strain was grown to mid-log in urea medium. The cells were pelleted and protein extracted (Protein extract). The media was collected and concentrated to the same volume as the protein extract in a centricon with 30 kDa cut-off (Medium). 150 µl of each sample was incubated in 66 mM urea solution and urease activity determined by Nessler's colour reagent.

B - The wild-type strain was grown to mid-log in urea medium and protein extract taken (Total). An aliquot was taken and insoluble matter pelleted by centrifugation, the supernatant was removed and kept (Soluble) and the pellet resuspended in the same volume (Membrane). 150 µl of each sample was incubated in 66 mM urea solution and urease activity determined by Nessler's colour reagent

Data points shown represent the mean of 3 repeats and error bars represent the standard deviation.

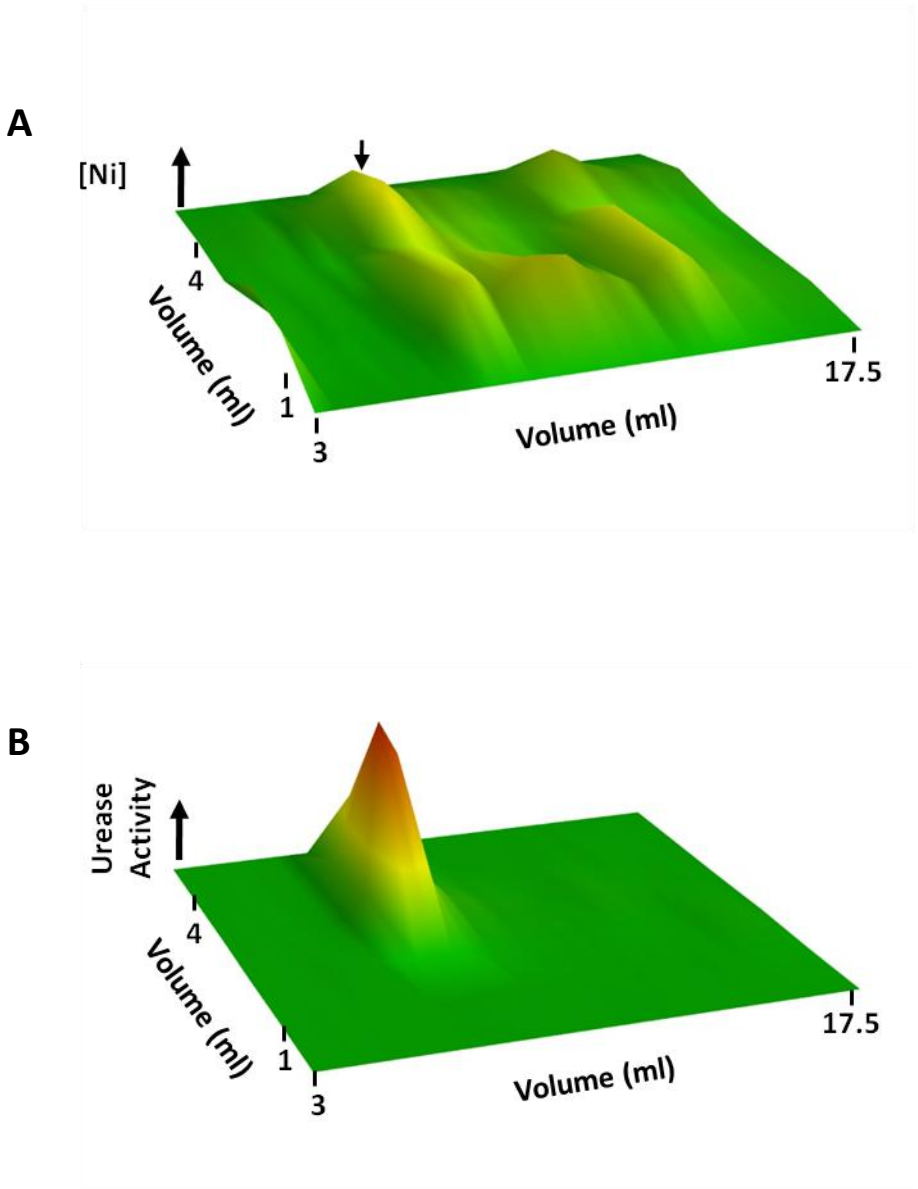

Figure 45 - Urease is a nickel binding enzyme.

The nickel concentration (z axis) (A) and urease activity (B) displayed for profiles showing two-dimensional chromatography based on size exclusion HPLC (y axis) and anion exchange chromatography (x axis) of the wild-type strain. The urease associated nickel peak is indicated by black arrows. Data are representative of 2 repeat experiments.

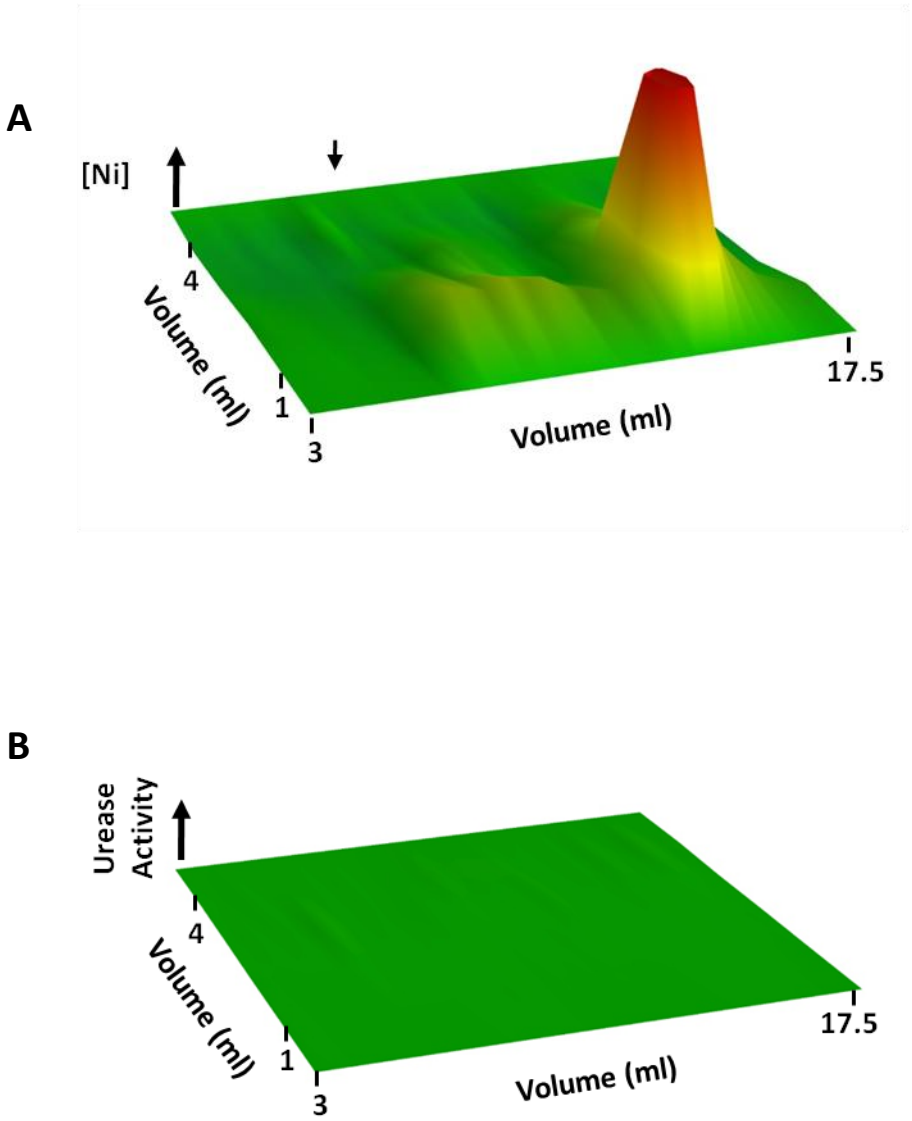

Figure 46 - The urease-associated nickel peak is absent in the *ure1Δ* strain.

The nickel concentration (z axis) (A) and urease activity (B) displayed for profiles showing two-dimensional chromatography based on size exclusion HPLC (y axis) and anion exchange chromatography (x axis) of the *ure1Δ* strain. The urease associated nickel peak is indicated by black arrows. Data are representative of 2 repeat experiments.

A

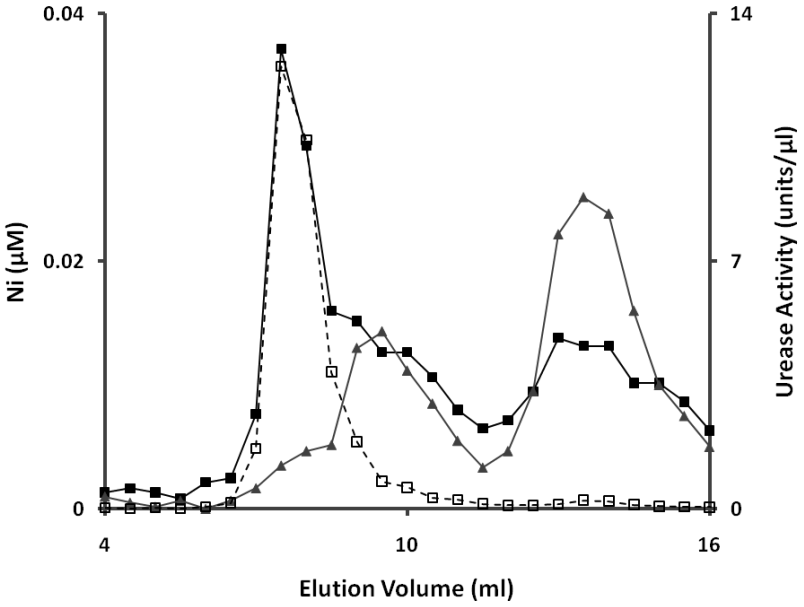
0.04
0.02
0
Ni (µM)
14
7
0
Urease Activity (units/µl)
4
10
16
Elution Volume (ml)

B

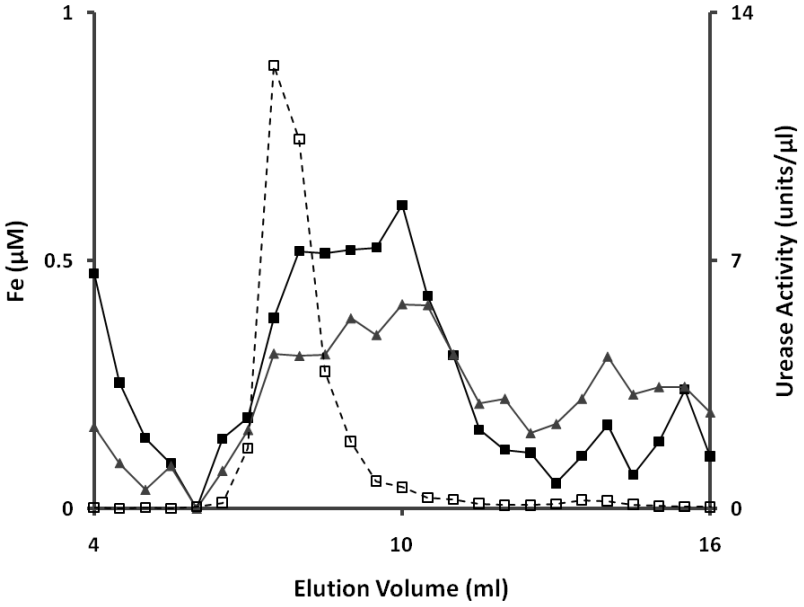
1
0.5
0
Fe (µM)
14
7
0
Urease Activity (units/µl)
4
10
16
Elution Volume (ml)

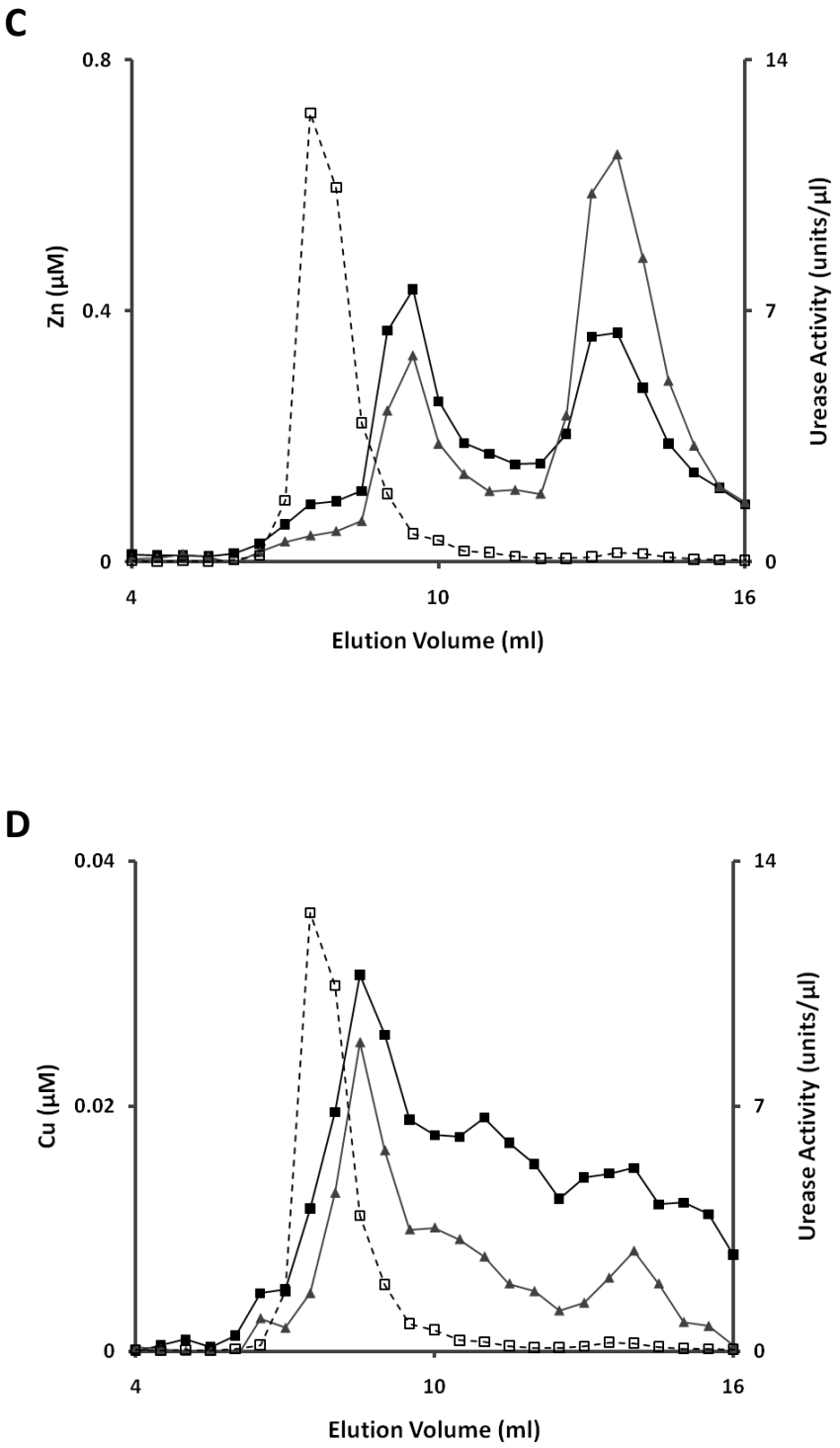

Figure 47 - Urease does not bind iron, zinc or copper.

The nickel (A), iron (B), zinc (C) and copper (D) concentrations of the 300 mM anion exchange elution resolved by size-exclusion HPLC for wild-type (black squares) and *ure1Δ* (grey triangles) glutamic acid grown cell extract. The urease activity of the wild-type (open squares) extract is over-laid on each. Data are representative of 2 repeat experiments.

The proteins associated with nickel peaks 1 and 2 are unknown and could not be determined by PCA. To investigate if these peaks were the result of mis-population of nickel into proteins that bound other metals, the nickel profiles were compared with those of other metals. It was observed that a large zinc peak co-migrated with nickel peak 1, although it was approximately 100 times the concentration (Figure 48A). A copper peak was observed to co-migrate with nickel peak 2, with approximately twice the concentration (Figure 48B). Nickel peak 1 was therefore attributed to mis-population of an unknown zinc protein with trace amounts of nickel. Due to the relatively high levels of nickel compared to copper in peak 2 it is unlikely that this represents a nickel mis-population of a native copper binding protein. Both the nickel and copper may be binding to a natively non-metal binding protein, however no protein could be identified by PCA.

5.3. Identification of a *Cn*UreG Dependent Nickel Pool

*Cn*UreG binds to nickel *in vitro* but it is not known if nickel binding occurs physiologically (Figure 33). To investigate this, the *ureGΔ* and *ureGΔ+UREG* strains were grown in glutamic acid medium, protein extract was isolated and separated by anion exchange and HPLC chromatography and the metal concentration of eluted fractions determined by ICP-MS. A single nickel peak was identified in the wild-type, *ure1Δ* and *ureGΔ+UREG* strains but is absent in the *ureGΔ* strain (Figure 49). This established the existence of a *Cn*UreG dependent nickel pool. Efforts to identify *Cn*UreG in this fraction failed because the protein concentration was too low and sample size too small to identify the nickel binding protein by PCA or to determine if *Cn*UreG was present in the sample by LC/MS/MS.

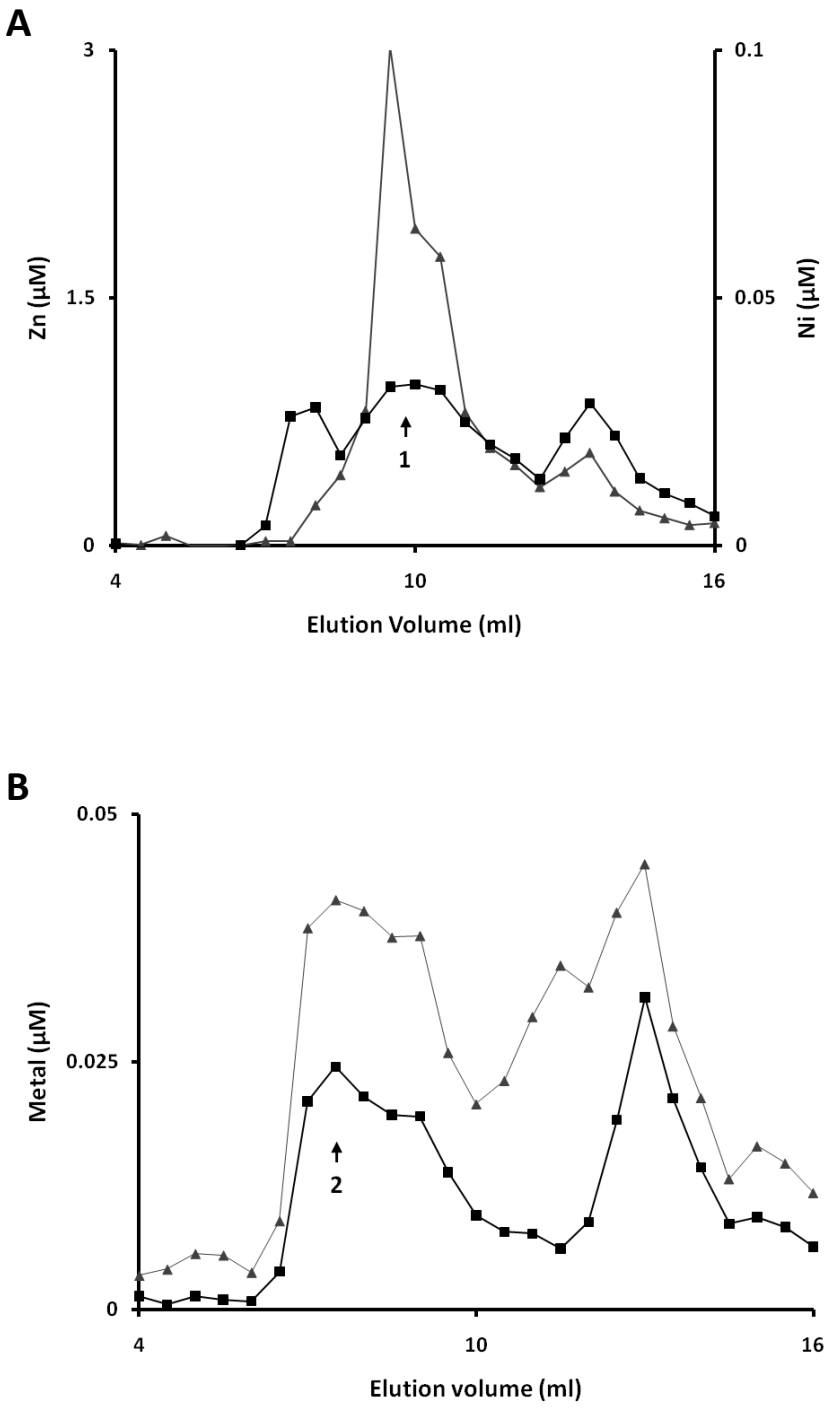

Figure 48 - Nickel peaks 1 and 2 co-migrate with other metals.

A - The nickel (black squares) and zinc (grey triangles) concentrations of the 100 mM anion exchange elution resolved by size-exclusion HPLC of wild-type cell extract from glutamic acid cultures. Nickel peak 1 is indicated by the black arrow.

B - The nickel (black squares) and copper (grey triangles) concentrations of the 200 mM anion exchange elution resolved by size-exclusion HPLC of wild-type cell extract from glutamic acid cultures. Nickel peak 2 is indicated by the black arrow.

Data are representative of 2 repeat experiments.

*Cn*UreG is able to bind zinc *in vitro* but zinc binding to UreG in any species has not been confirmed *in vivo* (Figure 33). To investigate if *Cn*UreG binds to zinc *in vivo*, the zinc profiles of the wild-type, *ureGΔ* and *ureGΔ+UREG* strains were examined. The zinc profiles were consistent between the three strains (Figure 49). This establishes that *Cn*UreG-zinc binding does not represent a significant zinc peak. However a *Cn*UreG associated zinc pool may be too small to distinguish from the background signal, therefore this does not prove that *Cn*UreG does not bind zinc *in vivo*.

5.4. Inhibition of Urease Activity by Cobalt

Incorporation of the incorrect metal into a protein has been demonstrated in a handful of cases *in vivo* (Waldron *et al*., 2009). Urease can be inhibited by binding other transition metals *in vitro* (Carter *et al*., 2009). To investigate if *C. neoformans* urease is inhibited *in vivo* by transition metals the wild-type strain was grown in urea medium supplemented with 10 μM of $NiSO_4$, $CoCl_2$, $Fe_2(SO_4)_3$, $CuSO_4$ or $ZnCl_2$. The urease activity of cells grown with added cobalt had significantly reduced urease activity compared to cells grown in unsupplemented media. The urease activity of cells grown in medium supplemented with the other metals was equal to the activity of cells grown in unsupplemented medium (Figure 50A). This established that cobalt inhibits urease activity in *C. neoformans in vivo*. To further investigate the inhibition of urease by cobalt the wild-type strain was grown in urea medium in the absence and presence of $CoCl_2$ added to 0.1, 1, 10 and 100 μM and the urease activity of protein extract determined. The activity was reduced to approximately half with the addition of 1 μM $CoCl_2$ and almost abolished with the addition of 100 μM $CoCl_2$ (Figure 50B).

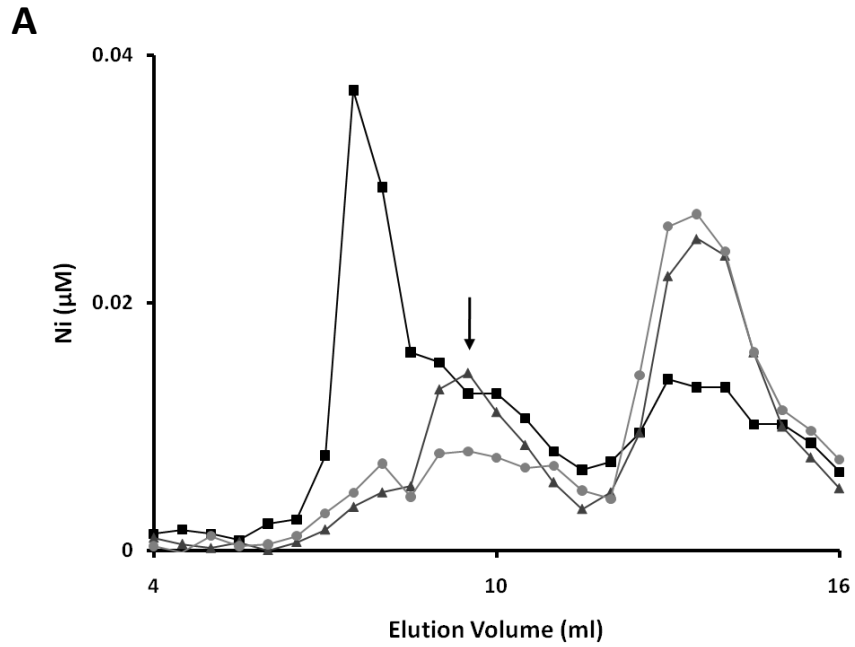
A
0.04
0.02
0
Ni (µM)
4
10
16
Elution Volume (ml)

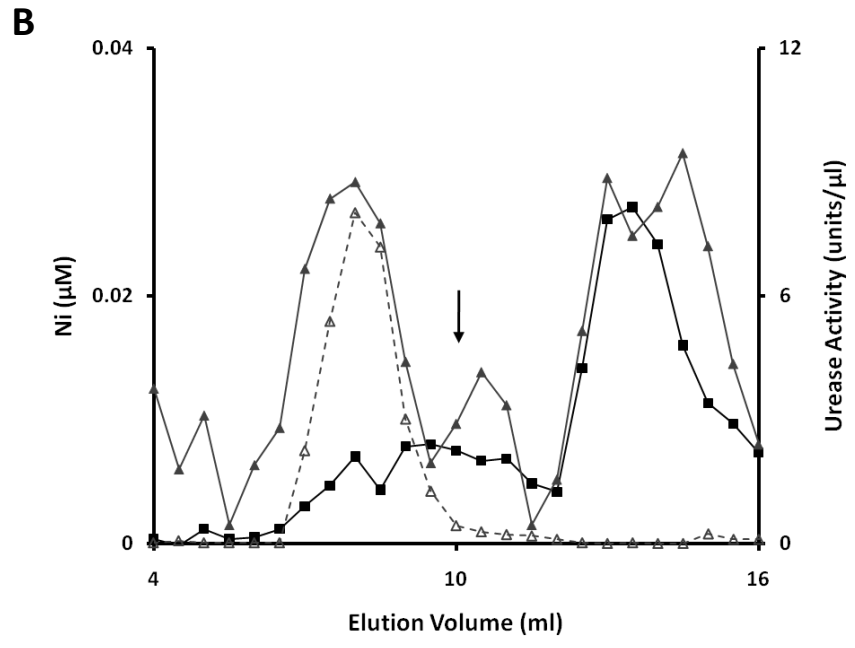
B
0.04
0.02
0
Ni (µM)
12
6
0
Urease Activity (units/µl)
4
10
16
Elution Volume (ml)

C

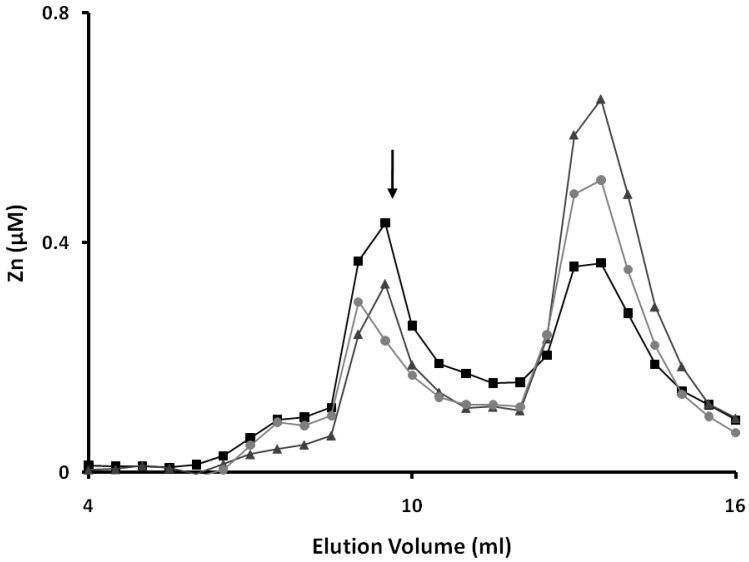
0.8
0.4
0
Zn (µM)
4
10
16
Elution Volume (ml)

D

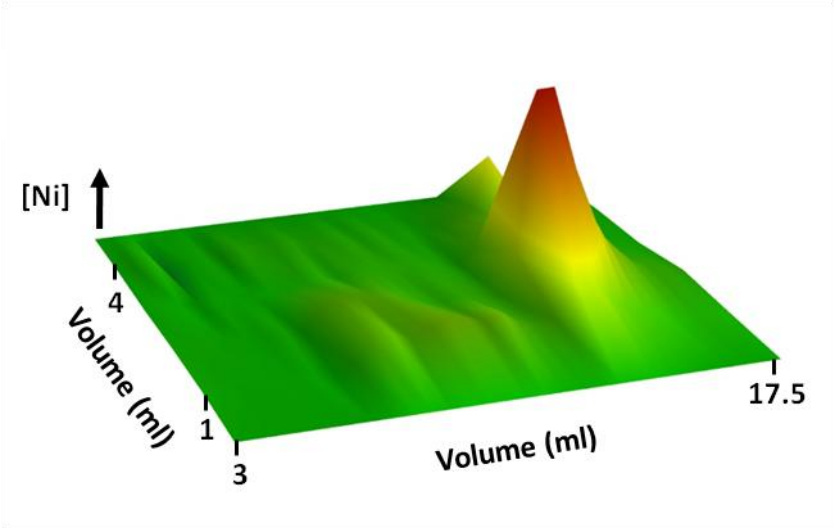
[Ni]
4
Volume (ml)
1
3
17.5
Volume (ml)

Figure 49 - Identification of a *Cn*UreG dependent nickel peak.

A - Nickel concentration of the 300 mM NaCl anion exchange elution resolved by size-exclusion HPLC of cell extract from the wild-type (black squares), *ure1Δ* (grey triangles) and *ureGΔ* (light grey circles) strains grown in glutamic acid medium. The UreG dependent nickel peak is indicated by the black arrow.

B - Nickel concentration of the 300 mM NaCl anion exchange elution resolved by size-exclusion HPLC of cell extract from the *ureGΔ* (black squares) and *ureGΔ+UREG* (grey triangles) strains grown in glutamic acid medium. The urease activity of the *ureGΔ+UREG* extract is over-laid (open triangles). The UreG dependent nickel peak is indicated by the black arrow.

C - Zinc concentration of the 300 mM NaCl anion exchange elution resolved by size-exclusion HPLC of cell extract from the wild-type (black squares), *ure1Δ* (grey triangles) and *ureGΔ* (light grey circles) strains grown in glutamic acid medium. The UreG dependent nickel peak location is indicated by the black arrow.

D - The nickel concentration (z axis) displayed for profiles showing two-dimensional chromatography based on size exclusion HPLC (y axis) and anion exchange chromatography (x axis) for the *ureGΔ* strain grown in glutamic acid medium.

Data are representative of 2 repeat experiments.

How cobalt inhibited urease activity was not clear. Cobalt may block nickel uptake into the cell or may prevent urease maturation by binding to urease or one of the accessory proteins. To determine if nickel is accumulated in the presence of cobalt the wild-type strain was grown in urea medium with and without 0.1, 1, 10 and 100 μM $CoCl_2$ added and the levels of cellular metal accumulation determined by ICP-MS. The levels of nickel accumulated were reduced by approximately 30% in cells grown in the presence of 100 μM cobalt compared to cells grown in unsupplemented medium (Figure 51A). The levels of cobalt accumulated increased significantly in cells grown with added cobalt (Figure 51Figure 51B). This established that nickel is accumulated at concentrations of cobalt which abolish urease activity. This also established that cobalt accumulation increases when cobalt concentration of the growth medium increases.

5.4.1. Inhibition of Capsule Formation by Cobalt

C. neoformans growth on urea induces capsule formation and it could not be determined if urease activity was required. To investigate if inhibition of urease activity by cobalt inhibits capsule formation the wild-type strain was plated in serial dilutions on urea medium with and without $CoCl_2$ added to 10 or 100 μM and incubated at 30^oC for 10 days. The colonies grown on unsupplemented medium developed a mucoid appearance and capsule formation was confirmed by India ink staining. The colonies grown in the presence of additional cobalt did not exhibit mucoid morphology and no capsule formation was observed (Figure 52). This established that capsule formation is inhibited by cobalt.

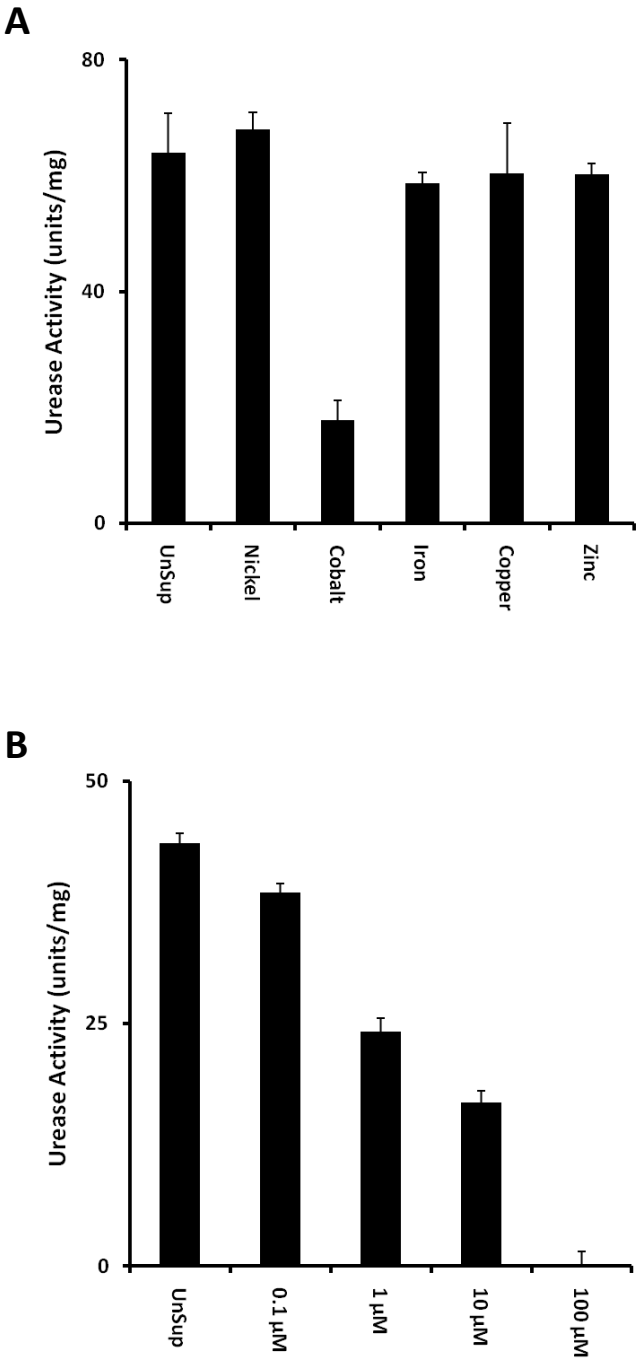

Figure 50 - Cobalt inhibits urease activity.

A - The wild-type strain was grown to mid-log in urea media either unsupplemented (UnSp) or with 10 µM $NiSO_4$, $CoCl_2$, $Fe_2(SO_4)_3$, $CuSO_4$ or $ZnCl_2$ added. Protein was extracted and the urease activity of each sample was determined.

B - The wild-type strain was grown to mid-log in urea media either unsupplemented (UnSp) or with 0.1, 1, 10 or 100 µM $CoCl_2$ added. Protein was extracted and the urease activity of each sample was determined

Data points shown represent the mean of 3 repeat experiments and error bars represent the standard deviation.

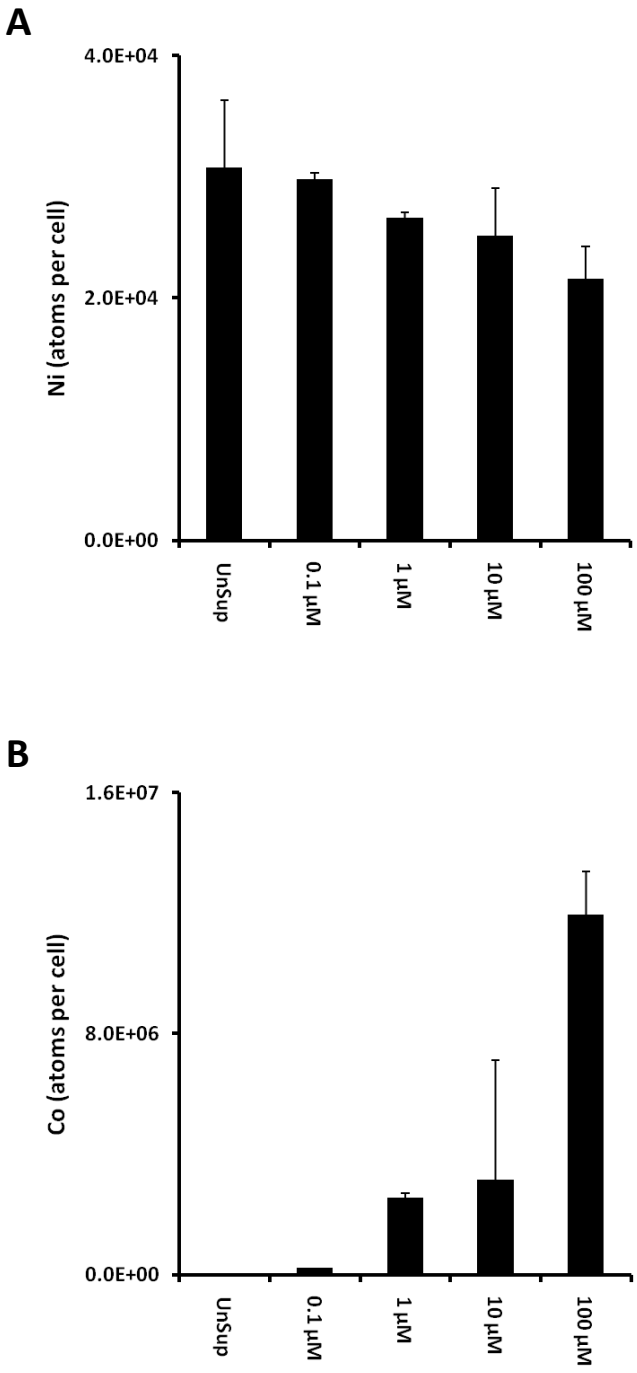

Figure 51 - Cobalt does not inhibit nickel accumulation.

The wild-type strain was grown to mid-log in urea media either unsupplemented (UnSp) or with 0.1, 1, 10 or 100 µM $CoCl_2$ added. The cellular concentration of nickel (A) and cobalt (B) was determined by ICP-MS. Data points shown represent the mean of 3 repeat experiments and error bars represent the standard deviation.

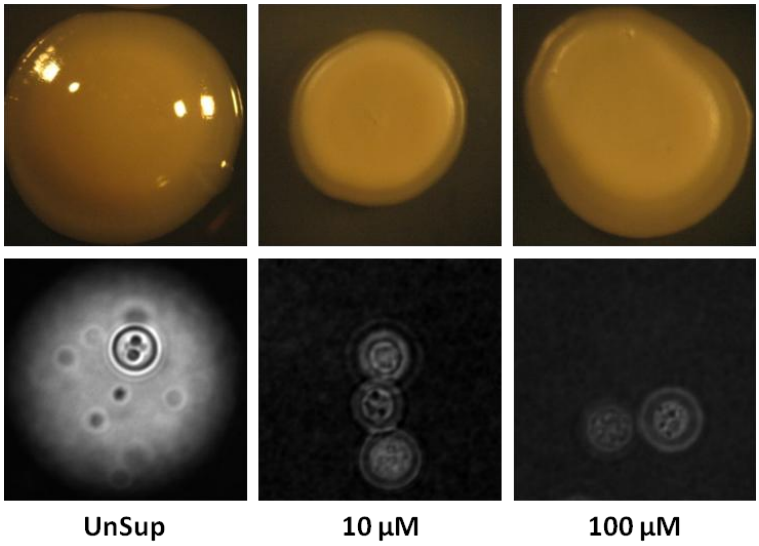

Figure 52 - Cobalt inhibits capsule formation.

Colonies of the wild-type strain were plated on urea medium either unsupplemented or with 10 or 100 µM $CoCl_2$ added and incubated for 10 days at 30°C. Colony morphology was photographed and capsule formation assayed by India ink. Data are representative of 3 repeat experiments.

5.4.2. Urease Binds Cobalt

Under the high cobalt conditions that inhibit urease activity cobalt is accumulated by the cell but the mechanism by which urease is inhibited is unclear. *K. aerogenes* urease activation can be inhibited *in vitro* by cobalt occupying the active site, or binding to a conserved cysteine residue near the active site (Yamaguchi and Hausinger, 1997). To investigate if *C. neoformans* urease is inhibited by cobalt binding the enzyme, the wild-type and *ure1Δ* strains were grown in glutamic acid medium with cobalt added to 100 μM and cell extracts resolved by anion exchange and HPLC. The eluate metal concentration and urease activity was quantified. In the wild-type strain a cobalt peak was associated with residual urease activity (Figure 53A, B). The nickel associated with urease was much lower than that of cells grown in medium without added cobalt (Figure 53C). This cobalt peak was significantly reduced in the *ure1Δ* mutant (Figure 53D). This is consistent with cobalt binding to urease and excluding nickel. The difference in cobalt concentration between the wild-type and *ure1Δ* strains at this peak is equivalent to the difference in nickel concentration between wild-type and *ure1Δ* strains grown in unsupplemented medium. This suggests that approximately equal amounts of cobalt and nickel bind to urease under these conditions.

*Cn*UreG is able to bind cobalt *in vitro* but it is unclear if cobalt reaches urease via this putative nickel chaperone. To investigate the role of *Cn*UreG in delivery of cobalt to urease the *ureGΔ* strain was grown in glutamic acid medium with cobalt added to 100 μM and cell extract resolved by anion exchange and HPLC, the metal concentration and urease activity were quantified. The *ureGΔ* profile included the urease associated cobalt peak and did not exhibit urease activity. This established that cobalt bound to urease by a *Cn*UreG independent mechanism.

A

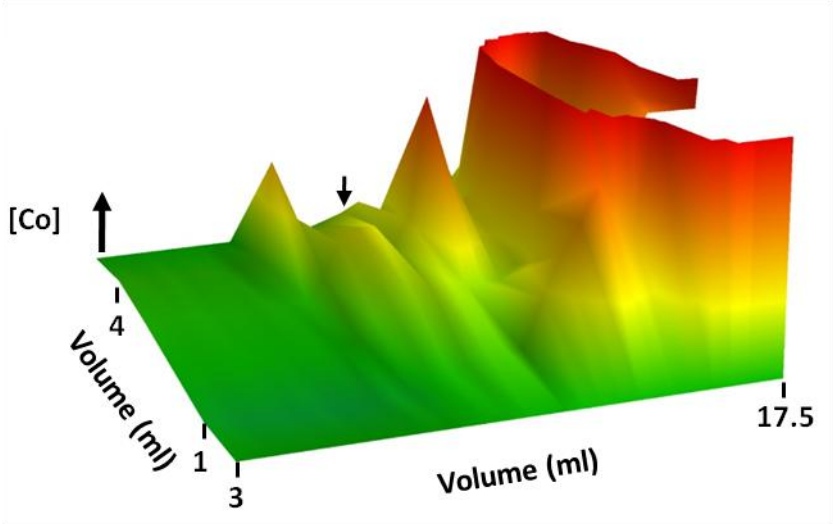
[Co]
4
Volume (ml)
1
3
17.5
Volume (ml)

B

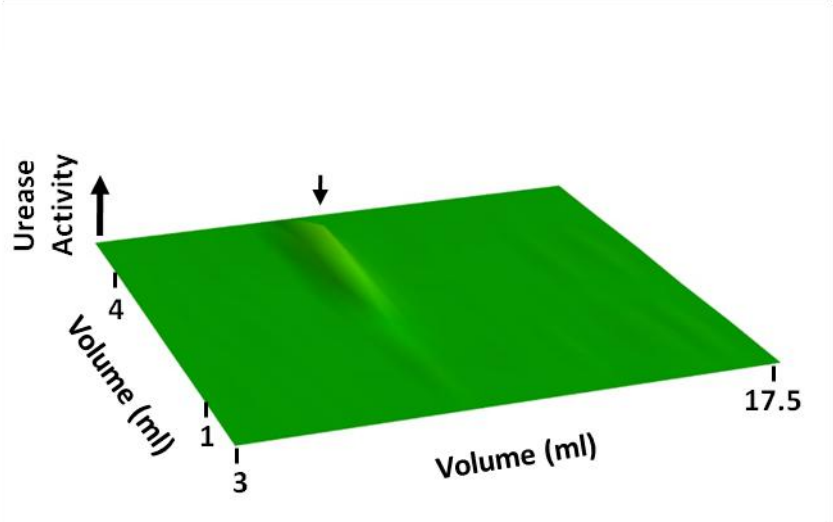
Urease Activity
4
Volume (ml)
1
3
17.5
Volume (ml)

C

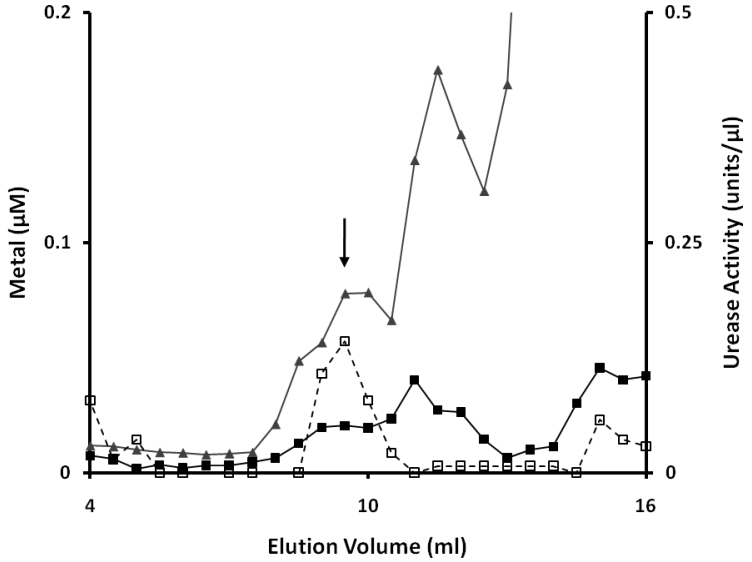
0.2
0.1
0
0.5
0.25
0
Metal (µM)
Urease Activity (units/µl)
4
10
16
Elution Volume (ml)

D

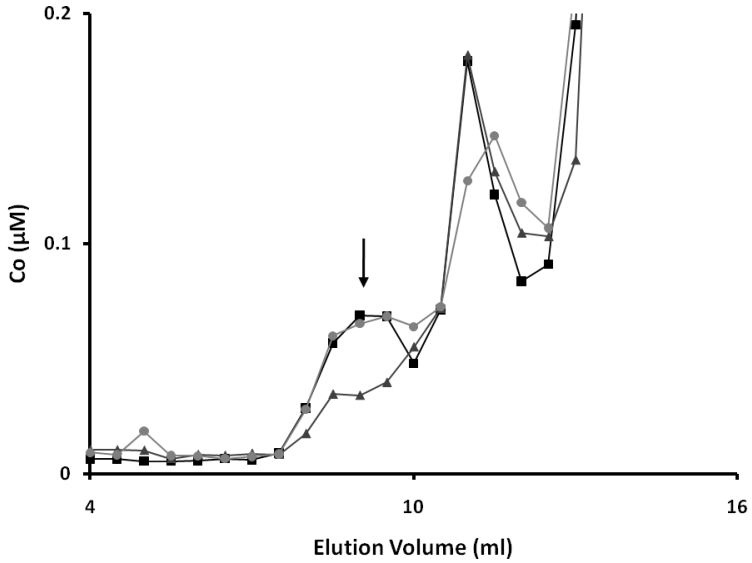
0.2
0.1
0
Co (µM)
4
10
16
Elution Volume (ml)

Figure 53 - Cobalt binds urease *in vivo* via a non-*Cn*UreG dependent mechanism.

A - The cobalt concentration (z axis) displayed for profiles showing two-dimensional chromatography based on size exclusion HPLC (y axis) and anion exchange chromatography (x axis) of wild-type cells grown in glutamic acid medium supplemented with 100 μM $CoCl_2$.

B - The urease activity of A.

C - 300 mM anion exchange elution cross-section of A. The nickel (black squares) and cobalt (grey triangles) concentration and the urease activity (open squares) are displayed. The urease associated cobalt peak is indicated by the black arrow.

D - Cobalt concentration of the 300 mM anion exchange elution step resolved by size-exclusion HPLC for the wild-type (black squares), *ure1Δ* (grey triangles) and *ureGΔ* (light grey circles) strains grown in glutamic acid medium supplemented with 100 μM $CoCl_2$.

Data are representative of 2 repeat experiments.

5.5. Discussion

Iron-binding urease enzymes have been identified in species of *Helicobacter* which infect carnivore stomachs where nickel is limiting but urease is required for colonisation. There is a high degree of homology between iron and nickel urease active sites and therefore the urease of any organism cannot be presumed to bind either metal (Carter *et al*., 2011). The urease of *C. neoformans* was shown to bind nickel specifically, which is consistent with fungal and plant urease proteins studied to date.

The nickel profiles of *C. neoformans* included three significant nickel peaks. One of these was established to be associated with urease but the other two peaks could not be associated with a protein by PCA. The first nickel peak showed significant overlap with a larger zinc peak and was therefore attributed to mis-population of a zinc-binding protein with nickel. Whether this mis-population is an artifact of analysis or represents physiological conditions is not clear. The second nickel peak showed overlap with a copper peak of comparable size. This peak is unlikely to be a natively nickel or copper binding protein as the proportion of nickel to copper is very high. These peaks are possibly due to metal binding a natively non-metal binding protein. The presence peaks which appear to be due to mis-population are apparent on the same scale as the urease-nickel peak demonstrates how little nickel is used in *C. neoformans* urease. Studies using the same method to investigate metal binding proteins in bacteria have not reported equivalent mis-population peaks and have been able to use PCA to identify the metal associated proteins (Tottey *et al*., 2008).

The identification of a small *Cn*UreG dependent nickel peak is the first time evidence of a UreG protein binding nickel *in vivo* has been presented. *Cn*UreG binds nickel *in vitro* with a much higher affinity than bacterial UreG proteins that have been studied and binding is comparable to their conjugate nickel chaperone, UreE. This indicates *Cn*UreG may act as a nickel chaperone. However, the protein associated with the *Cn*UreG dependent nickel peak could not be identified and therefore further investigation is required to confirm *Cn*UreG nickel binding *in vivo*. Increasing the protein concentration and resolution is necessary to identify the protein associated with the nickel peak. Therefore, refinement of the profile method is required.

The activity of *C. neoformans* urease is sensitive to inhibition by cobalt. Low levels of cobalt, 10 times that of nickel, reduce urease activity by approximately 50%. There is no known requirement for cobalt in *C. neoformans.* This is consistent with *C. neoformans* not having evolved to respond to environmental cobalt. The data presented here is consistent with inhibition of urease by cobalt binding and excluding nickel. The *in vitro* maturation of *K. aerogenes* urease can be inhibited by the binding of cobalt to a cysteine residue outside of the active site, C319, which may cause structural change in the active site that prevent metal binding. This residue is conserved in *C. neoformans* urease, C585. The site at which cobalt binds urease in *C. neoformans* has not been established. However, the approximately equal amount of nickel and cobalt binding to urease is consistent with cobalt occupying the active site. This could be investigated further by the expression of urease in which the conserved C585 residue had been mutated and analysis of cobalt inhibition and *in vivo* binding. The mechanism by which cobalt binds to urease is unclear but does not include *Cn*UreG, as cobalt binds to urease in the *ureGΔ* strain. *Cn*UreG is able to bind cobalt *in vitro* but with significantly lower affinity than nickel. It can therefore be concluded that cobalt does not replace nickel in the urease maturation pathway. Cobalt also inhibits the formation of capsule in response to urea growth. It is not clear if this is a direct result of urease inhibition. The [Fe-S] biogenesis pathway of *H. pylori* is disrupted by cobalt and as *C. neoformans* capsule formation is induced by low iron conditions cobalt may affect iron homeostasis and thus inhibit capsule formation (Vartivarian *et al*., 1993; Ranquet *et al*., 2007). Cobalt therefore inhibits two of *C. neoformans* virulence factors and may inhibit the same factors in other pathogenic fungi. The treatment of internal fungal infections with cobalt may be impractical, as high concentrations of cobalt are toxic to humans (Delaunay *et al*., 2010). However, superficial fungal infections could be treated by cobalt in conjunction with traditional anti-fungal therapies.

The urease of *C. neoformans* has previously been described as an excreted enzyme (Rodrigues *et al*., 2007; Rodrigues *et al*., 2008). When urease was reported as being excreted via vesicles, the growth phase of the cultures were not stated, however incubation times are given as 48 or 72 hours which would be consistent with stationary phase growth. Whether urease containing vesicles are excreted by living cells or are released as the result of cell death is not clear. The identification of

urease in extracellular vesicles by mass spectrometry does not indicate the relative abundance of urease in the cells and vesicles. Also, the urease activity of the vesicles is stated but the urease activity of the cell is not presented. Therefore, it is not clear from these data what proportion of urease is excreted in vesicles. The data presented in this chapter shows urease activity is detectable in the medium but is significantly lower than that of the cellular extract. Therefore, the detection of extracellular urease by *Rodrigues et al.* is consistent with the data presented here, but does not demonstrate that urease is an extracellular protein.

This study is the first time a metal profile assay of a eukaryote has been reported. A consistent problem with this method was the inability to identify metal-associated proteins by PCA. This puts a severe limitation on future studies using this method to investigate metal binding in *C. neoformans* and possibly other fungi. Attempts were made to increase the signal-noise ratio for both ICP-MS and SDS-PAGE analysis. This included using more sample in SDS-PAGE to increase the band intensity and running two HPLC size exclusion columns in tandem to increase the resolution but neither resulted in increased resolution or PCA protein identification. The assay could be refined for eukaryotic use by increasing the protein input and increasing resolution by tandem HPLC columns to generate a higher signal to noise ratio and greater resolution between the metal peaks.

6. Final Discussion

6.1. Project Summary

The over-arching aim of this project was to investigate the nickel homeostatic and urease maturation systems of *C. neoformans*. A primary goal was to establish whether nickel or iron is utilised by urease in *C. neoformans* and to determine under what conditions urease is activated. The aims were also to investigate the roles of the putative nickel transporter *Cn*Nic1 and the urease accessory protein *Cn*UreG in urease maturation and nickel accumulation.

The data presented in this thesis established that *C. neoformans* urease is a nickel-binding enzyme and that both urease activity and nickel accumulation are responsive to the available nitrogen source. *Cn*Nic1 is identified as the primary means of nickel accumulation and is proposed to be a high-affinity nickel importer. *Cn*UreG is demonstrated to bind nickel *in vitro* and evidence of *in vivo* nickel-binding by *Cn*UreG is presented. This indicated that *Cn*UreG has dual roles of putative GTPase and nickel chaperone to urease, in contrast to bacterial urease maturation systems which utilise a separate nickel chaperone.

The inhibition of urease activity by cobalt was observed *in vivo* and profiling experiments revealed that this was due to the binding of cobalt to urease which prevents nickel binding. However, cobalt binds to urease in the *ureGΔ* strain which demonstrates that cobalt does not replace nickel in the maturation process. This adds to the very limited list of observed mis-population of a protein metal-binding site.

6.2. *Cn*Nic1 as a Nickel Transporter

The *NIC1* gene in *C. neoformans* was identified by the close homology of its predicted product to the *Sp*Nic1p of *S. pombe* and HoxN of *C. necator* (Eitinger *et al*., 1997; Eitinger *et al*., 2000). Nickel accumulation and urease activity were significantly reduced in the *nic1Δ* strain, although in high nickel conditions urease activity was restored to wild-type levels. This clearly demonstrated that *Cn*Nic1 is required for nickel accumulation and may be a nickel importer. However it is not clear where *Cn*Nic1 is located in the cell, as it may be located at the cell surface and

mediate nickel import or could be on the vacuolar membrane and mediate nickel transport into or out of the vacuole. Localisation studies could be used to investigate if *Cn*Nic1 is at the cell surface. A fluorescent tag such as GFP or a small epitope tag could be used to localise *Cn*Nic1 microscopically. Localisation studies in live cells could also include investigation of *Cn*Nic1 regulation by exposure of the cells to high nickel and/or different nitrogen sources to determine if the localisation changes or if the protein is degraded. These studies, in conjunction with expression studies, could be used to identify if *C. neoformans* nickel import is regulated in response to nickel levels, the available nitrogen source or both. This would indicate if the nickel uptake system of *C. neoformans* is regulated in a similar manner to the iron uptake system of *S. cerevisiae*, which is responsive to both iron and glucose levels (Casas *et al*., 1997; Blaiseau *et al*., 2001).

The requirement of *Cn*Nic1 for urease activity only in low nickel conditions and the close homology of *Cn*Nic1 to HoxN and *Sp*Nic1p, both of which are high affinity transporters, indicate that *Cn*Nic1 may be a high-affinity nickel-transporter (Eitinger *et al*., 1997; Eitinger *et al*., 2000). Comparing the rate of nickel uptake in the wild-type and *nic1Δ* strains, using a radioactive isotope of nickel, across a range of concentrations could be used to determine the affinity of *Cn*Nic1 for nickel. In common with *Sp*Nic1p and HoxN, *Cn*Nic1 contains a HX_4DX motif. Mutation of either histidine residue results in a loss of function in HoxN (Eitinger *et al*., 1997). Expression of *Cn*Nic1 in *C. neoformans* with the equivalent histidine residues mutated could be used to investigate whether the mechanism of nickel transport is conserved between bacteria and fungi. The other residues in the motif (HGLDAH) are also of interest, *Cn*Nic1 has a leucine as third residue compared to valine in HoxN or phenylalanine in Nh1F, which transports both cobalt and nickel (Eitinger *et al*., 1997; Degen *et al*., 1999; Eitinger *et al*., 2000; Degen and Eitinger, 2002). Mutation studies of HoxN and Nh1F showed that this residue is important for determining specificity of metal transported and rate of transport. *Sp*Nic1p is a specific nickel transporter but can be inhibited by cobalt, unlike HoxN which is a specific nickel transporter but is not inhibited by cobalt. The presence of leucine rather than valine or phenylalanine may give rise to this combination of features in *Sp*Nic1p. However, *Cn*Nic1 also has a leucine at the third residue in the motif and is a specific nickel transporter, as the deletion of *Cn*Nic1 only affected nickel

accumulation, but is not inhibited by cobalt, as cobalt did not abolish nickel accumulation. *Cn*Nic1 has a glycine at the second residue of the motif compared to an alanine in each of the other transporters which may account for this difference. Therefore, mutation of residues other than the two histidines in this motif may give insight into how these residues control substrate specificity and affect the susceptibility to inhibition by cobalt in the NiCoT family.

6.3. *Cn*UreG as a Nickel Chaperone to Urease

*Cn*UreG was identified as a protein of interest due to the N-terminal histidine rich domain it contains which is conserved among fungal UreG proteins but absent in bacterial UreG proteins. Histidine is a good metal ligand and therefore this domain has the potential to bind metal physiologically. A similar domain which binds nickel is present in the nickel chaperones HypB protein of *Bradyrhizobium japonicum* and the UreE proteins of several bacterial species which bind nickel to chaperone it to their respective enzymes. An equivalent role for the N-terminal domain of *Cn*UreG is possible (Lee *et al*., 1993; Olson *et al*., 1997). This theory was supported by the lack of a homologue to UreE in fungal genomes in the NCBI database. The metal binding properties of *Cn*UreG were studied *in vitro* and revealed that *Cn*UreG binds nickel with an affinity much greater than that of bacterial UreG proteins and more consistent with bacterial UreE proteins. Profile experiments revealed a *Cn*UreG dependent nickel peak *in vivo*, however this could not be confirmed as nickel-bound *Cn*UreG due to experimental limitations. Likewise, binding of nickel to *Cn*UreG produced small changes in secondary structure that have not been previously reported for bacterial UreG proteins but similar changes have been observed for nickel binding to bacterial UreE (Won and Lee, 2004). These results are consistent with *Cn*UreG acting as the nickel chaperone to urease, assuming the difference in nickel binding characteristics of bacterial UreE and UreG proteins is directly related to their function. This suggests a model in which *Cn*UreG binds nickel, imported to the cell via *Cn*Nic1, and then binds to the urease-UreDF assembly complex. At this point nickel is passed to the urease active site in a GTP hydrolysis dependent manner (Figure 54). The role UreE in bacterial urease maturation systems is variable. In *K. aerogenes* UreE is required to sequester and deliver nickel to the urease-UreDFG complex, however in *H. pylori* a HypA-HypB complex delivers the nickel and UreE

is required to transfer nickel to UreG (Lee *et al*., 1993; Olson *et al*., 2001). The central binding site present in all UreE proteins is vital for urease maturation and is thought to be required for transfer of nickel to UreG (Stola *et al*., 2006). Therefore, the pivotal role for UreE is the transfer of nickel to UreG, and thereby to urease. In *C. neoformans*, *Cn*UreG may be able to transfer nickel from the N-terminal region to the urease active site potentially via the putative C173 metal binding site.

To confirm the theory outlined above further examination of the role of the *Cn*UreG N-terminal domain is required, investigating the effect of deletion of this region *in vitro* and *in vivo*. In addition, mutation studies could be used to determine if the putative C173 metal site binds nickel *in vitro* and if nickel binding at this site is required for urease activation *in vivo*. The other role for *Cn*UreG, as a GTPase, has not been addressed in this study. The GTPase activity of bacterial UreG proteins is very low and this is thought to be due to the requirement of other urease accessory proteins to activate the GTPase function. As the *C. neoformans* urease maturation system lacks UreE, which may be the required factor to activate bacterial UreG proteins, determination of *Cn*UreG GTPase activity *in vitro* would be of interest. Expression of *Cn*UreG lacking the N-terminal region *in vivo* would also allow for the GTPase role to be investigated separately from the chaperone role. If deletion of the N-terminal reduced urease activity, co-expression of a bacterial UreE or addition of excess nickel could be used to investigate if *Cn*UreG has the same role as bacterial UreG proteins.

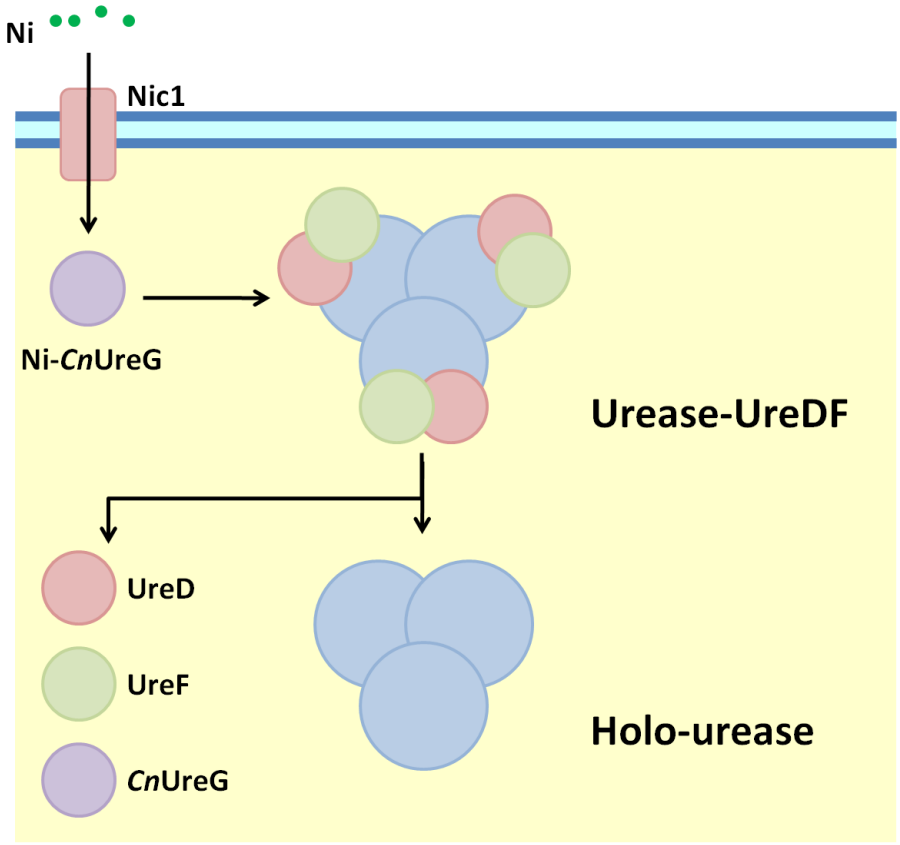

Figure 54 - The proposed model of urease maturation in *C. neoformans*.

The urease maturation complex is assembled by the binding to UreD and UreF to the urease apo-enzymes in the same manner as bacteria. Nickel loaded *Cn*UreG binds to the urease-UreDF complex and facilitates maturation by delivery of nickel to the active site in a potentially GTP hydrolysis dependent step.

6.4. The Inhibition of Urease by Cobalt

The urease activity of *C. neoformans* was inhibited by cobalt *in vivo* and relatively low levels of cobalt were able to significantly reduce activity, 1 μM of cobalt added to the growth media reduced urease activity to approximately half that of wild-type levels. This is very low compared to the 100 μM cobalt required to interrupt [Fe-S] cluster biogenesis in *H. pylori*, although this difference may reflect the relative concentrations of nickel and iron in the growth media of each organism (Ranquet *et al*., 2007). Profile studies revealed that cobalt bound to urease and that this prevented nickel binding, however where cobalt bound was not clear. Studies of *K. aerogenes* urease *in vitro* have established that cobalt can bind to a cysteine residue outside the active site and prevent maturation, therefore cobalt binding to the equivalent residue in *C. neoformans* urease may be inhibiting activity (Park and Hausinger, 1996; Yamaguchi and Hausinger, 1997). If cobalt is entering the active site of urease this is likely to take place prior to modification of the lysine residue and loading with nickel, as *in vitro* studies with *K. aerogenes* urease indicate that replacement of nickel in the active site by cobalt is extremely inefficient (King and Zerner, 1997). Therefore in the model of *C. neoformans* urease maturation outlined above, cobalt may bind before nickel loaded *Cn*UreG reaches the assembly complex (Figure 55). The binding of cobalt to urease in preference to other potential metal binding sites in the cell is probably due to the similarity between cobalt and nickel in binding geometries, which would allow cobalt to occupy the site utilising the same ligands as nickel.

A role of metallochaperones is to protect the target proteins from mis-population with the incorrect metal. Protein-protein specific interactions allow the control of which metal is exposed to the target protein. Profile studies with the *ureGΔ* strain established that cobalt bound to urease via a *Cn*UreG independent mechanism. This supports the theory that cobalt binds to urease before maturation. However, this also highlights that *Cn*UreG does not prevent exposure of urease to cobalt. This indicates that *C. neoformans* has not evolved in an environment where cobalt was bio-available and so has not evolved an effective means of preventing incorporation of cobalt into urease. Studies of *K. aerogenes* urease *in vitro* have demonstrated that urease can be activated by exposure to carbon dioxide and nickel and that activation is increased by binding of the accessory proteins to the apo-enzyme, therefore the

active site is accessible by metal atoms (Carter *et al*., 2009). The urease of *C. neoformans* may also be exposed during these stages of development and so allow cobalt access to the active site.

6.5. Concluding Remarks

The urease maturation system of *C. neoformans* is of interest due to the role urease plays during cryptococcal infection and as the first eukaryotic nickel homeostatic system to be studied in detail and which has novel features compared to the bacterial systems studied. In this thesis evidence has been presented and a model set out describing how nickel is imported via the *Cn*Nic1 transporter and chaperoned to the urease assembly complex by *Cn*UreG. The inhibition of urease by cobalt binding has been demonstrated and this adds to an extremely short list of recorded *in vivo* metal mis-population events. In addition the induction of capsule formation in response to urea and the inhibition of the process by cobalt has been recorded. However, there are still many areas of this project which require confirmation and further investigation, including; the transcriptional and protein turnover regulation of the nickel uptake system, investigation of the individual residues of the *Cn*Nic1 HX_4DH motif, elucidation of the metal binding residues and GTPase activity of *Cn*UreG, confirmation of *Cn*UreG nickel binding *in vivo* and determination of the cobalt binding site on urease.

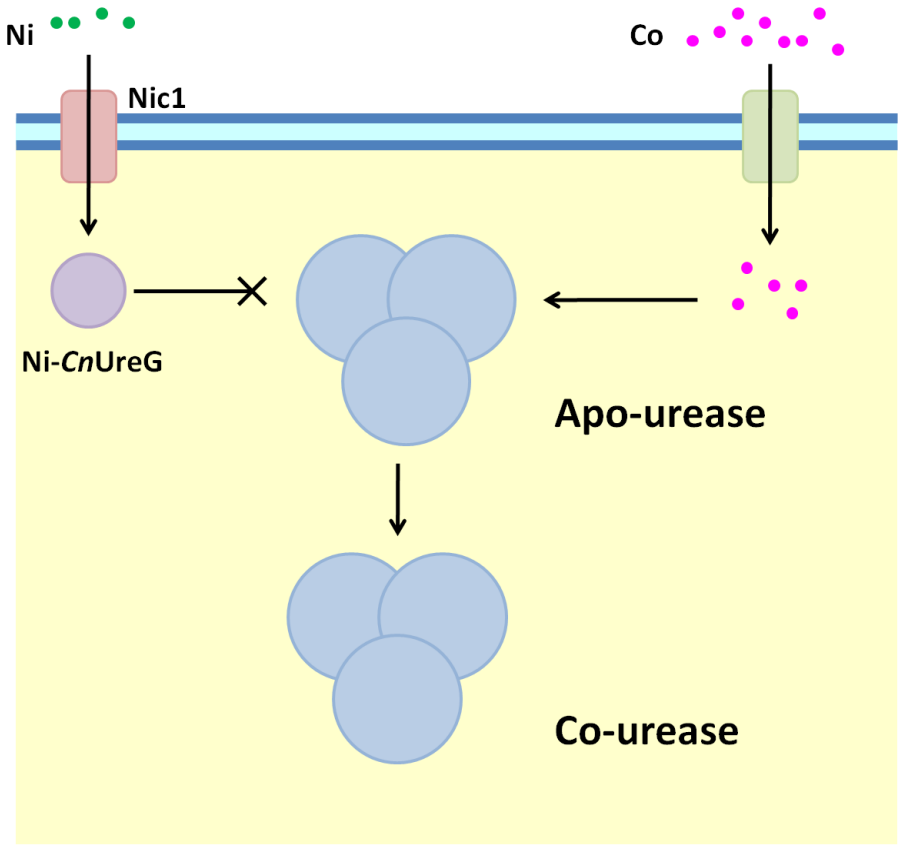

Figure 55 - The model of *C. neoformans* urease inhibition by cobalt.

Urease maturation is prevented by incorporation of cobalt into urease prior to nickel delivery by *Cn*UreG. The cobalt enters the cell via an unknown transporter (possibly Cramp or CorA).

7. References

Agranoff, D., Collins, L., Kehres, D., Harrison, T., Maguire, M., Krishna, S. (2005) 'The Nramp orthologue of *Cryptococcus neoformans* is a pH-dependent transporter of manganese, iron, cobalt and nickel.' *Biochemical Journal*, **385**: 225-32.

Al-Karadaghi, S., Hansson, M., Nikonov, S., Jönsson, B., Hederstedt, L. (1997) 'Crystal structure of ferrochelatase: the terminal enzyme in heme biosynthesis.' *Structure*, **5**: 1501-10.

Alagna, L., Hasnain, S.S., Piggott, B., Williams, D.J. (1984) 'The nickel ion environment in jack bean urease.' *Biochemical Journal*, **220**: 591-5.

Andrade, M.A., Chacón, P., Merelo, J.J., Morán, F. (1993) 'Evaluation of secondary structure of proteins from UV circular dichroism spectra using an unsupervised learning neural network.' *Protein Engineering*, **6**: 383-90.

Andrews, R.K., Dexter, A., Blakeley, R.L., Zerner, B. (1986) 'Jack bean urease (EC 3.5.1.5) VIII. On the inhibition of urease by amides and esters of phosphoric acid.' *Journal of the American Chemical Society*, **108**: 7124-5.

Anton, A., Grosse, C., Reissmann, J., Pribyl, T., Nies, D.H. (1999) 'CzcD is a heavy metal ion transporter involved in regulation of heavy metal resistance in *Ralstonia sp.* strain CH34.' *Journal of Bacteriology*, **181**: 6876-81.

Balasubramanian, A., **Ponnuraj**, K. (2010) 'Crystal structure of the first plant urease from jack bean: 83 years of journey from its first crystal to molecular structure.' *Journal of Molecular Biology*, **400**: 274-83.

Banci, L., Bertini, I., Ciofi-Baffoni, S., Finney, L.A., Outten, C.E., O'Halloran, T.V. (2002) 'A new zinc-protein coordination site in intracellular metal trafficking: solution structure of the Apo and Zn(II) forms of ZntA(46-118).' *Journal Molecular Biology*, **323**: 883-97.

Barras, F., Loiseau, L., Py, B. (2005) 'How *Escherichia coli* and *Saccharomyces cerevisiae* build Fe/S proteins.' *Advances in Microbial Physiology*, **50**: 41-101.

Bellucci, M., Zambelli, B., Musiani, F., Turano, P., Ciurli, S. (2009) '*Helicobacter pylori* UreE, a urease accessory protein: specific Ni(2+)- and Zn(2+)-binding properties and interaction with its cognate UreG.' *Biochemical Journal*, **422**: 91-100.

Benini, S., Rypniewski, W.R., Wilson, K.S., Miletti, S., Ciurli, S., Mangani, S. (1999) 'A new proposal for urease mechanism based on the crystal structures of the native and inhibited enzyme from *Bacillus pasteurii*: why urea hydrolysis costs two nickels.' *Structure,* **7**: 205-16.

Benoit, S., **Maier**, R.J. (2003) 'Dependence of *Helicobacter pylori* urease activity on the nickel-sequestering ability of the UreE accessory protein.' *Journal of Bacteriology*, **185**: 4787-95.

Benoit, S.L., Zbell, A.L., Maier, R.J. (2007) 'Nickel enzyme maturation in *Helicobacter hepaticus*: roles of accessory proteins in hydrogenase and urease activities.' *Microbiology*, **153**: 3748-56.

Beyer, W.F.Jr., Fridovich, I. (1991) 'In vivo competition between iron and manganese for occupancy of the active site region of the manganese-superoxide dismutase of *Escherichia coli*.' *Journal of Biological Chemistry*, **266**: 303-8.

Beinert, H., Holm, R.H., Münck, E. (1997) 'Iron-sulfur clusters: nature's modular, multipurpose structures.' *Science,* **277**: 653-9.

Bicanic, T., **Harrison**, T.S. (2004) 'Cryptococcal meningitis.' *British Medical Bulletin*, **72**: 99-118.

Bird, A.J., Zhao, H., Luo, H., Jensen, L.T., Srinivasan, C., Evans-Galen, M., Winge, D.R., Eide, D.J. (2000) 'A dual role for zinc fingers in both DNA binding and zinc sensing by the Zap1 transcriptional activator.' *EMBO Journal*, **19**: 34221-6.

Blaiseau, P.-L., Lesuisse, E., Camadro, J.-M. (2001) 'Aft2p, a novel iron-regulated transcription activator that modulates, with Aft1p, intracellular iron use and resistance to oxidative stress in yeast.' *Journal of Biological Chemistry*, **276**: 34221-6.

Boer, J.L., Quiroz-Valenzuela, S., Anderson, K.L., Hausinger, R.P. (2010) 'Mutagenesis of *Klebsiella aerogenes* UreG to probe nickel binding and interactions with other urease-related proteins.' *Biochemistry*, **49**: 5859-69.

Bose, I., Reese, A.J., Ory, J.J., Janbon, G., Doering, T.L. (2003) 'A yeast under cover: the capsule of *Cryptococcus neoformans*.' *Eukaryotic Cell*, **2**: 655-63.

Brayman, T.G., **Hausinger**, R.P. (1996) 'Purification, characterization, and functional analysis of a truncated *Klebsiella aerogenes* UreE urease accessory

protein lacking the histidine-rich carboxyl terminus.' *Journal of Bacteriology*, **178**: 5410-6.

Buchanan, K.L., **Murphy**, J.W. (1998) 'What makes *Cryptococcus neoformans* a pathogen?' *Emerging Infectious Diseases*, **4**: 71-83.

Camadro, J.M., **Labbé**, P. (1982) 'Kinetic studies of ferrochelatase in yeast. Zinc or iron as competing substrates.' *Biochemica et Biophysica Acta*, **707**: 280-8.

Camadro, J.M., Urban-Grimal, D., Labbé, P. (1982) 'A new assay for protoporphyrinogen oxidase - evidence for a total deficiency in that activity in a heme-less mutant of *Saccharomyces cerevisiae*.' *Biochemical and Biophysical Research Communications*, **106**: 724-30.

Canteros, C.E., Rodero, L., Rivas, M.C., Davel, G. (1996) 'A rapid urease test for presumptive identification of *Cryptococcus neoformans.*' *Mycopathologia*, **136**: 21-2.

Carter, E.L., Flugga, N., Boer, J.L., Mulrooney, S.B., Hausinger, R.P. (2009) 'Interplay of metal ions and urease.' *Metallomics*, **1**: 207-21.

Carter, E.L., **Hausinger**, R.P. (2010) 'Characterization of the *Klebsiella aerogenes* urease accessory protein UreD in fusion with the maltose binding protein.' *Journal of Bacteriology*, **192**: 2294-304.

Carter, E.L., Tronrud, D.E., Taber, S.R., Karplus, P.A., Hausinger, R.P. (2011) 'Iron-containing urease in a pathogenic bacterium.' *Proceedings of the National Academy of Sciences*, **108**: 13095-9.

Casadevall, A.P., **Perfect**, J.R. (1998) '*Cryptococcus neoformans.*' ASM Press, Washington, DC.

Casadevall, A.P., Steenbergen, J.N., Nosanchuk, J.D. (2003) "Ready made' virulence and 'dual use' virulence factors in pathogenic environmental fungi - the *Cryptococcus neoformans* paradigm.' *Current Opinion in Microbiology*, **6**: 332-7.

Casas, C., Aldea, M., Espinet, C., Gallego, C., Gil, R., Herrero, E. (1997) 'The AFT1 transcriptional factor is differentially required for expression of high-affinity iron uptake genes in *Saccharomyces cerevisiae*.' *Yeast*, **13**: 621-37.

Chai, H.C., **Tay**, S.T. (2009) 'Detection of IgM and IgG antibodies to *Cryptococcus neoformans* proteins in blood donors and HIV patients with active cryptococcosis.' *Mycoses*, **52**: 166-70.

Chang, Y.C., **Kwon-Chung**, K.J. (1994) 'Complementation of a capsule-deficient mutation of *Cryptococcus neoformans* restores its virulence.' *Molecular Cell Biology*, **14**: 4912-9.

Chang, Z., Kuchar, J., Hausinger, R.P. (2004) 'Chemical cross-linking and mass spectrometric identification of sites of interaction for UreD, UreF, and urease.' *Journal of Biological Chemistry*, **279**: 15305-13.

Changela, A., Chen, K., Xue, Y., Holschen, J., Outten, C.E., O'Halloran, T.V., Mondragon, A. (2003) 'Molecular Basis of Metal-Ion Selectivity and Zeptomolar Sensitivity by CueR.' *Science*, **301**: 1383-7

Cherniak, R., O'Neill, E.B., Sheng, S. (1998) 'Assimilation of xylose, mannose, and mannitol for synthesis of glucuronoxylomannan of *Cryptococcus neoformans* determined by 13C nuclear magnetic resonance spectroscopy.' *Infection and Immunity*, **66**: 2996-8.

Chillappagari, S., Seubert, A., Trip, H., Kuipers, O.P., Marahiel, M.A., Miethke, M. (2010) 'Copper stress affects iron homeostasis by destabilizing iron-sulfur cluster formation in *Bacillus subtilis*.' *Journal of Bacteriology*, **192**: 2512-24.

Clemens, D.L., Lee, B.Y., Horwitz, M.A. (1995) 'Purification, characterization, and genetic analysis of *Mycobacterium tuberculosis* urease, a potentially critical determinant of host-pathogen interaction.' *Journal of Bacteriology*, **177**: 5644-52.

Coffman, J.A., Rai, R., Cunningham, T., Svetlov, V., Cooper, T.G. (1996) 'Gat1p, a GATA family protein whose production is sensitive to nitrogen catabolite repression, participates in transcriptional activation of nitrogen-catabolic genes in *Saccharomyces cerevisiae*.' *Molecular and Cellular Biology*, **16**: 847-58.

Cooper, T.G., (1982) ' Nitrogen metabolism in *Saccharomyces cerevisiae*' in 'The Molecular Biology of the Yeast *Saccharomyces*: Metabolism and Gene Expression.' *Cold Spring Harbor Laboratory Press*, 39-99.

Colpas, G.J., Brayman, T.G., Ming, L.J., Hausinger, R.P. (1999) 'Identification of metal-binding residues in the *Klebsiella aerogenes* urease nickel metallochaperone, UreE.' *Biochemistry*, **38**: 4078-88.

Colpas, G.J., **Hausinger**, R.P. (2000) 'In vivo and in vitro kinetics of metal transfer by the *Klebsiella aerogenes* urease nickel metallochaperone, UreE.' *Journal of Biological Chemistry*, **275**: 10731-7.

Cox, G.M., Mukherjee, J., Cole, G. T., Casadevall, A., Perfect, J. R. (2000) 'Urease as a virulence factor in experimental cryptococcosis.' *Infection and Immunity*, **68**: 443-8.

Culotta, V.C., Yang, M., O'Halloran, T.V. (2006) 'Activation of superoxide dismutases: putting the metal to the pedal.' *Biochemica et Biophysica Acta*, **1763**: 747-58.

Cunningham, T.S., **Cooper**, T.G. (1991) 'Expression of the DAL80 gene, whose product is homologous to the GATA factors and is a negative regulator of multiple nitrogen catabolic genes in *Saccharomyces cerevisiae*, is sensitive to nitrogen catabolite repression.' *Molecular and Cellular Biology*, **11**: 6205-15.

Dancis, A. (1998) 'Genetic analysis of iron uptake in the yeast *Saccharomyces cerevisiae*.' *Journal of Pediatrics*, **132**: S24-9.

Daugherty, J.R., Rai, R., el Berry, H.M., Cooper, T.G. (1993) 'Regulatory circuit for responses of nitrogen catabolic gene expression to the GLN3 and DAL80 proteins and nitrogen catabolite repression in *Saccharomyces cerevisiae*.' *Journal of Bacteriology*, **175**: 64-73.

Degen, O., Kobayashi, M., Shimizu, S., Eitinger, T. (1999) 'Selective transport of divalent cations by transition metal permeases: the *Alcaligenes eutrophus* HoxN and the *Rhodococcus rhodochrous* NhlF.' *Archives of Microbiology*, **171**: 139-45.

Degen, O., **Eitinger**, T. (2002) 'Substrate specificity of nickel/cobalt permeases: insights from mutants altered in transmembrane domains I and II.' *Journal of Bacteriology*, **184**: 3569-77.

Delaunay, C., Blatter, G., Canciani, J.P., Jones, D.L., Laffargue, P., Neumann, H.W., Pap, G., Perka, C., Sutcliff, M.J., Zippel, H. (2010) 'Survival analysis of an asymmetric primary total knee replacement: a European multicenter prospective study.' *Orhopaedics and Traumatology, Surgery and Research*, **96**: 769-76.

Dixon, N.E., Gazzola, T.C., Blakeley, R.L., Zermer, B. (1975) 'Letter: Jack bean urease (EC 3.5.1.5). A metalloenzyme. A simple biological role for nickel?' *Journal of the American Chemical Society*, **97**: 4131-3.

Dixon, N.E., Riddles, P.W., Gazzola, C., Blakeley, R.L., Zerner, B. (1980) 'Jack bean urease (EC 3.5.1.5). V. On the mechanism of action of urease on urea, formamide, acetamide, N-methylurea, and related compounds.' *Canadian Journal of Biochemistry*, **58**: 1335-44.

Doering, T.L. (2009) 'How sweet it is! Cell wall biogenesis and polysaccharide capsule formation in C*ryptococcus neoformans.*' *Annual Review of Microbiology*, **63**: 223-47.

Eide, D.J. (2003) 'Multiple regulatory mechanisms maintain zinc homeostasis in *Saccharomyces cerevisiae*.' *Journal of Nutrition*, **133**: 1532S-5S.

Eitinger, T., **Friedrich**, B., (1991) 'Cloning, nucleotide sequence, and heterologous expression of a high-affinity nickel transport gene from *Alcaligenes eutrophus*.' *Journal of Biological Chemistry*, **266**: 3222-7.

Eitinger, T., Wolfram, L., Degen, O., Anthon, C. (1997) 'A Ni2+ binding motif is the basis of high affinity transport of the *Alcaligenes eutrophus* nickel permease.' *Journal of Biological Chemistry*, **272**: 17139-44.

Eitinger, T., **Mandrand-Berthelot**, M.A. (2000) 'Nickel transport systems in microorganisms.' *Archives of Microbiology*, **173**: 1-9.

Eitinger, T., Degen, O., Bohnke, U., Muller, M. (2000) 'Nic1p, a relative of bacterial transition metal permeases in *Schizosaccharomyces pombe*, provides nickel ion for urease biosynthesis.' *Archives of Microbiology*, **275**: 18029-33.

Eitinger, T., Suhr, J., Moore, L., Smith, J.A. (2005) 'Secondary transporters for nickel and cobalt ions: theme and variations.' *Biometals*, **18**: 399-405.

Ellis, D.H., **Pfeiffer**, T.J., (1990a) 'Ecology, life cycle, and infectious propagule of Cryptococcus neoformans.' *Lancet*, **13**: 923-5.

Ellis, D.H., **Pfeiffer**, T.J., (1990b) 'Natural habitat of *Cryptococcus neoformans var. gattii*.' *Journal of Clinical Microbiology*, **28**: 1642-4.

Ferguson, A.D., **Deisenhofer**, J. (2004) 'Metal import through microbial membranes'.' *Cell*, **116**: 15-24.

Fontecave, M., **Ollagnier-de-Choudens**, S. (2008) 'Iron-sulfur cluster biosynthesis in bacteria: Mechanisms of cluster assembly and transfer.' *Archives of Biochemistry and Biophysics*, **474**: 226-37.

Fraser, J.A., Subaran, R.L., Nichols, C.B., Heitman, J. (2003) 'Recapitulation of the Sexual Cycle of the Primary Fungal Pathogen Cryptococcus neoformans var. gattii: Implications for an Outbreak on Vancouver Island, Canada.' *Eukaryotic Cell*, **2**: 1036-1045.

Fraústo da Silva, J.J.R., **Williams**, R.J.P. (2001) 'The Biological Chemistry of the Elements: The Inorganic Chemistry of Life.' *Oxford University Press*.

Franzot, S.P., Salkin, I.F., Casadevall, A. (1999) *'Cryptococcus neoformans var. grubii*: separate varietal status for Cryptococcus neoformans serotype A isolates.' *Journal of Clinical Microbiology*, **37**: 838-40.

French, N., Gray, K., Watera, C., Nakiyingi, J., Lugada, E., Moore, M., Lalloo, D., Whitworth, J. A. G., Gilks, C. F. (2002) 'Cryptococcal infection in a cohort of HIV-1-infected Ugandan adults.' *AIDS* **16**: 1031-8.

Freyermuth, S.K., Bacanamwo, M., Polacco, J.C. (2000) 'The soybean Eu3 gene encodes an Ni-binding protein necessary for urease activity.' *Plant Journal*, **21**: 53-60.

Fu, Y.H., **Marzluf**, G.A. (1987a) 'Characterization of nit-2, the major nitrogen regulatory gene of *Neurospora crassa*.' *Molecular and Cellular Biology*, **7**: 1691-6.

Fu, Y.H., **Marzluf**, G.A. (1987b) 'Molecular cloning and analysis of the regulation of nit-3, the structural gene for nitrate reductase in *Neurospora crassa*.' *Proceedings of the National Academy of Sciences*, **84**: 8243-7.

Furukawa, Y., Torres, A.S., O'Halloran, T.V. (2004) 'Oxygen-induced maturation of SOD1: a key role for disulfide formation by the copper chaperone CCS.' *EMBO Journal*, **23**: 2872-81.

García-Rivera, J., Chang, Y.C., Kwon-Chung, K.J., Casadevall, A. (2004) '*Cryptococcus neoformans* induces alterations in the cytoskeleton of human brain microvascular endothelial cells.' *Eukaryotic Cell*, **3**: 385-92.

Ge, R., Zhang, Y., Sun, X., Watt, R.M., He, Q.Y., Huang, J.D., Wilcox, D.E., Sun, H. (2006) 'Thermodynamic and kinetic aspects of metal binding to the histidine-rich protein, Hpn.' *Journal of American Chemical Society*, **128**: 11330-1.

Ghasemi, M., Bakhtiari, M., Fallahpour, M., Noohi, A., Moazami, N., Amidi, Z. (2004) 'Screening of Urease Production by *Aspergillus niger* Strains.' *Iranian Biomedical Journal*, **8:** 47-50.

Gilbert, J.V., Ramakrishna, J., Sunderman, F.W.Jr., Wright, A., Plaut, A.G. (1995) 'Protein Hpn: cloning and characterization of a histidine-rich metal-binding polypeptide in *Helicobacter pylori* and *Helicobacter mustelae*.' *Infection and Immunity*, **63**: 2682-8.

Goldstein, A.L., and **McCusker**, J.H. (1999) 'Three new dominant drug resistance cassettes for gene disruption in Saccharomyces cerevisiae.' *Yeast*, **15:** 1541-15.

Granger, D.L., Perfect, J.R., Durack, D.T. (1985) 'Virulence of *Cryptococcus neoformans*. Regulation of capsule synthesis by carbon dioxide.' *Journal of Clinical Investigation*, **76**: 508-16.

Grenson, M. (1983) 'Inactivation-reactivation process and repression of permease formation regulate several ammonia-sensitive permeases in the yeast *Saccharomyces cerevisiae*.' *European Journal of Biochemistry*, **1**: 141-4.

Guimarães, A.J., Frases, S., Cordero, R.J., Nimrichter, L., Casadevall, A., Nosanchuk, J.D. (2010) '*Cryptococcus neoformans* responds to mannitol by increasing capsule size *in vitro* and *in vivo*.' *Cellular Microbiology*, **12**: 740-53.

Gupta, G., Fries, B.C., 'Variability of phenotypic traits in Cryptococcus varieties and species and the resulting implications for pathogenesis.' *Future Microbiology*, **5**: 775-87.

Ha, N.C., Oh, S.T., Sung, J.Y., Cha, K.A., Lee, M.H., Oh, B.H. (2001) 'Supramolecular assembly and acid resistance of *Helicobacter pylori* urease.' *Nature Structural Biology*, **8**: 505-9.

Haurie, V., Boucherie, H., Sagliocco, F. (2003) 'The Snf1 protein kinase controls the induction of genes of the iron uptake pathway at the diauxic shift in *Saccharomyces cerevisiae*.' *Journal of Biological Chemistry*, **278**: 45391-6.

Hausinger, R.P. (1994) 'Nickel enzymes in microbes.' *The Science of the Total Environment*, **148**: 157-66.

Higgins, C.F. (2001) 'ABC transporters: physiology, structure and mechanism--an overview.' *Research in Microbiology*, **152**: 205-10.

Hensel, M., Arst, H.N.Jr., Aufauvre-Brown, A., Holden, D.W. (1998) 'The role of the *Aspergillus fumigatus* areA gene in invasive pulmonary aspergillosis.' *Molecular and General Genetics*, **258**: 553-7.

Hmiel, S.P., Snavely, M.D., Miller, C.G., Maguire, M.E. (1986) 'Magnesium transport in *Salmonella typhimurium*: characterization of magnesium influx and cloning of a transport gene.' *Journal of Bacteriology*, **168**: 1444-50.

Huffman, D.L., **O'Halloran**, T.V. (2001) 'Function, structure, and mechanism of intracellular copper trafficking proteins.' *Annual Review of Biochemistry*, **70**: 677-701.

Idnurm, A., Bahn, Y., Nielsen, K., Lin, X., Fraser, J.A., Heitman, J. (2005) 'Deciphering the model pathogenic fungus *Cryptococcus neoformans*.' *Nature Reviews Microbiology*, **3**: 753-764.

Irving, H., **Williams**, R.J.P. (1948) 'Order of stability of metal complexes.' *Nature*, **162**: 746-747

Irving, H., **Williams**, R.J.P. (1953) 'The stability of transition-metal complexes.' *Journal of the Chemical Society*, 3192-3210.

Jabri, E., Carr, M.B., Hausinger, R.P., Karplus, P.A. (1995) 'The crystal structure of urease from *Klebsiella aerogenes*.' *Science*, **268**: 998-1004.

Jauniaux, J.C., Vandenbol, M., Vissers, S., Broman, K., Grenson, M. (1987) 'Nitrogen catabolite regulation of proline permease in *Saccharomyces cerevisiae*. Cloning of the PUT4 gene and study of PUT4 RNA levels in wild-type and mutant strains.' *European Journal of Biochemistry*, **164**: 601-6.

Jauniaux, J.C., **Grenson**, M. (1990) 'GAP1, the general amino acid permease gene of *Saccharomyces cerevisiae*. Nucleotide sequence, protein similarity with the other bakers yeast amino acid permeases, and nitrogen catabolite repression.' *European Journal of Biochemistry*, **31**: 39-44.

Jensen, L.T., **Winge**, D.R. (1998) 'Identification of a copper-induced intramolecular interaction in the transcription factor Mac1 from *Saccharomyces cerevisiae*.' *EMBO Journal*, **17**: 5400-8.

Kehres, D.G., Zaharik, M.L., Finlay, B.B., Maguire, M.E. (2000) 'The NRAMP proteins of *Salmonella typhimurium* and *Escherichia coli* are selective manganese transporters involved in the response to reactive oxygen.' *Molecular Microbiology*, **36**: 1085-100.

Kidd, S.E., Chow, Y., Mak, S., Bach, P.J., Chen, H., Hingston, A.O., Kronstad, J.W., Bartlett, K.H. (2007) 'Characterization of environmental sources of the human and animal pathogen *Cryptococcus gattii* in British Columbia, Canada, and the Pacific Northwest of the United States.' *Applied & Environmental Microbiology*, **73**: 1433-43.

Kim, K.Y., Yang, C.H., Lee, M.H. (1999) 'Expression of the recombinant *Klebsiella aerogenes* UreF protein as a MalE fusion.' *Archives of Pharmaceutical Research*, **22**: 274-8.

Kim, J.K., Mulrooney, S.B., Hausinger, R.P. (2006) 'The UreEF fusion protein provides a soluble and functional form of the UreF urease accessory protein.' *Journal of Bacteriology*, **188**: 8413-20.

King, G.J., **Zerner**, B. (1997) 'Jack bean urease: mixed-metal derivatives.' *Inorganica Chimica Acta*, **255**: 381-8.

Kmetzsch, L., Staats, C.C., Simon, E., Fonseca, F.L., Oliveira, D.L., Joffe, L.S., Rodrigues, J., Lourenço, R.F., Gomes, S.L., Nimrichter, L., Rodrigues, M.L., Schrank, A., Vainstein, M.H. (2011) 'The GATA-type transcriptional activator Gat1 regulates nitrogen uptake and metabolism in the human pathogen *Cryptococcus neoformans*.' *Fungal Genetics and Biology*, **48**: 192-9.

Koguchi, Y., **Kawakami**, K. (2002) 'Cryptococcal infection and Th1-Th2 cytokine balance.' *International Reviews of Immunology*, **21**: 423-38.

Kozel, T.R., Pfrommer, G.S., Guerlain, A.S., Highison, B.A., Highison, G.J. (1988) 'Role of the capsule in phagocytosis of *Cryptococcus neoformans*.' *Reviews of Infectious Diseases*, **2**: S436-9.

Leitch, S., Bradley, M.J., Rowe, J.L., Chivers, P.T., Maroney, M.J. (2007) 'Nickel-specific response in the transcriptional regulator, Escherichia coli NikR.' *Journal of the American Chemical Society*, **129**: 5085-95.

Labbé, S., Zhu, Z., Thiele, D.J. (1997) 'Copper-specific transcriptional repression of yeast genes encoding critical components in the copper transport pathway.' *Journal of Biological Chemistry*, **272**: 15951-8.

Labbé, R.F., **Dewanji**, A. (2004) 'Iron assessment tests: transferrin receptor vis-à-vis zinc protoporphyrin.' *Clinical Biochemistry,* **37**: 165-74.

Lange, H., Kispal, G., Lill, R. (1999) 'Mechanism of iron transport to the site of heme synthesis inside yeast mitochondria.' *Journal of Biological Chemistry*, **274**: 18989-96.

Lazera, M.S., Pires, F.D., Camillo-Coura, L., Nishikawa, M. M., Bezerra, C. C., Trilles, L. and Wanke, B. (1996) 'Natural habitat of Cryptococcus neoformans var. neoformans in decaying wood forming hollows in living trees.' *Journal of Medical & Veterinary Mycology*, **34**: 127-31.

Lee, I.R., Chow, E.W., Morrow, C.A., Djordjevic, J.T., Fraser, J.A. (2011) 'Nitrogen metabolite repression of metabolism and virulence in the human fungal pathogen *Cryptococcus neoformans.*' *Genetics*, **188**: 309-23.

Lee, M.H., Mulrooney, S.B., Hausinger, R.P. (1990) 'Purification, characterization, and in vivo reconstitution of Klebsiella aerogenes urease apoenzyme.' *Journal of Bacteriology*, **172**: 4427-31.

Lee, M.H., Mulrooney, S.B., Renner, M.J., Markowicz, Y., Hausinger, R.P. (1992) '*Klebsiella aerogenes* urease gene cluster: sequence of ureD and demonstration that four accessory genes (ureD, ureE, ureF, and ureG) are involved in nickel metallocenter biosynthesis.' *Journal of Bacteriology*, **174**: 4324-30.

Lee, M.H., Pankratz, H.S., Wang, S., Scott, R.A., Finnegan, M.G., Johnson, M.K., Ippolito, J.A., Christianson, D.W., Hausinger, R.P. (1993) 'Purification and characterization of *Klebsiella aerogenes* UreE protein: a nickel-binding protein that functions in urease metallocenter assembly.' *Protein Science*, **2**: 1042-52.

Lee, Y.H., Won, H.S., Lee, M.H., Lee, B.J. (2002a) 'Effects of salt and nickel ion on the conformational stability of *Bacillus pasteurii* UreE.' *FEBS letters*, **522**: 135-40.

Lee, Y.H., Won, H.S., Ahn, H.C., Park, S., Yagi, H., Akutsu, H., Lee, B.J. (2002b) 'Backbone NMR assignments of the metal-free UreE from *Bacillus pasteurii*.' *Journal of Biomolecular NMR*, **24**: 361-2.

Levitz, S. M., (1991) 'The ecology of Cryptococcus neoformans and the epidemiology of cryptococcosis.' *Reviews of Infectious Diseases*, **13**: 1163-9.

Li, L., Chen, O.S., McVey Ward, D., Kaplan, D. (2001) 'CCC1 is a transporter that mediates vacuolar iron storage in yeast.' *Journal of Biological Chemistry*, **276**: 29515-19.

Li, X., Chanroj, S., Wu, Z., Romanowsky, S.M., Harper, J.F., Sze, H. (2008) 'A distinct endosomal Ca2+/Mn2+ pump affects root growth through the secretory process.' *Plant Physiology*, **147**:1675-89.

Li, Y., Zamble, D.B. (2009) 'pH-responsive DNA-binding activity of *Helicobacter pylori* NikR.' *Biochemistry*, **48**: 2486-96.

Liochev, S.I., **Fridovich**, I. (2010) 'Mechanism of the peroxidase activity of Cu, Zn superoxide dismutase.' *Free Radical Biology and Medicine*, **15**: 1465-9

Liu, L., Tewari, R.P., Williamson, P.R. (1999) 'Laccase protects *Cryptococcus neoformans* from antifungal activity of alveolar macrophages.' *Infection and Immunity*, **67**: 6034-39.

Lorenz, M.C., **Heitman**, J. (1997) 'Yeast pseudohyphal growth is regulated by GPA2, a G protein alpha homolog.' *EMBO Journal*, **16**: 7008-18.

Lu, Z.H., **Solioz**, M. (2002) 'Bacterial copper transport.' *Advances in Protein chemistry*, **60**: 93-121

MacDiarmid, C.W., Gaither, L.A., Eide, D.J. (2000) 'Zinc transporters that regulate vacuolar zinc storage in *Saccharomyces cerevisiae*.' *EMBO Journal*, **19**: 2845-55.

MacDiarmid, C.W., Gaither, L.A., Eide, D.J. (2002) 'Biochemical properties of vacuolar zinc transport systems of *Saccharomyces cerevisiae*.' *Journal of Biological Chemistry*, **277**: 39187-94.

Macomber, L., **Imlay**, J.A. (2009) 'The iron-sulfur clusters of dehydratases are primary intracellular targets of copper toxicity.' *Proceedings of the National Academy of Sciences*, **106**: 8344-9.

Magasanik, B., **Kaiser**, C.A. (2002) 'Nitrogen regulation in *Saccharomyces cerevisiae*.' *Gene*, **290**: 1-18.

Maier, R.J., Benoit, S.L., Seshadri, S. (2007) 'Nickel-binding and accessory proteins facilitating Ni-enzyme maturation in *Helicobacter pylori*.' *Biometals,* **20**: 655-64.

Majtan, T., Frerman, F.E., Kraus, J.P. (2011) 'Effect of cobalt on *Escherichia coli* metabolism and metalloporphyrin formation.' *Biometals*, **24**: 335-47.

Matthews, J.M., Bhati, M., Lehtomaki, E., Mansfield, R.E., Cubeddu, L., Mackay, J.P. (2009) 'It takes two to tango: the structure and function of LIM, RING, PHD and MYND domains.' Current Pharmaceutical Design, 15: 3681-96.

Mehta, N., Benoit, S., Maier, R.J. (2003a) 'Roles of conserved nucleotide-binding domains in accessory proteins, HypB and UreG, in the maturation of nickel-enzymes required for efficient *Helicobacter pylori* colonization.' *Microbial Pathogenesis*, **35**: 229-34.

Mehta, N., Olson, J.W., Maier, R.J. (2003b) 'Characterization of *Helicobacter pylori* nickel metabolism accessory proteins needed for maturation of both urease and hydrogenase.' *Journal of Bacteriology*, **185**: 726-34.

Minehart, P.L., **Magasanik**, B. (1991) 'Sequence and expression of GLN3, a positive nitrogen regulatory gene of *Saccharomyces cerevisiae* encoding a protein with a putative zinc finger DNA-binding domain.' *Molecular and Cellular Biology*' **11**: 6216-28.

Mirbond-Donovan, F., Schaller, R., Hung, C.-Y., Xue, J., Reichard, U., Cole, G.T. (2006) 'Urease produced by Coccidioides posadasii contributes to the virulence of this respiratory pathogen.' *Infection and Immunity*, **74**: 504-15.

Mitchell, T.G., **Perfect**, J.R. (1995) 'Cryptococcosis in the era of AIDS - 100 years after the discovery of *Cryptococcus neoformans.*' *Clinical Microbiology Reviews*, **8**: 515-48.

Mizuno, K., Whittaker, M.M., Bachinger, H.P., Whittaker, J.W. (2004) 'Calorimetric studies on the tight binding metal interactions of *Escherichia coli* manganese superoxide dismutase.' *Journal of Biological Chemistry*, **279**: 27339-44.

Mobley, H.L., Island, M.D., Hausinger, R.P. (1995) 'Molecular biology of microbial ureases.' *Microbiological Reviews*, **59**: 451-80.

Moncrief, M.B., **Hausinger**, R.P. (1996) 'Purification and activation properties of UreD-UreF-urease apoprotein complexes.' *Journal of Bacteriology*, **178**: 5417-21.

Moncrief, M.B., **Hausinger**, R.P. (1997) 'Characterisation of UreG, identification of a UreD-UreF-UreG complex, and evidence suggesting that a nucleotide-binding site in UreG is required for *in vivo* metallocenter assembly of *Klebsiella aerogenes* urease.' *Journal of Bacteriology*, **179**: 4081-6.

Mulrooney, S.B., Ward, S.K., Hausinger, R.P. (2005) 'Purification and properties of the Klebsiella aerogenes UreE metal-binding domain, a functional metallochaperone of urease.' *Journal of Bacteriology*, **187**: 3581-5.

Musiani, F., Zambelli, B., Stola, M., Ciurli, S. (2004) 'Nickel trafficking: insights into the fold and function of UreE, a urease metallochaperone.' *Journal of Inorganic Biochemistry*, **98**: 803-13.

Navarro, C., Wu, L.F., Mandrand-Berthelot, M.A. (1993) 'The Nik operon of Escherichia coli encodes a periplasmic binding-protein-dependent transport system for nickel.' *Molecular Microbiology*, **9**: 1181-91.

Neyroz, P., Zambelli, B., Ciurli, S. (2006) 'Intrinsically disordered structure of *Bacillus pasteurii* UreG as revealed by steady-state and time-resolved fluorescence spectroscopy.' *Biochemistry*, **45**: 8918-30.

Niegowski, D., **Eshaghi**, S. (2007) 'The CorA family: structure and function revisited.' *Cellular and Molecular Life Sciences*, **64**: 2564-74.

Nielsen, K., De Obaldia, A. L., Heitman, J. (2007) '*Cryptococcus neoformans* mates on pigeon guano: implications for the realized ecological niche and globalization.' *Eukaryotic Cell*, **6**: 949-59.

Okagaki, L.H., Strain, A.K., Nielsen, J.N., Charlier, C., Baltes, N.J., Chrétien, F., Heitman, J., Dromer, F., Nielsen, K. (2010) 'Cryptococcal cell morphology affects host cell interactions and pathogenicity.' *PLoS Pathogens*, **6**: e1000953.

Okongo, M., Morgan, D., Mayanja, B., Ross, A., Whitworth, J. (1998) 'Causes of death in a rural, population-based human immunodeficiency virus type 1 (HIV-1) natural history cohort in Uganda.' *International Journal of Epidemiology*, **27**: 698-702.

Olson, J.W., Fu, C., Maier, R.J. (1997) 'The HypB protein from B*radyrhizobium japonicum* can store nickel and is required for the nickel-dependent transcriptional regulation of hydrogenase.' *Molecular Microbiology*, **24**: 119-28.

Olson, J.W., Mehta, N.S., Maier, R.J. (2001) 'Requirement of nickel metabolism proteins HypA and HypB for full activity of both hydrogenase and urease in *Helicobacter pylori*.' *Molecular Microbiology*, **39**: 176-82.

Olszewski, M.A., Noverr, M.C., Chen, G.-H., Toews, G.B., Cox, G.M., Perfect, J.R., Huffnagle, G.B. (2004) 'Urease expression by *Cryptococcus neoformans* promotes microvascular sequestration, thereby enhancing central nervous system invasion.' *American Journal of Pathology*, **164**: 1761-71.

Ooi, C.E., Rabinovich, E., Dancis, A., Bonifacino, J.S., Klausner, R.D. (1996) 'Copper-dependent degradation of the *Saccharomyces cerevisiae* plasma membrane copper transporter Ctr1p in the apparent absence of endocytosis.' *EMBO Journal*, **15**: 3515-23.

Outten, C.E., **O'Halloran**, T.V. (2001) 'Femtomolar sensitivity of metalloregulatory proteins controlling zinc homeostasis.' *Science*, **292**: 2488-92.

Park, I.S., Carr, M.B., Hausinger, R.P. (1994) 'In vitro activation of urease apoprotein and role of UreD as a chaperone required for nickel metallocenter assembly.' *Proceedings of the National Academy of Sciences*, **91**: 3233-7.

Park, I.S., **Hausinger**, R.P. (1995) 'Evidence for the presence of urease apoprotein complexes containing UreD, UreF, and UreG in cells that are competent for in vivo enzyme activation.' *Journal of Bacteriology*, **177**: 1947-51.

Park, I.S., **Hausinger**, R.P., (1996) 'Metal ion interaction with urease and UreD-urease apoproteins.' *Biochemistry*, **35**: 5345-52.

de **Pina**, K., Navarro, C., McWalter, L., Boxer, D.H., Price, N.C., Kelly, S.M. (1995) 'Purification and characterization of the periplasmic nickel-binding protein NikA of *Escherichia coli* K12.' *European Journal of Biochemistry*, **227**: 857-65.

Pearson, M.A., Michel, L.O., Hausinger, R.P., Karplus, P.A. (1997) 'Structures of Cys319 variants and acetohydroxamate-inhibited Klebsiella aerogenes urease.' *Biochemistry*, **36**: 8164-72.

Pot, R.G., Stoof, J., Nuijten, P.J., de Haan, L.A., Loeffen, P., Kuipers, E.J., van Vliet, A.H., Kusters, J.G. (2007) 'UreA2B2: a second urease system in the gastric

pathogen Helicobacter felis.' *FEMS Immunology and Medical Microbiology*, **50**: 273-9.

Portnoy, M.E., Schmidt, P.J., Rogers, R.S., Culotta, V.C. 'Metal transporters that contribute copper to metallochaperones in *Saccharomyces cerevisiae*.' *Molecular Genetics and Genomics*, **265**: 873-82.

Proctor, P. (1970) 'Similar functions of uric acid and ascorbate in man?' *Nature*, **28**: 868.

Perfect, J.R., Ketabchi, N., Cox, G.M., Ingram, C.W., Beiser, C.L. (1993) 'Karyotyping of *Cryptococcus neoformans* as an epidemiological tool.' *Journal of Clinical Microbiology*, **31**: 3305-9.

Perfect, J.R., Wong, B., Chang, Y. C., Kwon-Chung, K. J. and Williamson, P. R. (1998) '*Cryptococcus neoformans*: virulence and host defences.' *Medical Mycology*, **36**: 79-86.

Pierini, L.M., **Doering**, T.L. (2001) 'Spatial and temporal sequence of capsule construction in *Cryptococcus neoformans*.' *Molecular Microbiology*, **41**: 105-15.

Pujol-Carrion, N., Belli, G., Herrero, E., Nogues, A., de la Torre-Ruiz, M.A. (2006) 'Glutaredoxins Grx3 and Grx4 regulate nuclear localisation of Aft1 and the oxidative stress response in *Saccharomyces cerevisiae*.' *Journal of Cell Science*, **119** : 4554-64.

Ranquet, C., Ollagnier-de-Choudens, S., Loiseau, L., Barras, F., Fontecave, M. (2007) 'Cobalt stress in *Escherichia coli*. The effect on the iron-sulfur proteins.' *Journal of Biological Chemistry*, **282**: 30442-51.

Remaut, H., Safarov, N., Ciurli, S., Van Beeumen, J. (2001) 'Structural basis for Ni(2+) transport and assembly of the urease active site by the metallochaperone UreE from *Bacillus pasteurii*.' *Journal of Biological Chemistry*, **276**: 49365-70.

Rensing, C., Ghosh, M., Rosen, B.P. (1999) 'Families of soft-metal-ion-transporting ATPases.' *Journal of Bacteriology*, **181**: 5891-7.

Rivera, J., Feldmesser, M., Cammer, M., Casadevall, A. (1998) 'Organ-dependent variation of capsule thickness in *Cryptococcus neoformans* during experimental murine infection.' *Infection and Immunity*, **66**: 5027-30.

Robinson, P.A., Bauer, M., Leal, M.A., Evans, S.G., Holtom, P.D., Diamond, D.A., Leedom, J.M., Larsen, R.A. (1999) 'Early mycological treatment failure in AIDS-associated cryptococcal meningitis.' *Clinical Infectious Diseases*, **1**: 82-92.

Robinson, N.J., **Winge**, D.R. (2010) 'Copper metallochaperones.' *Annual Review of Biochemistry*, **79**: 537-62.

Rodrigues, M.L., Nakayasu, E.S., Oliveira, D.L., Nimrichter, L., Nosanchuk, J.D., Almeida, I.C., Casadevall, A. (2007) 'Extracellular vesicles produced by *Cryptococcus neoformans* contain protein components associated with virulence.' *Eukaryotic Cell*, **7**: 58-67.

Rodrigues, M.L., Nimrichter, L., Oliveira, D.L., Nosanchuk, J.D., Casadevall, A. (2008) 'Vesicular Trans-Cell Wall Transport in Fungi: A Mechanism for the Delivery of Virulence-Associated Macromolecules?' *Lipid Insights*, **2**: 27-40.

Ronne-Engström, E., Cesarini, K.G., Enblad, P., Hesselager, G., Marklund, N., Nilsson, P., Salci, K., Persson, L., Hillered, L. (2001) 'Intracerebral microdialysis in neurointensive care: the use of urea as an endogenous reference compound.' *Journal of Neurosurgery*, **94**: 397-402.

Rouf, M.A., **Lomprey**, R.F.Jr. (1968) 'Degradation of uric acid by certain aerobic bacteria.' *Journal of Bacteriology*, **96**: 617-22.

Rowe, J.L., Starnes, G.L., Chivers, P.T. (2005) 'Complex transcriptional control links NikABCDE-dependent nickel transport with hydrogenase expression in *Escherichia coli*.' *Journal of Bacteriology*, **187**: 6317-23.

Rulísek, L., **Vondrásek**, J. (1998) 'Coordination geometries of selected transition metal ions (Co2+, Ni2+, Cu2+, Zn2+, Cd2+, and Hg2+) in metalloproteins.' *Journal of Inorganic Biochemistry*, **71**: 115-27.

Rutherford, J.C., **Bird**, A.J. (2004) 'Metal-Responsive Transcription Factors that Regulate Iron, Zinc and Copper Homeostasis in Eukaryotic Cells.' *Eukaryotic Cell*, **3**: 1-13.

Saier, M.H.Jr., Tam, R., Reizer, A., Reizer, J. (1994) 'Two novel families of bacterial membrane proteins concerned with nodulation, cell division and transport.' *Molecular Microbiology*, **58**: 71-93.

Salomone-Stagni, M., Zambelli, B., Musiani, F., Ciurli, S. (2007) 'A model-based proposal for the role of UreF as a GTPase-activating protein in the urease active site biosynthesis.' *Proteins*, **68**: 749-61.

Schofield, C.J., **Ratcliffe**, P.J. (2004) 'Oxygen sensing by HIF hydroxylases.' *Nature Reviews. Molecular Cell Biology*, **5**: 343-54.

ter **Schure**, E.G., van Riel, N.A., Verrips, C.T. (2000) 'The role of ammonia metabolism in nitrogen catabolite repression in *Saccharomyces cerevisiae*.' *FEMS Microbiology Reviews*, **24**: 67-83.

Scott, D.R., Marcus, E.A., Weeks, D.L., Sachs, G. (2002) 'Mechanisms of acid resistance due to the urease system of *Helicobacter pylori*.' *Gastroenterology*, **123**: 187-85.

Sendide, K., Deghmane, A.-E., Reyrat, J.-M., Talal, A., Hmama, Z. (2004) '*Mycobacterium bovis* BCG urease attenuates major histocompatibility complex class II trafficking to the macrophage cell surface.' *Infection and Immunity*, **72**: 4200-9.

Seshadri, S., Benoit, S.L., Maier, R.J. (2007) 'Roles of His-rich hpn and hpn-like proteins in *Helicobacter pylori* nickel physiology.' *Journal of Bacteriology*, **189**: 4120-6.

Setty, S.R., Tenza, D., Sviderskaya, E.V., Bennett, D.C., Raposo, G., Marks, M.S. (2008) 'Cell-specific ATP7A transport sustains copper-dependent tyrosinase activity in melanosomes.' *Nature*, **454**:1142-6.

Sheridan, L., Wilmot, C.M., Cromie, K.D., van der Logt, P., Phillips, S.E. (2002) 'Crystallization and preliminary X-ray structure determination of jack bean urease with a bound antibody fragment.' *Acta Crystallographica. Section D, Biological Crystallography*, **58**: 374-6.

Shi, M. Li, S.S., Zheng, C., Jones, G.J., Kim, K.S., Zhou, H., Kubes, P., Mody, C.H. (2010a) 'Real-time imaging of trapping and urease-dependent transmigration of *Cryptococcus neoformans* in mouse brain.' *Journal of Clinical Investigation*, **120**: 1683-93.

Shi, R., Munger, C., Asinas, A., Benoit, S.L., Miller, E., Matte, A., Maier, R.J., Cygler, M. (2010b) 'Crystal structures of apo and metal-bound forms of the UreE protein from *Helicobacter pylori*: role of multiple metal binding sites.' *Biochemistry*, **49**: 7080-8.

Singleton, C., **Le Brun**, N.E. (2007) 'Atx1-like chaperones and their cognate P-type ATPases: copper-binding and transfer.' *Biometals*, **20**: 275-89.

Snavely, M.D., Florer, J.B., Miller, C.G., Maguire, M.E. (1989) 'Magnesium transport in *Salmonella typhimurium*: 28Mg2+ transport by the CorA, MgtA, and MgtB systems.' *Journal of Bacteriology*, **171**: 4761-6.

Solomons, N.W., Viteri, F., Shuler, T.R., Nielsen, F.H. (1982) 'Bioavailability of nickel in man: effects of foods and chemically-defined dietary constituents on the absorption of inorganic nickel.' *Journal of Nutrition*, **112**: 39-50.

Song, H.K., Mulrooney, S.B., Huber, R., Hausinger, R.P. (2001) 'Crystal structure of *Klebsiella aerogenes* UreE, a nickel-binding metallochaperone for urease activation.' *Journal of Biological Chemistry*, **276**: 49359-64.

Soriano, A., **Hausinger**, R.P. (1999) 'GTP-dependent activation of urease apoprotein in complex with the UreD, UreF, and UreG accessory proteins.' *Proceedings of the National Academy of Sciences*, **96**: 11140-4.

Soriano, A., Colpas, G.J., Hausinger, R.P. (2000) 'UreE stimulation of GTP-dependent urease activation in the UreD-UreF-UreG-urease apoprotein complex.' *Biochemistry*, **39**: 12435-40.

Sorrell, T.C., Brownlee, A.G., Ruma, P., Malik, R., Pfeiffer, T.J., Ellis, D.H. (1996) 'Natural environmental sources of *Cryptococcus neoformans var. gattii*.' *Journal of Clinical Microbiology*, **34**: 1261-3.

Stanbrough, M., **Magasanik**, B. (1995) 'Transcriptional and posttranslational regulation of the general amino acid permease of *Saccharomyces cerevisiae*.' *Journal of Bacteriology*, **177**: 94-102.

Stewart, V., **Vollmer**, S.J. (1986) 'Molecular cloning of nit-2, a regulatory gene required for nitrogen metabolite repression in *Neurospora crassa*.' *Gene*, **46**: 291-5.

Stola, M., Musiani, F., Mangani, S., Turano, P., Safarov, N., Zambelli, B., Ciurli, S. (2006) 'The nickel site of *Bacillus pasteurii* UreE, a urease metallo-chaperone, as revealed by metal-binding studies and X-ray absorption spectroscopy.' *Biochemistry*, **45**: 6495-509.

Stoof, J., Breijer, S., Pot, R.G., van der Neut, D., Kuipers, E.J., Kusters, J.G., van Vliet, A.H. (2008) 'Inverse nickel-responsive regulation of two urease enzymes in the gastric pathogen Helicobacter mustelae.' *Environmental Microbiology*, **10**: 2586-97.

Sukroongreung, S., Kitiniyom, K., Nilakul, C., Tantimavanich, S. (1998) 'Pathogenicity of basidiospores of *Filobasidiella neoformans var. neoformans*.' *Medical Mycology*, **6**: 419-24.

Sumner, J.B. (1926) 'The Isolation and Crystallization of the Enzyme Urease.' *Journal of Biological Chemistry*, **69**: 435-441.

Toffaletti, D.L., Rude, T.H., Johnston, S.A., Durack, D.T., Perfect, J.R. (1993) 'Gene transfer in Cryptococcus neoformans by use of biolistic delivery of DNA.' *Journal of Bacteriology*, **175**: 1405-11.

Tottey, S., Waldron, K.J., Firbank, S.J., Reale, B., Bessant, C., Sato, K., Cheek, T.R., Gray, J., Banfield, M.J., Dennison, C., Robinson, N.J. (2008) 'Protein-folding location can regulate manganese-binding versus copper- or zinc-binding.' *Nature*, **455**: 1138-42.

Tyvold, S.S., Solligård. E., Lyng, O., Steinshamn, S.L., Gunnes, S., Aadahl, P. (2007) 'Continuous monitoring of the bronchial epithelial lining fluid by microdialysis.' *Respiratory Research*, **8**: 78.

Ueta, R., Fujiwara, N., Iwai, K., Yamaguchi-Iwai, Y. (2007) 'Mechanism underlying the iron-dependent export of the iron-responsive transcription factor Aft1p in *Saccharomyces cerevisiae*.' *Molecular and Cellular Biology*, **18**: 2980-90.

Vartivarian, S.E., Anaissie, E.J., Cowart, R.E., Sprigg, H.A., Tingler, M.J., Jacobson, E.S. (1993) 'Regulation of cryptococcal capsular polysaccharide by iron.' *Journal of Infectious Diseases*, **167**: 186-90.

Voland, P., Weeks, D.L., Marcus, E.A., Prinz, C., Sachs, G., Scott, D. (2003) 'Interactions among the seven *Helicobacter pylori* proteins encoded by the urease gene cluster.' *American Journal of Physiology. Gastrointestinal and Liver Physiology*, **284**: G96-G106.

Waldron, K.J., **Robinson**, N.J. (2009) 'How do bacterial cells ensure that metalloproteins get the correct metal?' *Nature Reviews. Microbiology*, **7**: 25-35.

Waldron, K.J., Rutherford, J.C., Ford, D., Robinson, N.J. (2009) 'Metalloproteins and metal sensing.' *Nature*, **460**: 823-30.

Wayne Outten, F., Outten C.E., Hale, J., O'Halloran, T.V. (2000) 'Transcriptional Activation of an *Escherichia coli* Copper Efflux Regulon by the Chromosomal MerR Homologue, CueR.' *Journal of Biological Chemistry*, **275**: 31024-29.

Wang, S.Z., Chen, Y., Sun, Z.H., Zhou, Q., Sui, S.F. (2006) '*Escherichia coli* CorA periplasmic domain functions as a homotetramer to bind substrate.' *Journal of Biological Chemistry*, **281**: 26813-20.

Wang, Y., Aisen, P., Casadevall, A. (1995) 'Cryptococcus neoformans melanin and virulence: mechanism of actions.' *Infection and Immunity*, **63**: 3131-3136.

Wang, Y., Aisen, P., Casadevall, A. (1996) 'Melanin, melanin "ghosts," and melanin composition in *Cryptococcus neoformans*.' *Infection and Immunity*, **64**: 2420-2424.

Waring, W.S., Stephen, A.F., Robinson, O.D., Dow, M.A., Pettie, J.M. (2008) 'Serum urea concentration and the risk of hepatotoxicity after paracetamol overdose.' *QJM*, **101**: 359-63.

Waters, B.M., **Eide**, D.J. (2002) 'Combinatorial control of yeast FET4 gene expression by iron, zinc, and oxygen.' *Journal of Biological Chemistry*, **277**: 33749-57.

White, M., Cirrincione, C., Blevins, A., Armstrong, D. (1992) 'Cryptococcal meningitis: outcome in patients with AIDS and patients with neoplastic disease.' *Journal of Infectious Diseases*, **165**: 960-3.

Whittaker, J.W. (2003) 'The irony of manganese superoxide dismutase.' *Biochemical Society Transactions*, **31**: 1318-21.

Witte, C.P., Isidore, E., Tiller, S.A., Davies, H.V., Taylor, M.A. (2001) 'Functional characterisation of urease accessory protein G (ureG) from potato.' *Plant Molecular Biology*, **45**: 169-79.

Wiame, J.M., Grenson, M., Arst, H.N.Jr. (1985) 'Nitrogen catabolite repression in yeasts and filamentous fungi.' *Advances in Microbial Physiology*, **26**: 1-88.

Won, H.S., Lee, Y.H., Kim, J.H., Shin, I.S., Lee, M.H., Lee, B.J. (2004) 'Structural characterization of the nickel-binding properties of *Bacillus pasteurii* urease accessory protein (Ure)E in solution.' *Journal of Biological Chemistry*, **279**: 17466-72.

Won, H.S., **Lee**, B.J. (2004) 'Nickel-binding properties of the C-terminal tail peptide of *Bacillus pasteurii* UreE.' *Journal of Biochemistry*, **136**: 635-41.

Xiao, Z., **Wedd**, A.G. (2002) 'A C-terminal domain of the membrane copper pump Ctr1 exchanges copper(I) with the copper chaperone Atx1.' C*hemical Communications*, **6**: 588-9.

Yamaguchi, K., **Hausinger**, R.P. (1997) 'Substitution of the urease active site carbamate by dithiocarbamate and vanadate.' *Biochemistry*, **36**: 15118-22.

Yamaguchi-Iwai, Y., Stearman, R., Dancis, A., Klausner, R.D. (1996) 'Iron-regulated DNA binding by the AFT1 protein controls the iron regulon in yeast.' *EMBO journal*, **15**: 3377-84.

Yang, M., Cobine, P.A., Molik, S., Naranuntarat, A., Lill, R., Winge, D.R., Culotta, V.C. (2006) 'The effects of mitochondrial iron homeostasis on cofactor specificity of superoxide dismutase 2.' *EMBO Journal*, **25**: 1775-83.

Yonkovich, J., McKenndry, R., Shi, X., Zhu, Z. (2002) 'Copper ion-sensing transcription factor Mac1p post-translationally control the degradation of its target gene product Ctr1p.' *Journal of Biological Chemistry*, **277**: 23981-4.

Yun, C.W., Tiedeman, J.S., Moore, R.E., Philpott, C.C. (2000) 'Siderophore-iron uptake in *Saccharomyces cerevisiae*. Identification of ferrichrome and fusarinine transporters.' *Journal of Biological Chemistry*, **275**: 16354-9.

Zhao, H., **Eide**, D. (1996a) 'The yeast *ZRT1* gene encodes the zinc transporter protein of a high-affinity uptake system induced by zinc limitation.' *Proceedings of the National Academy of Sciences*, **93**: 2454-2458.

Zhao, H., **Eide**, D. (1996b)'The *ZRT2* gene encodes the low-affinity zinc transporter in *Saccharomyces cerevisiae*.' *Journal of Biological Chemistry*, **271**: 23203-23210.

Zambelli, B., Stola, M., Musiani, F., De Vriendt, K., Samyn, B., Devreese, B., Van Beeumen, J., Turano, P., Dikiy, A., Bryant, D.A., Ciurli, S. (2005) 'UreG, a chaperone in the urease assembly process, is an intrinsically unstructured GTPase that specifically binds Zn2+.' *Journal of Biological Chemistry*, **280**: 4684-95.

Zambelli, B., Musiani, F., Savini, M., Tucker, P., Ciurli, S. (2007) 'Biochemical studies on *Mycobacterium tuberculosis* UreG and comparative modelling reveal structural and functional conservation among the bacterial UreG family.' *Biochemistry*, **46**:3171-82.

Zambelli, B., Turano, P., Musiani, F., Neyroz, P., Ciurli, S. (2009) 'Zn2+-linked dimerization of UreG from *Helicobacter pylori*, a chaperone involved in nickel trafficking and urease activation.' *Proteins*, **74**: 222-39.

Zaragoza, O., García-Rodas, R., Nosanchuk, J.D., Cuenca-Estrella, M., Rodríguez-Tudela, J.L., Casadevall, A. (2010) 'Fungal cell gigantism during mammalian infection.' *PLoS Pathogens*, **6**: e1000945.

Zielinski, H., Mudway, I.S., Bérubé, K.A., Murphy, S., Richards, R., Kelly, F.J. (1999) 'Modeling the interactions of particulates with epithelial lining fluid antioxidants.' *American Journal of Physiology*, **277**: L719-26.

8. Appendix

8.1. The PCA of Nickel Peaks 1, 2 and 3

PCA was used to compare the distribution of nickel to protein across fractions of the metal profiles. In the main text a 3D representation of PC1, PC2 and PC3 of each peak was presented (Figure 43). Here 2D representations of PC1 vs. PC2, PC1 vs. PC3. PC2 vs. PC3 and the protein gel used to quantify the protein bands are presented for each nickel peak (Figure 56, Figure 57, Figure 58).

A

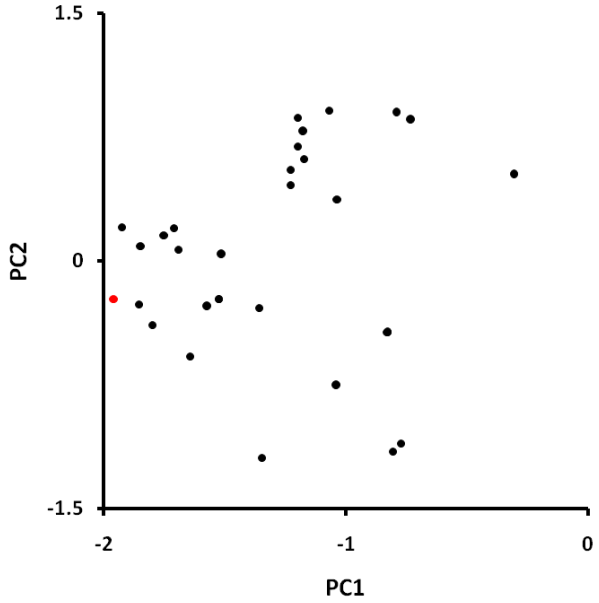

B

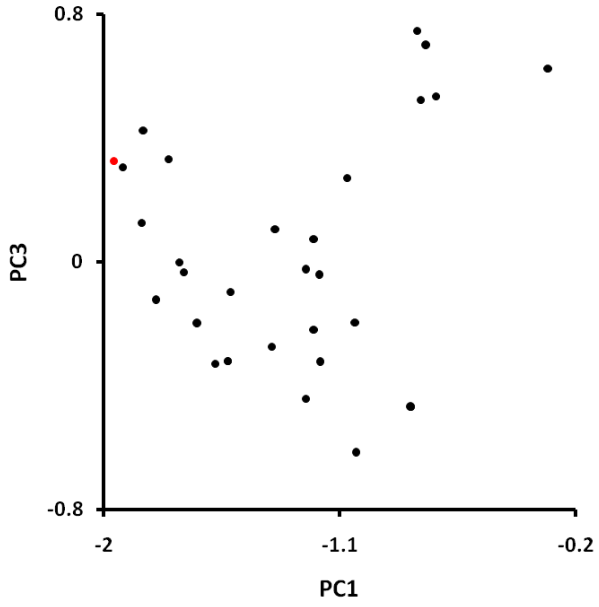

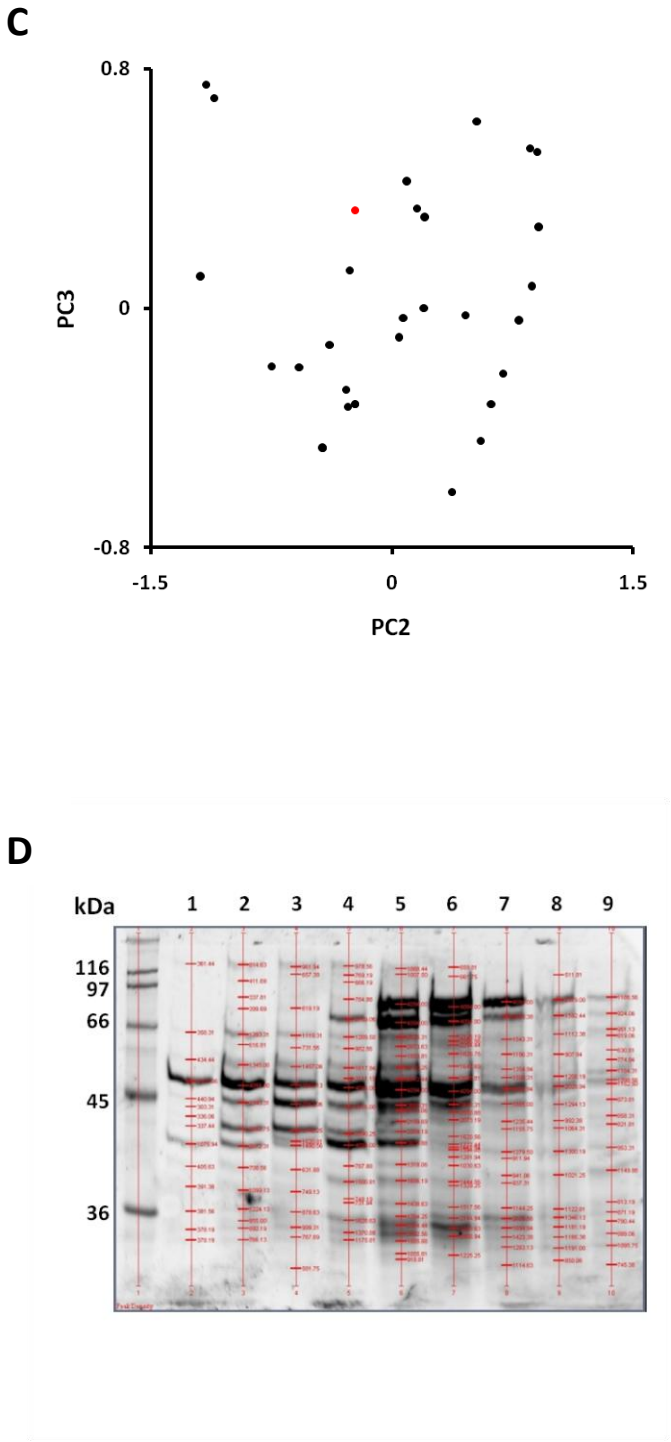

Figure 56 - PCA of nickel peak 1.

Two-dimensional plots (A-C) comparing the principle components 1, 2 and 3 (PC1, PC2 and PC3, respectively). The SDS-PAGE gel from which the protein distribution is measured is also displayed (D). Data are representative of 2 repeat experiments.

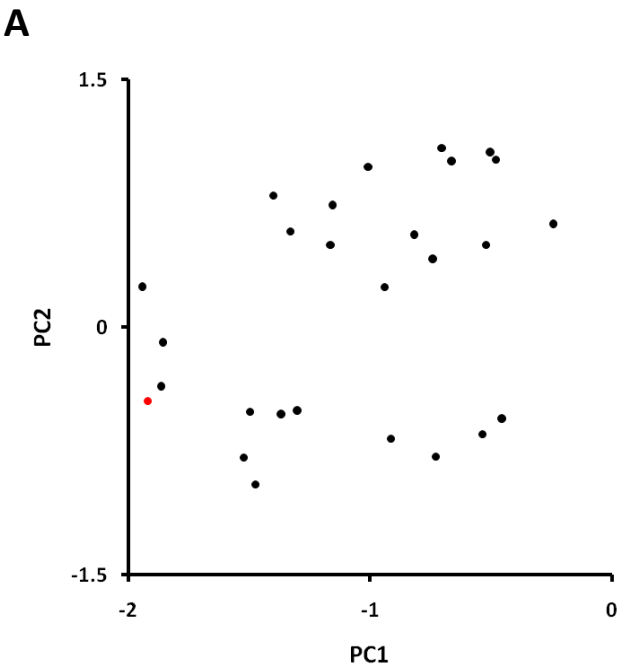
A
1.5
0
-1.5
PC2
-2
-1
0
PC1

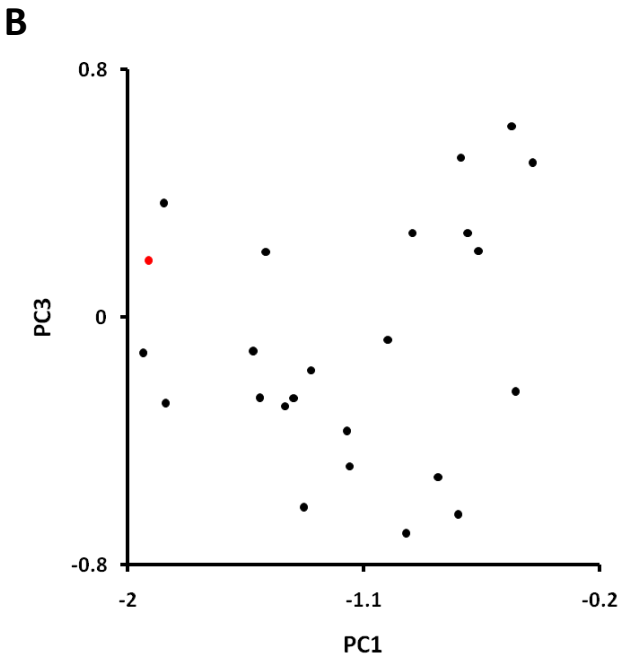
B
0.8
0
-0.8
PC3
-2
-1.1
-0.2
PC1

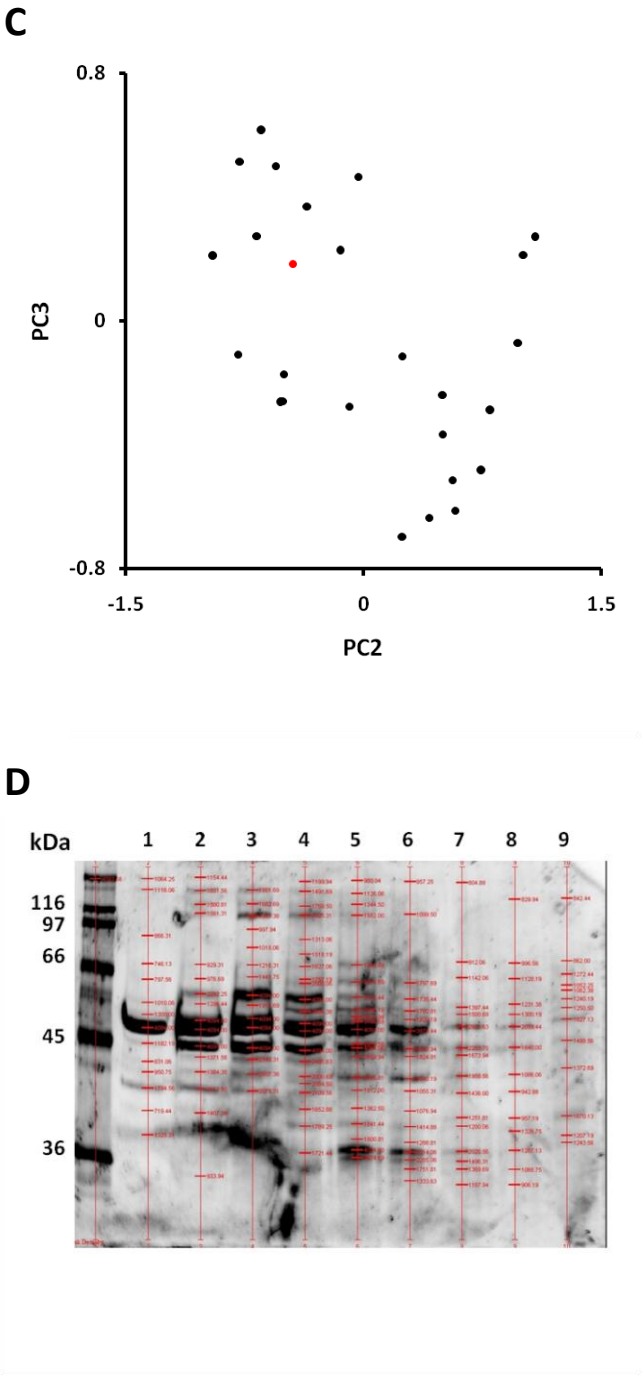

Figure 57 - PCA of nickel peak 2.

Two-dimensional plots (A-C) comparing the principle components 1, 2 and 3 (PC1, PC2 and PC3, respectively). The SDS-PAGE gel from which the protein distribution is measured is also displayed (D). Data are representative of 2 repeat experiments.

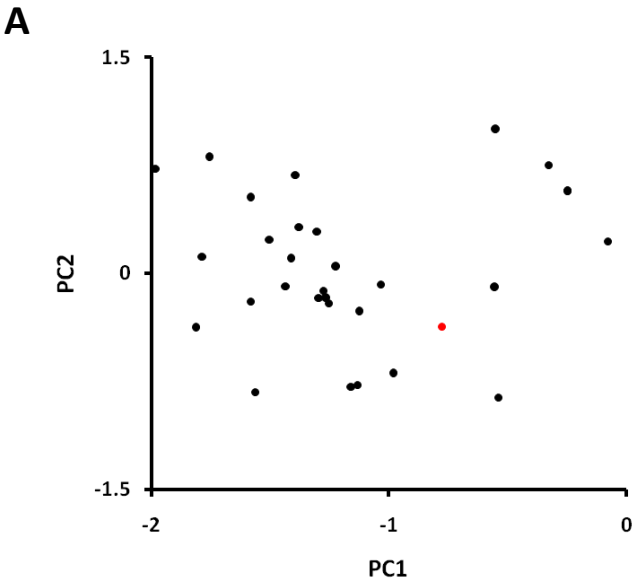
A
1.5
0
-1.5
PC2
-2
-1
0
PC1

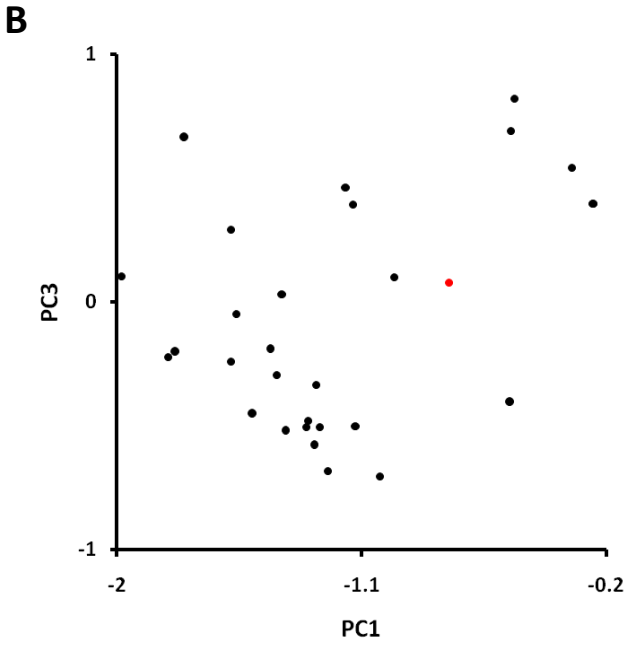
B
1
0
-1
PC3
-2
-1.1
-0.2
PC1

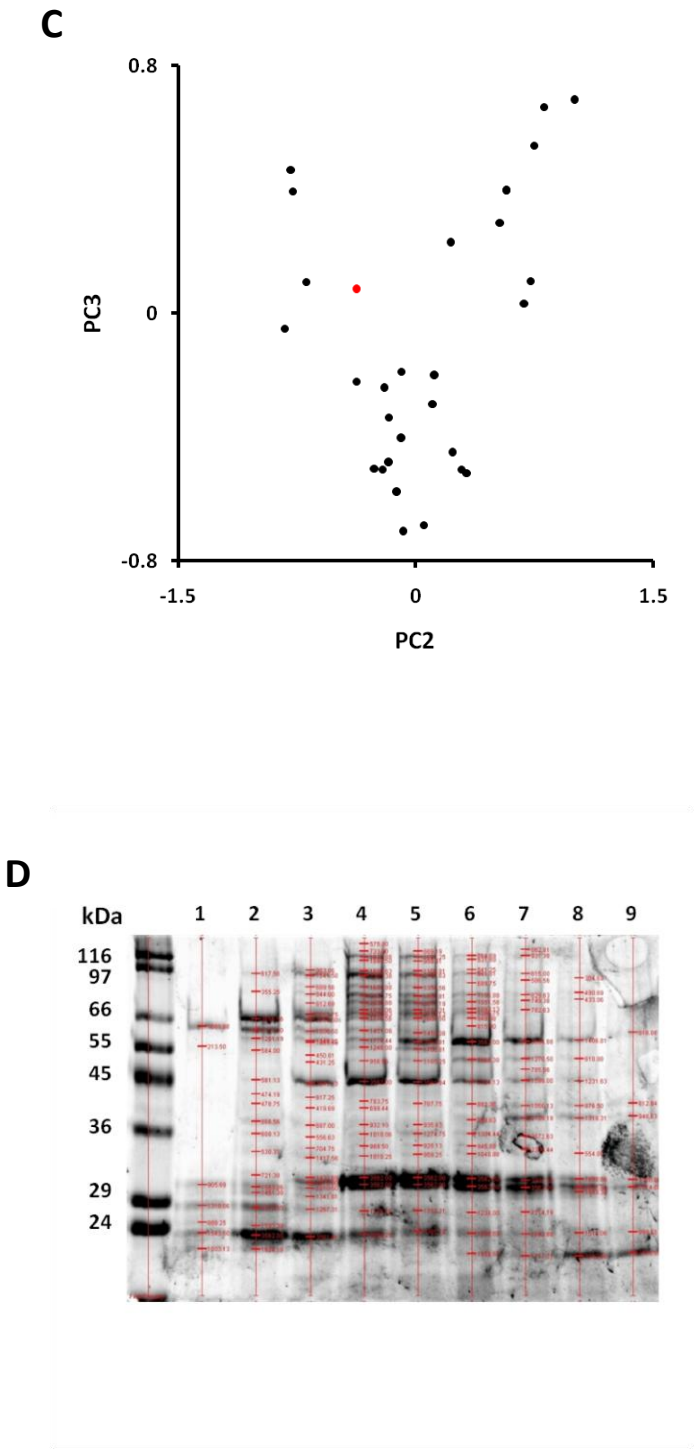

Figure 58 - PCA of nickel peak 3.

Two-dimensional plots (A-C) comparing the principle components 1, 2 and 3 (PC1, PC2 and PC3, respectively). The SDS-PAGE gel from which the protein distribution is measured is also displayed (D). Data are representative of 2 repeat experiments.